CRCLEME
Cooperative Research Centre for
Landscape Environments
and Mineral Exploration

CSIRO
EXPLORATION AND MINING

OPEN FILE REPORT SERIES

GEOLOGY, GEOCHEMISTRY AND MINERALOGY OF THE MURRIN MURRIN NICKEL LATERITE DEPOSIT

M.A. Wells and C.R.M. Butt

CRC LEME OPEN FILE REPORT 207 / CSIRO REPORT P2006/549

August 2006

(CRC LEME Report 126R, 2nd Impression 2006)

CRC AUSTRALIA

GEOLOGY, GEOCHEMISTRY AND MINERALOGY OF THE MURRIN MURRIN NICKEL LATERITE DEPOSIT

M.A. Wells and C.R.M. Butt

CRC LEME OPEN FILE REPORT 207 / CSIRO REPORT P2006/549

August 2006

(CRC LEME Report 126R, 2nd Impression 2006)

CRC LEME is an unincorporated joint venture between CSIRO-Exploration & Mining, and Land & Water, The Australian National University, Curtin University of Technology, University of Adelaide, Geoscience Australia, Primary Industries and Resources SA, NSW Department of Primary Industries and Minerals Council of Australia.

Headquarters: CRC LEME c/o CSIRO Exploration and Mining, PO Box 1130, Bentley WA 6102, Australia

Copies of this publication can be obtained from:

The Publications Officer, CRC LEME, c/- CSIRO Exploration & Mining, PO Box 1130, Bentley WA 6102, Australia. Information on other publications in this series may be obtained from the above, or from http://crcleme.org.au

Cataloguing-in-Publication

Geology, Geochemistry and Mineralogy of the Murrin Murrin Nickel Laterite Deposit

M.A. Wells & C.R.M. Butt

ISBN 1 921039 44 2

1. Geology
2. Geochemistry - Analytical
3. Mineralogy

I. M.A. Wells & C.R.M. Butt

II. Title

CRC LEME Open File Report

ISSN 1329-4768

Addresses and affiliations of authors

Martin R. Wells	**Charles Butt**
Cooperative Research Centre for Landscape Environments and Mineral Exploration, University of Canberra	Cooperative Research Centre for Landscape Environments and Mineral Exploration
c/- CSIRO Exploration & Mining	c/- CSIRO Exploration & Mining
PO Box 1130	PO Box 1130
Bentley	Bentley
WA 6102	WA 6102
Western Australia	Western Australia

Table of Contents

Executive summary iii

1.0 Introduction 1

1.1 Background 1

1.2 Geological setting 1

1.3 Geomorphology 3

1.4 Climate and vegetation 5

1.5 Formation of Ni-Laterites 5

1.6 Murrin Murrin Ni-laterite 6

1.7 Project objectives 8

1.8 Specific project objectives 8

1.9 Project work program 9

1.10 Other research projects 10

1.10.1 Palaeomagnetic dating 10

1.10.2 Stable O-isotope dating 10

1.11 Methodology 11

1.11.1 Infrared analysis 11

1.11.2 3-D Modelling (MVS) 13

1.11.3 Limitations to MVS modelling 13

1.11.4 Geochemistry 14

1.11.5 X-ray diffraction 15

1.11.6 Mass balance 15

1.11.7 Stable O-isotope analysis of kaolinite; preparation. 16

1.11.8 Cluster analysis 17

1.11.9 Normative mineral analyses 17

1.12 Limitations of the study 17

2.0 Murrin Murrin region regolith-landform map 19

2.1 Introduction 19

2.2 Regolith mapping and terminology 19

2.3 Methodology 19

2.3.1 Aerial photographs 20

2.3.2 Magnetic and radiometric data 20

2.3.3 Digital elevation model 20

2.3.4 Landsat thematic data 21

2.4 Remote sensing of regolith-landform units 22

2.5 Regolith-landform units and relationships 28

2.5.1 Relict regime 31

2.5.2 Erosional regime 34

2.5.3 Depositional regime 34

3.0 Regolith Units 36

3.1 Introduction 36

3.2 Geomorphology and site description 36

3.3 Mineral identification 37

3.3.1 PIMA-II 37

3.3.2 X-ray diffraction analysis 39

3.4 Regolith stratigraphy 43

3.5 Regolith models for MM2 and MM3 45
3.5.1 Bedrock geology 50
3.6 CIPW-Norm abundances 53
3.6.1 Criteria and order of element allocation for calculations of CIPW-Norm abundances for MM2 and MM3. 54
3.6.2 Criteria and order of element allocation for calculations of CIPW-Norm abundances for the channel-clay unit, MM2. 56
3.7 Normative mineralogy for MM2 and MM3 57
3.7.1 Normative mineralogy of channel clays for MM2 71
3.8 Summary 73
4.0 Geochemistry: Element-regolith associations 75
4.1 Introduction 75
4.2 MVS modelling: block models for MM2 and MM3 75
4.2.1 MM2 75
4.2.2 MM3 78
4.3 MVS modelling: slices and regolith surfaces 78
4.3.1 MM2 79
4.3.2 MM3 97
4.4 Cluster Analysis 99
4.4.1 Cluster analysis: global and individual deposits 102
4.4.2 Cluster analysis; regolith geochemistry 102
4.5 Mass balance analysis 103
4.6 Mass balance profiles: MM2 and MM3 105
4.7 Summary 111
5.0 Summary and discussion 113
6.0 Aknowledgements 119
7.0 References 120

EXECUTIVE SUMMARY

A regional and deposit scale examination was undertaken of the characteristics and factors controlling enrichment of Ni and Co within the Ni-laterite deposits at Murrin Murrin. Compilation of a 1:50000 regolith-landform map by a combined approach that incorporated aerial photographic interpretation and magnetic, radiometric and Landsat TM image analysis established the regional regolith-landform setting of the deposits within the north and south tenements at Murrin Murrin. The regolith-landform map is also available as a separate report (Wells, 1999) and is available on CD as a MapInfo project.

Examination of the factors controlling Ni and Co enrichment at the deposit scale was achieved by characterization of element-regolith associations for two sites, MM2 and MM3, within the north and south tenements, respectively. Regolith characteristics of the Ni-laterite profiles at the two sites were modelled using the Mining Visualization Software (MVS) system, mass balance studies cluster analysis and from determinations of CIPW-Norm mineral abundances.

The mineralogy and element associations within regolith units at depth for both sites was similar because of the similar bulk chemistry (*i.e.,* high Mg; low Si, Al and Fe) of the underlying serpentinized cumulate and because of the minimal effect of weathering at these depths. The greater effect of weathering in the upper portion (*i.e.,* near surface) of profiles highlighted differences in the chemistry of the underlying cumulate bedrock, which were expressed as relative differences in CIPW-Norm abundances of chlorite, saponite and nontronite between MM2 and MM3. Understanding of the variations in regolith mineralogy within and between deposits may have important metallurgical implications for ore processing.

The prevailing landform processes also influence element-regolith associations within the deposit and expression of the Ni-laterite profile at the surface. Introduction of locally derived felsic sediments (high in Al, Si, Ca and Ti) at the surface of the laterite profile at MM2 confused the element-regolith associations expected in profiles formed from weathered ultramafics. The depositional landform regime that prevails at MM2 is reflected in the subdued relief and minimal outcrop of laterite, which hinders exploration in the area. The more prominent relief at MM3 is a reflection of the prevailing relict and erosional landforms of the area that provides a better exposure of the laterite profile.

Mineralization of Ni and Co at MM2 is strongly controlled by structural overprinting of underlying ortho- and mesocumulates, which is expressed as a normally displaced, intersecting fault-set. Nickel and Co occur mainly within the nontronite unit in profiles formed over variably weathered ortho- and mesocumulates along the fault planes. Probable reactivation during weathering resulted

in the localized depletion of Ni and Co (and other metals) along fault shear planes. Three-dimensional modelling, using MVS, of the fault-set within the regolith at MM2 was important to understanding the distribution of Ni and Co.

Enrichment of Ni and Co at MM3 is controlled strongly by lithology; variations in cumulate lithology were well correlated to values of the Ni/Ni+Al ratio. Mineralization occurs mainly within the nontronite unit of profiles developed from ortho- and mesocumulates where the nontronite unit was thickest, presumably because leaching was minimal. Ortho- and mesocumulates have weathered to variable depths that possibly reflect local variations in porosity of the serpentinized cumulate. Regolith profiles over adcumulates were more uniformly developed but to a shallower depth. Secondary silicification associated with initial stages of adcumulate weathering probably inhibited extensive profile development by impeding drainage. This also prevented enrichment of Ni and Co over adcumulates due to silicification either diluting enrichment or impeding the mobilization of Ni and Co within the profile.

1.0 INTRODUCTION

1.1 Background

The Murrin Murrin Ni-laterite deposit is situated approximately 60km east of Leonora within the north-eastern Yilgarn Craton of Western Australia (Figure 1.1) at 28° 50'S and 121° 54'E on the Laverton 1:250 000 (SH/51-2) map sheet.

The area has experienced an extensive and varied exploration and mining history with early gold prospecting and mining beginning in the 1890's. This was followed by the production of copper between 1899 and 1908 from the Anaconda, Rio Tinto and Nangeroo mines after the discovery of small Cu-Zn sulphide deposits (Gower, 1976). Exploration for Ni commenced some 60 years later for Ni-sulphide hosted deposits, which although unsuccessful, realized the smectite hosted Ni-laterite deposits in the area (Monti and Fazakerley, 1996). These deposits were to wait nearly 30 years before undergoing commercial development by Anaconda Nickel NL. These deposits are one of three Ni-laterite deposits in the northeastern Yilgarn Craton that began production in 1999.

1.2 Geological setting

A detailed account of the regional and ore-deposit geology is beyond the scope of the present study. Hallberg (1985) and Hammond (1996), as summarized by Monti and Fazakerley (1996), provide a more detailed account of the geological and structural setting of the Murrin Murrin Ni-deposits. However, a summary of the main geological features is provided in the following discussion. A generalized geological and structural setting of the deposits is given in Figure 1.1.

The Murrin Murrin deposits are formed from serpentinized peridotite (*i.e.*, komatiitic olivine cumulates) host rocks within the Archaean Norseman-Wiluna greenstone belt (Monti and Fazakerley, 1996). These tend to form the lower stratigraphic sequences with feldspathic, clastic and volcaniclastic sedimentary rocks, and mafic volcanics and intrusives tending to comprise the upper units (Monti and Fazakerley, 1996). Granite, granodiorite and adamellite rocks have also intruded the sequence.

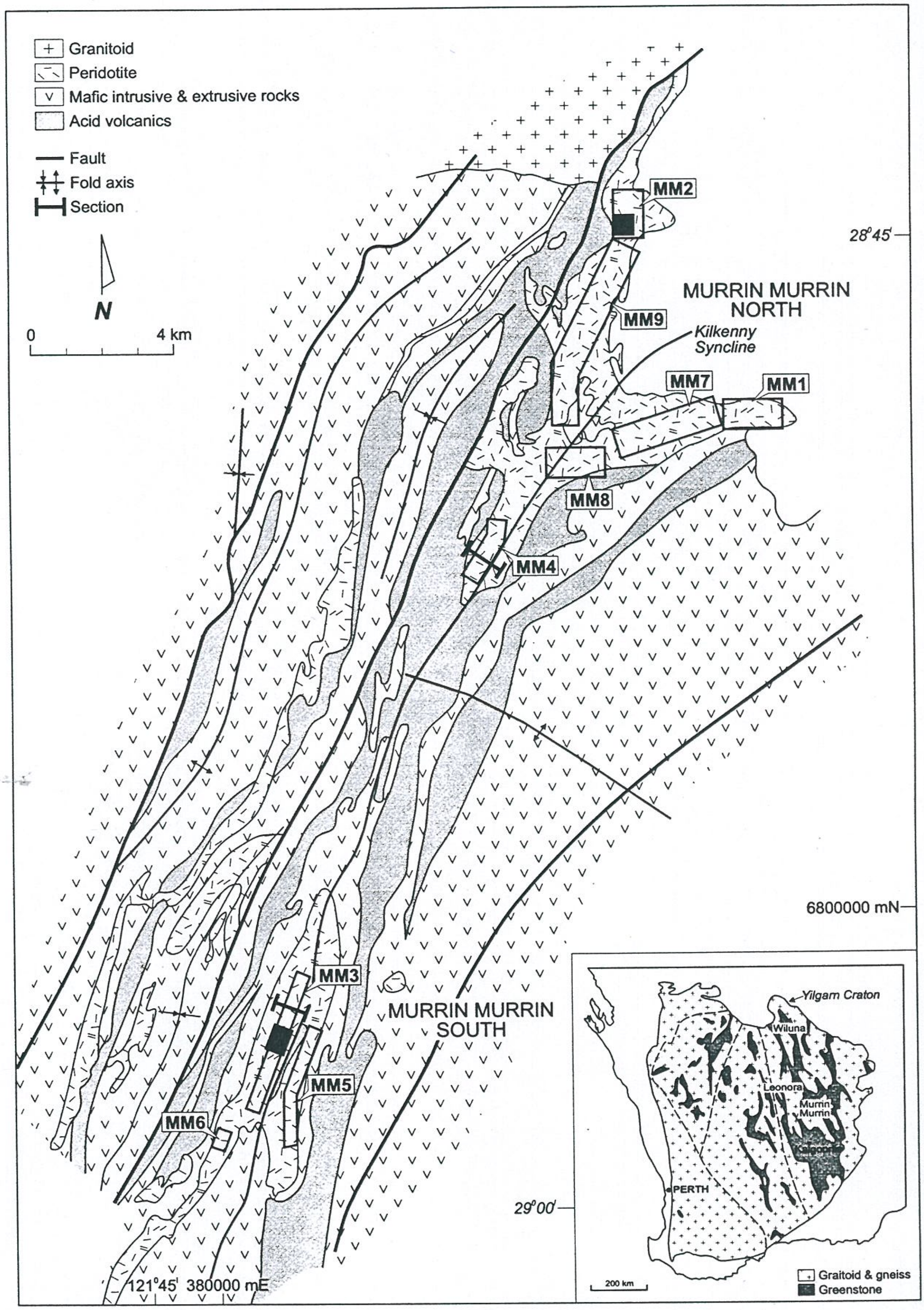

Figure 1.1. Location and generalized geological and structural setting for the Murrin Murrin Ni-deposits (modified from Monti and Fazakerley, 1996). Two areas (■) were selected within the MM2 and MM3 deposits for further detailed study.

A regional scale, north plunging anticlinorium to the east of the Murrin Murrin ultramafic sequences and a synclinorium, developed on a similar scale to the west, have constrained the Murrin Murrin ultramafic rocks to a NNE-SSW striking sequence (Hammond, 1996). The sequence is further constrained by regional scale NNE striking, westerly dipping faults (Fig. 1.1) which are offshoots of the NW striking Keith-Kilkenny fault to the SW (Monti and Fazakerley, 1996). Emplacement of felsic (*i.e.*, granite, granodiorite) intrusives has further complicated the deformational history of the greenstone belts with tightly folded synclinal features (*i.e.*, the Kilkenny syncline) that shows plunge reversals (Fig. 1.1). This has ultimately resulted in the formation of two outcrops of serpentinized peridotite designated as Murrin Murrin North and Murrin Murrin South (Fig. 1.1). These areas will hereafter be referred to throughout this report as MM North and MM South.

1.3 Geomorphology

The Murrin Murrin Ni-laterite deposits occur within a gently undulating terrain of generally low relief. Weathered ultramafic sequences generally provide the few high points in the landscape consisting of sub-parallel, elongated ridges and hills, and isolated hills (*i.e.*, mesas and buttes) and minor breakaways capped by ferruginous duricrust. To the north granite-granodiorite-adamellite rocks (*i.e.*, East Terrace area and Minerie Hill) have formed significant, residual breakaways with extensive plateau surfaces and associated backslopes.

Extensive depositional sediments as alluvial and colluvial plains blanket large areas to the NW, SW and ESE of the Ni deposits. These alluvial sediments form part of an extensive NW-SE trending, sub-parallel palaeodrainage system (Fig. 1.2) which drains to the SE bounded by the Lake Carey palaeochannel system to the NE and the Lake Raeside system to the SW (Pringle *et al.*, 1994). The NNE-SSW striking ultramafic sequences have formed a drainage divide in the north of the area and are part of a regional NW – SE striking drainage divide (Fig. 1.2) (Pringle *et al.*, 1994). Katata Creek has made a westerly incision into the ultramafic sequences and connects with Maleta and Bummer Creeks, which drain to the south-west. Kilkenny Creek, which runs sub-parallel to the strike of the ultramafic sequences that outcrop in MM south, also drains to the SW. These systems ultimately drain into the Lake Raeside palaeochannel system. The main drainage system to the NE of MM north (*i.e.*, Garden Cement Creek) runs to the east and ultimately flows into Lake Carey.

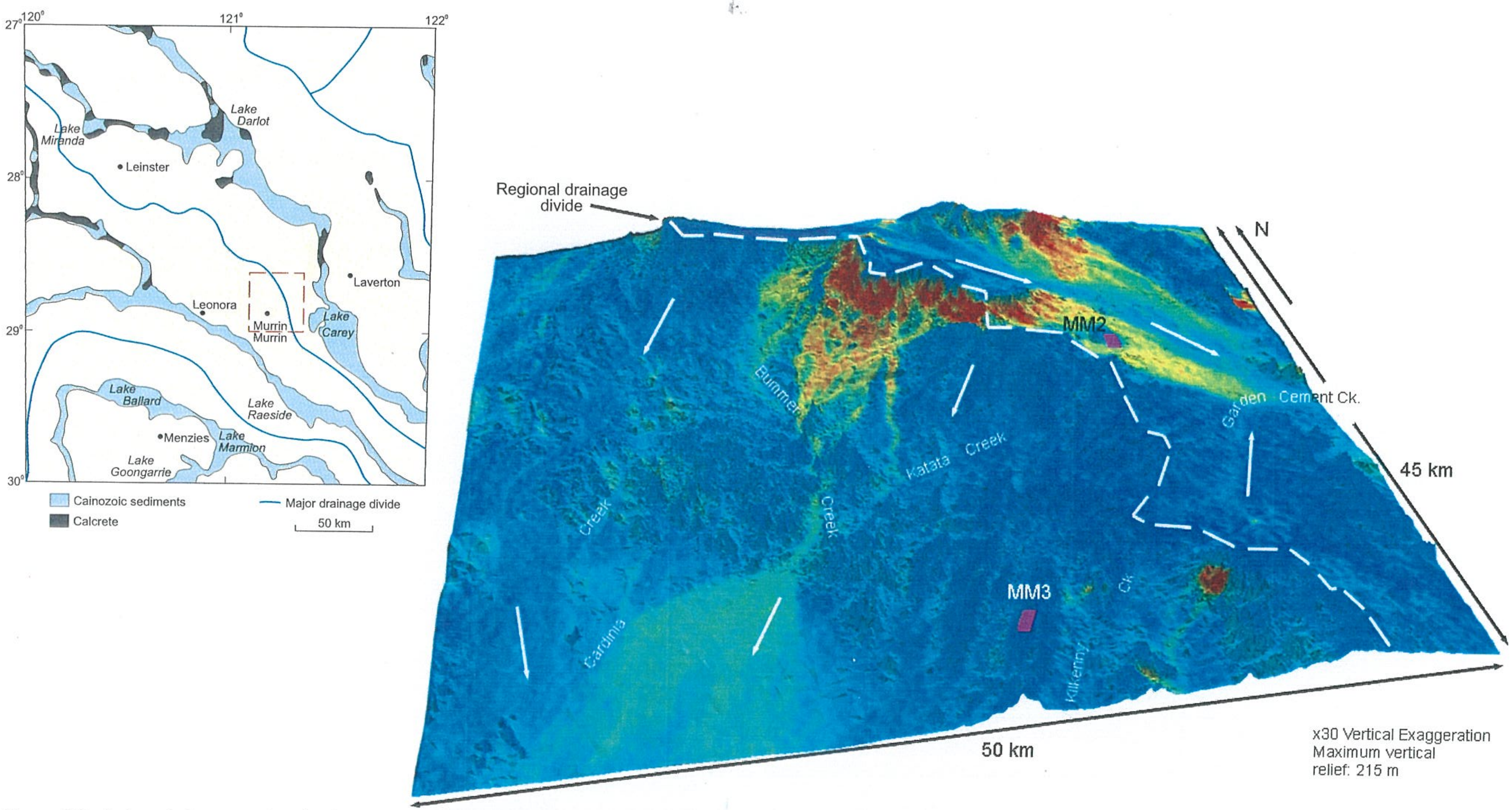

Figure 1.2. Palaeodrainage system for the Leonora-Laverton area (inset) and a three dimensional perspective view of the Kγ-ray image draped over the DEM for the Minerie 1:100 000 map sheet, with the location of study areas MM2 and MM3 also shown (■). A regional NW-SE trending drainage divide effectively separates MM north from MM south. The radiometric image for K highlights the division of drainage for the area and shows very well the movement of recent K-bearing sediments (orange/yellow and cyan hues) which originate from outcrops of granite/adamellite saprock at the base of the breakaway (bright red hues). Drainage to the NE of the divide is associated with the Lake Carey palaeochannel system (see inset). To the SW of the divide, drainage is associated with the Lake Raeside system (see inset). The direction of drainage is shown by the white arrows.

1.4 Climate and vegetation

The climate is semi-arid, with generally hot, dry summers and cool, wet winters. The mean annual rainfall for both Leonora and Laverton is 222 mm (Pringle *et al.,* 1994). Summer rainfall does occur from sporadic thunderstorms associated with cyclonic depressions. An average maximum temperature for January of 37.1° C with an average minimum of 21.5° C is recorded for Leonora. The coolest month for Leonora is July with mean maximum and minimum temperatures of 18.2 and 6.0° C, respectively (Pringle *et al.,* 1994).

Vegetation is mainly open woodland dominated by acacia (*e.g., Acacia aneura* – mulga) and eremophila species (*e.g.,* poverty bush). Low shrublands are also present characterized by *Maireana sedifolia* (pearl bluebush), *M. pyramidata* (sago bush), *Casuarina cristata* (black oak tree), *Ptilotus obovatus* (cotton bush) and Wanderrie grasses (Pringle *et al.,* 1994). Various eucalypts (*e.g., Eucalyptus camaldulensis* - river red gum) can be found in the area but these are restricted to the main drainage lines. Salt-tolerant shrubs are also present occurring mainly in open alluvial plain areas and include various saltbush (atriplex) species (*e.g., Atriplex bunburyana* - silver saltbush). Isolated populations of the declared rare flora (DRF) *Hemigenia exilis* occur in the MM south area restricted mainly to duricrust ridges and hills, but also occur in down slope positions along creek lines.

1.5 Formation of Ni-Laterites

Lateritic Ni-deposits form by the chemical weathering of ultramafic Ni-host rocks. Most Ni-laterites of commercial significance appear to have formed from serpentinized peridotite, containing forsteritic (Fo) olivine as the main Ni source, and their metamorphic derivatives having a minimum Ni content of >2500 ppm (Burger, 1996).

Nickel laterite profiles are zoned consisting of a general sequence from bedrock to surface of: unweathered serpentinized ultramafic; saprolite zone; clay (smectite-rich) zone; ferruginous zone and soil cover. Brand *et al.,* (1998) have classified lateritic Ni-deposits into three main groups on the basis of the dominant mineralogy of the main Ni-bearing phases:

A. Garnieritic silicates. Dominated by 'garnierite-like' phases (essentially hydrated Mg-Ni-silicates) that occur generally deep in the saprolite. High grade: global mean 1.53 % Ni. *Examples*: Thio-Nakety districts, New Caledonia; Cerro Matoso, Colombia; Marlborough, Qld (Butt, 1974; Golightly, 1979, 1981; Parianos and Rivers, 1996).

B. Smectite silicates. Consisting mainly of smectitic clays (*e.g.*, nontronite), commonly occurring in the upper saprolite and/or pedolith. Low grade: global mean 1.21 % Ni. *Examples*: Brazil; **Murrin Murrin**, W.A.; Bulong, W.A. (Monti and Fazakerley, 1996; Monti. 1999; Burger, 1996, 1999; de Oliveira *et al.*, 1992).

C. Oxide. These are dominated by Fe oxides (*e.g.*, goethite and hematite), commonly occurring in the upper saprolite and/or pedolith. They are characterized by low Ni grades with a global mean of 1.06 % Ni. *Examples*: Goro, New Caledonia; Moa Bay, Cuba; Ivory Coast, west Africa; Cawse, W.A.; Ravensthorpe, W.A. (Brand *et al.*, 1996; Denn, 1999; Lipton *et al.*, 1999; Nahon *et al.*, 1982).

The presence of Co in these deposits is associated with Mn oxides (Mn being derived from primary Mn-bearing pyroxene in the host rock) which occur generally higher in the profile under suitable conditions of Eh and pH near the smectite/ferruginous zone contact. The Mn oxides account for only a minor amount of Ni within these deposits but appear to be the main host for Co (Butt and Nickel, 1981; Elias *et al.*, 1981: Llorca, 1993).

The characteristics of each Ni-laterite type, including Ni-grade and mineralogy are the result of the combined interaction of a range of climatic, geomorphological and geological (*i.e.*, lithology, structure) factors. Garnieritic silicate Ni-deposits account for the majority of continental Ni-deposits and are developed mainly from obducted Miocene and Pliocene ophiolite sequences, mainly harzburgite-olivine dunite cumulates (Brand *et al.*, 1998). Examples include, the Ni-deposits of Philippines and Australia (*e.g.*, Marlborough), and some deposits of New Caledonia. These deposits are characterized by typically high Ni-grades (2.5-5.0% Ni), in areas of very high relief in seasonally humid, tropical climates. In contrast, lateritic Ni-deposits such as Murrin Murrin are generally characterized by low Ni-grades (1.0-1.2% Ni) developed from weathered ultramafics (*i.e.*, komatiitic olivine cumulates) in a now, semi-arid environment of low relief.

1.6 Murrin Murrin Ni-laterite

Monti and Fazakerley (1996) and Camuti and Riel (1996) have described a generic profile for the Murrin Murrin Ni-laterite with a detailed description of unit mineralogy provided by these authors. A diagrammatic representation of the Murrin Murrin Ni-laterite profile is given in Figure 1.3. The Ni-laterite profile 'stratigraphy' has been compiled by Anaconda Exploration Staff with unit identification based on the criteria outlined in the Murrin Murrin Feasibility study (Volume 2).

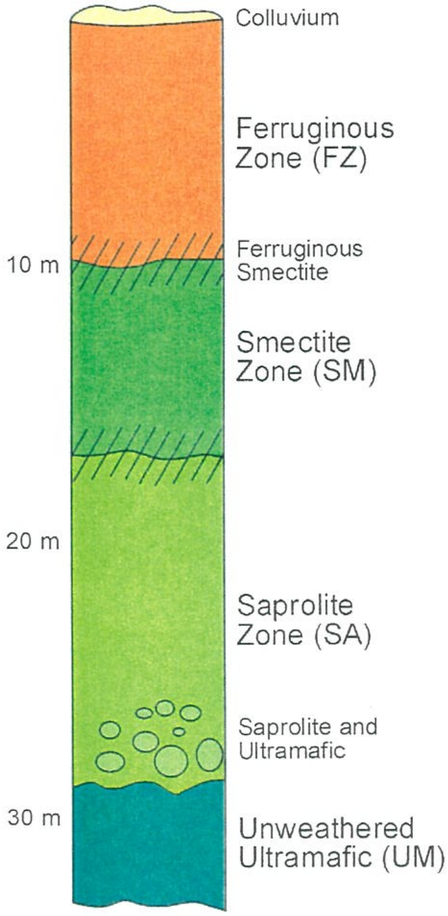

Figure 1.3. Generic profile for the Murrin Murrin Ni-laterite deposits (from Monti and Fazakerley, 1996).

However, this profile is not a 'regolith' profile as such. Criteria used for unit classification relied mainly upon logging in the field of RC drill pulps by identification of colour and texture variations. Some unit identification criteria are open to subjective interpretation by the observer/s. For example, identification of the SM zone relied upon identification of moderate levels (*i.e.* >25%) of smectite (Murrin Murrin Feasibility study, Volume 2, Section 3, p3-37). This approach, although suitable for general descriptive purposes of identifying relative trends in profile mineralogy in two dimensions, is not suitable for an objective examination of the structural and lithological factors that control the distribution of Ni and Co in these deposits in three dimensions. This is particularly important in light of the, at times, highly variable nature of the Ni-laterite profile at Murrin Murrin. For example, the complex contact between the FZ and SM zones as shown in Figure 1.4 which may also cause problems in volume estimates for grade control calculations.

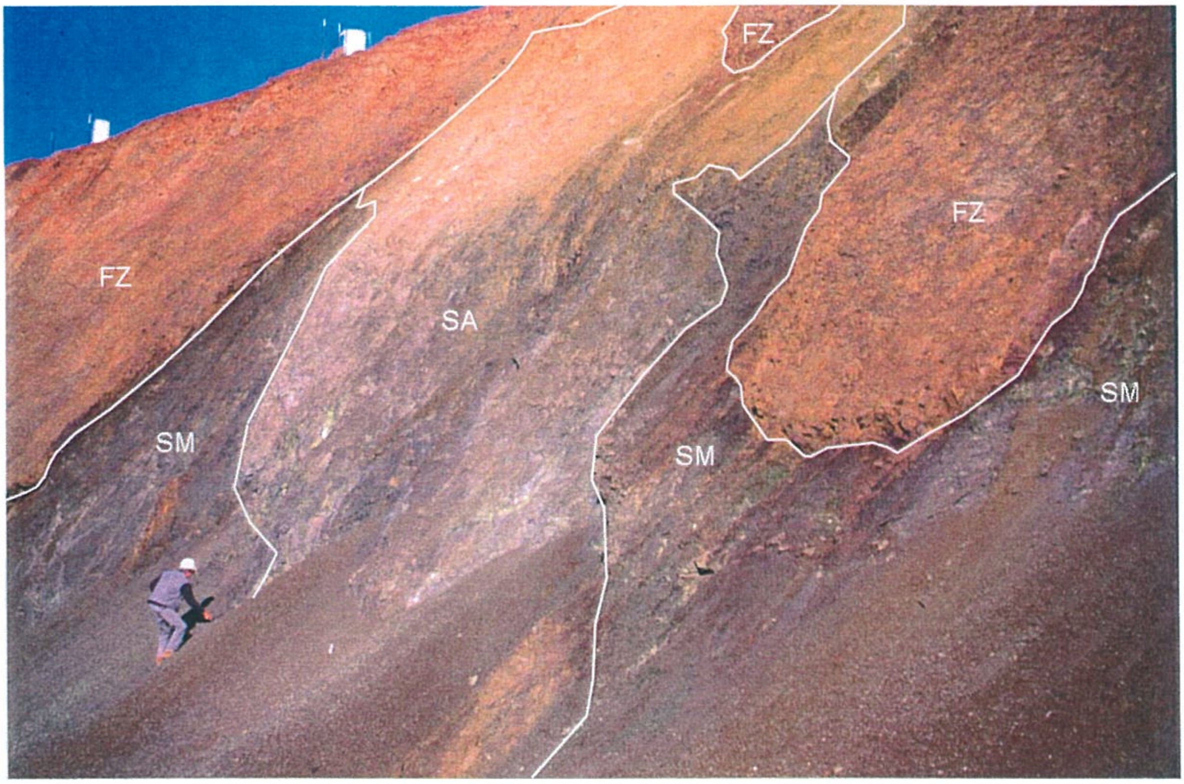

Figure 1.4. View of the western face of the trial pit at MM2 illustrating the highly variable and complex nature of the weathering profile at Murrin Murrin, in particular the contact between the ferruginous zone (FZ) and underlying smectite (SM) and saprolite (SA) zones (Anaconda Nickel unit classification terminology).

1.7 Project objectives

To determine the characteristics and distribution of nickel and cobalt enrichment in smectitic Murrin Murrin Ni-laterite deposit, and to determine its origin in terms of regolith and landform evolution.

1.8 Specific project objectives

1. Determine the evolution of the Murrin Murrin deposits within the context of their local and regional landscape setting.
2. Establish the mineralogical and geochemical characteristics of the Murrin Murrin Ni-deposits.
3. Determine the mineralogical controls on Ni/Co distribution within the deposits.
4. Evaluate the primary controls (*i.e.*, lithology/structure) to the distribution of Ni and Co and other elements.

5. Develop 3-D visualization models of the bedrock and regolith.

6. Establish a chronology of Ni-laterite formation in terms of local and regional landscape evolution by dating suitable primary and secondary mineralogical assemblages.

1.9 Project work program

A combined regional to local site scale approach was used to address each of the project objectives. A regional scale, regolith-landform map was compiled at 1:50 000 of the Murrin Murrin Ni-laterite deposits and surrounding tenements. This was to aid in establishing a regional landform setting for the evolution of the Ni-laterite deposits. The regolith-landform map was compiled from aerial photographic interpretation in conjunction with remotely sensed, reflected and emitted data. A detailed discussion of the regolith-landform map produced is provided in the following chapter. This was also provided as a separate report (Wells, 1999).

Two study areas were selected within the Murrin Murrin deposits (Fig. 1.1) to provide local-scale examination of the mineralogical and chemical factors influencing Ni and Co enrichment. A 600 x 900 m area within the MM2 deposit (9200 to 9800 mE; 26000 to 26900 mN) and a 500 x 800 m area within the MM3 deposit (9100 to 9600 mE; 71700 to 72500 mN) were selected to provide a comparative study of factors influencing mineralization at Murrin Murrin. The two study areas are hereafter referred to throughout this report as MM2 and MM3, respectively.

MM2 occupies part of the western limb of the northern expression of the Kilkenny syncline (Fig. 1.1) and is underlain by predominantly olivine ortho- and mesocumulates (Hill *et al.,* 1996). MM3 occupies part of the western limb of the southern expression of the Kilkenny syncline (Fig. 1.1). The ultramafic sequence here consists of a tightly folded (isoclinal?), olivine cumulate that grades from orthocumulate on the western margin of the limb to meso- and adcumulate lithologies in the centre, through to meso- and orthocumulates on the eastern margin of the limb towards the centre of the fold (Hill *et al.,* 1996). A more detailed summary of individual deposit geology is provided in the Murrin Murrin Feasibility Study (Volume 2).

Investigation of the regolith mineralogy and geochemistry for each of the study areas was conducted using a combination of x-ray diffraction (XRD), infrared analysis (IR) and x-ray fluorescence (XRF). Most analyses were performed on RC drill sample pulps, prepared according to the guidelines and procedures used by analytical laboratories Analabs and UltraTrace as outlined in the Murrin Murrin Feasibility Study (Volume 2).

Bulk, 'grab-bag' samples were collected from RC riffle split samples at the MM2 and MM3 sample farms on site. Northing transects of 200 m line spacings were taken across the MM2 and MM3 study areas with selected holes sampled for bulk density, XRD and some infrared analyses. Drill holes selected in transects depended primarily on the condition of the plastic sample bags at the sample farms. Three-dimensional models of Ni/Co (and other element) distributions in relation to regolith mineralogy were visualized from combining IR analyses and geochemical data, provided by Anaconda, using the Mining Visualization System (MVS).

1.10 Other research projects

Collaborative research programs were established to help address the final objective of the research project; establishing a chronology of weathering events and dating of the Ni-laterite deposits. This was undertaken by two methods:

1. Paleomagnetic dating.

2. Stable oxygen isotope dating of clay minerals (*e.g.*, kaolinite).

1.10.1 Palaeomagnetic dating

Dating of suitable material collected during field trips to the MM2 and MM7 trial was conducted by Dr. Brad Pillans (Australian National University). A report of the research undertaken and results obtained is presented in Appendix 1.

1.10.2 Stable O-isotope dating

Stable oxygen-isotope dating of suitable, kaolinite-rich material collected during a number of field trips to the trial pits at MM2 and MM7, and from RC drill pulps was conducted by Dr. Yves Noack and Dr. Alain Decarreau both of the Centre European de Recherches et d'Enseignement des Geosciences de l'Environment (CEREGE), France. Research undertaken by Drs Noack and Deacarreau also included detailed crystal-chemical investigations of smectite-rich, core samples using x-ray diffraction (XRD), Fourier transform infrared (FTIR) analysis and scanning electron microscopy (SEM). A report of the research undertaken and results obtained is presented in Appendix 2.

Kaolinite-rich samples, selected from RC bulk samples, were prepared for isotopic dating in the CSIRO laboratories at Floreat Park.

The results of both collaborative studies have been integrated within the final discussion of the report, particularly in relation to the evolution of the Murrin Murrin deposits.

1.11 Methodology

1.11.1 Infrared analysis

Accurate logging of regolith mineralogy in the MM2 and MM3 study areas was achieved using the Portable Infrared Mineral Analyzer (PIMA-II), N$^{o.}$ 37 instrument. Infrared analysis of RC pulp samples using PIMA was selected as the primary means of mineralogical characterization as analysis is rapid (approximately 45 seconds per measurement), semi-quantitative and required minimum sample preparation unlike more traditional methods of analysis such as x-ray diffraction (XRD) and thermal analysis, which are more costly and time consuming.

Reflected infrared measurements were determined between the 1300 and 2500 nm wavelength region relative to an internal, sputtered gold standard. Contact measurements were made with the sample placed in a small petri dish against a 10 mm diameter viewer port. The instrument was calibrated prior to spectra capture and spectra were obtained using an Enhance (*i.e.,* sensitivity) value of 1. Each one-metre interval composite sample for RC holes drilled to a 50 x 50 m grid within MM2 and MM3 was analyzed. In order to keep the number of samples analyzed to a manageable level, it was not possible for every drill hole within the selected study areas to be analyzed. A list of the drill holes selected for MM2 and MM3 is provided in Appendix 3.

Logging of infrared spectra was achieved using the Windows based software program, The Spectral Geologist (TSG), version 2.0. The raw spectra were processed using the Hull Quotient technique which was used to enhance small variations within the spectra. An example of a mineralogical logging profile is presented in Figure 1.5. Classification of the main regolith units was made primarily on the dominant mineral (*i.e.,* silicate) phase identified. Kaolinite was identified from Al-OH absorption peaks at 1390 and 1410 nm, and 2208 nm. A Mg-OH absorption peak between 2290 and 2300 nm indicated the presence of Nontronite. A shift in the Mg-OH absorption peak to between 2300 and 2317 nm indicated the presence of saponite.

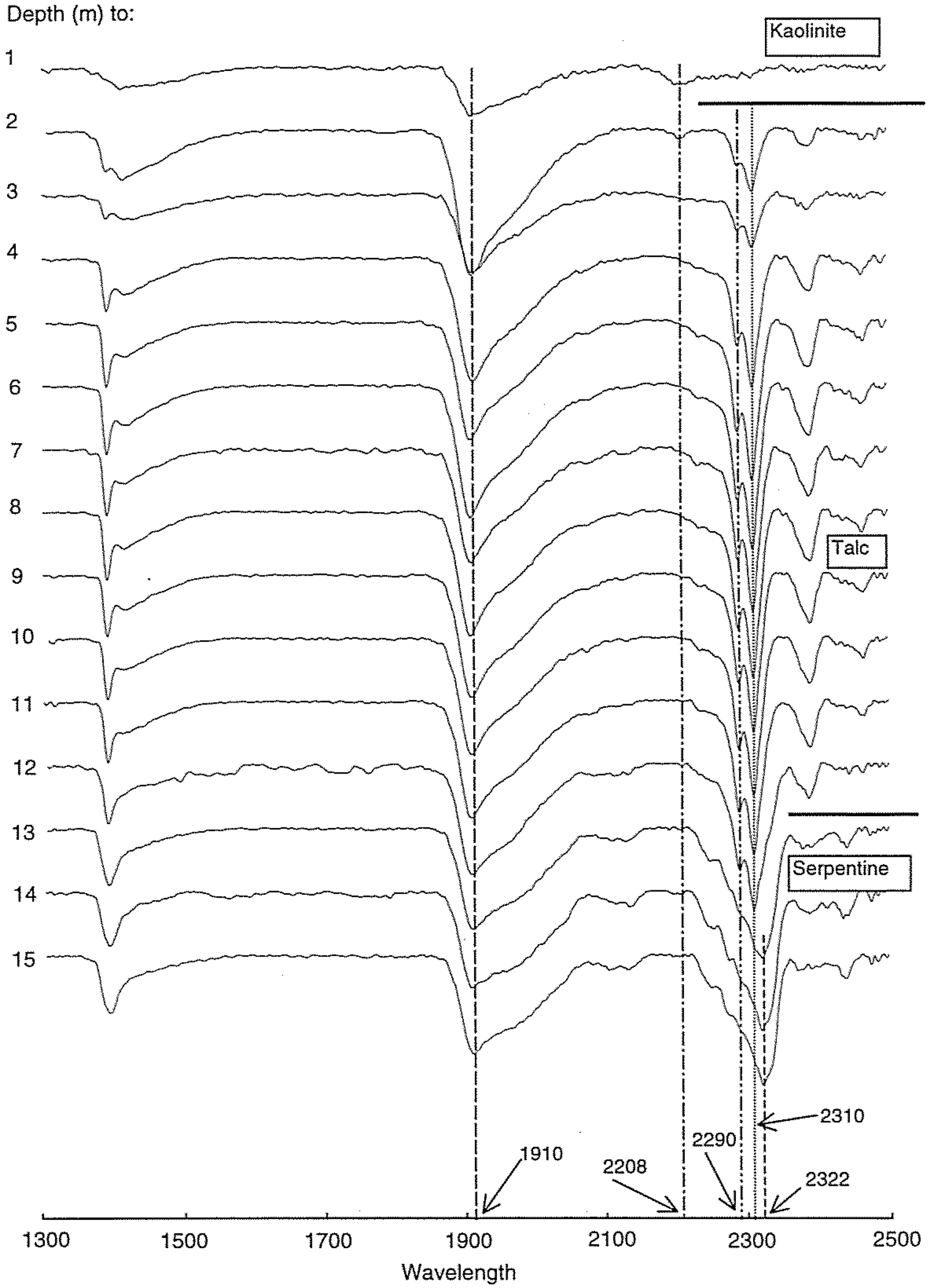

Figure 1.5. Infrared logging profile for RC hole ARC0601, MM3 (9099 mE, 71700 mN, 421 RL) showing some of the absorption features discriminated by PIMA. Spectra are presented as the Hull Quotient of the raw spectra, which flattens the background and enhances variations in the spectra. The absorption feature at 2208 nm is the Al-OH band for kaolinite. Talc is indicated by Mg-OH bands at 2290 and 2310 nm, whereas serpentine is indicated by an absorption band at 2322 nm. The feature at 1910 nm is adsorped water. Features near 1400 nm, for this drill hole, are related to talc or serpentine. The main regolith units have been marked according to the main Al-Mg-silicate identified in the spectra.

Serpentine was identified by the Mg-OH absorption peak occurring between 2317 and 2323 nm. These somewhat arbitrary criteria for mineral identification were necessary and take into account the variable hydration and base exchangeable cation saturation state of, in particular, smectitic clays.

Opaline-Si was also detected by the presence of a broad absorption feature between 2210 and 2270 nm. Large amounts of opaline-Si acted as a diluent strongly reducing the infrared signal of other silicate phases, in particular smectitic clays.

A comparison of PIMA spectra for RC drill pulps and bulk, grab-bag samples for the same drill hole showed no significant difference in the positions of Al-OH/Mg-OH absorption bands, for the purposes of this study, as a result of the methods used (*i.e.,* drying at 110° C and pulverizing) by Analabs and UltraTrace to prepare the pulps.

1.11.2 3-D Modelling (MVS)

Interpreted regolith mineralogy profiles for MM2 and MM3 were imported into MVS through the KRIG_3D_GEOLOGY module as separate Excel .geo files. Multi-element geochemical data, as obtained from Anaconda Nickel NL, were prepared and tabulated as Excel .csv files. Minimum element concentrations were set to half the detection limit of each element as indicated in Tables 3.4.8 and 3.4.9 for assays performed by Analabs and UltraTrace, respectively (Murrin Murrin Feasibility study, Volume 2, p 3-26) to remove any zero assay values. Kriging of geochemistry with mineralogy for both MM2 and MM3 was facilitated through the MVS KRIG_3D module based on a 15 m grid mesh (*i.e.* approximately 1/3 of the spacing of RC drill holes). Block models for MM2 and MM3 were generated with XYZ (*i.e.,* eastings, northings, RL) resolutions of 48 x 68 x 74 m and 39 x 61 x 72 m, respectively. Regions of low confidence were removed using the MVS SELECT_CELLS and ISOVOLUME modules using arbitrarily determined confidence limits. For example, in the case of Ni for MM2 and MM3, only concentrations with a confidence of greater than 99.9999% are presented. Confidence limits for each element within the 3-D models generated for MM2 and MM3 are presented in Table 1.1.

1.11.3 Limitations to MVS modelling

The geochemical data set provided by Anaconda Nickel NL for MM2 and MM3 was incomplete. Abundances of elements other than Ni and Co were determined only where either Ni or Co grades were greater than 0.7 and 0.05%, respectively (Murrin Murrin Feasibility study, Volume 2, page 3-25). Consequently, up to 20 to 30% of samples in the MM2 and MM3 study areas do not have a complete geochemical data set. Samples for which no data were recorded were removed prior to kriging being initiated. This partly accounts for the low confidence limits indicated for most of the elements (Table 1.1). In the case of Co, however, even though an assay was recorded for all samples within the study areas, the low C.L. is a reflection of the marked heterogeneous or localized distribution of Co within the regolith. Nickel is much more evenly distributed throughout the profiles, which accounts for the very high C.L. obtained.

Table 1.1. Confidence limits (% C.L.) for kriged element concentrations for study areas MM2 and MM3.

MM2		MM3	
Element	%C.L.	Element	%C.L.
Ni	99.9999	Ni	99.9999
Co	8.5	Co	8.5
Mg	31.0	Mg	21.0
Fe	9.0	Fe	7.0
Al	9.0	Al	7.0
Ca	9.0	Ca	7.0
Mn	7.5	Mn	6.3
Cr	(unfiltered)	Cr	73.0
Zn	7.5	Zn	5.8
Cu	(unfiltered)	Cu	(unfiltered)
As	(unfiltered)	As	5.8

1.11.4 Geochemistry

Samples pulps from selected intervals from RC drill holes (analyzed by PIMA) for geochemical analysis by x-ray fluorescence (XRF) were prepared by SGS Australia Pty. Ltd., by fusion of approximately 6.6 g of lithium metaborate 12:22 flux with 1.0 g of pulverized sample at 1100° C for 12 minutes in platinum crucibles. Major and trace elements were determined for a total of 495 samples using a Philips PW1220C XRF in the CSIRO analytical laboratories at Floreat Park. Elements determined and detection limits are presented in Table 1.2. A list of the RC drill holes analyzed and element abundances is provided in Appendix 4.

Loss on drying was determined gravimetrically using 1 g samples after drying in a muffle furnace at 105° C for one hour. Loss on ignition was determined on the sample after heating to 1050° C.

1.11.5 X-ray diffraction

X-ray diffraction (XRD) analysis was performed on a selected number of pulps from RC drill holes (analyzed by PIMA) to provide a check on the mineralogical logging using PIMA and as a means verifying CIPW-norm calculations performed using the XRF data. Random powder diffraction patterns were obtained using a Philips PW1050 goniometer with CuKα radiation and a graphite beam monochromator. Diffraction patterns were obtained by scanning from 2 to 65° 2θ in 0.01° 2θ increments scanning at 1.0° 2θ/min.

Table 1.2. Elements and detection limits for multi-element suite determined by XRF analysis.

Element (Majors)	Detection Limit (%)#	Element (Trace)	Detection Limit (ppm)
Si	0.01	Ba	20
Al	0.01	Ce	15
Fe	0.005	Cl	20
Mn	0.002	Cr	10
Mg	0.01	Co	10
Ca	0.001	Cu	10
Na	0.01	Ga	3
K	0.001	La	10
Ti	0.003	Ni	10
P	0.002	Nb	4
		Pb	5
		Rb	5
		S	10
		Sr	5
		V	5
		Y	5
		Zn	5
		Zr	5

Detection limits for major elements are for their respective oxides (*e.g.*, D.L for Si as SiO_2 equals 0.01%).

1.11.6 Mass balance

Determinations of the relative accumulation or depletion of elements within the regolith at MM2 and MM3 were calculated, assuming the immobility of Zr in the laterite profile by the equation (Porto and Hale, 1995):

$$E = [C_w.C_{pi}/C_p.C_{wi}] - 1$$

Where:

E = Enrichment factor. A negative value for E indicates depletion, whereas positive values indicate accumulation of the element in question.

C_w = Element concentration in the weathered material.

C_{pi} = Immobile element concentration (*i.e.*, Zr) in the weathered material.

C_p = Element concentration in bedrock.

C_{pi} = Immobile element concentration (*i.e.*, Zr) in bedrock.

Assays for Zr and other elements were obtained from the XRF analyses of 495 samples of selected RC drill pulps (Section 1.11.4). The geochemical data supplied by Anaconda Nickel NL was not used because of the absence of several important elements (*e.g.*, Zr) required to perform the mass balance calculations.

1.11.7 Stable O-isotope analysis of kaolinite; preparation.

Initial XRD analysis identified the presence of kaolin in pulps of four RC drill holes selected for preliminary PIMA spectroscopy. The presence of kaolin was confirmed by XRD analysis of K-saturated and K-saturated, oriented clay plates heated to 550° C for 2 hours. Identification of kaolinite from halloysite was obtained using the formamide intercalation method of Churchman *et al.*, (1984). Subsequent analysis by PIMA confirmed the presence of kaolinite from Al-OH absorptions at 1396, 1412 and 2208 nm in drill holes CBRC 0724, CBRC 0796, ARC 0786 and ARC 1008. Drill holes CBRC 0724 and CBRC 0796 were selected for isotope analysis, which contained kaolinite to depths of 16 and 11 m, respectively.

Samples for isotope analysis were taken from drill hole splits collected in the field. A representative sub-sample was riffle-split and gently crushed to obtain the <2 mm fraction. Kaolinite was concentrated by removal of iron oxide and smectite clay contaminants. Iron oxides, mainly as goethite, hematite and minor amounts of maghemite were removed by treatment with citrate-bicarbonate-dithionite (CBD) according to the method of Jackson *et al.*, (1986), incorporating modifications to the method as outlined by Stace (1956). Removal of iron oxides was indicated by samples obtaining a pale blue-grey-green colour. Treatment with CBD is not considered to have a significant effect on the stable-isotope composition of clay minerals (Yeh, 1980; McMurty *et al.*, 1983; Bird and Chivas, 1989).

Smectite clays were removed by the method of Gibbs (1967). Smectite clays were converted to Na-saturated forms and removed by centrifuging samples solvated in a 15% ethanol solution. Na-saturated smectite has a lower specific gravity than kaolinite (and illite) in ethanol and can, therefore, be removed by centrifugation (Gibbs, 1967).

The purity of the resulting residues was tested by XRD which indicated that the samples consisted of >95% kaolinite. Trace amounts of smectite were detected in the kaolinite-rich concentrates but this was considered not significant. Isotope analysis was conducted in the CEREGE analytical laboratories, France according to the methods outlined by Clayton and Mayeda (1963) and Girard *et al.*, (1997).

1.11.8 Cluster analysis

Cluster analysis of the geochemical data provided by Anaconda Nickel NL for drill holes within the MM2 and MM3 study areas was performed using STATISTICA™ (Volume III) for Windows. Zero assay values were removed from the data set before analysis. In order to reduce the effect of the magnitude of element concentration (*i.e.*, % versus ppm) the data was standardized using the Data Management Module within STATISTICA™ by the equation:

$$x_{SD} = (x - x_{AV})/\sigma$$

Where:

x_{SD} = Standardized assay value for the element.

x = The concentration of the element, either as % or ppm.

x_{AV} = The average element abundance (% or ppm).

σ = Standard deviation.

1.11.9 Normative mineral analyses

Determination of CIPW-Norm mineral abundances were calculated from XRF analyses of samples from selected intervals for RC drill holes (see Section 1.11.4). Normative abundances of up to 19 phases were calculated from concentrations of Si, Al, Fe, Mn, Mg, Ca, Na, K, Ti, P, S, Co, Cr and Ni according to the guidelines in Ragland (1989), with elements allocated to phases identified from XRD and PIMA logging of RC pulps. A detailed discussion of the criteria used and assumptions made in order to complete the calculations is given in Chapter 3.

1.12 Limitations of the study

Infrared analysis using PIMA is not sensitive to very dark (*i.e.*, black) minerals such as Mn oxides. This is not a significant problem as Mn oxides generally occur as small, localized bodies and do not comprise a significant unit within the regolith. The presence of very bright (*i.e.*, white) minerals such as carbonates may cause problems due to their very high albedo and oversaturate the detector. This may be a problem, particularly towards the base of profiles in regard to mis-identification of the carbonate mineralogy and where high amounts of carbonate (*i.e.,* magnesite and dolomite) may dilute the signal of associated silicate phases. In addition, the characteristic absorption bands of common Fe oxides, such as goethite, hematite and maghemite, occur within the short-wave infrared region (*e.g.,* 400 to 1000 nm), outside the wavelength range covered by PIMA. This is not a significant problem for smectite hosted Ni-deposits with a mineralogy dominated by Al-Mg-clay silicates (*e.g.,* serpentine, chlorite, talc, smectite and kaolinite) which all show characteristic Al-OH, Mg-OH absorptions within the wavelength range 1300 to 2500 nm.

As a result of the initial assaying procedures (Murrin Murrin Feasibility Study, Volume 2) adopted by Anaconda Nickel NL, abundances of elements other than Ni or Co were incomplete. This is a major limitation to the 3-D modelling performed using MVS and may have caused artefacts during kriging and it is not known whether areas of low confidence in the data are a result of missing data or not.

Due to budget and time constraints only a select number of samples could be analyzed by XRF. This was to supplement the geochemical data supplied and to provide abundances for additional, important elements, such as Si, Zr, Ti, K and Na. In addition, no LOI (as total weight loss, SO_2 or CO_2) data were available for the geochemical data supplied by Anaconda Nickel NL. As a result of this, no CIPW-Norm calculations could be made using the Anaconda data.

It could be argued that the spacing of RC drill holes selected for MVS modelling (*i.e.,* 50 x 50 m) was too coarse considering that in some areas within the MM2 and MM3 study areas RC holes were drilled to a grid of 6.25 m. The 50 x 50 m spacing was selected to, firstly, provide a consistent density of drilling over the areas of interest, and secondly, to keep the number of samples analyzed by PIMA to a realistic and manageable level.

Despite these limitations the results of the project do provide valuable information regarding the evolution of the Murrin Murrin Ni-deposits and the factors influencing Ni-Co mineralization within these deposits.

2.0 MURRIN MURRIN REGION REGOLITH-LANDFORM MAP

2.1 Introduction

A map of the regolith-landform (RL) relationships at 1:50 000 of the tenement areas surrounding and including Murrin Murrin has been produced. The RL map (Map 1) covers an area of some 660 km^2 and is located on the Minerie 1:100 000 sheet (Sheet 3240) within the Laverton 1:250 000 sheet (SH/51-2).

This discussion is a reproduction of the RL map report, previously submitted to Anaconda Nickel NL (Wells, 1999). The RL map is also available as a hard copy and in digital, GIS format on CD as a Map Info project.

2.2 Regolith mapping and terminology

Regolith-landform mapping attempts to define areas of similar regolith and landform characteristics that can be represented at the scale of mapping. The term regolith includes all weathered and eroded material the covers the underlying bedrock. Other definitions of regolith are given in Pain *et al.*, (1991). Specific regolith materials (*e.g.*, duricrust, alluvium) can be related to particular landforms (*e.g.*, breakaways, depositional plains) and it is these associations that are identified and recognized to define a regolith-landform mapping unit (RLU) (Anand *et al.*, 1993). Due to the compositional and spatial variability of most regolith materials, the purity or homogeneity of the RLU being defined is very much dependent on the scale of mapping. The larger the scale (*i.e.*, the more detailed the observation) the greater the variability that can be represented.

The boundary that delineates each RLU is referred to as a polygon. The position of the polygon boundary on a regolith-landform map defines the greatest rate of change in characteristics between adjacent RLU's (Anand *et al.*, 1993).

2.3 Methodology

A number of data types were used to compile the RL map, the principle data type among these being interpretation from aerial photographs supplemented with field mapping and observations.

Other data types were used as an adjunct to aerial photographic interpretation and included remotely sensed reflected and emitted data (*e.g.*, radiometric and Landsat Thematic Mapper data).

2.3.1 Aerial photographs

Colour, and black and white (B/W) 1:50 000 aerial photographs were purchased from the Department of Land Administration (DOLA). The colour photographs, flown by TS and Environs in January 1998, covered only the central and western region of the mapped area. The B/W photographs, flown in May 1996, were purchased to extend coverage to the eastern margin of the surveyed area. Flight lines for each of the series of colour and B/W photographs are shown in Figure 2.1.

Regolith-landform units were identified and interpreted using stereoscopic photographic pairs and mapped using a x3 magnification binocular eyepiece to give an effective scale of observation of approximately 1:17 000. Regolith-landform units were interpreted from tonal and textural variations in the aerial photographs with confirmation by field mapping. Unit boundaries were then modified and take into account additional information obtained from radiometric and Landsat TM imaged data. RLU classification followed that recommended by Pain *et al.*, (1991).

2.3.2 Magnetic and radiometric data

Fully rectified, airborne geophysical and radiometric images were supplied by Anaconda Nickel NL, covering the Minerie 1:100 000 sheet (3240). About 90% of total gamma-ray radiation emanates from within the top 30-45 cm of surficial cover or exposed bedrock (Gunn *et al.*, 1997; Wilford *et al.*, 1997). Radiometric imaging can thus provide some information regarding the affects of near surface weathering and pedogenesis.

2.3.3 Digital elevation model

A digital elevation model (DEM) of the Minerie 1:100 000 sheet was also obtained from Anaconda Nickel NL. The DEM has a pixel xy resolution of 50 m on the ground and a vertical z resolution of 5 m. The DEM was used to generate three-dimensional perspective images of the Landsat TM and radiometric images, which greatly enhanced interpretation of the regolith distribution within the landscape.

2.3.4 Landsat thematic data

Landsat LS5 satellite thematic (TM) band data (*e.g.*, bands 1 to 7), covering a 26 x 26 km area of the Minerie 1:100 000 sheet was purchased from the Australian Centre for Remote Sensing (ACRES) through World Geoscience Corporation. The Landsat TM image sampled was taken in January 1997 to ensure that there was little vegetative cover, thus minimizing any interference to reflected band data from surface vegetation.

Table 2.1. Expected response of surface mineralogy and vegetation for interband ratios 5/7, 4/7 and 4/2 (from Tapley and Gozzard, 1992).

Ratio 5/7		Ratio 4/7			Ratio 4/2	
High	Clay-rich	High	Low Fe	High clay	High	High Fe
Low	Clay-poor	Med-High	Low Fe	Med. clay	Low	Low Fe
		Medium	Low Fe	Low clay		
		Medium	Med. Fe	Med. clay		
		Low-Med.	High Fe	High clay		
		Low	High Fe	Low clay		

Green vegetation has a medium response in all ratios

Previous studies using remotely sensed data imaged for deeply weathered terrains in Australia have demonstrated the usefulness of applying interband TM ratios to interpreting surface geological information (Fraser *et al.*, 1986; Cudahy, 1989). Ratios of bands 2, 4, 5 and 7 as 5/7, 4/7 and 4/2 presented as a false colour red, green and blue image have been used to map the surface distribution of iron and clay-rich materials in weathered felsic and mafic terrains of the north eastern Yilgarn (Drury and Hunt, 1988; 1989; Tapley and Gozzard, 1992). One main advantage of using interband ratios is in reducing the influence of topography to the spectral reflectance characteristics of the area being imaged. Similar materials will show the same spectral response regardless of differences in brightness in the original image caused by variations in topography (such as aspect and slope) (Tapley and Gozzard, 1992). Table 2.1 shows the type of response expected for each band ratio. Table 2.2 shows the expected colour response for different surface materials and vegetation.

Band data were initially corrected for any atmospheric interference and processed to produce an unrectified, false colour red, green, blue image using band ratios 5/7, 4/7 and 4/2, respectively. Referencing to a 1:50 000 base drainage map was used to rectify the resulting image. This was performed using the Digital Image Resampling, Rectification and Registering software program, RIFT, within ArcView, version 3.0. Ground control reference points (GCP) were located within the TM image to be rectified and the base map. A nearest neighbour, 3rd order polynomial function was applied to warp the TM image when a sufficient number of ground control pairs were located (about 50 pairs were used). A check of the root mean square error (RMS) associated with each GCP pair identified the least reliable points, which were removed before final rectification of the TM image. A final RMS of approximately 30 m was obtained (*i.e.*, equivalent to one pixel resolution of the TM image). A map-image (Map 2) of the TM scene with interband ratios 5/7, 4/7 and 4/2 as false colour red, green and blue, for the Minerie sheet is available on CD, to be printed as a hard copy if desired, within the Map Info project.

Table 2.2. Expected colour (*i.e.*, hue) of surface mineralogy and vegetation for the composite image and for individual interband ratios (from Tapley and Gozzard, 1992).

Image	5/7	4/7	4/2	Mineralogy	
(RGB)	(Red)	(Green)	(Blue)	Fe-O	Clay
Black	L	L	L	L	L
White	M-H	M-H	M-H	Green biomass	
Red	H	L	L	M-H	H
Orange	H	M	L	M	H-M
Yellow	M-H	M	L	L	M-H
Green	L	H	L	L	M
Green (dark)	L	L-M	L	L-M	L-M
Green (Olive)	L-M	L-M	L	M	L
Blue	L	L	H	H	L
Purple (dark)	L-M	L	L-M	L-M	L
Purple (light)	L-M	L	M	M	L-M
Magenta	M	L	M	M	M
Cyan	L	M	M	L-M	M
Brown	L-M	L-M	L-M	L-M	L-M

L = Low; M = Medium; H = High

2.4 Remote sensing of regolith-landform units

The following discussion relates the types and distribution of surficial weathered materials as revealed by remotely sensed aeromagnetic, Landsat TM and radiometric imaging to regolith-landform units within the surveyed area.

Greenstone belts within the Murrin-Murrin area are easily identifiable in the aeromagnetic data as elongated, high amplitude (*i.e.*, red hues) anomalies (Fig. 2.2). These result from serpentinized ultramafics and ferruginous duricrust, which may cap the weathered greenstones. Greenstone belts outcrop as sub-parallel, elongated ridges and minor, Relict breakaways and generally comprise the few high points in the mapped area. Felsic rocks (*e.g.*, granite, adamellite, and granodiorite) occur as subdued, low contrast blues and blue-green (cyan) colours in the aeromagnetic data. These tend to show a subdued relief or form elevated, relict plateaux bounded by significant breakaways developed to the north of the surveyed area (*e.g.*, at Minerie Hill).

Ultramafic rocks are also easily identified in remotely sensed radiometric and TM images. As mafic and ultramafic rocks are typically depleted in K, Th and U (Gunn *et al.*, 1997) these show as dark blue to black hues in the ternary gamma-ray response image (Fig. 2.3 A). Landsat TM imaging also shows greenstone belts as dark blue to purple colours (Fig. 2.4 A). Scree and colluvial material derived directly from exposed mafic and ultramafic saprolite, on lower erosional slopes, also shows as dark blue-purple to lilac colours (Fig. 2.4 A). These correlate to the erosional low hills (RL map unit, *Wel12*) and rise units (RL map unit, *SSer11*) as mapped on the regolith-landform map with a surrounding apron of scree material (RL map unit, *CMel/er9*).

Ferruginous duricrust that caps weathered ultramafic profiles with a mineralogy dominated by goethite and hematite and only minor clays (*i.e.*, kaolinite) present in the TM image as magenta to pale red hues (Fig. 2.4 B). Lag derived from these ferruginous duricrusts will also appear as magenta to red in the TM image. Duricrust associated with minor breakaways also show as magenta-pale red hues. However, lag and soils developed on the backslopes, due to the increased quartz and clay content (*i.e.*, kaolinite and gibbsite), appear as dark green hues. Thicker vegetative cover on breakaway backslopes may also be a component of the green colour in these areas. Both duricrust types are commonly associated with an apron of clay rich, Fe-poor material that appears as a rim of pale yellow hues (Fig. 2.4 C) which confuses with felsic saprolitic material (Fig. 2.4 D).

Deep weathering of granite to granodiorite rocks (Gower, 1976) to the north of the mapped area, encompassing the area known as the East Terrace, has also resulted in a total radiometric depletion

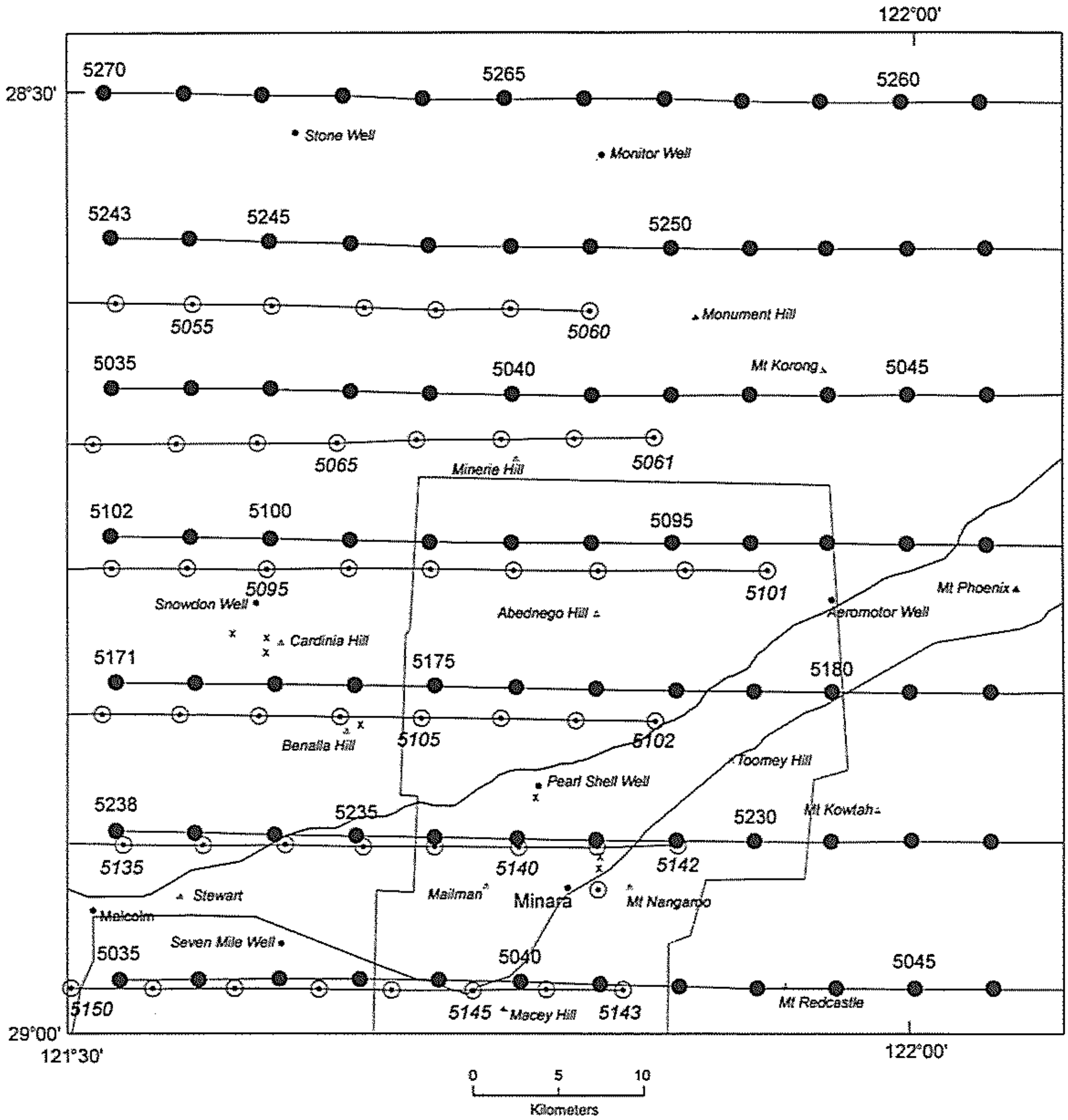

Figure 2.1. Flight line diagram for the surveyed area. Open circles (photo numbers in Italics) represent colour aerial photographs, whereas solid circles represent black and white aerial photographs. Colour aerial photographs were used for the bulk of the interpretation. Some B/W photographs were used for interpreting the eastern margin of the mapped area.

giving the dark blue-black hues (Fig. 2.3 B) which can be confused with greenstone outcrops. The deeply weathered plateau surface developed from more radiometrically active granite/adamellite, which encompasses Minerie Hill, also shows dark blue to black hues due to the leaching of K-bearing phases, such as K-feldspar (orthoclase, $KAlSi_3O_8$) and K-mica (muscovite,

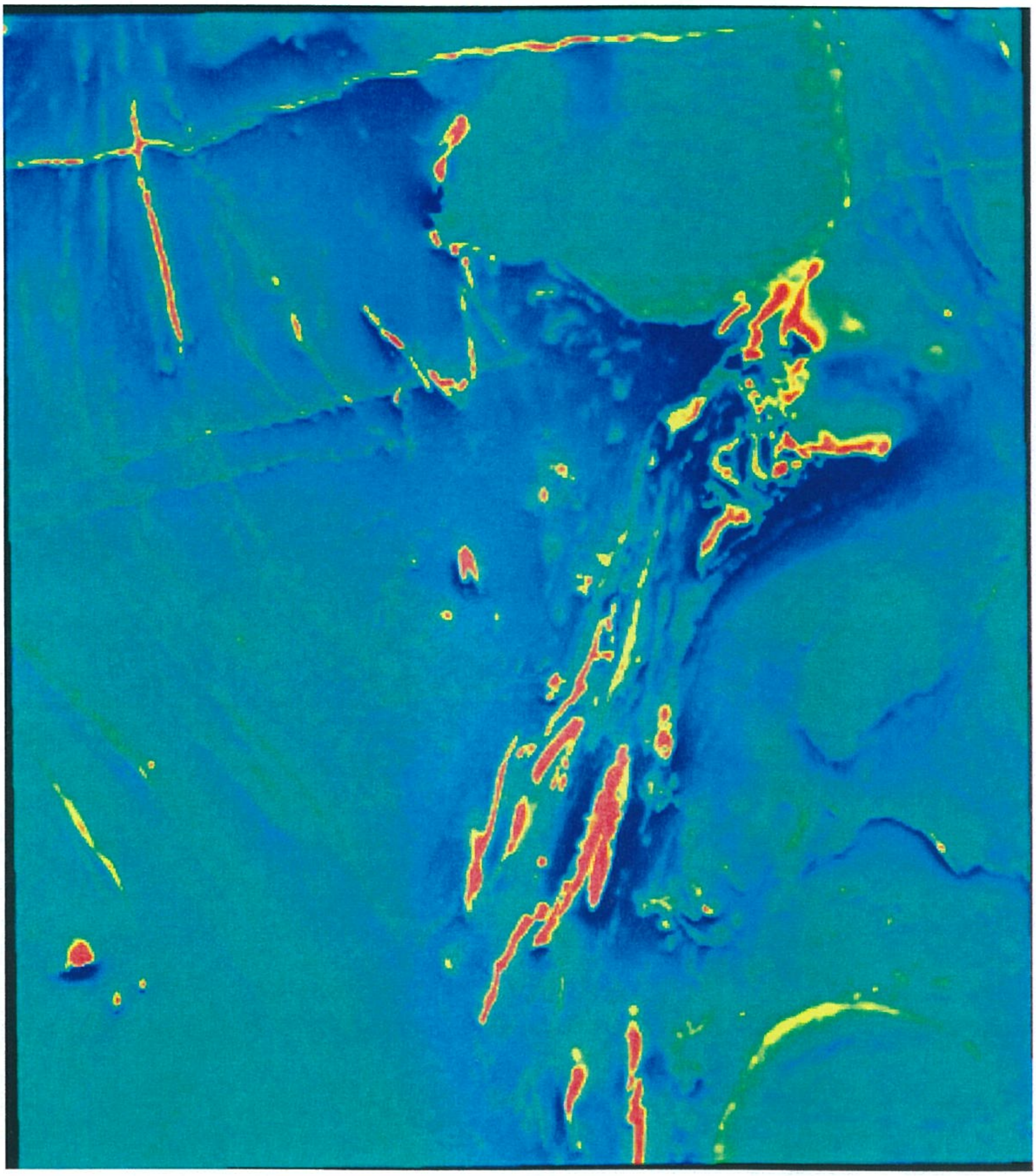

Figure 2.2. Aeromagnetic image for the Minerie 1:100 000 map sheet. Greenstone belts are easily distinguished, appearing as high contrast, red anomalies. Granitoid rocks appear as more subdued, low contrast blue and cyan colours.

$K_2Al_4(Si_6Al_2O_{20})(OH,F)_4$), and the removal Th and U-bearing minerals, such as zircon and monazite ($(Ce,La,Th)PO_4$), from the upper part of the weathering profile (Fig. 2.3 C).

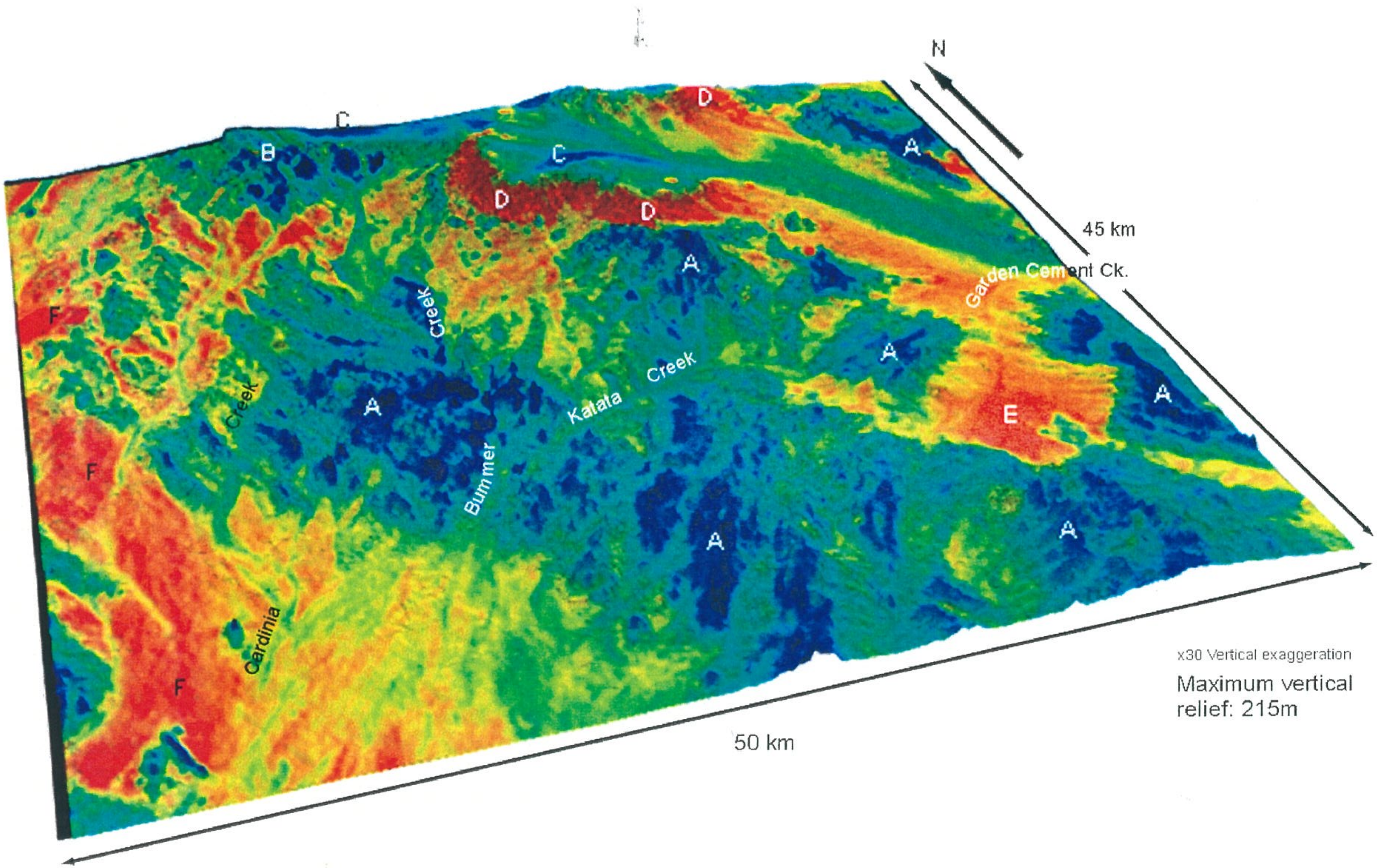

Figure 2.3. Three dimensional perspective view of the total gamma-ray response for the Minerie sheet draped over the Minerie DEM. A number of regolith materials can be distinguished and related to various landforms. A (dark blue to black): Mafic and ultramafic rocks (*i.e.,* greenstones); B (dark blue): Kaolinized granitoids (granite/adamellite); C (blue): Weathered upper surface of plateau, D (bright red): Exposed granite/granodiorite saprolite. E (red-orange): Weathered sediments of a likely, mixed Fe-oxide/carbonate dominated mineralogy. F (orange): Weathered sediments of a mixed origin consisting of clays, of a felsic origin, and Fe-oxides with near surface carbonate.

Dark red colours in the total radiometric image at the base of the breakaway relate to outcrops of granite/adamellite saprolite or saprock (Fig. 2.3 D) that have not undergone significant weathering. Granitic saprolite is also indicated by bright yellow hues in the TM image indicating high amounts of feldspathic derived clays (*e.g.*, kaolinite) (Fig. 2.4 D).

Examination of the radiometric images for K and U (Figures 2.5 and 2.6, respectively) reveals areas that indicate more recent sediment movement within the landscape. Bright red hues in the K and U gamma-ray image indicate outcrops of granite, at the base of the breakaway, containing K-bearing phases (*e.g.*, feldspar and mica) (Fig. 2.5 A) and U-bearing minerals such as zircon (Fig. 2.6 A). The gamma-ray response for K shows very well the movement of felsic derived material onto lower erosional slopes below the breakaway, shown as yellow-orange hues (Fig. 2.5 B), that feed into the catchment of Bummer Creek and, to a lesser extent, Maleta Creek. The K response decreases due to the combined effects of the leaching of K-bearing phases as material is transported as channel sediments and due to the introduction of more Fe-rich material from mafic and ultramafic sources. In addition, most K-bearing phases are shown to concentrate in the coarser sized sand and silt fractions (Wilford *et al.,* 1997) so that increasing distance from the source would decrease the contribution of these coarser, K-bearing sediments to the gamma-ray signal. This is shown in the TM image as pale green hues (Fig 2.4 E) due to the mixing of feldspathic clays (*i.e.,* kaolinite-rich) and Fe-rich material derived from ultramafic rocks adjacent to Maleta Creek, for example. Final deposition occurs in the lower reaches of Bummer Creek, shown in cyan hues (Fig. 2.5 C), which forms a broad, deltaic, alluvial plain. Retention of K in this area may be associated with the formation of secondary K-bearing phases such as illite ($K_2Al_4(Si_6Al_2)O_{20}(OH)_4$).

To the north-east of Minerie Hill an additional granite/adamellite outcrop (Fig. 2.5 F) encompassing Monument Hill, outlines a catchment area with K-bearing felsic material, as orange-yellow hues mixing with Fe-rich material (Fig. 2.5 D) feeding into the alluvial plain that drains to the east into Garden Cement Creek. This is also shown in the TM image as cyan and pale blue hues (Fig. 2.4 F), which results from the mixing of feldspathic (*i.e.,* kaolinitic) clays and Fe-rich materials.

Several smaller felsic (*i.e.,* granite/granodiorite) outcrops are also indicated in the south east of the mapped area, shown as isolated red 'patches' in the K gamma-ray image (Fig. 2.5 F), although these are not revealed in the TM image. Movement of felsic derived sediments are also clearly shown being restricted to localized, recent channel deposits.

White hues in the TM image (Fig. 2.4 H) indicate areas of vegetative cover restricted to the main drainage lines (*e.g.*, Bummer, Kilkenny, Garden Cement and Katata creeks) and to alluvial plain areas (*e.g.*, the deltaic fan of Bummer Creek). Pale blue colours of recent channel sediments (*e.g.*, Kilkenny and Garden Cement creeks) are consistent with a mineralogy dominated by quartz and Fe-oxides and with a low clay content (*i.e.*, kaolinite).

Bright orange-red hues in the ternary gamma-ray image in the area west of Mt Kowtah (Fig 2.3 E) result from a low to medium Th response (cyan hues, Fig. 2.7 A) and a high U gamma-ray response (orange-yellow hues, Fig. 2.6 B). This suggests that the surface materials consist of a mixed Fe-oxide/carbonate mineralogy. Surface concentrations of U and Th indicate the presence of resistate minerals such as xenotime, zircon and monazite. However, once released U tends to associate and be concentrated in calcrete deposits (Deutscher *et al.*, 1980) and Th associates mainly with Fe-oxide/oxyhydroxide phases (Short *et al.*, 1989; Dickson and Scott, 1990). Green to cyan hues in this area of the TM image are consistent with a surface mixed clay/Fe-oxide mineralogy (Fig. 2.4 G) consisting of a mixed lag of Fe-rich nodules, quartz and carbonate over a depositional, alluvial plain.

Red-orange and yellow hues for the total gamma-ray image (Fig. 2.3 F) along the western margin of the survey area, including Cardinia Creek and other drainage lines further to the west, reflect the felsic lithology of the source material. This most probably originates from granite/granodiorite outcrops to the north at East Terrace. The low K response for this area (Fig 2.5) reflects the deep weathering overprint of the felsic source rocks (*i.e.*, granite/granodiorite at the East Terrace). Uranium and Th have most probably been concentrated by Fe oxides (Th) and near surface carbonate (*i.e.*, calcrete) deposits (U). The main response in this area appears to originate from U associated with calcrete deposits. The more deeply weathered surface materials intermix with the western margin of the broad alluvial, depositional plains of Bummer Creek. This area was not covered in the Landsat TM image.

2.5 Regolith-landform units and relationships

A total of 17 units were identified within the mapped area (Map 1). These have been classified within the Relict, Erosional and Depositional (RED) landscape scheme (Anand *et al.*, 1993). Relict landform regimes are defined as those areas where lateritic residuum has been preserved. For example, duricrusts and breakaways which are expressions of an ancient, weathered landscape (Anand *et al.*, 1993). Erosional landform regimes are characterized with erosion as the main

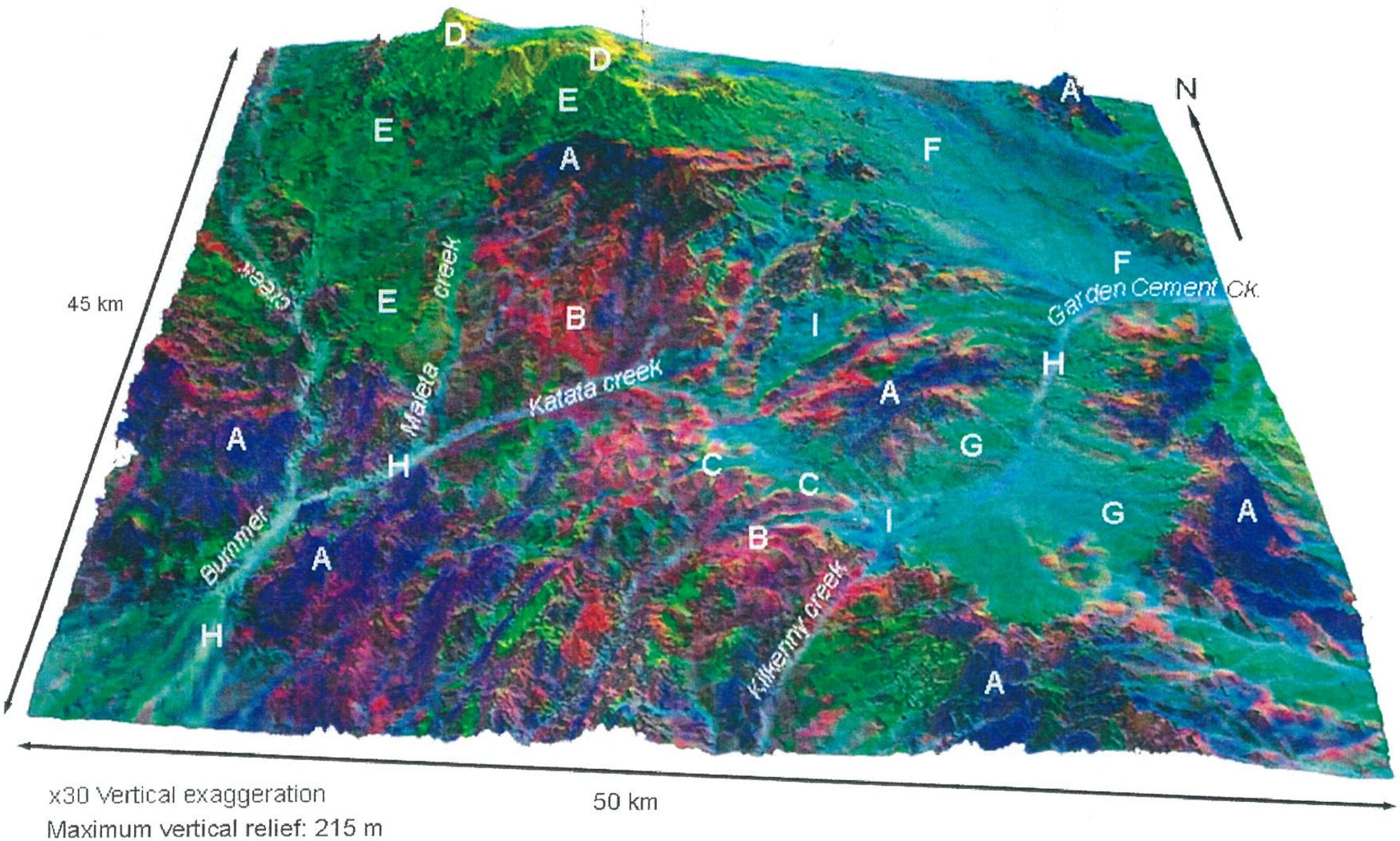

Figure 2.4. Landsat TM image of the area surveyed for the regolith-landform map presented in false colour R, G, B for interband ratios 5/7, 4/7 and 4/2, respectively, draped over the DEM of the Minerie sheet. A (dark blue to purple and lilac): Greenstone belts with associated scree and alluvial material derived from outcrops. B (magenta to red): Ferruginous duricrust with a mineralogy dominated by Fe oxides (mainly goethite and hematite) with a low clay content, developed mainly from ultramafic rocks. C (Light pink with yellow): Duricrust forming small breakaways with a more mixed mineralogy of Fe oxides and clays (*i.e.,* kaolinite and gibbsite). A 'rim' of pale yellow hues outlines both duricrust types indicating the presence of clay-rich materials (*i.e.,* kaolinite) from exposed mottled zones. D (bright yellow): Granitic saprolite at the base of the breakaway high in feldspathic clays. E (pale green): Kaolinite-rich clays derived from granitic saprolite, mixing with Fe-rich material derived from adjacent mafic/ultramafic rocks. F (cyan): Felsic derived clays (*i.e.,* kaolinite-rich) with high Fe-rich material. G (green to cyan): Mixed alluvial plain sediments of medium Fe-rich material, low in clay (*i.e.* kaolinite). H (white): Vegetation occurring along the main drainage lines. I (pale blue): Fe-rich clays/Fe-oxides mainly as channel sediment deposits.

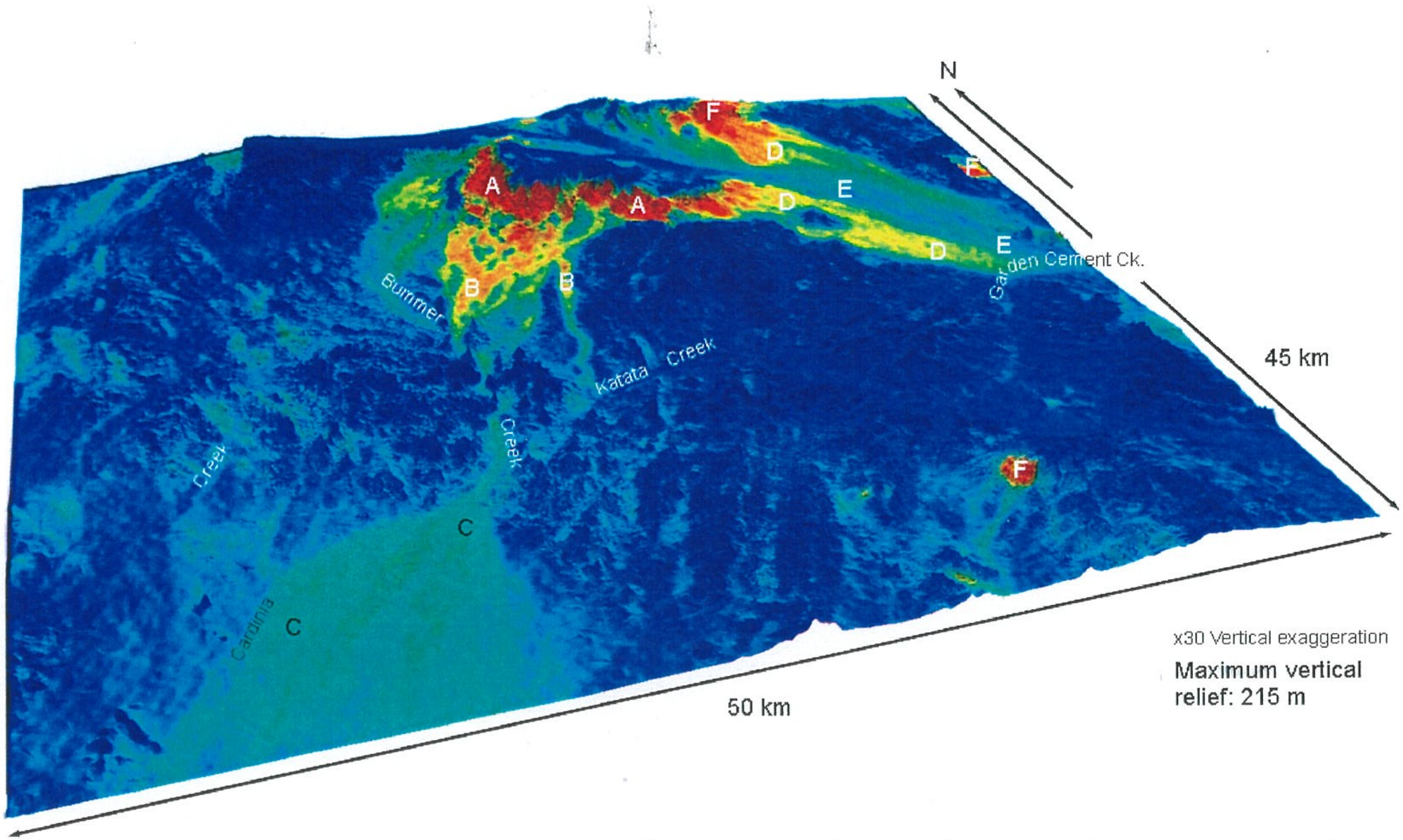

Figure 2.5. Three dimensional perspective view of the gamma-ray response for K draped over the DEM for the Minerie sheet. The γ–ray response for K can provide a good indication of the movement of more recently derived (*i.e.,* of felsic origin), poorly weathered materials within the landscape. Primary K-bearing minerals such as orthoclase are comparatively easily weathered and do not persist in weathering profiles. Secondary bearing K-phases such as illite are also comparatively short-lived. A (bright red): Granite/adamellite saprolite exposed at the base of the breakaway. Potassium bearing phases in the plateau surface of the breakaway have been leached producing the dark blue colours. B (orange-yellow): K-bearing sediments derived from granite saprolite washing onto lower erosional slopes below the breakaway. C (cyan): Depositional alluvial fan of K-depleted sediments. D (orange-yellow): K-bearing, felsic sediments outwashing onto the broad alluvial plain that feeds into the Garden Cement Creek. E (cyan to pale blue): Sediments depleted of K due to the leaching of primary K-bearing phases and due to the incorporation of Fe-rich materials. F (bright red): Other localized outcrops of fresh or saprolitic granitoid rock.

geomorphological process. Overlying material has been removed to a level that exposes the underlying weathered material and/or fresh bedrock. A thin, locally derived sediment cover may also be present in these regimes (Anand *et al.*, 1993). These sediments may overlie complete or partly eroded deep weathering profiles or fresh rock. Depositional regimes include those areas where the deposition and accumulation of eroded material (*i.e.*, sediment) is the dominant landform process and produces an overlying sediment cover that can be many tens of meters thick (Anand *et al.*, 1993).

A description of each regolith-landform unit is given in the legend accompanying the RL map. Regolith-landform units identified within the RED classification scheme can be broadly grouped as comprising mainly ferruginous duricrusts and gravel (*i.e.*, relict), saprock and saprolite (*i.e.*, erosional), and alluvial and colluvial material (*i.e.*, depositional). The following is a summary of the regolith-landform units identified in the surveyed area.

2.5.1 Relict regime

Four units were identified within the relict regime with RL map units *Wl1, RFel2, Rel3* and *SVee4* (Map 1, legend). Dark red-brown to black, well indurated, ferruginous duricrust occurs as a localized capping, up to 4-5 m thick but generally 2-3 m in thickness, of weathering profiles developed from mafic and ultramafic rocks (RL map units, *RFel2* and *Wl1*). These tend to form isolated mesas and buttes of low relief (about 30 m) but also may occur as minor breakaways. The upper slopes of isolated hills and slopes immediately below the breakaway escarpment line are covered by boulders of duricrust and nodules which fine to a thin veneer of polished black, Fe-rich gravel (< 10 mm) on the lower footslopes.

The mineralogy of duricrust that caps ultramafic rocks is dominated by Fe-oxides as hematite and goethite with maghemite, rutile, kaolinite and quartz as minor phases. For duricrusts forming minor breakaways, goethite and hematite are the main Fe oxides with kaolinite and gibbsite, and trace amounts of quartz and rutile. The mineralogy of scree and lag of Fe-rich gravel reflects the mineralogy of the duricrust from which they are derived.

There are elongated relict ridges of chert and BIF (RL map unit, *Rel3*). These consist of outcrops to 5-10 m wide of highly indurated, cryptocrystalline quartz with angular to blocky quartz gibber covering the immediately adjacent upper scree slopes. Less coarse, slightly more rounded, Fe-stained quartz cobbles cover the lower slopes. Thin mammilliary forms of hematite and goethite stain on exposed fracture surfaces. These ridges constitute only a minor relict landform element within the mapped area and are not well delineated in either the TM or radiometric images.

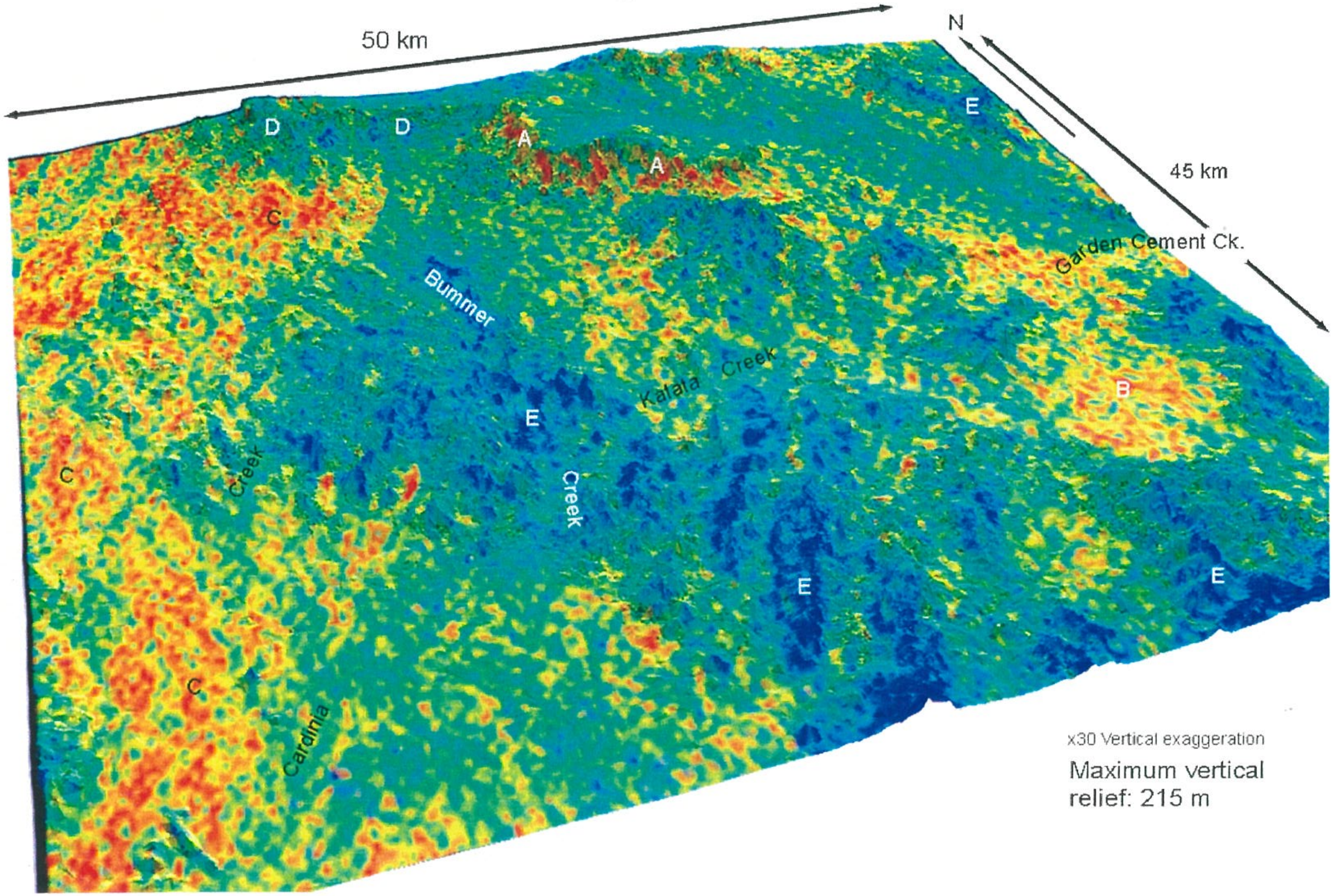

Figure 2.6. Three dimensional perspective view of the gamma-ray response for U draped over the DEM for the Minerie sheet. A (red-orange): Exposed granite/adamellite saprolite at the base of the breakaway. B (orange-yellow): Locally derived more deeply weathered alluvial sediments with U most likely concentrated by near surface carbonate (*i.e.*, calcrete) deposits. C (orange-yellow): Felsic derived, sediments with U associated with near surface carbonate deposits. D (cyan to blue): Deeply weathered granite/granodiorite. Uranium bearing phases such as zircon have been leached from the weathering profile. E (dark blue): Greenstone belts.

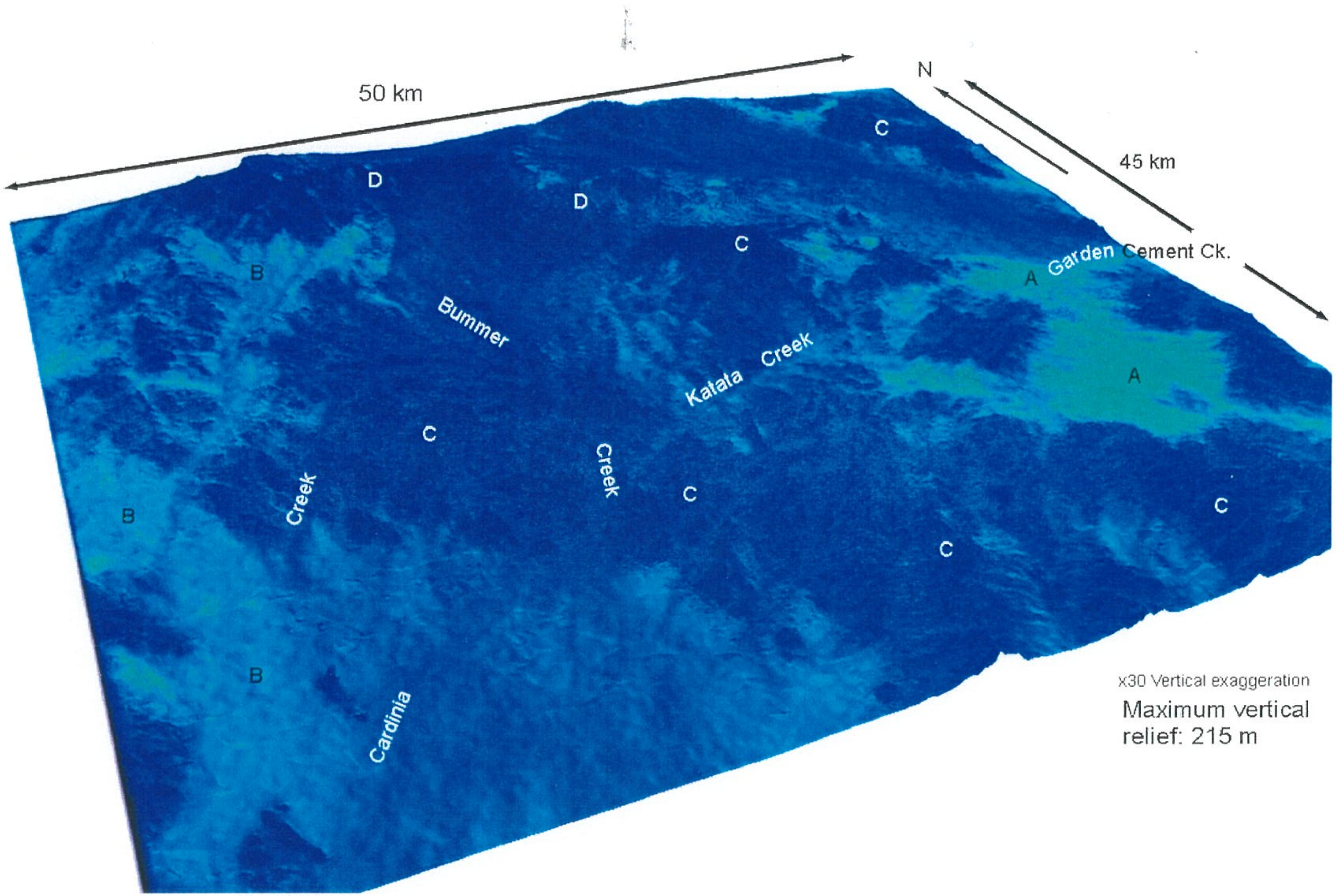

Figure 2.7. Three dimensional perspective view of the gamma-ray response for Th draped over the DEM for the Minerie sheet. A (cyan): Fe-rich material. B (pale blue to cyan): Sediments that have a medium Fe-oxide and clay mineral content. C (dark blue): Greenstone belts. D (blue): Granitic saprolite.

2.5.2 Erosional regime

The main erosional landform elements comprise profiles of weathered ultramafic rock, expressed as a series of sub-parallel hills of low relief (*i.e.*, 9-30 m, Pain *et al.*, 1991) and broad, rounded rises of subdued relief (*i.e.*, <9 m, Pain *et al.*, 1991) developed mainly from mafic rocks (*i.e.*, gabbro and basalt). These are represented by map units, *Wel12* and *SSer11*, respectively. Low hills developed from ultramafic rocks may be capped by a relict, ferruginous duricrust generally 2-3 m thick, that helps to preserve the weathering profile, in which case these hills may occur in isolation as mesas and buttes, as previously discussed.

Erosional rises are marked by very coarse (20-30 cm) lag of angular, blocky cobbles of basalt or gabbroic saprock. These broad, low rises are covered by thin, immature soils on the lower slopes. Sub-crops of basalt and gabbro saprock/saprolite also occur in gently undulating, erosional plain areas (RL map unit, *SSep7*) which generally show an extensive cover of fine, mixed quartz and polished, black Fe-rich lag covering poorly developed soils.

Mafic and ultramafic saprolite is also exposed on a more local scale in minor outwash areas where drainage lines have dissected the weathering profiles.

2.5.3 Depositional regime

Alluvial and colluvial channel sediments are restricted to drainage lines and adjacent areas throughout the mapped area. These are represented by map units *Aa13* and *Cfc16* (Map 1, legend). Alluvial plains (units, *Aap14* and *Aap15*) form extensive covers of sediment in the NW, NE to E and SE areas of the mapped area (Map 1) and represent the main depositional landform in the area.

Alluvial plain surfaces are covered with a polymictic lag of variable amounts of angular quartz fragments and coarse, ironstone gravel indicative of the locally derived nature of these deposits. Sheet-wash flooding is the main erosional element in this part of the landscape. Locally, Wanderrie banks may be developed particularly in the east and southeast of the mapped area (RL map unit, *Aap15*). Wanderrie banks are micro-topographical relief features generally less than 30 cm in height and are usually found in the lower portions of alluvial plain areas (Mabbutt, 1963). They generally consist of fine to coarse sands deposited parallel to local topographic contours by the combined action of wind and sheet-wash erosion (Mabbutt, 1963; Pringle *et al.*, 1994).

Uniform, orange-brown, sandy-clay sediments, of variable thickness to about 30 cm, and containing many fine (*i.e.*, < 2mm) ironstone gravel give way to hardpanized (*i.e.*, hyalite, SiO_2)

alluvial sediments also containing many fine, ironstone gravel. The mineralogy of the hardpanized sediments is dominated by quartz with minor plagioclase, goethite, hematite, maghemite, kaolinite, illite/mica, talc and rutile. The presence of plagioclase and talc in the near surface sediments reflects the recent and locally derived nature of the alluvial cover most probably derived from exposed mafic and ultramafic saprolite or saprock.

Channel sediments (RL map unit, *Aa13*) associated with shallow, open creeks and streams are similar to alluvial plain deposits. These consist of unconsolidated, red-brown clayey-sands with many polished black Fe-stone gravel/nodules overlying hardpanized (*i.e.*, hyalite, SiO_2) clayey-sands. The absence of cutans coating the Fe-stone nodules and gravel is also testament to the transported nature of the channel sediments (Anand *et al.*, 1991). The hardpanized sediments are dominated by quartz with plagioclase, hematite and kaolinite as minor phases, and rutile in trace amounts.

In more deeply incised channels, poorly developed soil profiles with immature horizons may form. A general profile consists of 0–30 cm of red-brown, fine clayey-sands, dominated by quartz with minor plagioclase, kaolinite, hematite and rutile, overlying calcareous sandy-clays to about 60-70 cm. A stone line of angular, quartz and lithic fragments to 50 mm appear to mark the transition to the lower calcareous horizon. The mineralogy of the pedogenic carbonate horizon consists of calcite and quartz as the main phases with minor hematite, plagioclase, kaolinite and gypsum.

3.0 REGOLITH UNITS

3.1 Introduction

This chapter provides a discussion of the regolith characteristics of the two study areas, MM2 and MM3, that were selected to provide deposit and profile scale examination of the regolith mineralogy at Murrin Murrin. Investigation of the regolith at MM2 and MM3 was conducted mainly by reflected infrared analysis (*e.g.*, PIMA) of RC drill pulps supplemented by X-ray diffraction (XRD) analysis. This helped to establish the weathering profiles or regolith stratigraphy for MM2 and MM3, which, in conjunction with geochemical data supplied by Anaconda, was used as the basis for developing 3-D models using the visualization software MVS.

3.2 Geomorphology and site description

MM2 occurs mainly within a depositional landform regime with dominantly alluvial and colluvial surficial material. Regolith-landform units *Aa13*, *Aap14* and *Cfc16* cover approximately 75% of the area (Fig. 3.1). The high total radiometric response for the area, shown in red-orange hues in Figure 3.1, is due mainly to γ-ray responses for K and U associated with recent felsic sediments that originate from granite/adamellite outcrops that occur to the NW of the area (see Fig. 1.2). MM2 is located to the NE of a regional drainage divide with local drainage associated with the Lake Carey palaeochannel system (Fig. 1.2). Deposition of felsic sediments along drainage lines that feed into Garden Cement Creek has blanketed the area resulting in a more subdued expression of relief.

In contrast, MM3 occurs within an area of more prominent relief characterized by relict and erosional landforms with low hills (<30 m) of weathered ultramafics that may be capped by a ferruginous duricrust; regolith-landform units *Wel12* and *RFel2*, respectively (Figure 3.1 and Chapter 2). Ultramafic rocks have low radiometric signatures and show as dark blue to blue hues (Fig. 3.1). The low total γ-ray response for the area (*i.e.*, green colours in Figure 3.1) is due mainly to low concentrations of U associated with drainage lines and erosional landforms that may have a thin cover of deposited material. Uranium is probably associated with near surface pedogenic carbonate and groundwater calcrete deposits in valley areas. MM3 occurs to the SW of the main drainage divide with local drainage associated with the Lake Raeside palaeochannel system (Fig. 1.2). Locally, drainage has developed sub-parallel to strike of the greenstone belts, which has resulted in the more prominent relief for the area.

3.3 Mineral identification

Reflected infrared analysis of RC pulps using the PIMA-II instrument, as described in Section 1.11.1, was used as an objective and efficient means of drill hole logging. This enabled the regolith mineralogy to be more precisely determined and allowed a high degree of uniformity to descriptions of the regolith within and between the study areas.

3.3.1 PIMA-II

Logging of RC drill pulps using PIMA identified several mineralogically distinct regolith units based upon the dominant clay silicate phase present. For MM2 and MM3, the main minerals were from the base of profiles to the surface: serpentine, talc, saponite, nontronite and kaolinite. Other phases identified included gibbsite and alunite but these were present in only minor amounts and were only locally developed being restricted to the near surface of profiles.

Within MM2, drill holes CBRC 0721 (with a depth of 36 m), 1384 (12 m), 1387 (30 m), 1391 (30 m), 1392 (39 m), 1393 (27 m) and 1395 (33 m) were distinguished by a near monotonous mineralogy of well crystalline (*i.e.*, well ordered) kaolinite as indicated by resolution of the Al-OH absorption doublets at 1390-1410 nm and 2162-2208 nm (Appendix5). Minor amounts of Fe replacing Al were indicated by the presence of an absorption feature at 2240 nm. Illite and smectite (montmorillonite) were locally developed but only at depth for some of these drill holes.

The well crystalline kaolinite was different from that identified in all other RC holes logged within MM2 and MM3. In this case the kaolinite was generally not as well ordered (*i.e.*, absorption doublets were poorly developed in PIMA spectra) and kaolinite also generally occurred in association with smectite and/or opaline silica (Appendix 5).

Within MM3, serpentine was identified in surface and sub-surface samples for RC holes ARC 0049 (to a depth of 6 m), 0050 (3 m), 0120 (1 m), 0128 (1 m), 0132 (2 m) and 0134 (11 m). This is unexpected, as serpentine is commonly destroyed during weathering and, indeed, was absent in units overlying serpentine in most profiles.

Crossover contamination of consecutive RC holes during drilling was eliminated as a possible source of serpentine for some of the holes. Serpentine is not likely to have been mis-identified and PIMA is not over sensitive to serpentine. Identification of serpentine as silicified and ferruginized olivine cumulate in outcrops confirmed the PIMA results. Serpentine generally occurred in ferruginous duricrust on hill crests and adjacent upper slope positions. Primary serpentine may have been coated with secondary silica and Fe oxides enabling its preservation to, in some cases, considerable depth (*e.g.*, to 11 m for ARC0134).

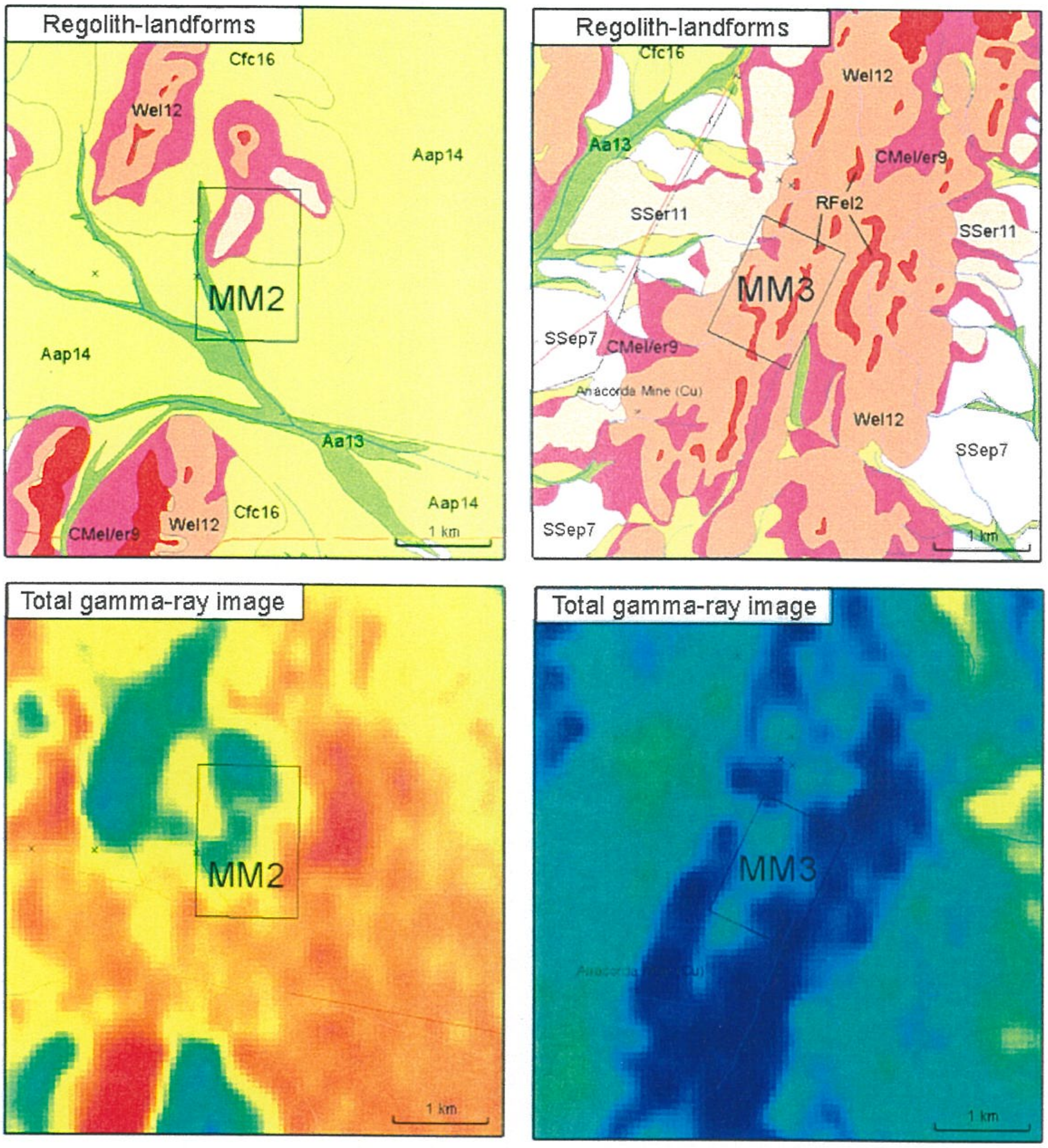

Figure 3.1. Regolith-landform units for the MM2 and MM3 study areas and the corresponding total radiometric γ-ray response for the areas. Regolith-landform images were taken from the regolith-landform map. Red-orange hues for the total γ-ray image of MM2 indicate a high response mainly from K and U associated with felsic sediments derived from granitic outcrops to the NW of the area. Radiometrically poor greenstone belts present as very low response, dark blue hues in the total γ-ray image for MM3. Cyan hues for the γ-ray image of MM3 indicate a low response mainly for U associated with thin covers of surface material in erosional landforms. Refer to the Regolith-Landform map legend and Chapter 2 for a more complete description of each regolith-landform unit.

3.3.2 X-ray diffraction analysis

Random powder X-ray diffraction (XRD) analysis of selected RC drill holes representative of the main changes in mineralogy, as identified by PIMA, provided a more comprehensive examination of regolith mineralogy and was used to establish the mineral 'suite' for calculations of normative abundances (Section 3.6). Drill holes CBRC 0724 and 0796 were selected as representative of MM2 (Table 3.1). For MM3, drill holes ARC 0786 and 1008 were selected for examination. The mineralogy for these drill holes with the units identified by PIMA is presented in Table 3.2. Changes in clay silicate mineralogy as identified by XRD generally coincided with the units as distinguished using PIMA.

The clay silicate mineralogy of the serpentine unit, as identified by PIMA, is comprised mainly of serpentine with lesser amounts of chlorite and, in some profiles, minor amounts of talc. Although magnesite and dolomite can occur with serpentine, magnesite occurs mainly with talc and, with dolomite comprises the main non-silicate phase for the talc unit (Table 3.2). The presence of talc, in association with ultramafic rocks, most probably occurs by the alteration (*i.e.*, steatization) of serpentine (Deer *et al.*, 1980):

$$\underset{\text{(Serpentine)}}{Mg_3Si_2O_5(OH)_4} + 3CO_2 \rightarrow \underset{\text{(Talc)}}{Mg_3Si_4O_{10}(OH)_2} + \underset{\text{(Magnesite)}}{3MgCO_3} + 3H_2O$$

Talc may also form by the addition of Si and removal of Mg (Deer *et al.*, 1980). Calcium present during alteration may form, with excess Mg, as dolomite. The presence of minor amounts of talc within the serpentine unit and, conversely the presence of minor amounts of serpentine within the talc unit (Table 3.2) for some profiles, suggests that in these cases talc may be of secondary origin.

Iron released during the serpentinization of primary olivine is generally not incorporated to any great extent within serpentine (Deer *et al.*, 1980; Delvigne, 1998) and forms, instead magnetite ($FeO.Fe_2O_3$). Subsequent oxidation of magnetite (*i.e.*, martitization) forms maghemite (γFe_2O_3) and/or hematite (αFe_2O_3). Maghemite is the main Fe oxide that occurs within the serpentine unit, whereas hematite is the main Fe oxide in that occurs in association with talc (Tables 3.1 and 3.2).

Chlorite is the main Al-bearing phase within the serpentine, talc and saponite units and continues up the weathering profile into the lower portion of the nontronite unit where it may represent the main alumino-silicate (Tables 3.1 and 3.2). Kaolinite replaces chlorite in the upper portion of the nontronite unit and the former mineral then continues to the surface as the main Al-bearing phase. Chlorite was not easily identified in PIMA spectra.

Table 3.1. Mineralogy for RC holes CBRC0724 and CBRC0796 for MM2 by XRD, with the main regolith units identified using PIMA.

RD drill hole CBRC0724.

Sample ID	Depth (m)	Clay silicates	Oxide phases	
26872	1	K, sm	Gth, hm	Kaolinite (PIMA)
26873	2	K, sm	Gth, hm	
26874	3	K, sm	Gth, hm, mgh (tr)	
26875	4	K, sm	Gth, hm	
26876	5	K, sm	Gth, hm, mgh (tr)	
26877	6	K, sm	Gth, hm, mgh (tr)	
26878	7	K, sm (tr)	Gth, hm, mgh (tr)	
26879	8	K, sm	Gth, hm, mgh (tr)	
26880	9	K, sm	Gth, hm, mgh (tr)	
26881	10	K, sm	Gth, mgh, hm	
26882	11	K, sm	Gth, mgh, hm (tr)	
26883	12	K, sm	Gth, mgh	
26884	13	Sm, K	Gth, mgh	Nontronite (PIMA)
26885	14	Sm, K	Gth, mgh, hm (tr)	
26886	15	Sm, K, ill (tr)	Gth, mgh, hm (tr)	
26887	16	Sm, K, ill (tr)	Gth, mgh, hm (tr)	
26888	17	Sm, k (tr)	Gth, mgh	
26890	18	Sm, k (tr)	Mgh, Gth	
26891	19	Sm, cht	Mgh, hm, gth (tr)	
26892	20	Sm, cht	Mgh, hm	
26893	21	Cht, sm	Mgh, hm	
26894	22	Cht, sm, talc? (tr)	Mgh, hm, Mn-oxide (tr)	
26895	23	Cht, Sm, talc? (tr)	Mgh, hm, Mn-oxide (tr)	Saponite (PIMA)
26896	24	Cht, Sm, talc? (tr)	Mgh, hm, Mn-oxide (tr)	

RC drill hole CBRC0796.

Sample ID	Depth (m)	Clay silicates	Oxide phases	
30379	1	K, sm	Gth, hm, qtz, clt	Kaolinite (PIMA)
30380	2	K, sm	Gth, Clt, bass, hm (tr)	
30381	3	K, sm	Gth, Bass, hm (tr)	
30383	4	K, sm	Gth	
30384	5	Sm, K	Gth	
30385	6	Sm, K	Gth, clt (tr)	Nontronite (PIMA)
30386	7	Sm, K	Gth, clt, dmt, hm (tr)	
30387	8	Sm, K	Gth, mgh, clt	
30388	9	Sm, K	Gth	
30389	10	Sm, K	Gth	
30390	11	Sm, K	Gth	
30391	12	Sm, K	Gth	
30392	13	Sm, cht, k? (tr)	Gth, mgh	
30393	14	Cht, sm, k? (tr)	Mgh, hm, dmt, gth (tr)	
30394	15	Cht, sm	Mgh, hm, dmt, gth (tr)	
30395	16	Cht, sm	Mgh, hm, dmt, gth (tr)	
30396	17	Cht, sm	Mgh, hm, dmt, gth (tr)	
30397	18	Cht, sm	Mgh, dmt, hm	
30398	19	Cht, sm	Mgh, hm, dmt	
30399	20	Cht, sm	Mgh, hm, dmt	
30400	21	Cht, sm	Mgh, hm, dmt	
30401	22	Cht, sm	Mgh, hm, dmt	
30402	23	Cht, sm	Mgh, hm, dmt	
30403	24	Cht, sm	Mgh, hm, dmt	
30404	25	Cht, sm	Mgh, hm, dmt	

k = kaolinite; sm = smectite; cht = chlorite; spt = serpentine; ill = illite; gth = goethite; hm = hematite; mgh = maghemite; clt = calcite; dmt = dolomite; mst = magnesite; rt = rutile; gb = gibbsite; bass = bassanite; qtz = quartz. Mineral name abbreviations shown with the first letter in capitals (*e.g.*, Sm) indicates that the mineral is the major phase. Mineral name abbreviations in lower case indicate that the phase is present in minor amounts.

Table 3.2. Mineralogy of RC drill holes ARC0786 and ARC1008 for MM3 by XRD, with the main regolith units identified using PIMA.

RC drill hole ARC0786.

Sample ID	Depth (m)	Clay silicates	Oxide phases	Regolith unit
37969	1	K, sm (tr), talc (tr)	Qtz, Gth, Hm, mgh, clt, gb	Talc (PIMA)
37970	2	K, talc, sm	Qtz, rt, clt, hm, gth, mst, gb (tr)	
37971	3	Talc, cht, sm (tr)	Mst, Dmt, qtz, hm	
37972	4	Talc, cht, sm (tr)	Mst, Dmt, hm	
37973	5	Talc, cht, sm (tr)	Mst, Dmt, hm	
37974	6	Talc, cht, sm (tr)	Mst, Dmt, hm	
37975	7	Talc, cht, sm (tr)	Mst, Dmt, hm (tr)	
37976	8	Talc, cht, sm (tr)	Mst, Dmt, hm (tr)	
37977	9	Talc, cht, sm	Mst, Dmt, hm (tr)	
37978	10	Talc, Cht, sm	Mst, Dmt, hm (tr)	
37979	11	Talc, Spt, Cht	Mst, Dmt, hm (tr), mgh (tr)	
37980	12	Spt, Cht, talc	Mst, Dmt, hm	Serpentine (PIMA)
37981	13	Cht, Spt, talc	Dmt, Mst, mgh, hm (tr)	
37982	14	Spt, cht	Mst, dmt, mgh? (tr)	
37983	15	Spt, cht	Mst, dmt, mgh? (tr)	

RC drill hole ARC1008.

Sample ID	Depth (m)	Clay silicates	Oxide phases	Regolith unit
83610	1	K, sm? (tr)	Gth, Qtz, hm	Kaolinite (PIMA)
83611	2	K, sm? (tr)	Gth, hm	
83612	3	K, Sm, ill	Gth, Dmt, hm	
83613	4	Sm, ill, k	Gth, Qtz, Dmt, hm	Nontronite (PIMA)
83614	5	Sm, ill, k	Qtz, gth, hm (tr)	
83615	6	Sm, k? (tr)	Gth, hm, mgh	
83616	7	Sm, k? (tr)	Gth, hm, mgh	
83617	8	Sm, k? (tr)	Gth, Qtz, hm, mgh	
83618	9	sm (tr)	Qtz, gth (tr), hm (tr)	
83619	10	Sm	Gth, qtz, hm, mgh (tr)	
83620	11	Sm, k? (tr)	Gth, hm, qtz, mgh	
83621	12	Sm	Gth, hm, mgh	
83622	13	Sm, k? (tr)	Gth, Hm, Mgh, qtz	
83623	14	Sm, spt	Gth, Mgh, hm	
83624	15	Spt, sm	Hm, Gth, mgh	Serpentine (PIMA)
83625	16	Spt, cht, sm (tr)	Mgh, gth, hm	
83626	17	Spt, cht, sm (tr)	Mgh, hm, qtz (tr)	
83627	18	Spt, cht, sm (tr)	Mgh, hm	
83628	19	Spt, cht, sm (tr)	Mgh, Hm	
83629	20	Spt, cht, sm (tr)	Hm, mgh	
83630	21	Spt, cht, sm (tr)	Hm, mgh	
83631	22	Spt, cht, sm (tr)	Hm, mgh	
83632	23	Spt, cht, sm (tr)	Hm, Mst, mgh	
83633	24	Spt, cht, sm (tr)	Hm, mgh	
83634	25	Spt, cht, sm (tr)	Hm, mgh	
83635	26	Spt, cht, sm (tr)	Hm, mgh	
83636	27	Spt, cht, sm (tr)	Hm, mst, mgh, dmt (tr)	
83637	28	Spt, cht, sm (tr)	Hm, mgh	

k = kaolinite; sm = smectite; cht = chlorite; spt = serpentine; ill = illite; gth = goethite; hm = hematite; mgh = maghemite; clt = calcite; dmt = dolomite; mst = magnesite; rt = rutile; gb = gibbsite; bass = bassanite; qtz = quartz. Mineral name abbreviations shown with the first letter in capitals (*e.g.*, Sm) indicates that the mineral is the major phase. Mineral name abbreviations in lower case indicate that the phase is present in minor amounts.

Smectite, as nontronite and minor, locally developed montmorillonite are the main clay-silicate phases within the nontronite unit, particularly for the middle to upper portion of the unit (Tables 3.1 and 3.2). As is the case for chlorite, maghemite may also continue into the lower portion of the nontronite unit as the main Fe oxide phase, but is replaced by goethite in the upper portion of the unit and, with minor amounts of hematite, comprise the main Fe-bearing phases (Tables 3.1 and 3.2).

The clay mineralogy of the kaolinite unit (PIMA) is dominated by kaolinite with minor amounts of smectite and lesser amounts of illite, if present. The oxide mineralogy of the kaolinite unit is dominated by goethite with minor hematite and trace amounts of maghemite.

Near surface samples contain accessory rutile, gibbsite, calcite, dolomite and bassanite, $Ca_2(SO_4)_2.H_2O$ (Table 3.1). Bassanite may be present in significant amounts: *e.g.*, it is a major phase in RC hole CBRC0796 (Table 3.1). Bassanite has probably formed by the partial dehydration of original gypsum, as a result of the methods used by Analabs and UltraTrace to prepare the sample pulps (*i.e.*, drying at 110° C). Dehydration of gypsum can be initiated at temperatures above 80° C. Dolomite and calcite also occur in near surface samples, associated with the kaolinite/nontronite contact. Dolomite may also be present locally throughout the profile.

Quartz generally occurs as a minor phase of the oxide mineralogy, being present sporadically throughout the profiles (Table 3.1 and 3.2). High amounts of quartz may be present locally (*e.g.*, for RC hole ARC1008, sample 83618) where it may comprise the major phase but, the vertical distribution of quartz is generally limited. Opaline silica was not detected by XRD because it is x-ray amorphous.

For MM2, drill hole CBRC0721 was selected as representative of the well crystalline kaolinite as identified by PIMA. Results of the XRD analysis of RC pulps are presented in Table 3.3. Quartz is the major oxide phase present throughout the profile. Plagioclase and K-feldspar occur as the other main oxide phases, which decrease in abundance towards the surface of the profile.

Illite or muscovite occur as the main Al-bearing clay silicate phases at depth which are replaced by kaolinite as the main alumino-clay silicate moving up the profile. Minor amounts of smectite and illite occur in the central portion of the profile. Goethite is present in minor amounts as the only Fe oxide phase identified (Table 3.3).

The mineralogy of this profile is distinct and is representative of a weathering profile of either *in-situ* felsic bedrock or of material originating from a felsic source, rather than having an ultramafic origin. The presence of nontronite at the base of some drill holes identified with this mineralogy suggests that the profile is depositional in origin. The location of RC holes identified with this mineralogy at 9200 to 9275 mE and 26300 to 26500 mN, on the western margin of MM2, indicates that these profiles are associated with either current surface drainage or is a palaeochannel remnant associated with the Lake Carey palaeochannel drainage system (Fig. 1.2). The source of the felsic material is most probably derived from granitic outcrops that form the prominent breakaway to the NW (see Figure 1.2).

Table 3.3. Mineralogy of RC drill hole CBRC0721.

Sample ID	Depth (m)	Clay silicates	Oxide phases
26821	1	Kaolinite	Quartz, goethite, calcite
26823	3	Kaolinite	Quartz, goethite, hematite? (tr)
26826	6	Kaolinite	Quartz, goethite
26829	9	Kaolinite, illite*	Quartz, plagioclase, goethite (tr)
26832	12	Kaolinite, smectite?	Quartz, goethite (tr), calcite (tr)
26835	15	Smectite, Kaolinite	Plagioclase, K-feldspar?
26839	18	Kaolinite, smectite, illite*	Quartz, plagioclase
26842	21	Kaolinite, smectite, illite*	Quartz, goethite (tr)
26845	24	Kaolinite, smectite	Quartz, plagioclase, K-feldspar
26848	27	Kaolinite, smectite, illite*	Quartz, K-feldspar
26851	30	Illite*, Kaolinite, smectite	Quartz, K-feldspar
26854	33	Kaolinite, smectite, illite*	Quartz,
26857	36	Illite*, smectite, kaolinite	Quartz, Plagioclase, K-feldspar, calcite

Mineral names shown with the first letter in capitals (*e.g.,* Kaolinite) indicates that the mineral is present in major amounts. Mineral names in lower case (*e.g.,* plagioclase) indicate that the phase is present in minor amounts. For the XRD analysis of these samples illite* is used as a general term that includes muscovite and K-depleted forms such as illite, proper.

3.4 Regolith stratigraphy

Profiles of the regolith 'stratigraphy' for MM2 and MM3, compiled based mainly on PIMA spectroscopy with some XRD analysis, are presented in Table 3.4. Regolith developed at MM2 and MM3 shows a very similar stratigraphy, as would be expected from the weathering of ultramafic rocks (*i.e.,* peridotites) that have a similar bulk chemical composition (*i.e.,* high Mg and low Si, Al, and Fe contents, Hill *et al.,* 1996). However, small variations in the chemistry of the underlying bedrock are reflected in the relative abundances of minerals that form in the regolith. This is discussed in more detail in Section 3.5 and 3.6.

Table 3.4. Regolith stratigraphy for MM2 and MM3, as identified by PIMA and interpreted regolith units.

		Interpreted units*	
MM2: PIMA unit	**Description and comments**	**Anaconda**	**Generic**
#0: Kaolinite-1	Well crystalline kaolinite, with some illite and minor smectite at depth.	FZ or PC	Channel clays
#1: Kaolinite-2	Poorly crystalline kaolinite with locally developed opaline-Si. Gibbsite an alunite occur as local, minor phases.	FZ	Fe-rich, partially collapsed saprolite
#2: Nontronite	Locally developed opaline-Si, with minor amounts of kaolinite. Minor montmorillonite also locally present.	SM	Smectite
#3: Saponite	Some nontronite may occur with some locally developed opaline-Si.	SM/SA?	Saprolite
#4: Talc	Mainly talc with minor amounts of kaolinite, smectite (as nontronite and montmorillonite) and opaline-Si.	SA	Saprolite
#5: Serpentine	Dominantly serpentine with some local alteration to saponite.	SA/UM	Saprock to fresh ultramafic
#6: Mixed serpentine	Variably weathered serpentine, with local alteration to saponite and talc.	SA/UM	
MM3: PIMA unit			
#0: Kaolinite with serpentine	Mainly kaolinite with minor serpentine preserved at the surface.	FZ	Lateritic duricrust and preserved saprolite
#1: Kaolinite	Dominantly kaolinite with variably developed local opaline-Si.	FZ	Fe-rich, partially collapsed saprolite
#2: Nontronite	Locally developed opaline-Si, kaolinite and minor talc.	SM	Smectite
#3: Saponite	Mainly saponite with locally developed opaline-Si.	SM/SA?	Saprolite
#4: Talc	Local kaolinization and minor amounts of smectite (as nontronite with some saponite).	SA	Saprolite
#5: Serpentine	Mainly serpentine with some minor, variable alteration to saponite and talc.	UM	Saprock to fresh ultramafic

*Terms used by Anaconda for profile description: PC = plastic clays; FZ = Ferruginous zone; SM = smectite zone; SA = saprolite; UM = ultramafic.

In addition, the influence that local geomorphological factors (*i.e.*, drainage, topography) have to profile development is reflected mainly in the upper portion (*i.e.*, kaolinitic units) of the profiles for the two sites. Interpretation of the kaolinite units is complex with the regolith having both a transported and residual component. At MM2, the well crystalline kaolinite is associated with deposits of channel clay sediments of felsic origin. Kaolinite associated with weathered ultramafics may also have a transported component, particularly in the upper portion of the unit. This is most evident at MM2, where input of Al (which may account for the presence of gibbsite within kaolinite, Table 3.4) and Si-rich material at the surface occurs, due to location of the site within the outwash of granitic material that feeds into the Lake Carey palaeodrainage system (Fig. 1.2).

Regolith boundaries within the weathering profiles at MM2 and MM3 are somewhat gradational with some phases continuing into overlying units. Locally, development or alteration occurs within regolith units, which complicates the profile stratigraphy. Development of opaline-Si from the central portion of the profiles through to the surface is a feature of the profiles at both sites (Table 3.4).

The descriptive scheme used by Anaconda to describe the Ni-laterite profiles is generally too broad and does not permit detailed discrimination of units within the regolith. For example, in the case of the kaolinite units at MM2, Anaconda's classification scheme does not enable discrimination of the genetic significance of these units (Table 3.4). This is important when considering the influence of local site factors to the formation of the deposits.

3.5 Regolith models for MM2 and MM3

The regolith profiles for MM2 and MM3, as presented in Table 3.4, were subsequently used as the basis for developing three-dimensional block models using the 3-D visualization program MVS. Block models of the regolith stratigraphy for MM2 and MM3 are presented in Figures 3.2 and 3.3, respectively. Initial comparison of the two areas emphasizes the subdued relief of MM2 relative to MM3. This is a reflection of the depositional landforms that dominate at MM2 (Section 3.2). Drainage incision running sub-parallel to the strike of ultramafic rocks has produced the more prominent relief at MM3 (Fig 3.3), which is characterized by relict and erosional regolith-landform regimes (Chapter 2).

Northing slices through the block models provide a better indication of the variation in, and complex nature of, the regolith stratigraphy for MM2 (Fig. 3.4) and MM3 (Fig. 3.5). Nontronite appears as a significant unit at both sites. Fault planes or fractures are evident in MM2 for transects at 26700 mN and 26500 mN (Fig. 3.4). Within MM3, talc appears restricted to the western margin of the deposit (Fig. 3.5). In comparison, talc shows a more uniform distribution within MM2, particularly in the northern part of the area (*i.e.,* transects 26700 and 26500 mN, Fig. 3.4).

As a means of enabling a semi-quantitative comparison of regolith developed at both sites, the volume of each unit at MM2 and MM3 was determined using the SELECT_CELLS and VOLUME_MASS modules in MVS, and is expressed as a percentage of the total regolith volume in Figure 3.6. Such calculations can, however, be biased by the, somewhat, arbitrary depth of drilling at the two sites. Despite this, the comparison in this case remains valid because, if the

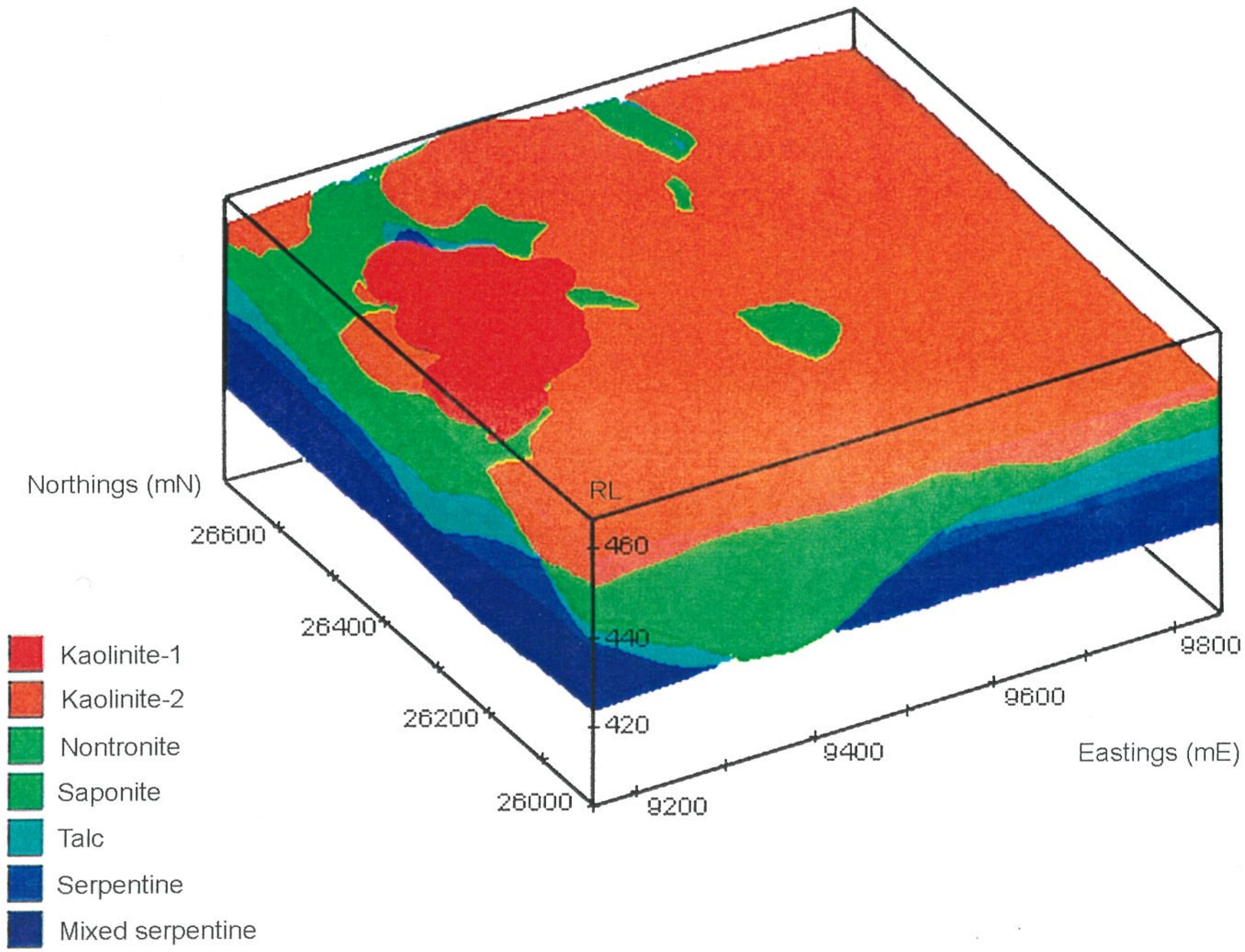

Figure 3.2. Block model, produced using MVS, of the regolith at MM2. Notice the subdued relief for the area. Profiles with well crystalline kaolinite that occur on the western margin of the area may be associated with the present day drainage or may be a remnant of the Lake Carey palaeochannel system to the SE of the area. View is at 210° azimuth and 30° elevation, with x5 vertical exaggeration.

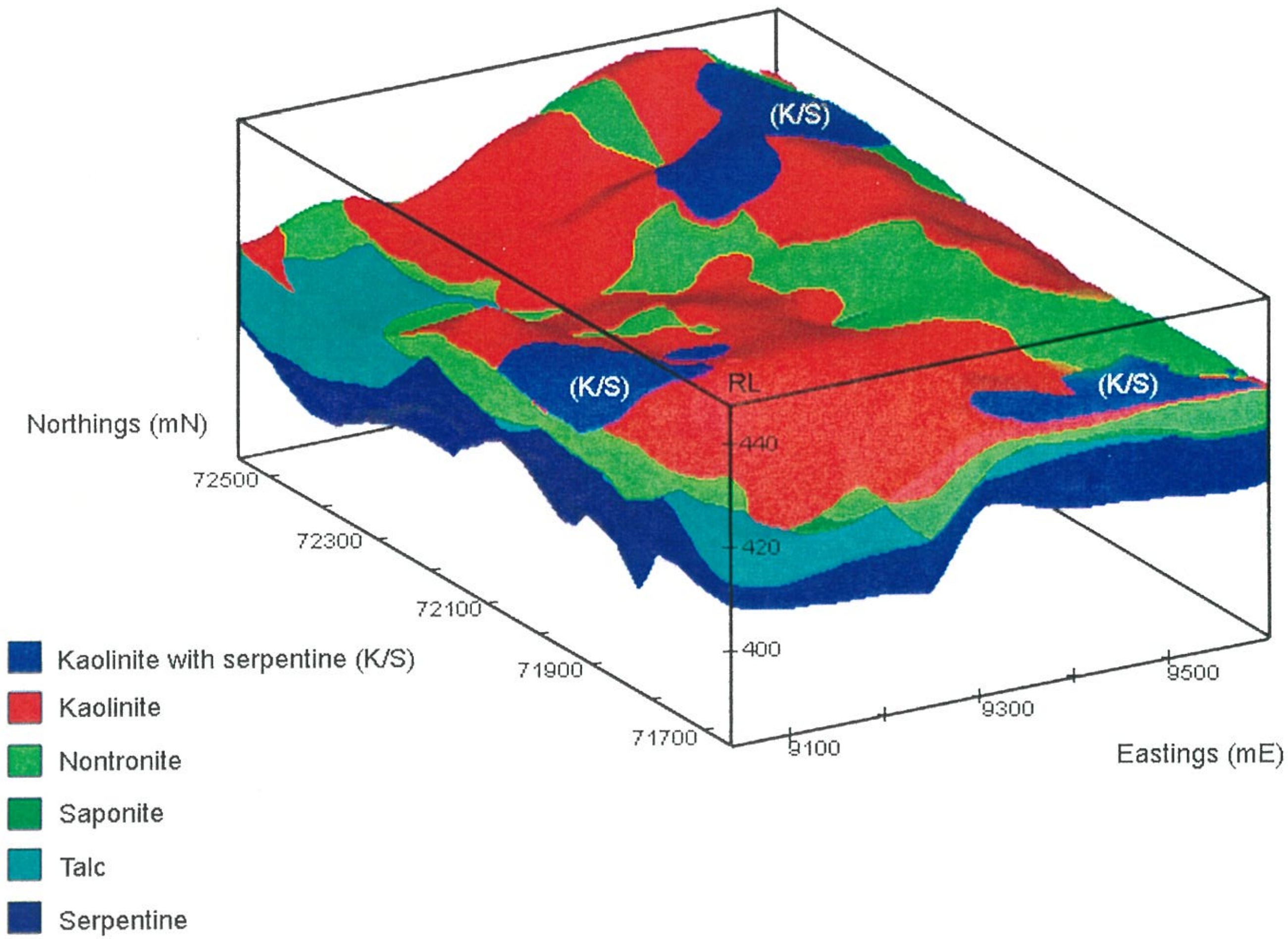

Figure 3.3. Block model, produced using MVS, of the regolith at MM3. Compare the more prominent relief of the area to that at MM2 (Figure 3.2). Talc appears restricted to the western margin of the study area (See slices of northing transects through the area, in Figure 3.5). View is at 210° azimuth and 20° elevation, with x5 vertical exaggeration.

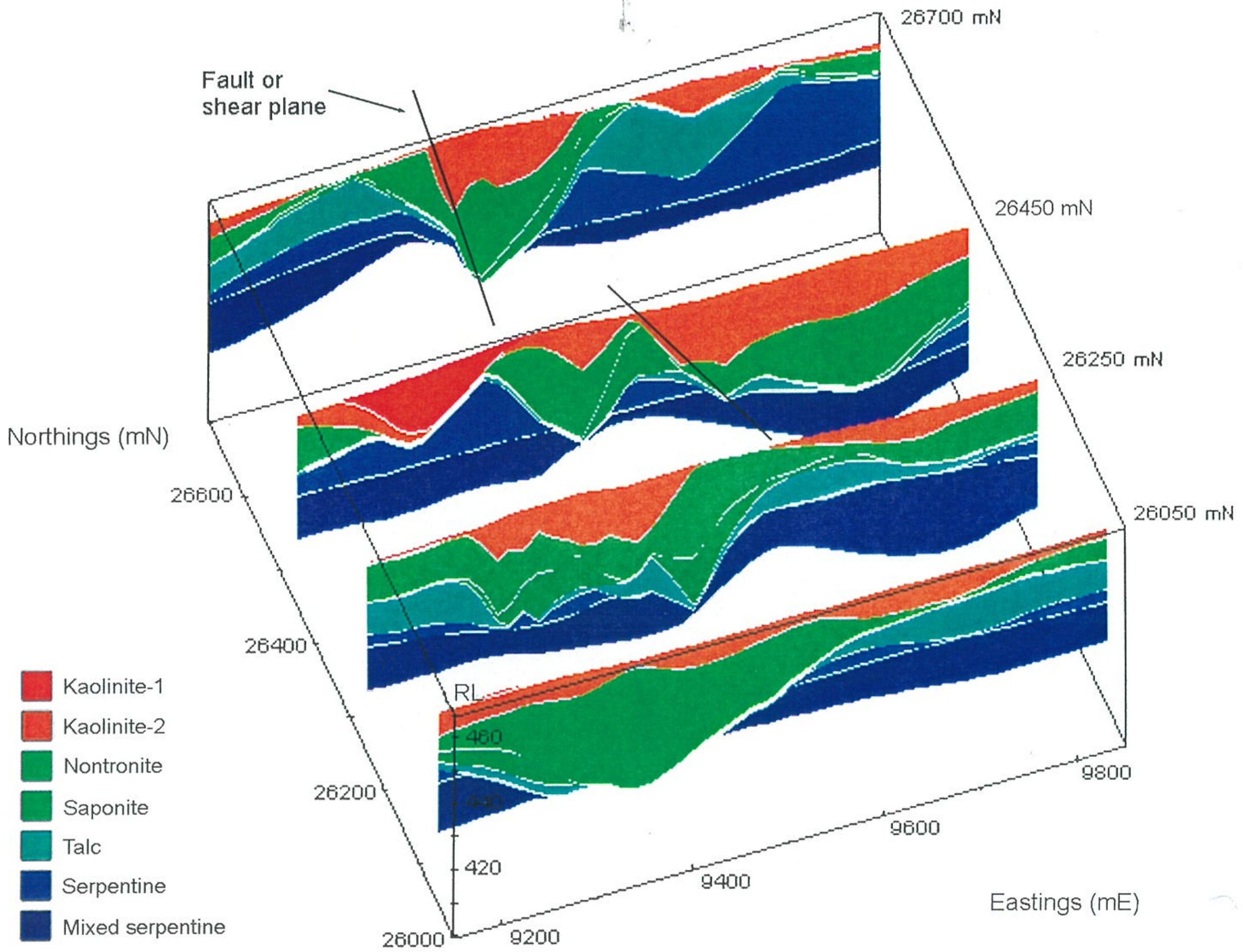

Figure 3.4. Northing slices through the regolith at MM2. A shear or fault plane is evident in transects 26700 and 26500 mN, offsetting the nontronite unit. Regolith units have been separated (*i.e.*, white lines in slices) to show individual units. View is at 200° azimuth and 50° elevation, with x5 vertical exaggeration.

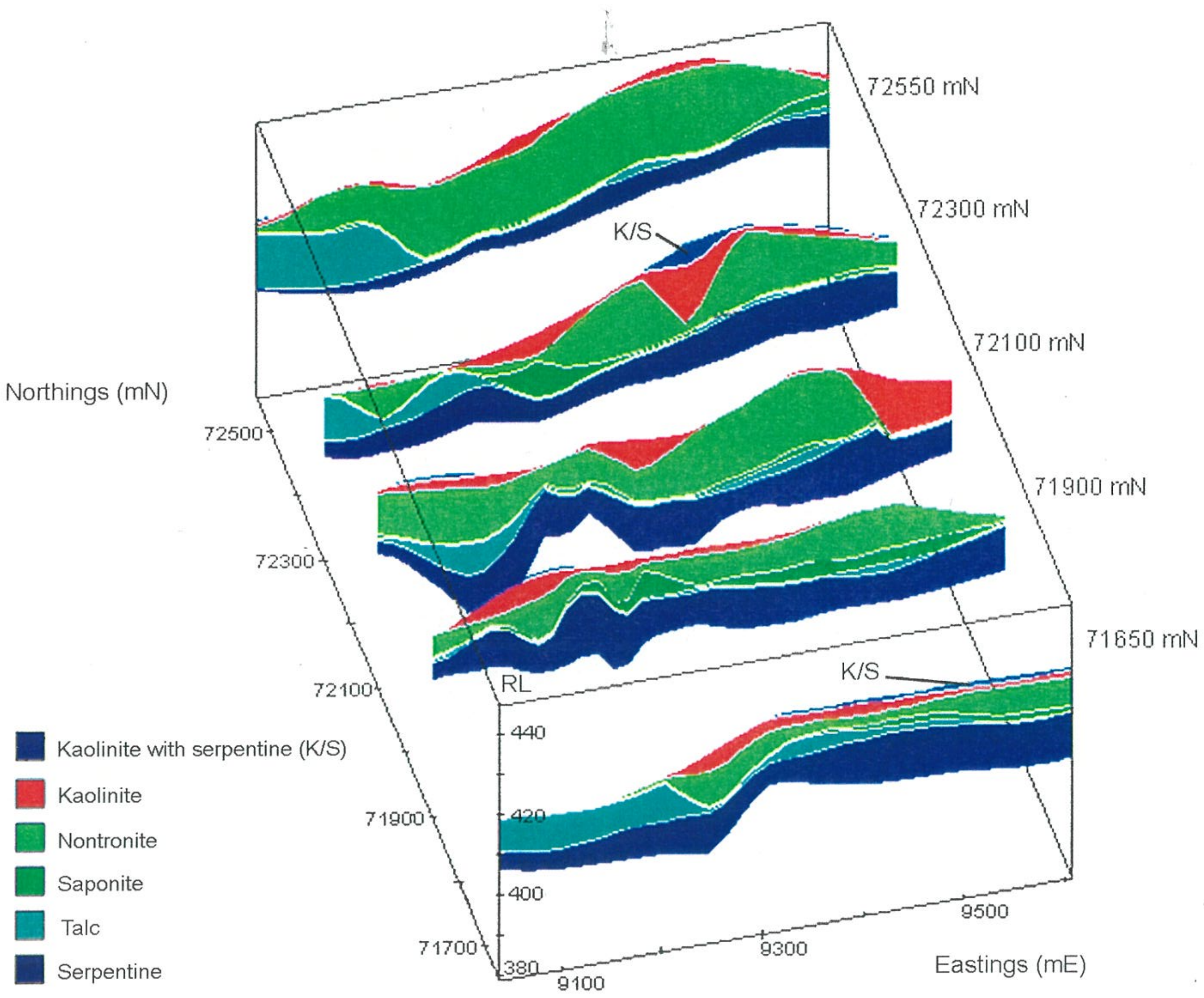

Figure 3.5. Northing slices through the regolith at MM3. Talc appears mainly along the western margin and may reflect differences in the underlying lithology (see discussion in Section 4.4). Regolith units have been separated (*i.e.*, white lines in slices) to show individual units. View is at 195° azimuth and 40° elevation, with x5 vertical exaggeration.

serpentine and mixed serpentine units at MM2 are considered as a single unit, then values of the volume% that serpentine occupies at MM2 and MM3 are very similar, at 39 and 41%, respectively (Figure 3.6). Overall, the proportions of the other units at the two sites are similar, except that MM2 has a slightly greater proportion of kaolinitic material (channel clays and kaolinite units), at the expense of the nontronite unit. This may, in part, reflect the input of Al-rich sediments derived from granitic outcrops to the NW of MM2.

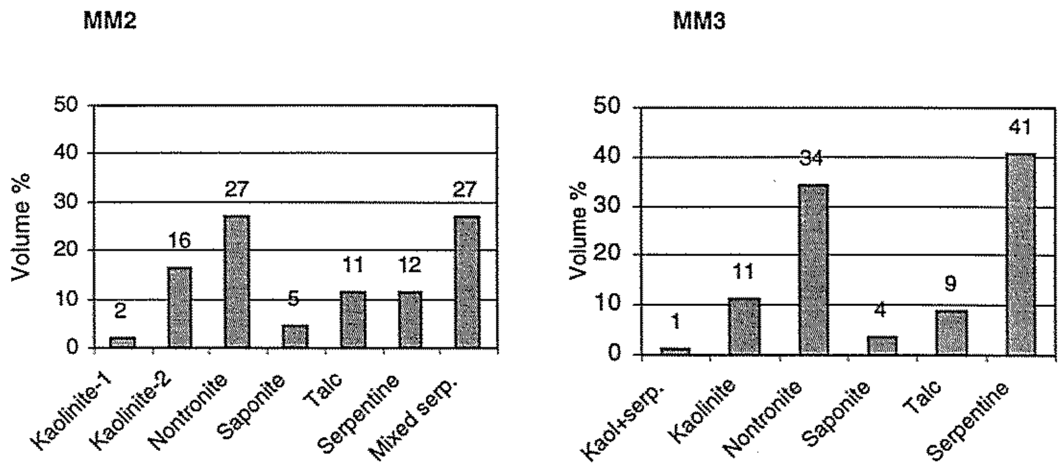

Figure 3.6. The volume % of regolith units at MM2 and MM3 as a percentage of the total regolith volume.

3.5.1 Bedrock geology

In a separate study of the bedrock geology at Murrin Murrin, Hill *et al.*, (1996) distinguished olivine cumulate lithologies (*i.e.*, ortho-, meso- and adcumulates) based on their Ni/Ni+Al ratios (Table 3.5). This classification groups all other lithologies (*e.g.*, basalt, gabbro, felsic volcanics) into the one unit 'Felsic volcanics'.

The Ni/Ni+Al ratio was used for distinguishing fresh rock but it appears that it may also provide useful results when applied to the regolith. Similar volume calculations performed using MVS were undertaken to estimate the lithological content to profile development and regolith units at MM2 and MM3. Use of this lithological discriminant in the present study is based purely on geochemical grounds and takes no account of any possible lateral or vertical dispersion of either Ni or Al (*i.e.*, assumes that they are immobile during weathering).

Distribution of the Ni/Ni+Al ratio at MM2 and MM3 was modelled using MVS and the volume percentage that each of the rock types listed in Table 3.5 occupies within MM2 and MM3 was determined (Fig. 3.7). The dominant lithology at MM2 consists of olivine ortho- and mesocumulates, which occupy about 82% of the total volume, with a minor amount of felsic volcanic rocks (Fig. 3.7). In contrast, olivine meso- and adcumulate lithologies are the main rock types at MM3 occupying 86% of the total volume, with adcumulates alone comprising 50% of the total volume (Fig. 3.7). These findings are consistent to the 'bottom-of-hole' geological logging observations of Hill *et al.*, (1996), which reported the underlying bedrock for tenements MM2 and MM9 as consisting of predominantly ortho- and meso-cumulates. For MM south, a more or less complete gradational sequence of ortho-cumulates through to adcumulates was recorded (Hill *et al.*, 1996).

Table 3.5. Distinction of different rock types based on their (Ni/Ni+Al) ratio.

Rock type	(Ni/Ni+Al) ratio
'Felsic volcanics'	<0.05
Olivine orthocumulate	0.05 - 0.2
Olivine mesocumulate	0.2 - 0.4
Olivine adcumulate	>0.4

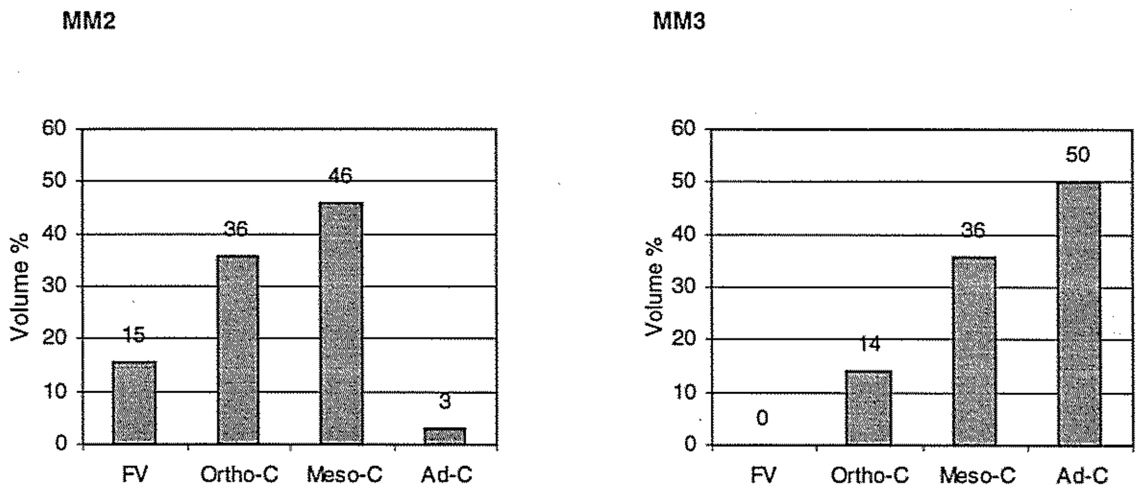

Figure 3.7. Volume % of rock types, distinguished on the basis of their (Ni/Ni+Al) ratios (Hill *et al.*, 1996), as a percentage of the total volume of regolith at MM2 and MM3.

The volume of each regolith unit (Table 3.4) as a percentage of the volume of each rock type is presented in Figures 3.8 and 3.9 for MM2 and MM3, respectively. Surprisingly, regolith developed with 'felsic volcanic' rocks at MM2 is comprised mainly of kaolinite and serpentine

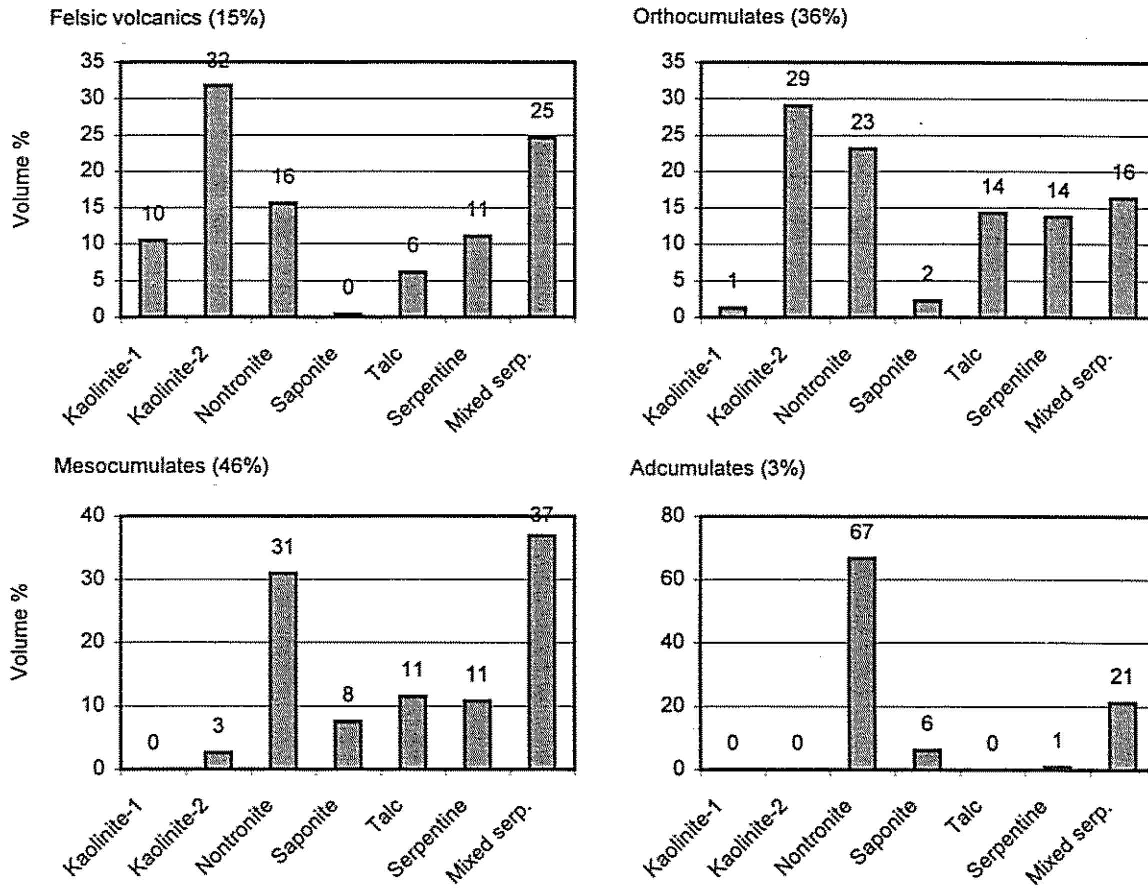

Figure 3.8. Volumes of regolith units developed from different lithologies in MM2, based on their Ni/Ni+Al ratios. Volumes are a percentage of the volume that each rock type occupies.

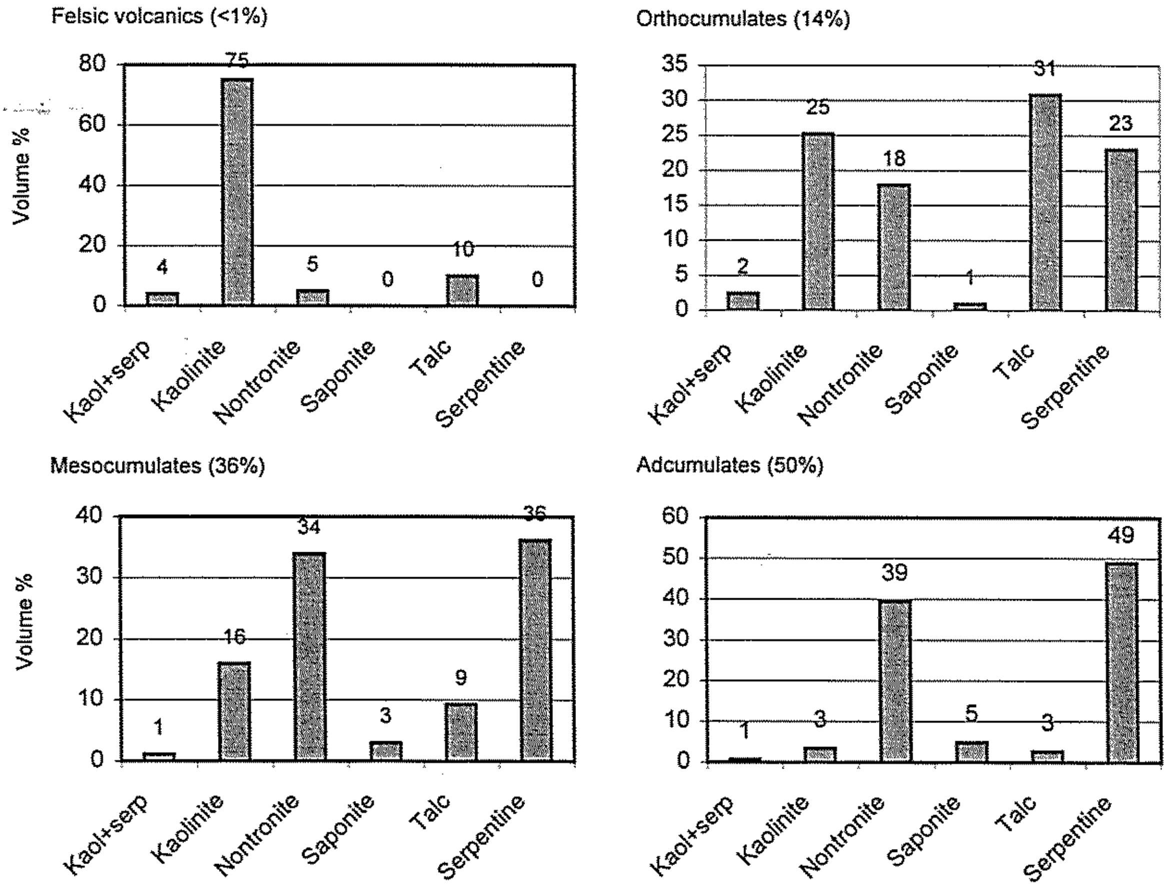

Figure 3.9. Volumes of regolith units developed from different lithologies in MM3, based on their Ni/Ni+Al ratios. Volumes are a percentage of the volume that each raock type occupies.

(Fig. 3.8). According to average geochemical compositions of cumulate lithologies for the Norseman-Wiluna belt, komatiite rocks tend to have very low Ni/Ni+Al values of about 0.03 (Hill *et al.,* 1996). Serpentine developed from rocks with Ni/Ni+Al values of <0.05 suggests the presence of komatiitic lithologies at MM2. This may also account for the talc and nontronite units also associated with the felsic volcanics in MM2 (Fig. 3.8). At MM3, FV rocks comprise <1% of the total rock volume, with the kaolininte as the dominant unit (75%, Fig. 3.9).

Regolith units over the different cumulate lithologies are very similar in both deposits, particularly for olivine meso- and adcumulate lithologies. Orthocumulates alter to a generally mixed regolith profile. Mesocumulates and, in particular, adcumulates alter to regolith dominated by nontronite and serpentine units in which talc is a major component (Fig. 3.9). The saponite unit is only a minor component in both areas.

3.6 CIPW-Norm abundances

To provide a more detailed examination of regolith mineralogy at MM2 and MM3 than can be provided by infrared analysis (*e.g.,* PIMA is not sensitive to Fe oxides) and that is cost effective (the cost of XRD analysis of a large number of samples would be prohibitive), mineral abundances were calculated as CIPW-Norms on the basis of the XRF analysis of 495 samples from selected RC drill pulps (Section 1.11.4). The geochemical data supplied by Anaconda was not used as it did not have assays for several important elements including, in particular, Si. Minerals used in the calculations are based on the 19 phases identified from XRD analysis of sample pulps from RC drill holes CBRC0721, CBRC0724, CBRC0796, ARC0786 and ARC1008, and from PIMA logging of pulps. Results are presented in Appendix 6, Tables A6.1, A6.2 and A6.3.

Weight loss attributed to volatilization of CO_2 during fusion of pulps for XRF analysis was not determined and hence was not included in the calculations. This causes problems with samples that have high carbonate contents (*i.e.,* > 10%) as dolomite and magnesite contain 47 % and 52 % CO_2, respectively. Consequently, where high amounts of carbonate occur (as shown in Appendix 6, with the regolith unit highlighted in bold) abundances of other minerals should be considered as overestimates. It also must be noted that CIPW-Norm determinations can only provide an indication of the phases that <u>may</u> be present not what <u>is</u> present.

The Norm set of minerals for MM2 and MM3 included: bassanite, alunite, chromite, rutile, apatite, asbolan, illite, nontronite, saponite, chlorite, kaolinite, gibbsite, magnesite, dolomite, calcite, talc, serpentine, opaline-Si/quartz and Fe oxides. As the mineralogy for the channel clay sediments in

MM2 was distinct, a separate mineral set was required and included: chromite, rutile, asbolan, vermiculite, nontronite, illite, muscovite, plagioclase, magnesite, dolomite, calcite, kaolinite, gibbsite, opaline-Si/quartz and Fe oxides.

Several assumptions regarding the composition of some minerals and the association of minerals within some of the regolith units were required. The following discussion provides an outline of the assumptions made and presents a general order in which mineral abundances were calculated.

3.6.1 Criteria and order of element allocation for calculations of CIPW-Norm abundances for MM2 and MM3.

1. Sulphur was initially assigned to bassanite, $Ca_2(SO_4)_2.H_2O$, the intermediate phase of the gypsum–anhydrite dehydration series. Remaining S was assigned to alunite $KAl_3(SO_4)_2(OH)_6$. Other S-bearing phases such as jarosite, $KFe_3(SO_4)_2(OH)_6$, and the Na-rich equivalents of alunite and jarosite were not considered. No other discrete Na phases such as halite, NaCl, were detected in either XRD patterns or PIMA spectra.

2. All Cr was allocated to chromite, $FeCr_2O_4$.

3. All Ti was presented as rutile, TiO_2. Rutile is generally pure although substitution of Fe^{2+}/Fe^{3+} and major amounts of Nb and Ta can occur. Tantalum rich varieties may also contain Sn, Cr, and V (Deer *et al.*, 1980). In practice, Ti may also present as anatase, TiO_2, in the regolith, but the assumptions, calculations and results are the same, regardless. It is noted, however, that only rutile was detected in samples by XRD.

4. Mn was assigned as asbolan, $(Co,Ni)Mn_2O_4(OH)_2.xH_2O$, with x = 2. Random powder XRD of Mn-rich samples collected from the trial pits at MM2 and MM7 confirmed the presence of asbolan. Co and Ni were assigned in equivalent amounts to asbolan. Chemical analysis of asbolan confirmed a Co:Ni ratio of approximately 1:1, with an average Co/Mn ratio of 0.33.

5. All P was present as apatite, $Ca_5P_3O_{12}(OH)$.

6. Potassium remaining from the allocation to alunite was assigned to illite. The composition of illite was taken as, $K_{0.75}(Al_{1.1},Fe_{0.7},Mg_{0.2})(Si_{3.5},Al_{0.5})O_{20}(OH)_4$.

7. All Na was assigned to either nontronite, $Na_{0.66}(Fe_{3.2},Ni_{0.2},Mg_{0.6})(Si_{7.6},Al_{0.4})O_{20}.2H_2O$, or saponite, $Na_{0.66}(Mg_{5.3},Fe_{0.62},Ni_{0.08})(Si_{7.34},Al_{0.66})O_{20}.2H_20$. No Ca was allocated to either phase. The Ni contents for nontronite and saponite were set to about 2% Ni, taken as the average of the range of Ni contents reported for these phases (Camuti and Riel, 1996).

8. Remaining Ca was assigned to dolomite, $(Ca,Mg)(CO_3)_2$.

9. Calcium not allocated to dolomite due to the lack of Mg, was taken up by calcite, $CaCO_3$. Calcite and dolomite have a generally pure composition, although Sr, Ba, Co and Zn can be important substituents in calcite and small amounts of Fe^{2+} may replace Mg in dolomite (Deer *et al.*, 1980).

10. Chlorite of composition, $(Mg_{3.5},Al_{1.0},Fe_{1.30},Ni_{0.2})(Si_{2.6},Al_{1.4})(OH)_{16}$, was determined using Al as the limiting element. The Ni content of chlorite was set to 2% based on the average Ni contents reported for chlorite analyses for samples from Murrin Murrin (Camuti and Riel, 1996). Other important substitutions that can occur in chlorite, but not considered in this study, include Cr, Mn, V, Cu or Li (Deer *et al.*, 1980).

11. Any remaining Al was assigned to kaolinite, $Al_2Si_2O_5(OH)_4$, and gibbsite, $Al(OH)_3$. Kaolinite and gibbsite are generally chemically pure although small amounts of Fe can replace Al, and Ti can substitute for Si in kaolinite (Deer *et al.*, 1980). Although minor amounts of Fe substitution were indicated in PIMA spectra this was not a consistent feature of kaolinite and was not considered in the normative calculations.

12. Any remaining Fe was allocated to Fe oxides, as Fe_2O_3. No distinction of the different Fe phases goethite, hematite or maghemite was possible. Cobalt and Ni remaining after allocation to asbolan, nontronite, saponite and chlorite was assigned to Fe oxides.

13. Talc, $Mg_3Si_4O_{10}(OH)_4$. Talc is generally pure, but Al and Ti can replace Si, and the substitution of Mg by small amounts of Fe, Mn and Al does occur. Minnesotaite is the Fe equivalent of talc, but Fe-rich varieties only generally show up to about 33% Fe (Bailey, 1980).

14. Serpentine, $Mg_3Si_2O_5(OH)_4$. As for talc, small amounts of Al can replace Si, and Al and Fe can substitute for Mg in serpentine. The Ni-rich variety of serpentine, a type of garnierite, can occur, but most serpentines generally have <0.25% Ni. Garnierite has not been identified within the Murrin Murrin Ni deposits.

15. Remaining Si is presented as SiO_2. No distinction could be made between amorphous (*i.e.*, opaline) or crystalline SiO_2.

16. Any remaining Mg is presented as magnesite, $MgCO_3$. As for dolomite and calcite, magnesite has a generally pure chemistry, although the intermediate Fe-Mg-carbonate phase, breunnerite

$(Mg,Fe)CO_3$, for the magnesite-siderite series does occur (Deer *et al.*, 1980) and has been described in the MM south area (Wells, 1998).

Certain assumptions regarding the association (*i.e.*, 'paragenesis') of particular phases were also required for normative determinations of certain minerals. Nontronite and saponite are considered mutually exclusive, as were kaolinite and chlorite. No talc could be present with serpentine. Saponite is considered the only smectite phase present in the Saponite, Talc and Serpentine units. Other phases such as montmorillonite, sepiolite, hectorite and palygorskite, have been reported as local occurrences in these deposits (Camuti and Riel, 1996), but were not considered in the normative calculations. These assumptions, however, do reflect the general mineralogy observed in the regolith at MM2 and MM3 (see Table 3.4).

3.6.2 Criteria and order of element allocation for calculations of CIPW-Norm abundances for the channel-clay unit, MM2.

1. Abundances for chromite, rutile (or anatase), apatite and asbolan were calculated following the assumptions outlined previously. Sulphur was not present in significant amounts and consequently no S-bearing phases were included in the normative calculations.

2. Vermiculite, $Mg_2(Mg_{5.5}Fe_{0.5})(Al_2Si_6)O_{20}(OH)_4$, was calculated using Mg as the limiting element.

3. Nontronite, $(Ca_{0.01},Na_{0.65})(Fe_{3.53},Ni_{0.02},Mg_{0.45})(Si_{7.5},Al_{0.5})_{20}.2H_2O$, was determined for samples at the base of some of the profiles. Nontronite was determined using Na as the limiting element and included some Ca.

4. Illite, $K_{0.75}(Al_{1.1},Fe_{0.7},Mg_{0.2})(Si_{3.5},Al_{0.5})O_{20}(OH)_4$, was determined as the main K-bearing phase in association with nontronite.

5. Dolomite, magnesite and calcite were calculated from remaining Mg and Ca.

6. All K, other than that assigned to illite, was assigned to muscovite, $KAl_2(Si_3Al)O_{20}(OH)_4$.

7. Plagioclase was determined as equivalents of albite, $NaAlSi_3O_8$, and anorthite, $CaAl_2Si_2O_8$. Normative abundances of other feldspars as identified by XRD, such as orthoclase, $KAlSi_3O_8$, (Table 3.3) could not be determined.

8. Remaining Al was assigned to kaolinite, $Al_2Si_2O_5(OH)_4$.

9. Remaining Fe was assigned to Fe oxides. Similarly, no discrimination between goethite, hematite or maghemite was possible. Nickel and cobalt remaining from allocation to asbolan and nontronite was incorporated with Fe oxides.

10. Remaining Si was allocated to SiO_2, without distinction between either amorphous, opaline or crystalline phases.

3.7 Normative mineralogy for MM2 and MM3

Plots of the normative mineralogy of selected RC holes for northing transects across MM2 and MM3 are presented in Figures 3.10 to 3.13, and 3.14 to 3.19, respectively. Only those silicate and oxide phases present in significant amounts are shown. For example, as there is no saponite, talc or serpentine in the nontronite unit at either site (Table 3.4), these were not plotted for the purposes of clarity. Interpretations based on trends in the variations of mineral abundances need to be treated with some caution because of the assumptions and criteria used to determine normative abundances *e.g.,* no talc was allowed within the serpentine unit, although in reality some cross-over of serpentine into talc does occur. Normative abundances for accessory gibbsite, bassanite, alunite, chromite, rutile, apatite and asbolan were also not plotted as these were, with few exceptions, generally present in very low amounts (*e.g.,* < 0.5-1.0%) (Appendix 6, Tables A6.1 and A6.2).

Chlorite, as the main Al-bearing phase at depth in these profiles, increases in abundance moving up the weathering profiles from the serpentine and talc units, as the amount of available Al increases, where it tends to be mainly associated with nontronite in MM2 and MM3 and often shows the greatest abundance in association with this unit (Figures 3.10-3.19). Where chlorite does occur in association with either nontronite or saponite in MM2, it is generally the more abundant phase (Figures 3.10-3.13), whereas within MM3, nontronite and saponite are more abundant (Figures 3.14-3.19). This may reflect the greater Al content of the dominantly ortho- and meso-cumulate lithology of the underlying bedrock at MM2. In comparison, the bedrock at MM3 is predominantly adcumulate, which is relatively Al-poor (Hill *et al.,* 1996).

Surprisingly, quite low amounts of nontronite and saponite, of up to 20% but generally <10%, are present within the corresponding regolith units for MM2 (Figures 3.10-3.13). In contrast, abundances of nontronite and saponite within MM3 were generally greater than amounts for

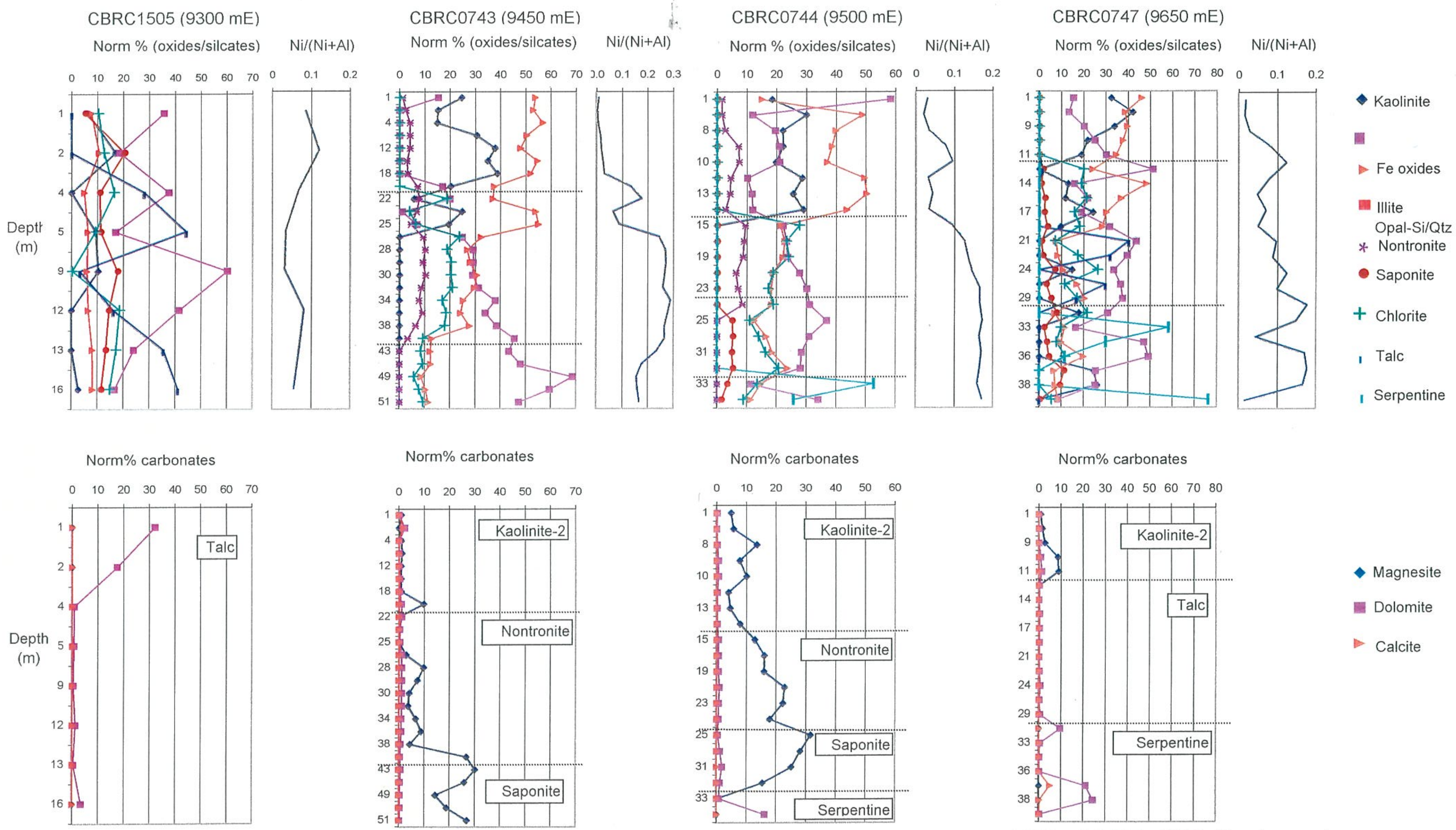

Figure 3.10. Normative mineral abundances for the main silicate, oxide and carbonate phases of selected RC holes along transect 26700 mN (MM2). Ni/(Ni+Al) ratios are also plotted for each drill hole. The main regolith units (PIMA) are also shown.

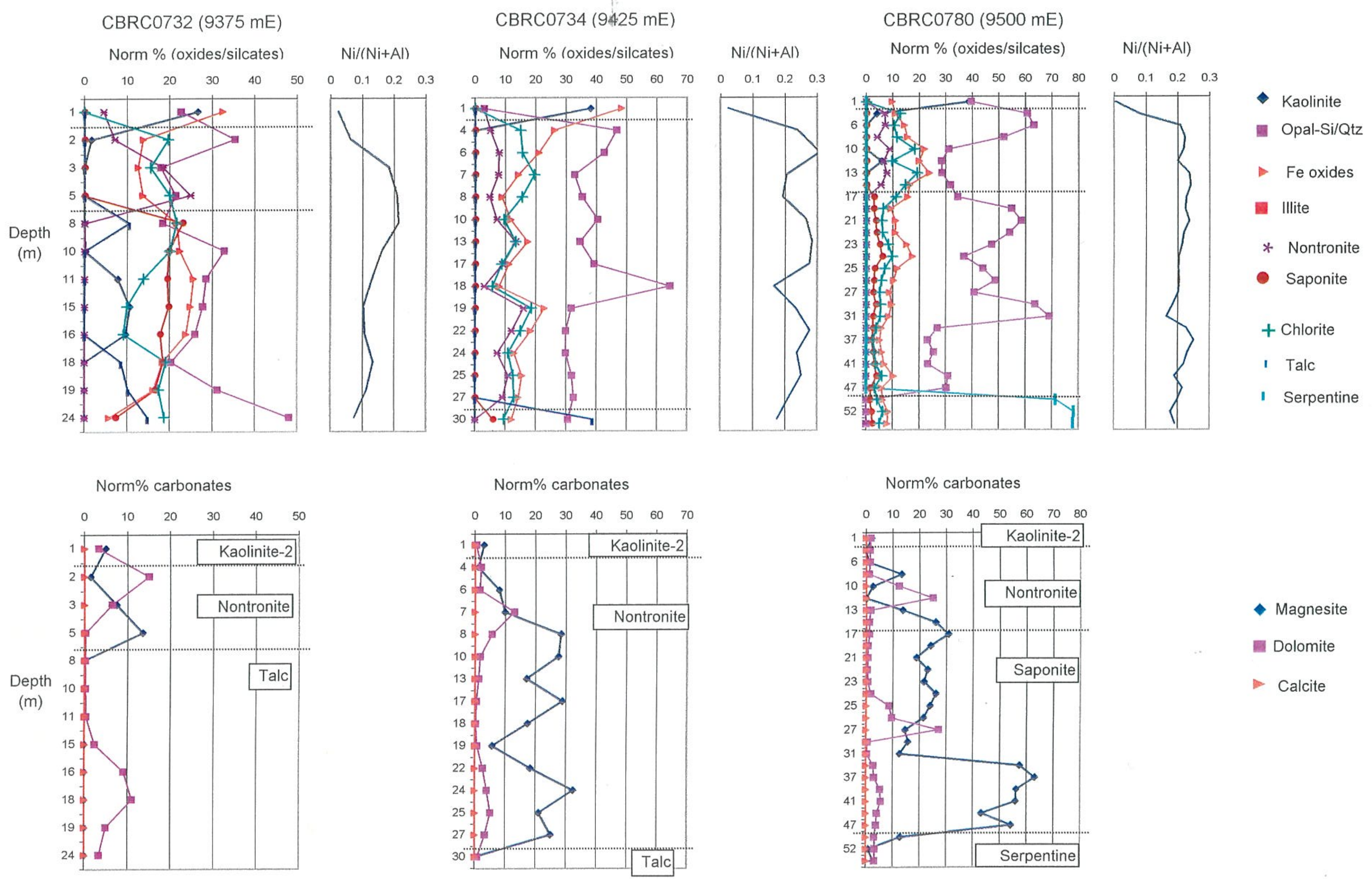

Figure 3.11. Normative mineral abundances for the main silicate, oxide and carbonate phases of selected RC holes along transect 26500 mN (MM2). Ni/(Ni+Al) ratios are also plotted for each drill hole. The main regolith units (PIMA) are also shown.

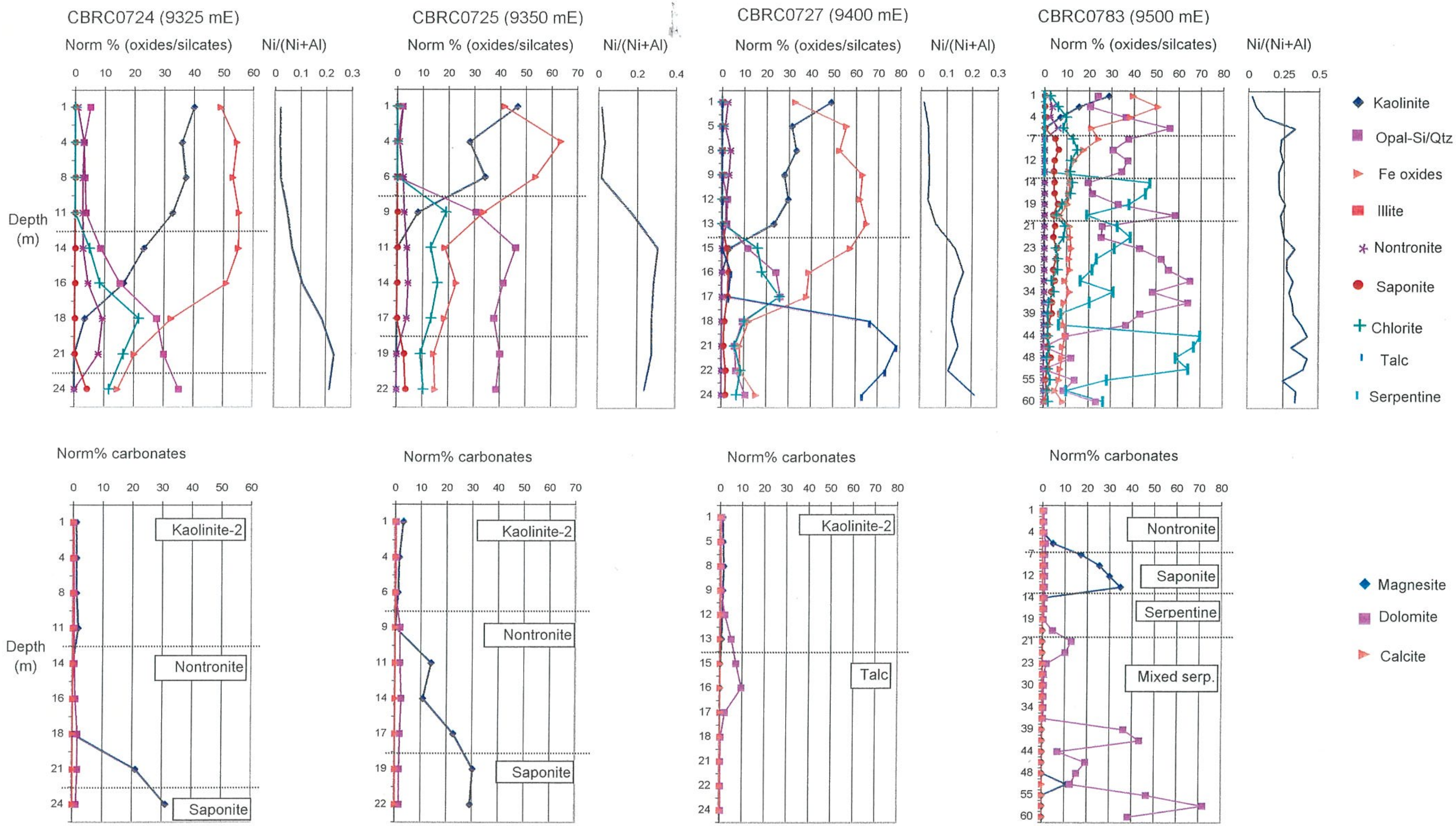

Figure 3.12. Normative mineral abundances for the main silicate, oxide and carbonate phases of selected RC holes along transect 26300 mN (MM2). Ni/(Ni+Al) ratios are also plotted for each drill hole. The main regolith units (PIMA) are also shown.

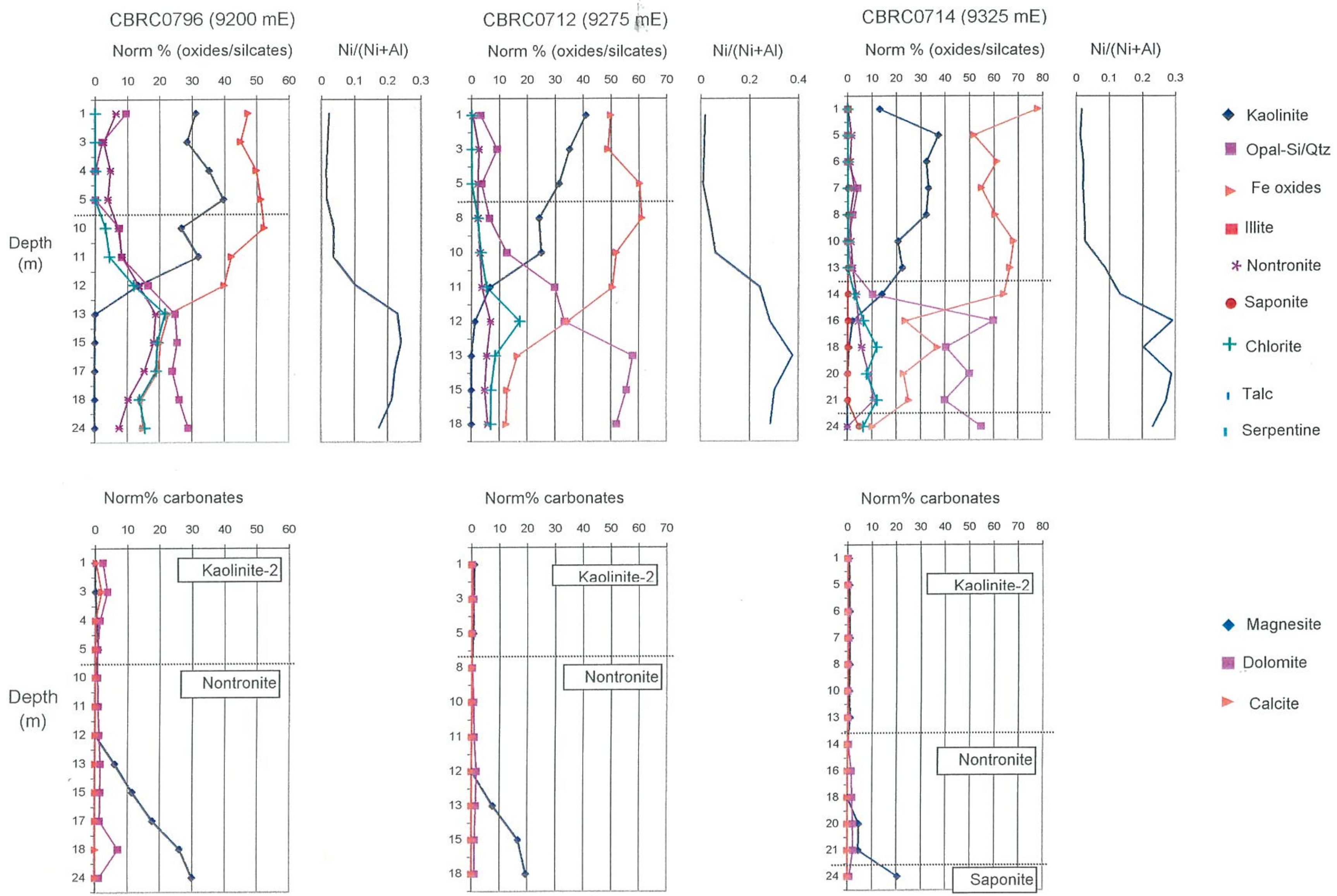

Figure 3.13. Normative mineral abundances for the main silicate, oxide and carbonate phases of selected RC holes along transect 26100 mN (MM2). Ni/(Ni+Al) ratios are also plotted for each drill hole. The main regolith units (PIMA) are also shown.

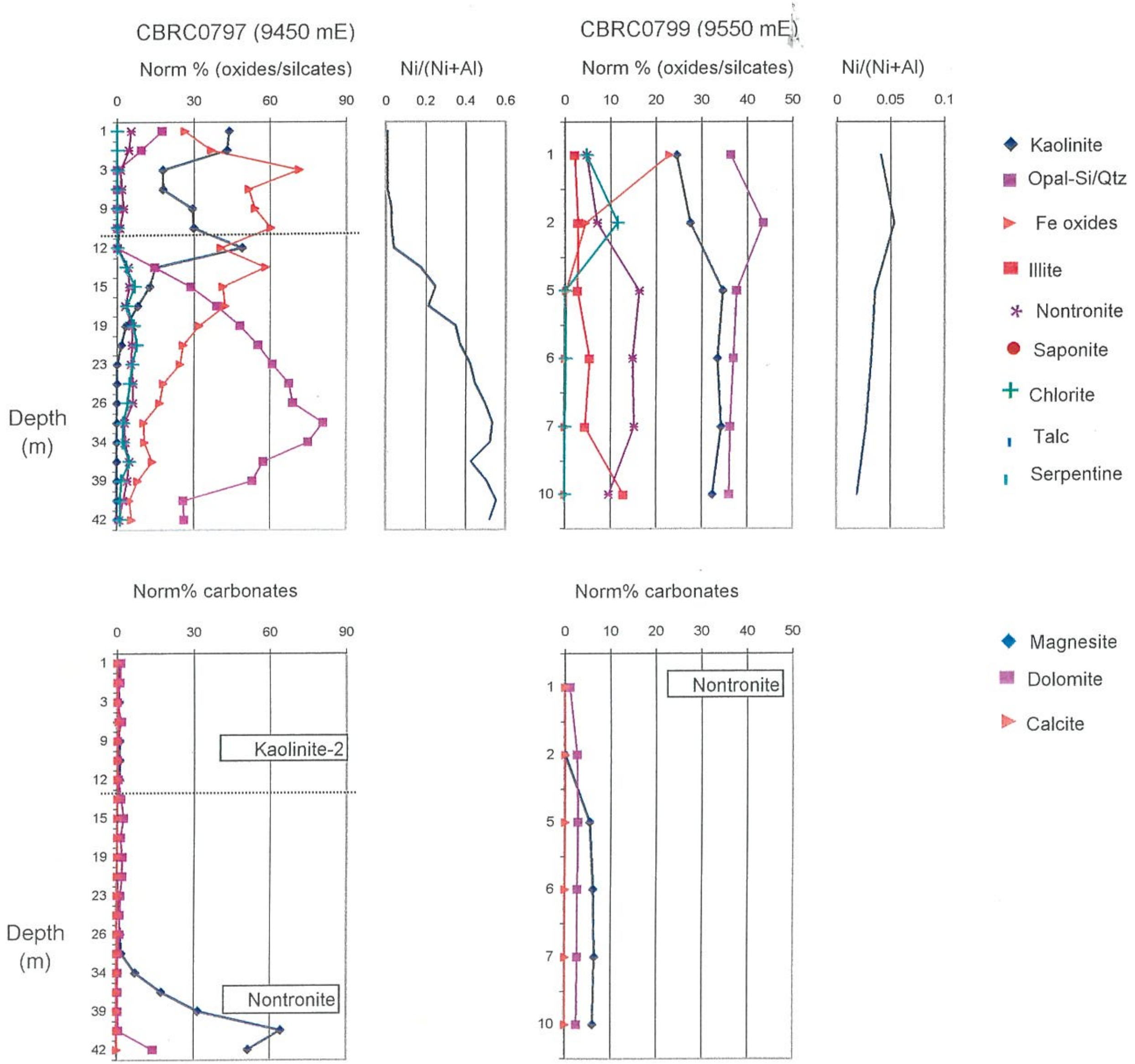

Figure 3.13. Continued..

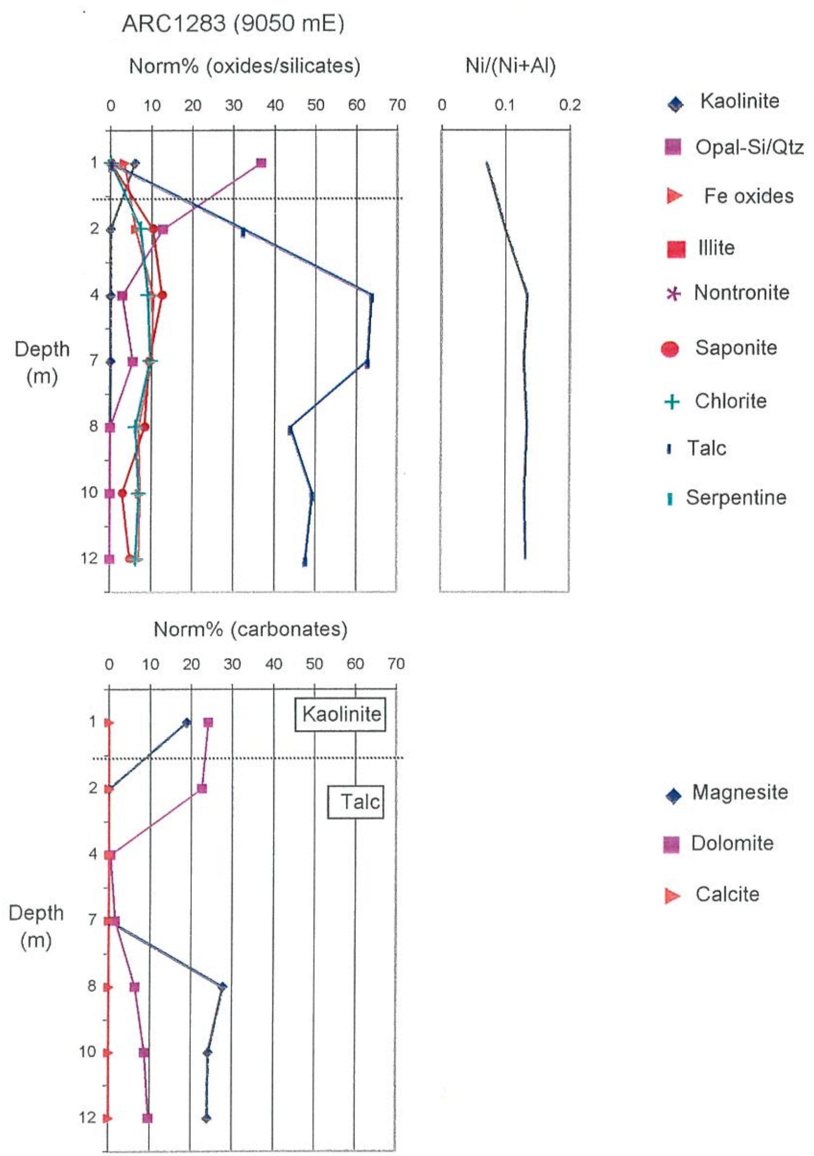

Figure 3.14. Normative mineral abundances for the main silicate, oxide and carbonate phases, and Ni/(Ni+Al) ratios of selected RC holes along transect 72550 mN (MM3). The main regolith units (PIMA) are also shown.

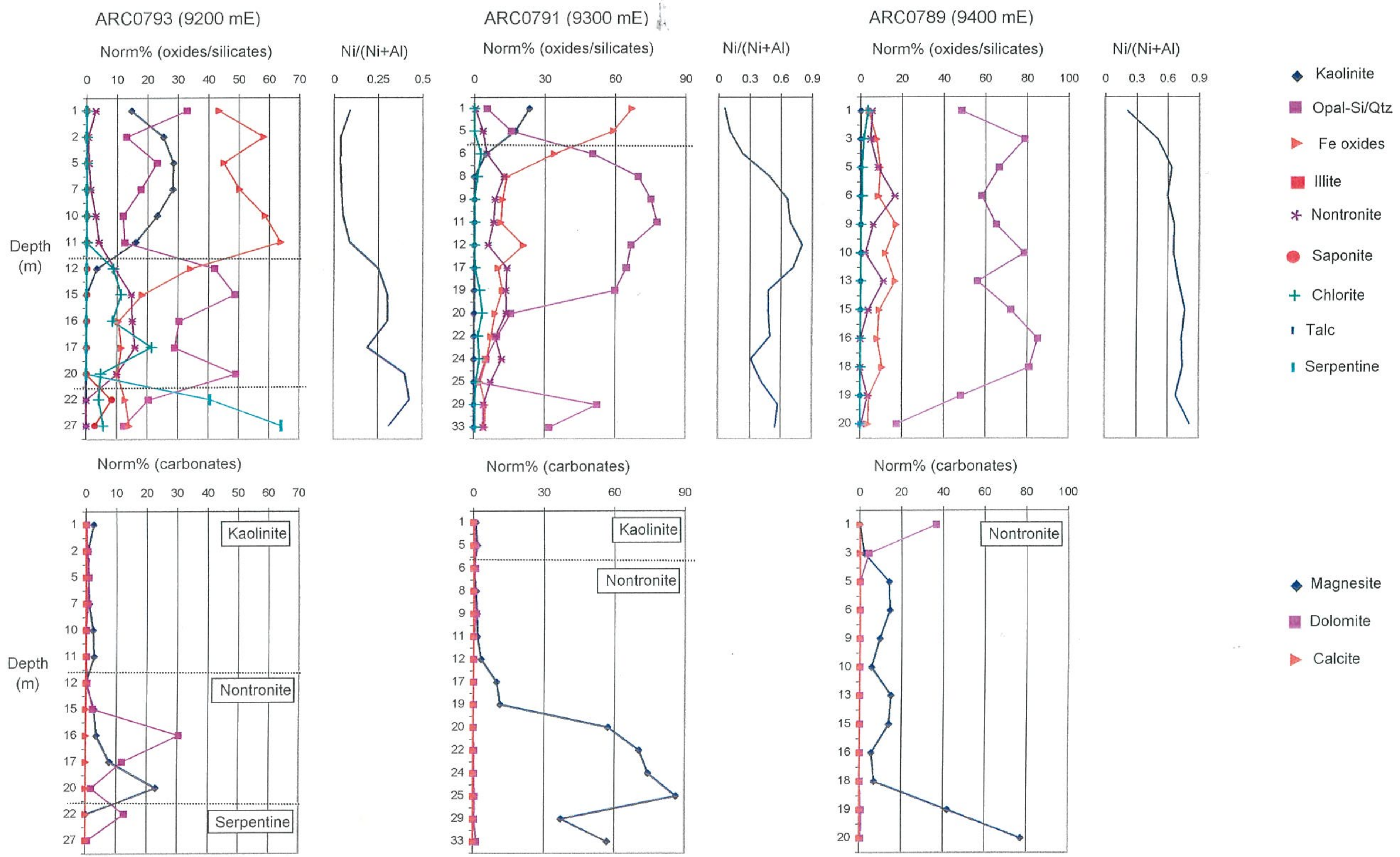

Figure 3.15. Normative mineral abundances for the main silicate, oxide and carbonate phases, and Ni/(Ni+Al) ratios of selected RC holes along transect 72500 mN (MM3). The main regolith units (PIMA) are also shown.

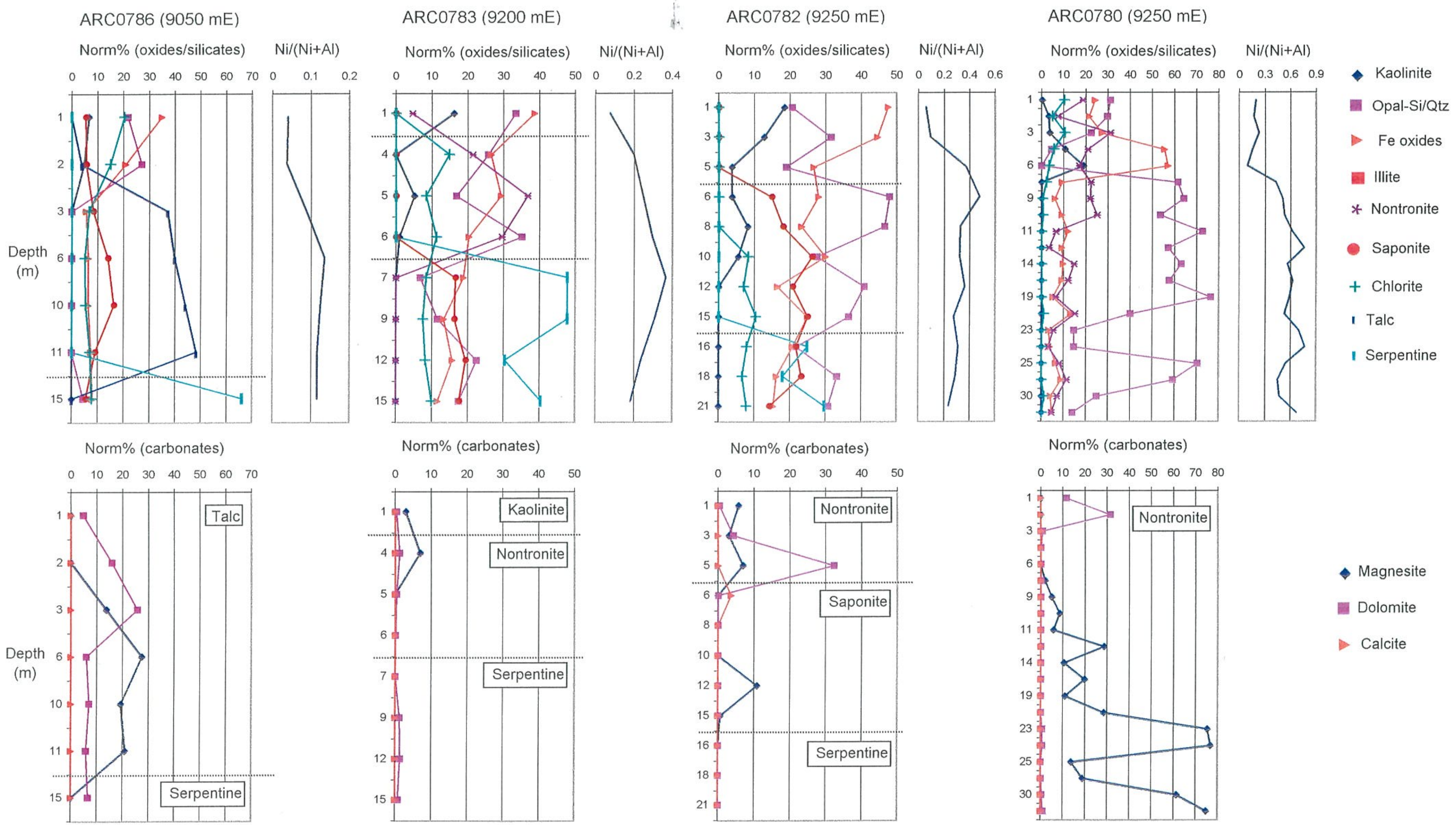

Figure 3.16. Normative mineral abundances for the main silicate, oxide and carbonate phases, and Ni/(Ni+Al) ratios of selected RC holes along transect 72300 mN (MM3). The main regolith units (PIMA) are also shown.

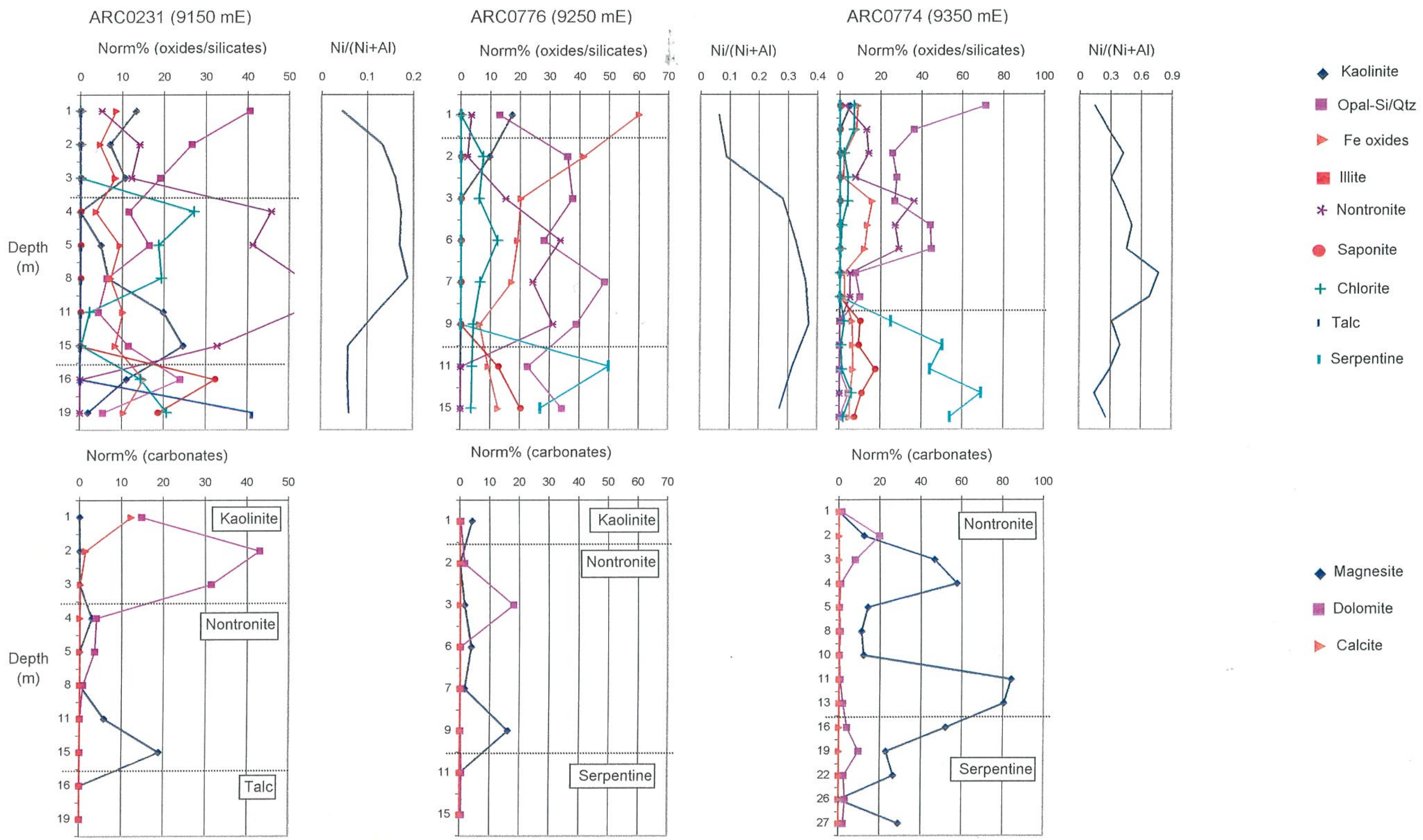

Figure 3.17. Normative mineral abundances for the main silicate, oxide and carbonate phases, and Ni/(Ni+Al) ratios of selected RC holes along transect 72100 mN (MM3). The main regolith units (PIMA) are also shown.

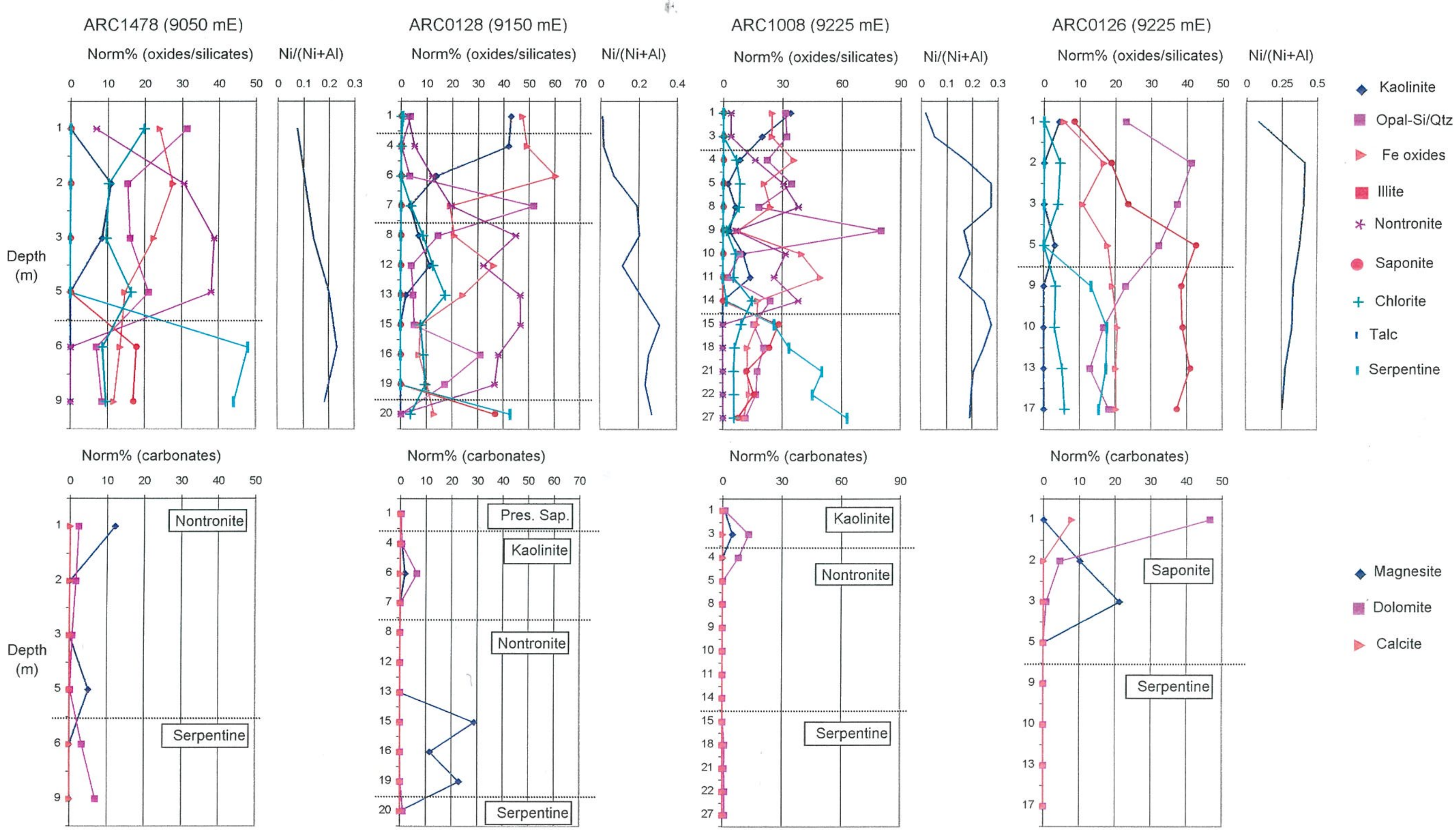

Figure 3.18. Normative mineral abundances for the main silicate, oxide and carbonate phases, and Ni/(Ni+Al) ratios of selected RC holes along transect 71900 mN (MM3). The main regolith units (PIMA) are also shown.

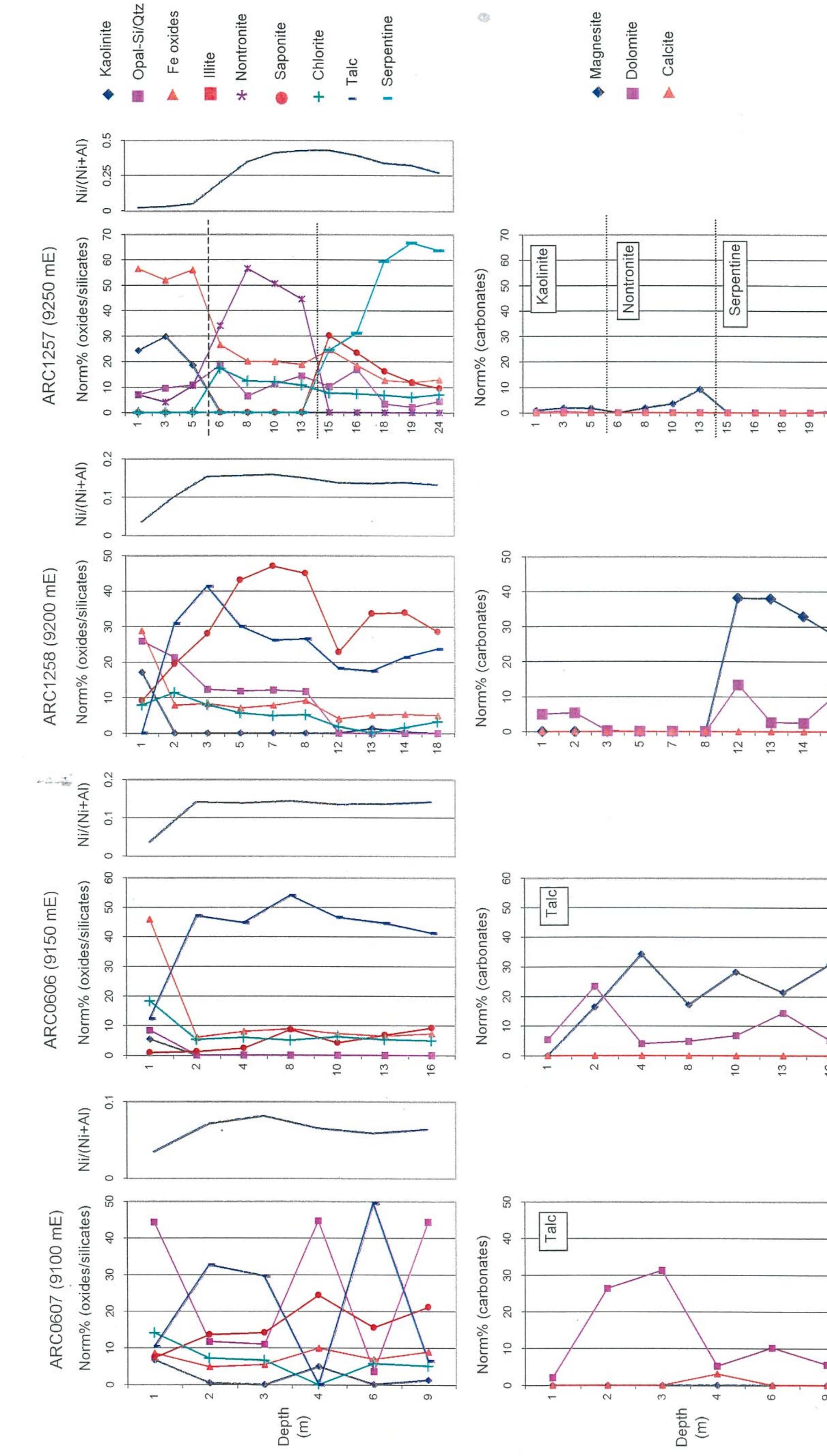

Figure 3.19. Normative mineral abundances for the main silicate, oxide and carbonate phases, and Ni/(Ni+Al) ratios of selected RC holes along transect 71650 mN (MM3). The main regolith units (PIMA) are also shown.

MM2, and amounted to 30-50 % of the normative mineralogy of the nontronite and saponite units for MM3, *e.g.*, RC holes ARC0231 (Fig. 3.17), ARC1478, ARC0128 (Fig. 3.18), and ARC01257 (Fig. 3.19).

Amounts of chlorite and nontronite decreased towards the nontronite/kaolinite contact, where the amount of kaolinite increases and replaces chlorite as the main Al-bearing, clay silicate phase and nontronite essentially disappears. Iron oxides are generally low in abundance within the serpentine and talc units, comprising in general 5-10 Norm%, but up to 10-20 Norm%, of the normative mineralogy of these units. Amounts of Fe oxides increase markedly from the upper portion of the nontronite unit and into the kaolinite unit where the abundance of Fe oxides can amount to 50-70 Norm%. Not surprisingly, kaolinite also shows the greatest abundance within the kaolinite unit for both MM2 and MM3, and can comprise up to 30-50 % of the normative mineralogy.

Amounts of SiO_2 for MM2 and MM3 are highly variable and, although can amount to 60-80% of the total phases present, were not related to depth even where Ni/Ni+Al values remained relatively constant at depth (Figures 3.10-3.19). In general, the greatest abundances of SiO_2 occurred within MM3 where the Ni/Ni+Al ratio suggested an adcumulate lithology for the parent rock. For example, RC holes CBRC0796 (Fig. 3.13), ARC0791, 0789 (Fig. 3.15), and ARC0780 (Fig. 3.16).

Magnesite and dolomite, as the main carbonate phases within profiles for MM2 and MM3, are present in quite variable amounts, which are unrelated to depth and can be equivalent to amounts of SiO2 (Figures 3.10-3.19). However, the presence of carbonate appear to be exclusive of SiO_2, with high amounts of carbonate, mainly as magnesite, correlating to low amounts of SiO_2. The occurrence of high amounts of one carbonate does not necessarily indicate high amounts of the other. Amounts of calcite are generally very low, with some near surface occurrences in MM2 and MM3, *e.g.*, holes CBRC0743 (Fig. 3.10), CBRC0796 (Fig.3.13), ARC0231 (Fig. 3.17) and ARC0126 (Fig. 3.18), which are most probably pedogenic carbonate or calcrete deposits.

Bassanite was present in significant amounts in MM2 for RC holes CBRC0796 (15 %) and CBRC0732 (18 %) (Appendix 6, Table A6.1) and in MM3 for RC holes ARC0126 (2 %), ARC0231 (15 %) and ARC1283 (7 %) (Appendix 6, Table A6.2) occurring in near surface samples. Major amounts of gibbsite are present for MM2 RC holes CBRC0797 (22 %), CBRC0727 (10 %), CBRC0743 (20 %), CBRC0725 (5 %) and CBRC0714 (4 %), occurring in the top 10-12 m within the kaolinite unit. Gibbsite was not present in regolith units below the kaolinite unit. No normative gibbsite was present in any RC holes at MM3 (Appendix 6, Table A6.2).

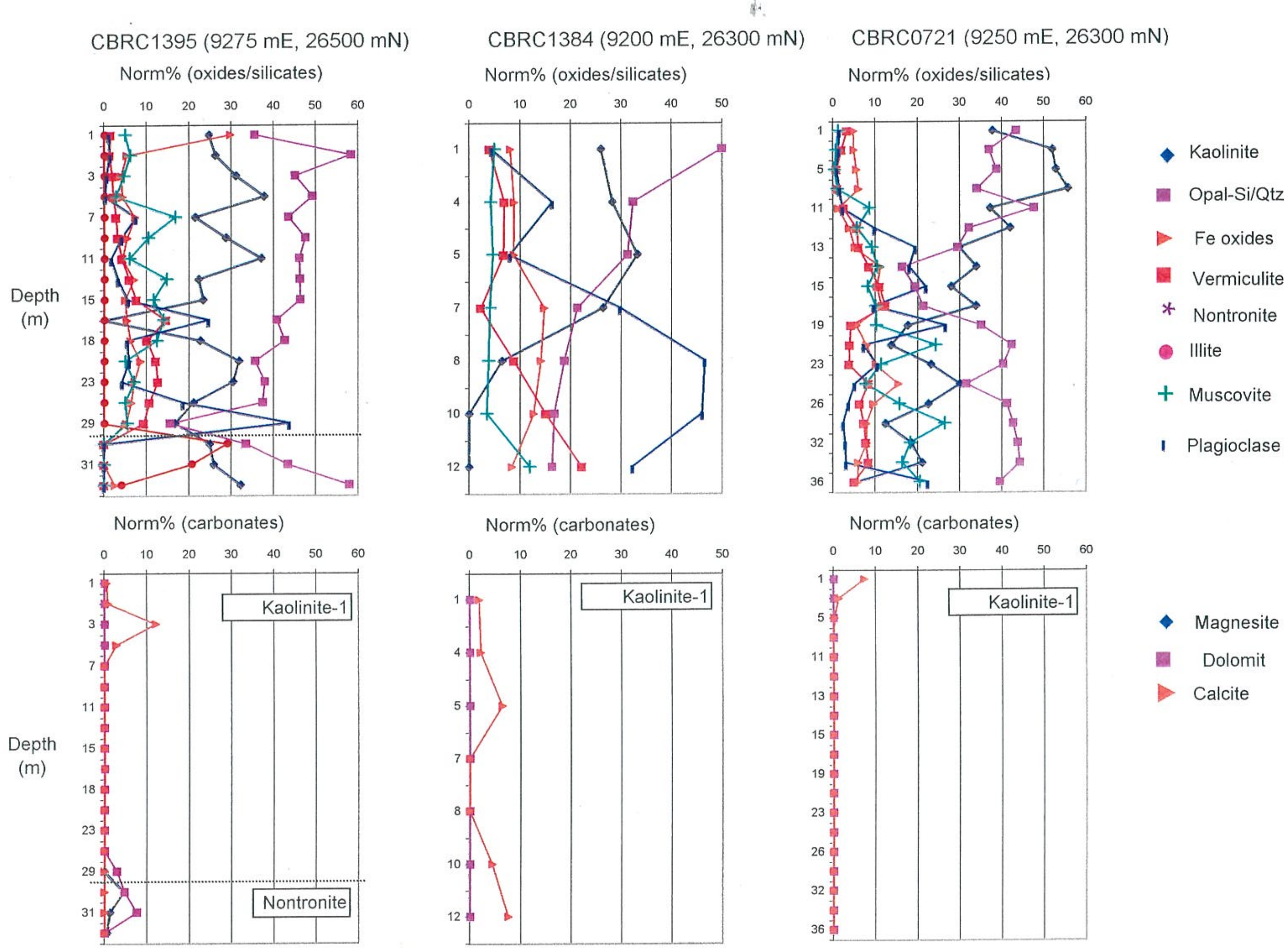

Figure 3.20. Normative mineral abundances for the main silicate, oxide and carbonate phases of selected RC holes representative of the kaolinite-1 (*I.e.,* channels clays) unit for MM2. The main regolith units (PIMA) are also shown.

Normative abundances for chromite within MM2 generally ranged from 0.1-1.0 %, whilst abundances within MM3 were greater, averaging between 1-2 % (Appendix 6). However, significant amounts of chromite were indicated for several RC holes within MM2: CBRC0714 (5.5%), CBRC0783 (5.2%), CBRC0747 (6.8%) and CBRC0743 (7.2%) (Appendix 6, Table A6.1). The greatest abundances of chromite generally occurred in sub-surface samples at or near the kaolinite/nontronite contact. In the case of RC hole CBRC0747 the greatest amounts of chromite occurred in the central portion of the talc unit (Appendix 6).

Amounts of rutile remained at background abundances of between 0 to 0.1 Norm% (Tables A6.1 and A6.2) throughout most of the profile, but increased in abundance to between 0.5-1.0 Norm% towards the top 5-10 m in MM2 and in the top 1-3 m in MM3, (Tables A6.1 and A6.2). Greatest abundances of rutile occurred in MM2 for RC holes CBRC0797 (2.4% at 3m) and CBRC0714 (2.6% at 1m) (Appendix 6, Table A6.1). Rutile is the ubiquitous form of Ti in acid, plutonic rocks (Deer *et al.*, 1980); high amounts of rutile in near surface samples at MM2 may, therefore, indicate input of Ti from an external source.

3.7.1 Normative mineralogy of channel clays for MM2

Normative mineral abundances for the channel clay regolith unit within MM2 are presented in Figure 3.20. Accessory phases chromite, rutile, apatite and asbolan, not shown in Figure 3.20, were present in only very low amounts of generally <0.5 %, with rutile being the most common. In addition, only those silicate and oxide phases present in significant amounts are plotted in Figure 3.20 for the purposes of clarity.

Amounts of the primary alumino-silicates plagioclase and muscovite are variable, but tend to decrease moving up the profiles (Fig. 3.20) reflecting the greater affect of weathering towards the surface. Consequently, the abundance of kaolinite increases towards the surface as the amount of available Al increases from the weathering of muscovite and, in particular, plagioclase. Indeed, kaolinite together with SiO_2, most likely as quartz, form the major phases of these profiles, and together comprise up to 80-90 % of the normative mineralogy (Fig. 3.20). These sediments have most probably accumulated by a series of depositional events, however, this is not clearly shown in trends of the mineralogy for these profiles.

Magnesite and dolomite are not the important carbonate minerals in these profiles. Minor amounts of magnesite to about 5% do occur in RC hole CBRC1395 (Fig. 3.20) but this is associated with the underlying nontronite unit. Calcite appears as the main carbonate phase but its occurrence is mainly restricted to within the top 5 m (Fig. 3.20).

Table 3.6. Summary of the regolith characteristics for the deposits at MM2 and MM3.

MM2: PIMA unit	Description and comments	Normative mineralogy	Interpreted regolith units: Anaconda^	Interpreted regolith units: Generic
#0: Kaolinite-1	Well crystalline kaolinite, with some illite and minor smectite at depth.	Kaolinite+SiO_2 ↑ up profile, to 80-90 Norm%. Plagioclase > muscovite ↓ up profile. <10% calcite in top 5m of profile	FZ or PC	Channel clays
#1: Kaolinite-2	Poorly crystalline kaolinite with locally developed opaline-Si. Gibbsite and alunite occur as local, minor phases.	Fe oxides ≥ kaolinite >> SiO_2 > nontronite > carbonate	FZ	Fe-rich, partially collapsed saprolite
#2: Nontronite	Locally developed opaline-Si, with minor amounts of kaolinite. Minor montmorillonite also locally present.	Fe oxides ≈ SiO_2 (≈ carbonate*) ≥ chlorite > nontronite	SM	Smectite
#3: Saponite	Saponite with some nontronite and opaline-Si locally developed.	SiO_2 (≈ carbonate*) > Fe oxides ≈ chlorite > saponite	SM (SA?)	Saprolite
#4: Talc	Mainly talc with minor amounts of kaolinite, smectite (as nontronite and montmorillonite) and opaline-Si.	SiO_2 ≥ talc ≈ chlorite ≈ Fe oxides ≥ saponite ≈ carbonate	SA	Saprolite
#5: Serpentine	Dominantly serpentine with some local alteration to saponite.	Serpentine ≈ SiO_2 > Fe oxides ≈ chlorite (≈ carbonate) > saponite	SA/UM	Saprock to fresh ultramafic
#6: Mixed serpentine	Variably weathered serpentine, with local alteration to saponite and talc.		SA/UM	

MM3: PIMA unit				
#0: Kaolinite with serpentine	Mainly kaolinite with minor serpentine preserved at the surface.	Kaolinite ≈ Fe oxides >>> serpentine > carbonate	FZ	Lateritic duricrust and preserved saprolite
#1: Kaolinite	Dominantly kaolinite with variably developed, local opaline-Si.	Fe oxides ≥ SiO_2 ≈ kaolinite >> nontronite > carbonate	FZ	Fe-rich, partially collapsed saprolite
#2: Nontronite	Locally developed opaline-Si, kaolinite and minor talc.	SiO_2 (≈ carbonate*) > nontronite ≈ Fe oxides > chlorite	SM	Smectite
#3: Saponite	Mainly saponite with locally developed opaline-Si.	SiO_2 > Fe oxides ≈ saponite > chlorite ≈ carbonate	SM (SA?)	Saprolite
#4: Talc	Local kaolinization and minor amounts of smectite (as nontronite with some saponite).	Talc (≈ carbonate) > saponite ≈ chlorite ≈ Fe oxides ≈ SiO_2	SA	Saprolite
#5: Serpentine	Mainly serpentine with some minor, variable alteration to saponite and talc.	Serpentine > saponite ≈ carbonate ≈ Fe oxides ≈ SiO_2 ≈ chlorite	UM	Saprock to fresh ultramafic

^ Abbreviations of the regolith terms used by Anaconda: PC = plastic clays; FZ = ferruginous zone; SM = smectite zone; SA = saprolite; UM = ultramafic.

* Indicates that abundances of the carbonate phases, magnesite and dolomite, are highly variable, but can be equivalent to amounts of SiO_2. However, in these cases carbonate and SiO_2 appear mutually exclusive (*i.e.*, high amounts of SiO_2 correlate with low amounts of carbonate, mainly as magnesite).

3.8 Summary

Regolith at the two deposits selected for this study was described primarily by using short-wave (SW) reflected infrared analysis (*i.e.*, PIMA) which identified the main regolith units within MM2 and MM3. PIMA spectroscopy, however, only provides an indication of the main Al-Mg-silicate phases present. Infrared analysis of the iron oxide mineralogy would necessitate a separate study and require the use of an infrared spectrometer, such as the Infrared Intelligent Spectrometer (IRIS) that covers the spectral characteristics of common iron oxide minerals, such as goethite and hematite, in the visible near infrared (VNIR) spectrum.

A more detailed examination of regolith mineralogy, than that provided by PIMA, was achieved by determination of normative mineral abundances based on geochemical data from the XRF analyses of selected RC drill samples.

However, this approach required a number of assumptions regarding the composition of several important phases, such as nontronite, saponite and chlorite. Other methods that could have been used as a check against the normative calculations, such as quantitative XRD (*i.e.*, Reitvelt analysis), themselves require a number of assumptions regarding the composition, structure and crystallinity of polymorphic phases, such as smectite. Despite this, the assumptions made for calculations of CIPW-Norms reflected the changes in the regolith mineralogy and, provided that carbonates comprise < 10 % of the sample, such calculations can provide useful information about the regolith.

A summary of the main regolith units, mineralogy and equivalent interpreted units of the deposits at MM2 and MM3 are presented in Table 3.6. Table 3.6 is the same as Table 3.4, but includes the dominant silicate and oxide mineralogy for each unit as determined from the normative calculations.

The regolith stratigraphy of the deposits is very similar, but the relative abundances of minerals within the regolith vary and reflect the general composition of the underlying bedrock at the two sites. For example, abundances of chlorite in the nontronite and saponite units at MM2 were greater than amounts of nontronite and saponite. In comparison, amounts of nontronite and saponite in MM3 were greater than abundances of chlorite in these units. This is a reflection of the greater Al content of ortho- and mesocumulates that comprise the main bedrock type at MM2, compared to Al-poor adcumulate which comprise the main bedrock type at MM3. The influence that local geomorphological factors, such as drainage and topography, have to the development of regolith mineralogy is also reflected in the mineralogy at the surface of the profiles for MM2 and

MM3 (Table 3.6). Interestingly, the kaolinite and nontronite units, in particular for those at MM2, show very high normative abundances of Fe oxides; a feature that was not detected using PIMA.

4.0 GEOCHEMISTRY: ELEMENT-REGOLITH ASSOCIATIONS

4.1 Introduction

This chapter provides a discussion of the geochemical characteristics of the regolith at MM2 and MM3. Element associations within MM2 and MM3 and their relationship to the regolith were investigated using MVS (Section 1.11.2), mass balance calculations (Section 1.11.6) and cluster analysis (Section 1.11.8). The geochemical data, supplied by Anaconda, was used to perform the 3-D modelling using MVS and cluster analysis. Mass balance calculations were based on the assumption that Zr is immobile during weathering. Zirconium data were obtained from XRF analyses of selected RC drill pulps. A better means of performing the mass balance calculations would to have been to use bulk density measurements. However, time constraints and the lack of suitable samples precluded this approach.

4.2 MVS modelling: block models for MM2 and MM3

Profiles of the regolith stratigraphy established for the study areas (Table 3.4) were kriged in conjunction with the geochemical data, supplied by Anaconda, using MVS. Areas of low confidence were removed by filtering of the raw data according to the confidence limits defined in Table 1.3. Block models of the distribution of Ni and Co at MM2 and MM3, produced using the 3D_PLUME module in MVS, at different cut-off grades are presented in Figures 4.1 and 4.2, respectively.

The models confirmed that the bulk of Ni and Co mineralization occurs in the nontronite unit at MM2, especially at higher concentrations (*e.g.*, > 1.0 % Ni and > 0.07 % Co) (Fig. 4.1). However, at lower cut-offs (*i.e.*, 0.2 % Ni and 0.02 % Co) in MM3 both metals are widely distributed in all units at both sites except for the uppermost kaolinite unit (*i.e.*, duricrust with preserved serpentine) (Fig. 4.2). Specific details of the distribution of Ni and Co (and other elements) at each site are discussed in the following sections.

4.2.1 MM2

A prominent Ni-poor zone (*i.e.*, <0.5 % Ni) is located at the NW-W corner of MM2 that is more or less coincident to the channel clay unit (*i.e.*, kaolinite-1). This is also shown for the lower Ni cut-

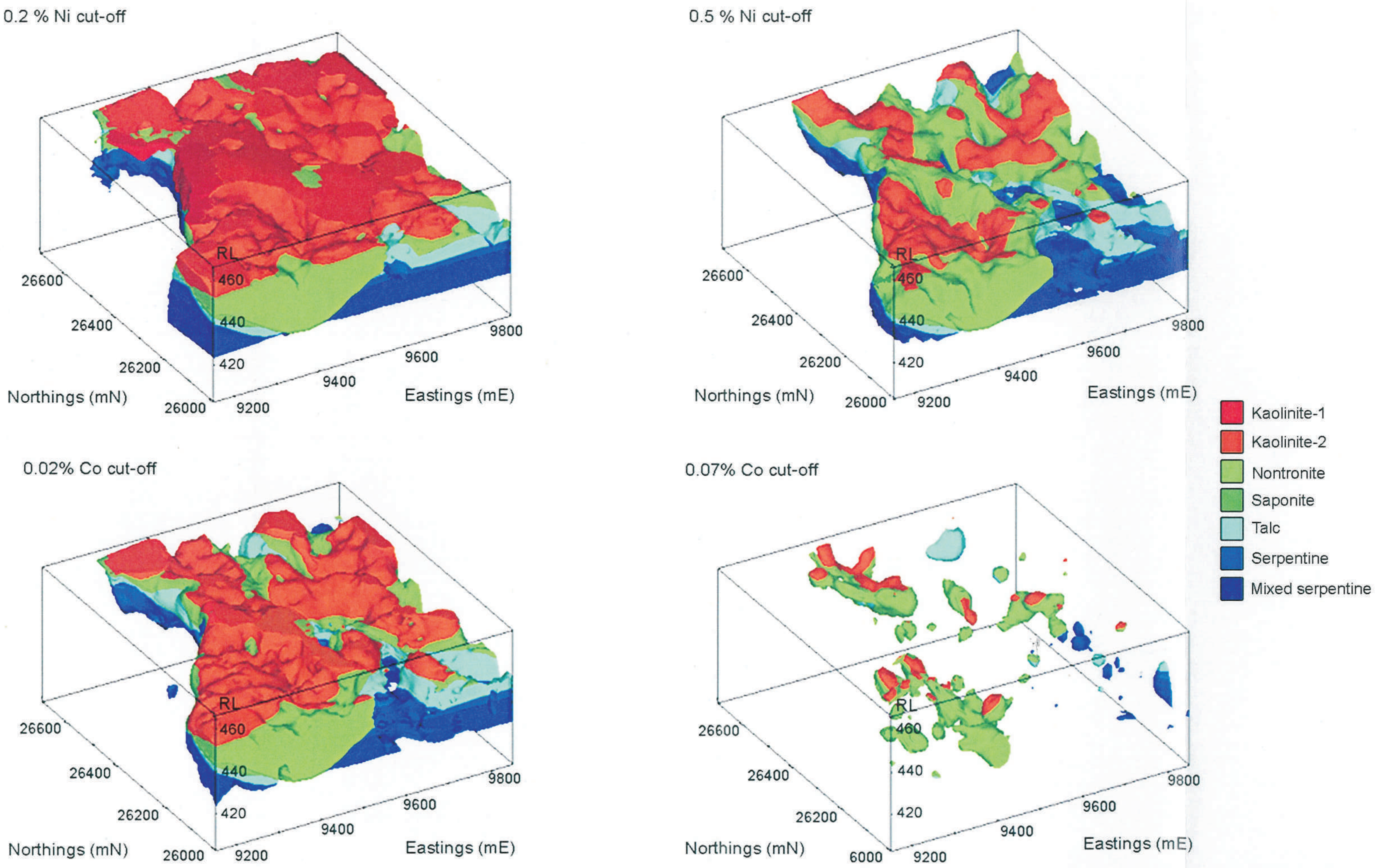

Figure 4.1. Three dimensional perspective views of the distribution of Ni and Co, for different cut-off grades, in the regolith at MM2. View is at 200° azimuth and 45° elevation, with x5 vertical exaggeration. The 'kaolinite-2' unit for MM2 is equivalent to the 'kaolinite' unit at MM3 (see Figure 4.2).

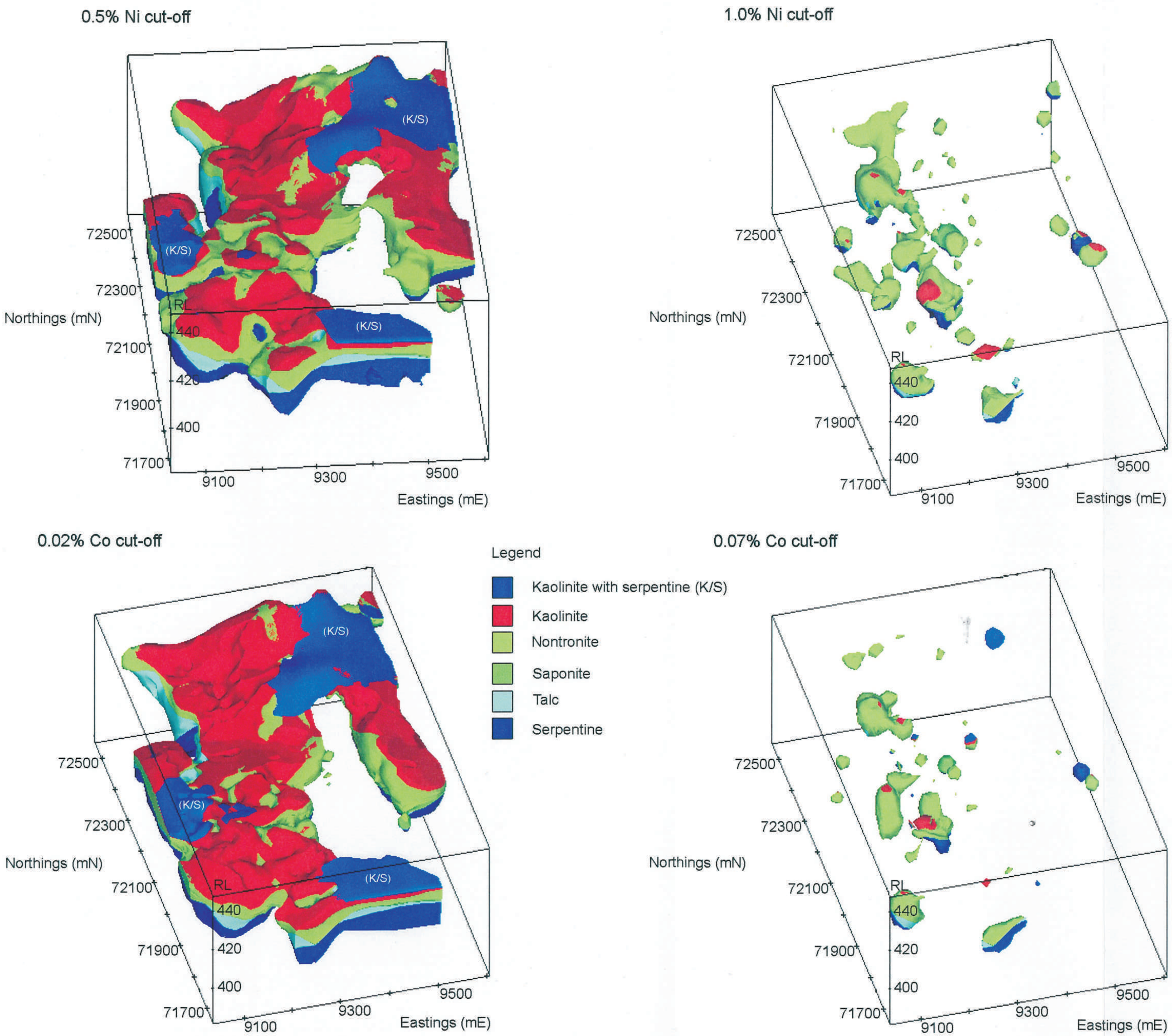

Figure 4.2. Three dimensional perspective views of the distribution of Ni and Co, for different cut-off grades, in the regolith at MM3. View of the >0.5 % Ni plume is at 185° azimuth and 30° elevation, with x5 vertical exaggeration. Remaining views are at 195° azimuth and 40° elevation, with x5 vertical exaggeration. The 'kaolinite' unit is equivalent to the' kaolinite-2' unit at MM2.

off >0.2 % and emphasizes the Ni-poor nature of these clays. The distribution of Co, for grades of >0.02 %, is very similar to that of Ni at 0.2 % and indicates that there has been very little lateral movement of either Ni or Co into these sediments at least for these concentrations.

A cross-shaped (*i.e.,* 'X'), topographical feature is evident, expressed mainly at the nontronite/kaolinite-2 contact and defines the western margin of the 0.5 % and 0.2 % Ni plumes and boundary to the channel clay unit (Fig. 4.1). This feature is discussed in more detail in Section 4.3.1.

4.2.2 MM3

A prominent Ni- and Co-poor zone is shown for the central region of MM3 at about 9400 mE at grades of >0.5 % Ni and 0.02 % Co (Fig. 4.2). Cobalt has a very similar distribution to that of Ni (Fig. 4.2), probably reflecting variations in the underlying cumulate lithology, with the Ni- and Co-poor areas relating to olivine adcumulate bedrock. This is discussed in more detail in Section 4.3.2.

The distributions of high grades of Ni (> 1.0 %) and, to a lesser extent, high grades of Co (>0.07%), reflects an enriched zone along the western-margin of the deposit as a sub-linear, 'boudinage' feature at about 9250 mE (Fig. 4.2). This zone of Ni and Co enrichment corresponds to areas where the underlying lithology is comprised mainly of olivine ortho- and meso-cumulates (Hill *et al.,* 1996).

4.3 MVS modelling: slices and regolith surfaces

Models of the distribution of Ni and Co, and other elements from the Anaconda data set, as slices through the regolith and for different regolith surfaces within MM2 and MM3 have been used to illustrate the influence that deposit scale lithological and structural features have on mineralization. Slices, as northing transects, through the regolith at MM2 and MM3, and views of regolith surfaces within the deposits were produced using the NORTHING_SLICE and GEOLOGICAL_SURFACE modules, respectively, within MVS.

The Ni/Ni+Al ratio has been used as a means of distinguishing olivine cumulate lithologies (*i.e.,* ortho-, meso and adcumulate) in fresh rock (Hill *et al.,* 1996). Models of the distribution of the Ni/Ni+Al ratio for different slices and regolith surfaces in MM2 and MM3 may also provide useful results when applied to the regolith and aid interpretation of element distributions in these deposits.

Slices through MM2 and MM3 are the same as those shown in Figures 3.4 (MM2) and 3.5 (MM3). Values of the Ni/Ni+Al ratio, kriged in conjunction with the regolith stratigraphy established for MM2 and MM3 (Table 3.4), were not filtered before processing in MVS, due to the very high and identical maximum and minimum confidence limits of 99.99998 % for the raw data. Element distributions and Ni/Ni+Al values are shown for three surfaces:

1. The top of the nontronite unit (or base of the kaolinite unit).

2. The top of the saponite unit (or base of the nontronite unit).

3. The top of the serpentine unit (or base of the talc unit).

These surfaces were considered the most informative for discussion; models for other regolith surfaces are not presented, but can be generated upon request. In addition, distributions of Cu, As and Ca for these surfaces were not presented, but can also be generated if requested.

Slices as northing transects through the regolith are presented in Figures 4.3 to 4.5 for MM2 and in Figures 4.6 to 4.8 for MM3. Views of the Ni/Ni+Al ratio for the different regolith surfaces within MM2 and MM3 are presented in Figure 4.9. Three-dimensional perspective views of element distributions for surfaces of the nontronite, saponite and serpentine units are shown in Figures 4.10 to 4.13 for MM2 and in Figures 4.14 to 4.17 for MM3.

The following discussion, therefore, integrates the results for the different views through the regolith (*i.e.*, as slices and surfaces) at MM2 and MM3.

4.3.1 MM2

General features and element distribution

Inspection of Figures 4.9 to 4.13 emphasizes the channel-like nature of the kaolinite-1 unit (*i.e.*, channel clays) overlying the nontronite unit at the western margin of the deposit. Concentrations of Ni, Co, Mg, Fe, Mn, Zn, Cr and values of the Ni/Ni+Al ratio are all very low in this unit, whereas the distribution of Al defines its shape very well, especially at the saponite and serpentine surfaces (Fig. 4.12). Modelling of more closely spaced drill holes (*e.g.*, <25 m spacings) would of course, given better definition of the unit.

The distributions of Fe, Al and Mg appear to be partly structurally controlled. High Al and Fe values coincide to low values of Mg; a result of the normal weathering of ultramafic rocks. An Al-poor zone within the serpentine and saponite units (Fig. 4.12), that may continue up into the lower portion of the nontronite unit (Fig. 4.4), may be related to the underlying lithology. The increase in Al and Fe contents towards the surface of the profile, in some cases defines very well the nontronite/kaolinite contact. For example, in transect 26250 mN (Fig. 4.4).

The highest concentrations of Cr (Figure 4.5) generally occur with the highest concentrations of Fe (Figure 4.4) in the upper profile (*i.e.,* kaolinite-2 unit) associated with the north and south apical zones of the conjugate fault-set. The distribution of Zn (Figures 4.5 and 4.13) is associated with the occurrence of Ni (Figures 4.3 and 4.10). This is discussed in more detail in Section 4.4.

The distribution of Co appears generally related to that of Ni (see Figures 4.3 and 4.10). However, the highest Co grades do not correlate with the highest grades of Ni. This is particularly evident in comparisons of the Ni and Co distribution for slices through the regolith (Fig. 4.3). In addition, Co mineralization occurs mainly at or below the kaolinite/nontronite boundary (*e.g.,* see transect 26700 mN, Fig. 4.3).

Lithological controls

Interpretation of the distribution of the Ni/Ni+Al ratio at MM2 is confused by strong structural overprinting as evidenced by faulting that appears unrelated to any lithological controls. A generally mixed, underlying lithology of ortho- and mesocumulates is indicated by values of the Ni/Ni+Al ratio of mainly < 0.4, with no specific lithological features evident within the talc and serpentine units that may be related to structural or bedrock characteristics of the Kilkenny syncline (*i.e.,* there is no evidence of easterly dipping features with the serpentine unit). High Ni/Ni+Al values > 0.4 in the south area of the deposit (Fig. 4.3) are located in the apex of the southern extension of the fault-set (Fig. 4.9). This may represent a local gradation to an adcumulate parent rock, which is reflected in the serpentine-talc-saponite units (Fig. 4.3) due mainly to low Al (Fig. 4.4) rather than to high Ni contents (Fig. 4.3).

Structural controls

A strong structural control is reflected well by values of the Ni/Ni+Al ratio (Fig. 4.9) and in element distributions for regolith surfaces within the deposit (Figures 4.10 to 4.13). An approximately NW-SE and NNE-SSW, cross-shaped (*i.e.,* 'X') topographical feature, expressed mainly by tighter contour intervals, is evident in the surface of the serpentine unit (Fig. 4.9).

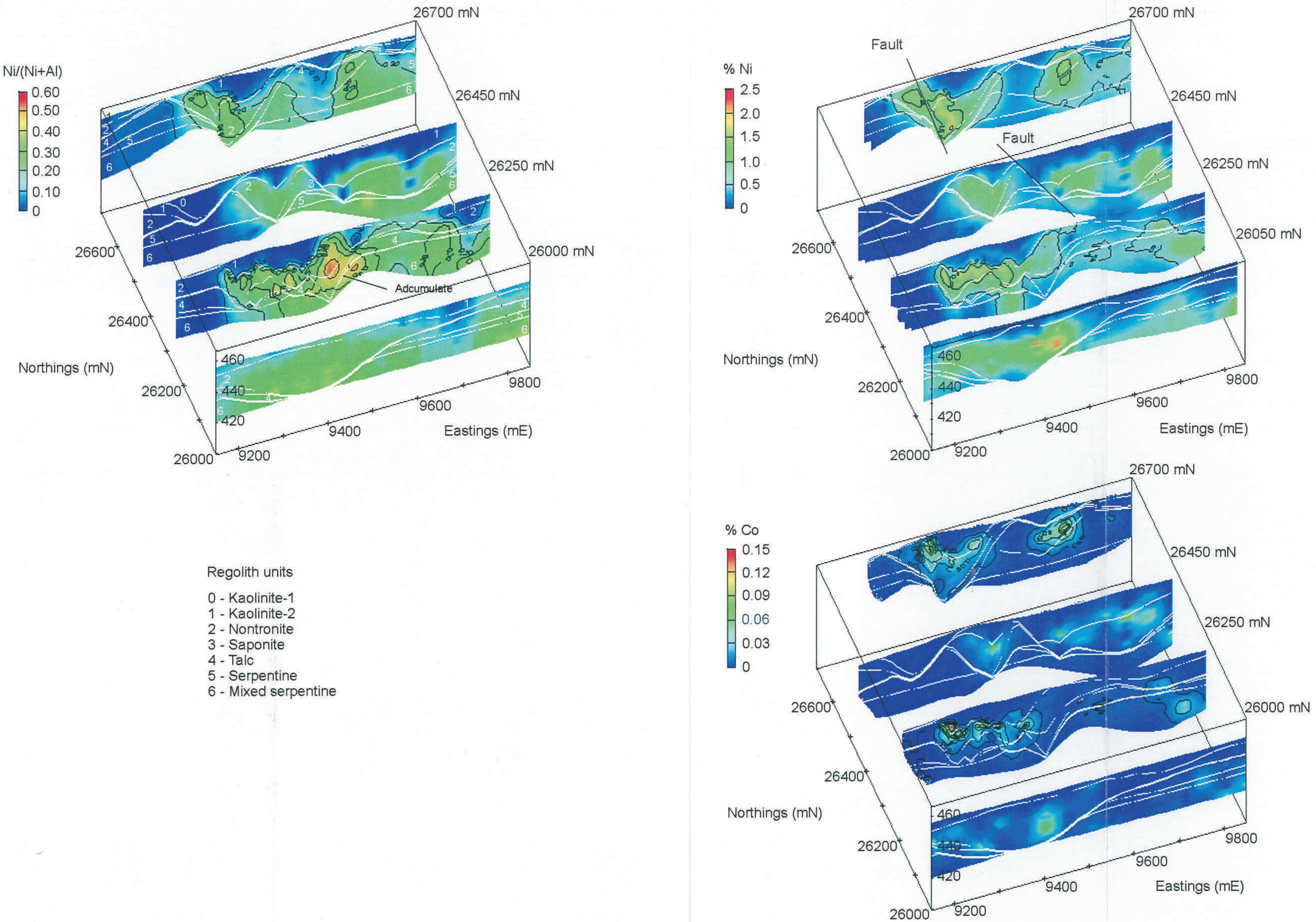

Figure 4.3. Three dimensional perspective views of the distribution of values of the Ni/Ni+Al ratio, Ni and Co for transects through the regolith at MM2. Transects are the same as in Figure 3.4. Regolith units have been separated (*i.e.*, white lines in slices) to show individual units. Views are at 200° azimuth and 50° elevation, with x5 vertical exaggeration.

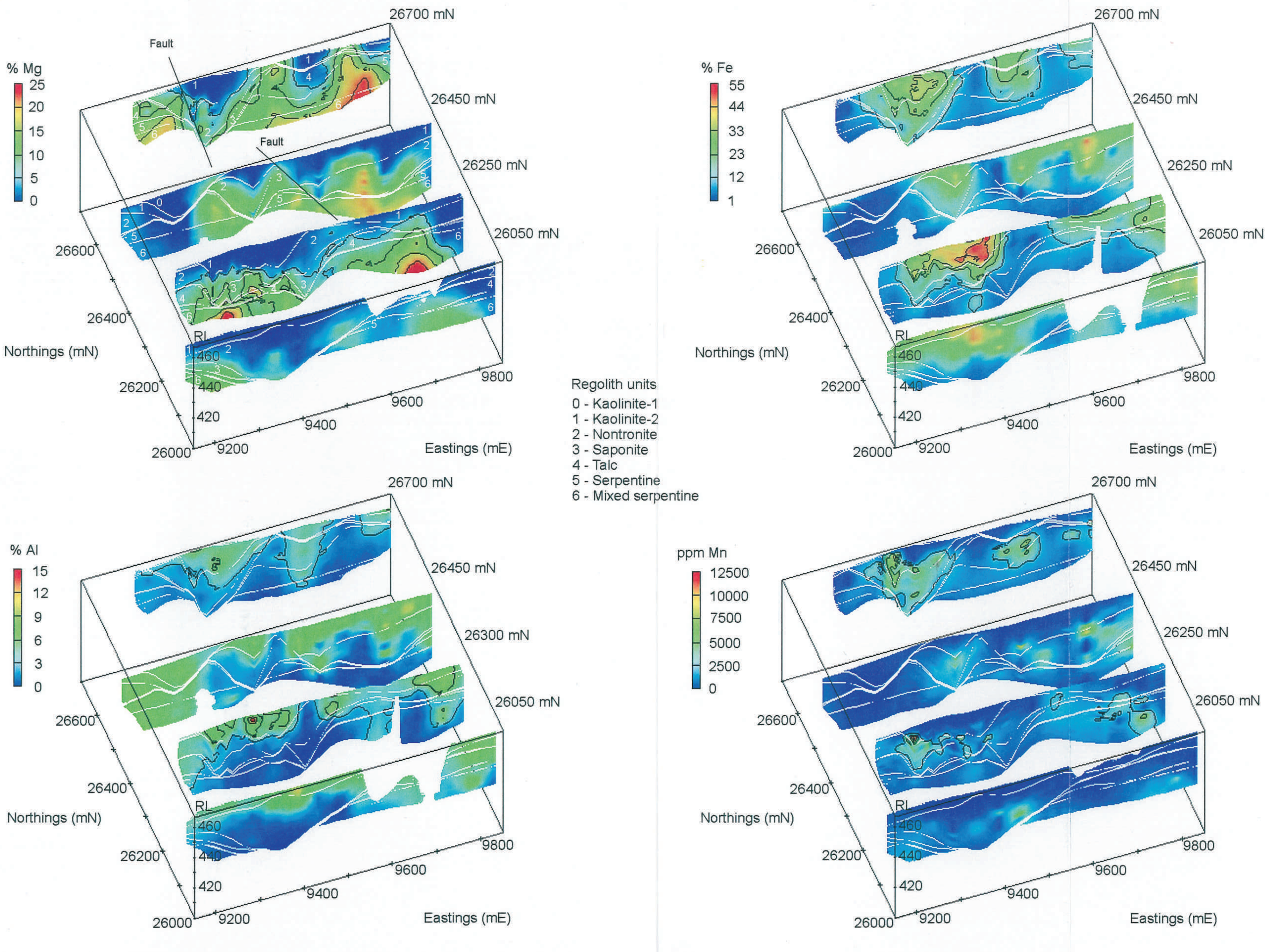

Figure 4.4. Three dimensional perspective views of the distribution of Mg, Fe, Al and Mn for transects through the regolith at MM2. Transects are the same as in Figure 3.4. Regolith units have been separated (*i.e.*, white lines in slices) to show individual units. View is at 200° azimuth and 50° elevation, with x5 vertical exaggeration. Blank (*i.e.*, white) areas for some transects are areas of low confidence that have been filtered out of the data.

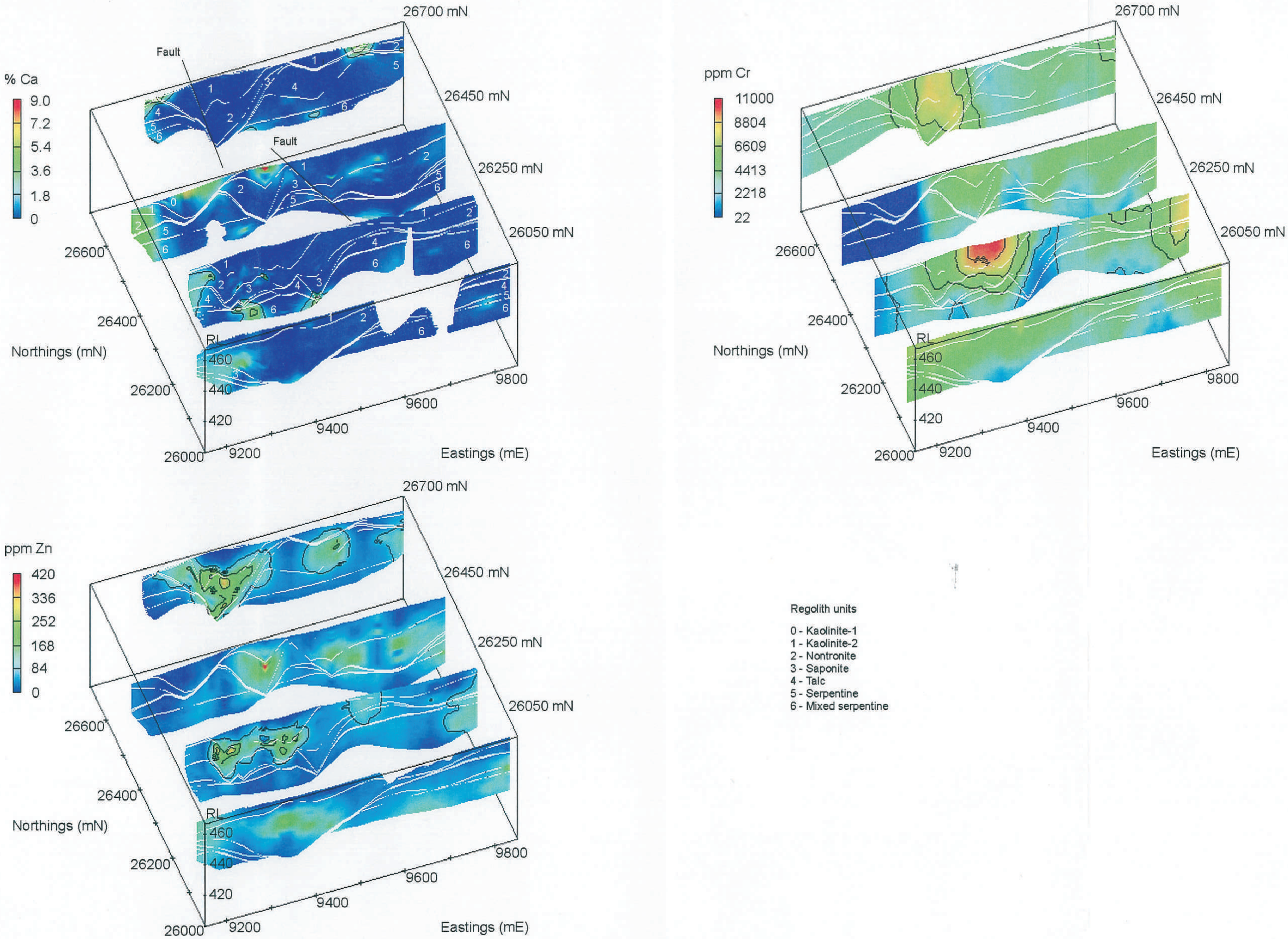

Figure 4.5. Three dimensional perspective views of the distribution of Ca, Cr and Zn for transects through the regolith at MM2. Transects are the same as for Figure 3.4. Regolith units have been separated (*i.e.*, white lines in slices) to show individual units. View is at 200° azimuth and 50° elevation, with a x5 vertical exaggeration. Blank (*i.e.*, white) areas for some transects are areas of low confidence that have been filtered out of the data.

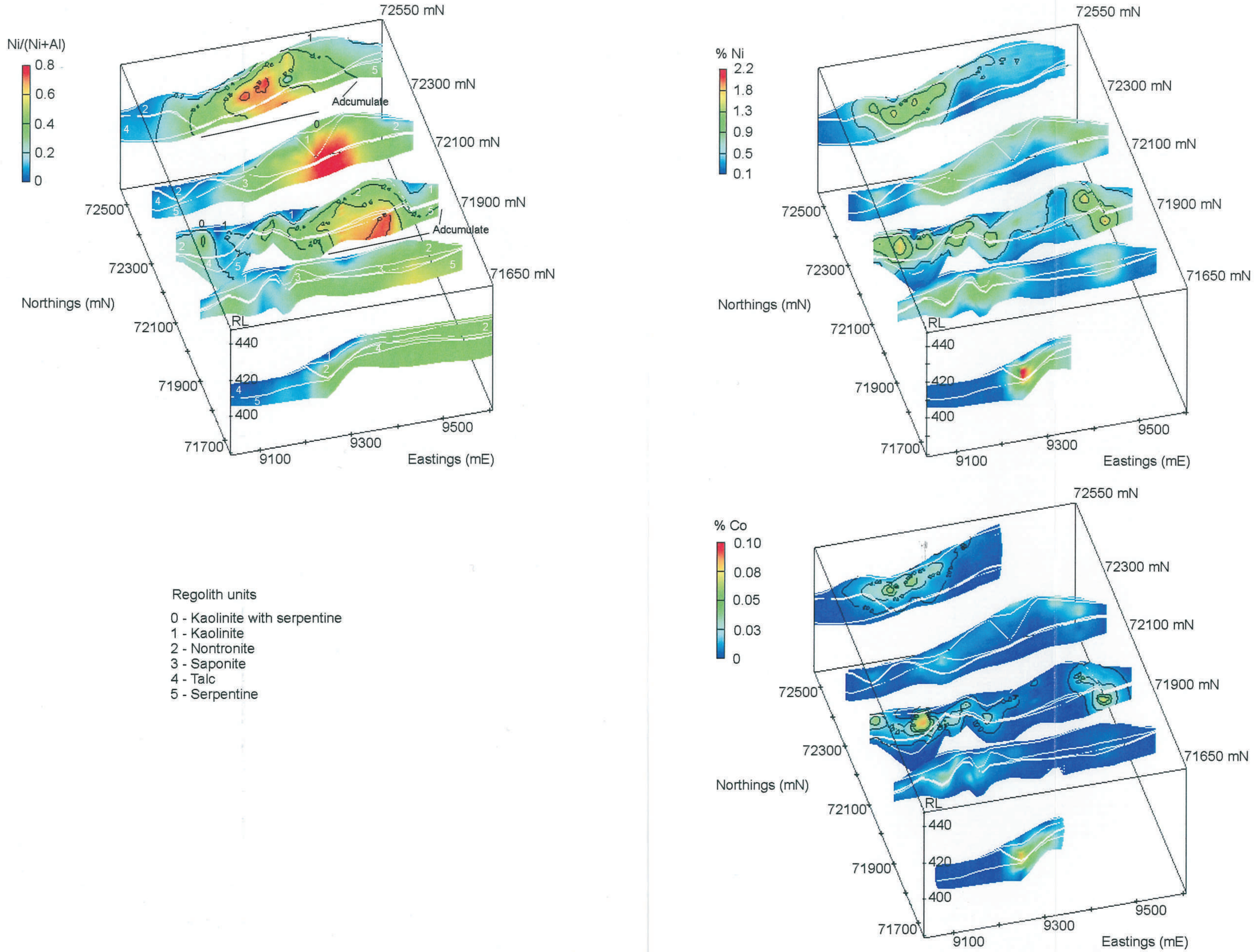

Figure 4.6. Three dimensional perspective views of the distribution of the Ni/Ni+Al ratio, Ni and Co for transects through the regolith at MM3. Transects are the same as in Figure 3.5. Regolith units have been separated (*i.e.*, white lines in slices) to individual units. Views are at 195° azimuth and 40° elevation, with x5 vertical exaggeration.

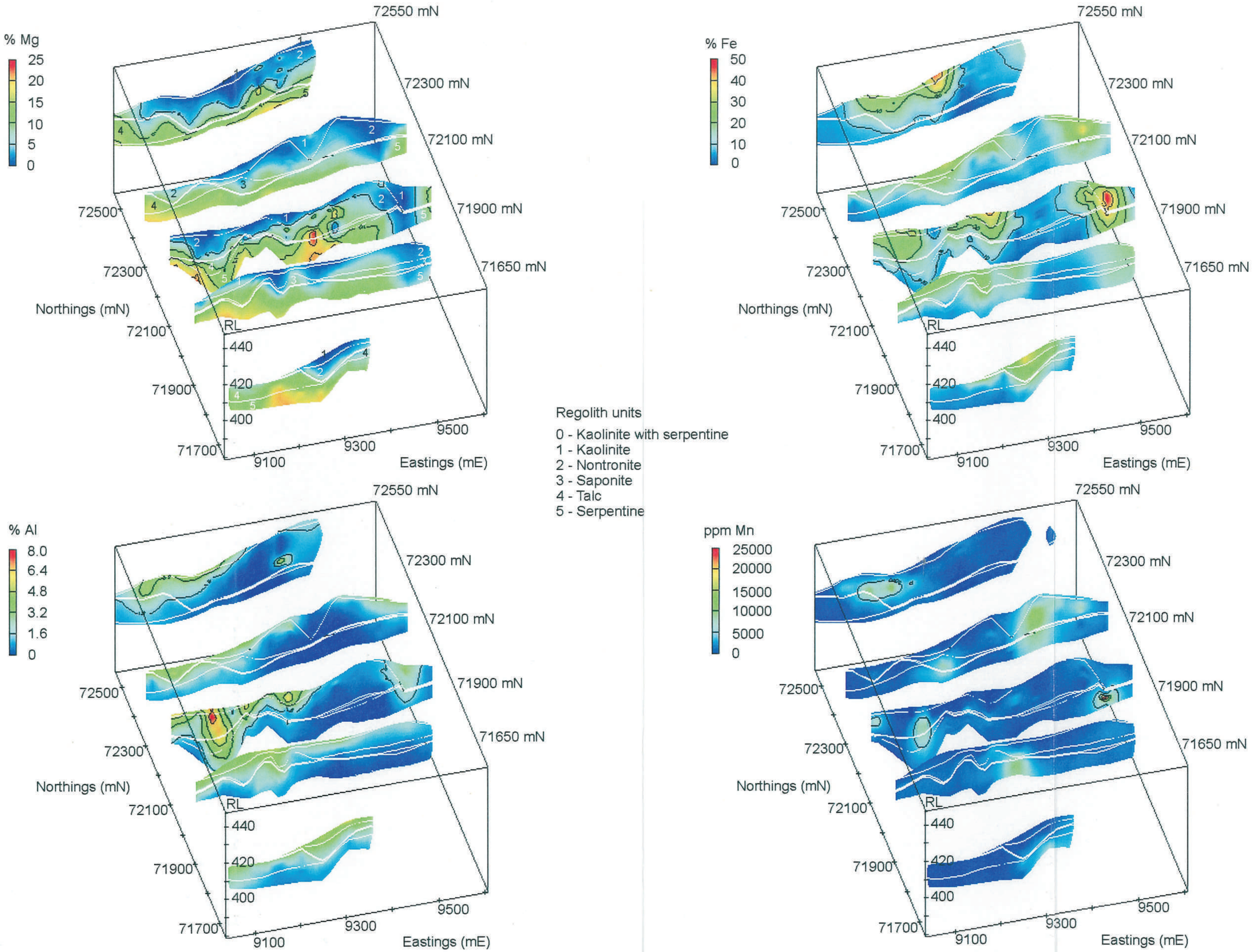

Figure 4.7. Three dimensional perspective views of the distribution of Mg, Fe, Al and Mn for transects through the regolith at MM3. Transects are the same as in Figure 3.5. Regolith units have been separated (*i.e.*, white lines in slices) to show individual units. Views are at 195° azimuth and 40° elevation, with x5 vertical exaggeration. Blank (*i.e.*, white) areas for some transects are areas of low confidence that have been filtered out of the data.

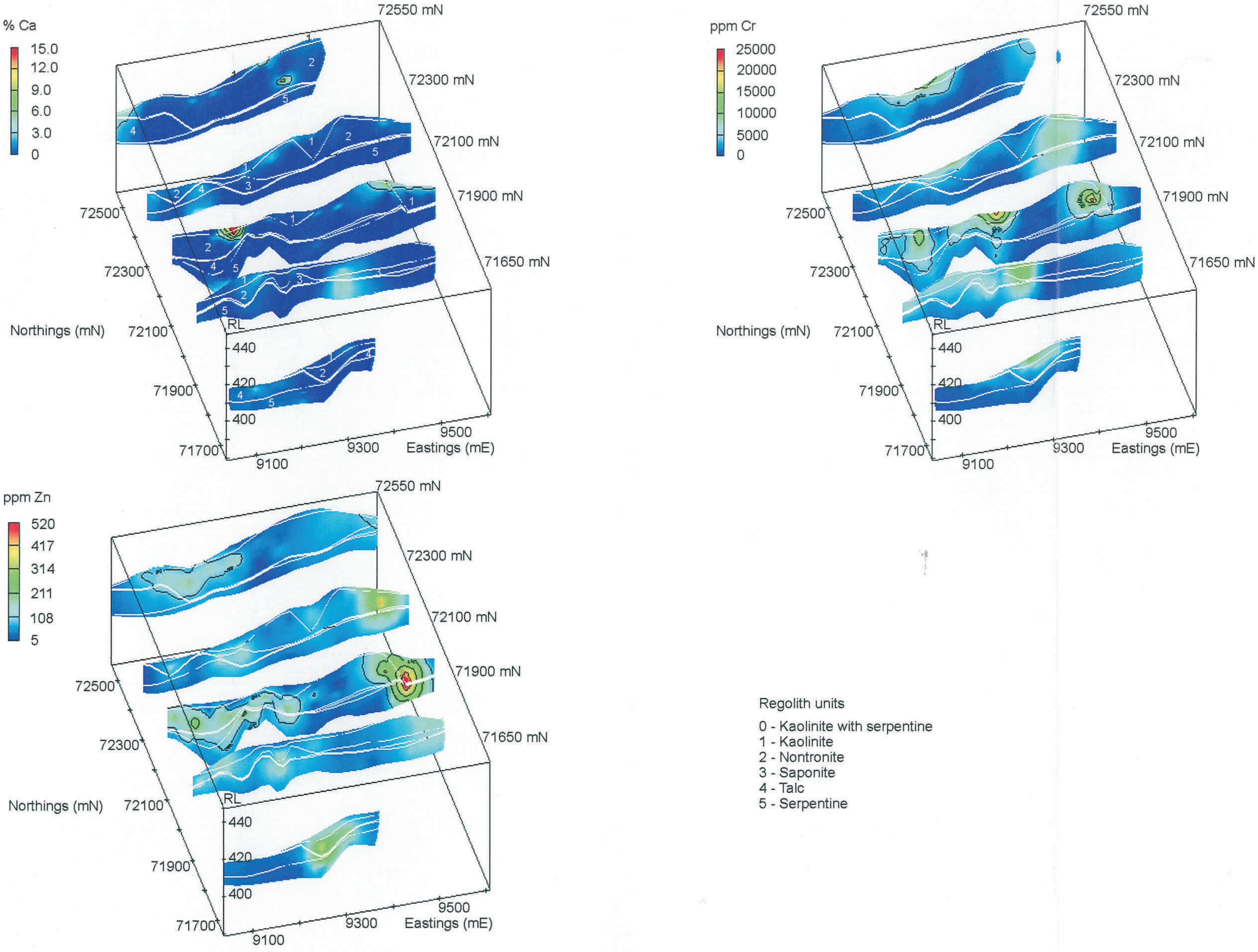

Figure 4.8. Three dimensional perspective views of the distribution of Ca, Cr and Zn for transects through the regolith at MM3. Transects are the same as for Figure 3.5. Regolith units have been separated (*i.e.*,white lines in slices) to show individual units. View is at 195° azimuth and 50° elevation, with x5 vertical exaggeration.

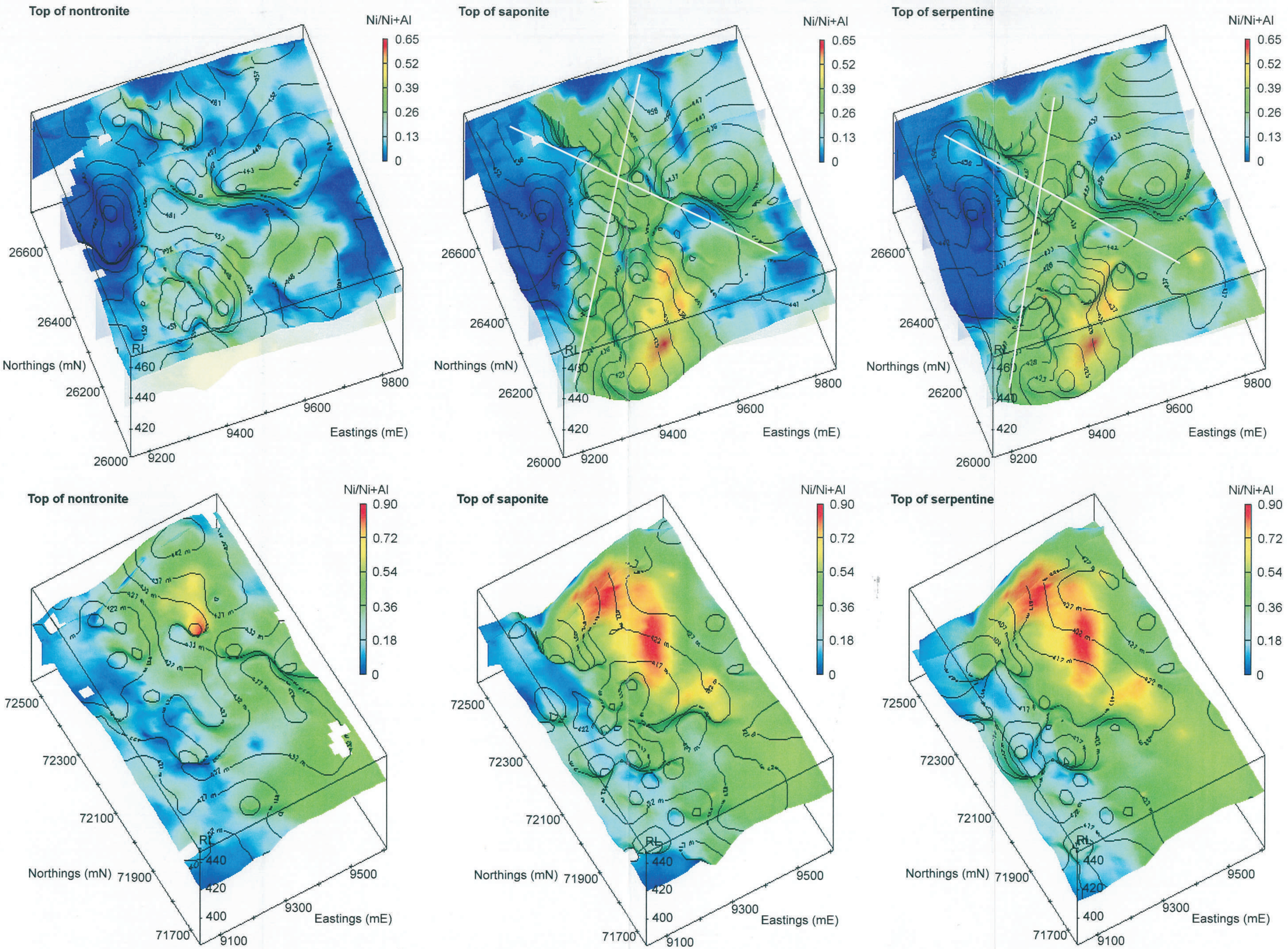

Figure 4.9. Distribution of Ni/Ni+Al values for different surfaces in the regolith at MM2 and MM3. Transects for northings 26050, 26250, 26450 and 26700 mN are shown in MM2 as transparent slices through the regolith. Transect 72500 mN is also shown as a slice through the regolith at MM3. RL contours are shown (*i.e.*, black lines) for each surface. Views for both MM2 and MM3 are at 200° azimuth and 50° elevation, with x5 vertical exaggeration. Blocked out (*i.e.*, white) areas for some surfaces are areas of low confidence that have been filtered out of the data. White lines at the surface of the saponite and serpentine units represent the expression of an intersecting fault-set within MM2.

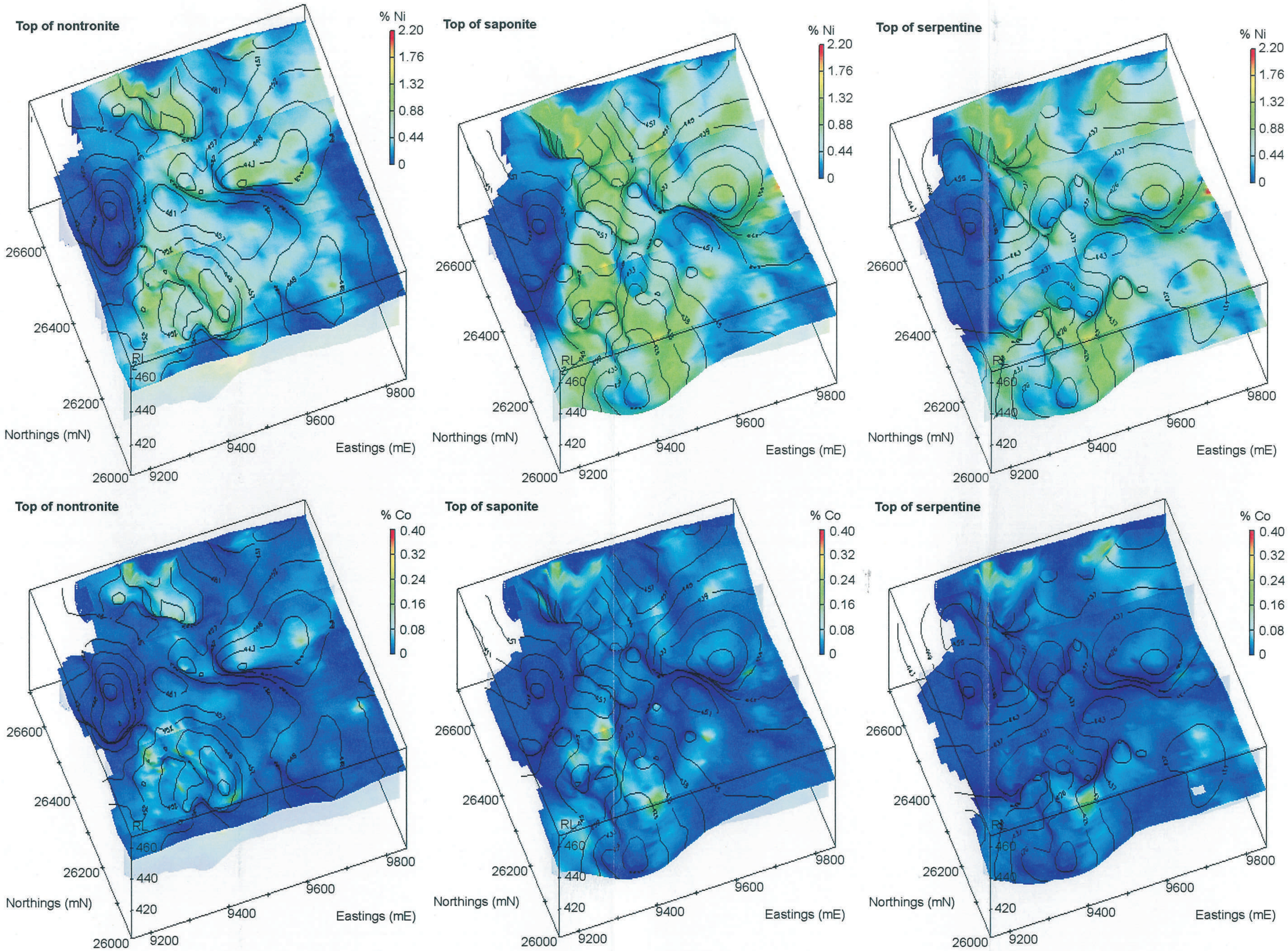

Figure 4.10. Distribution of Ni and Co for different regolith surfaces at MM2. RL contours, at either 4 or 5 m intervals, are shown (*i.e.*, black lines) for each surface. View is at 200° azimuth and 50° elevation, with x5 vertical exaggeration. Transects for northings 26050, 26250, 26450 and 26700 mN are also shown as transparent slices through the regolith. Blocked out (*i.e.*, white) areas for some surfaces are areas of low confidence that have been filtered out of the data.

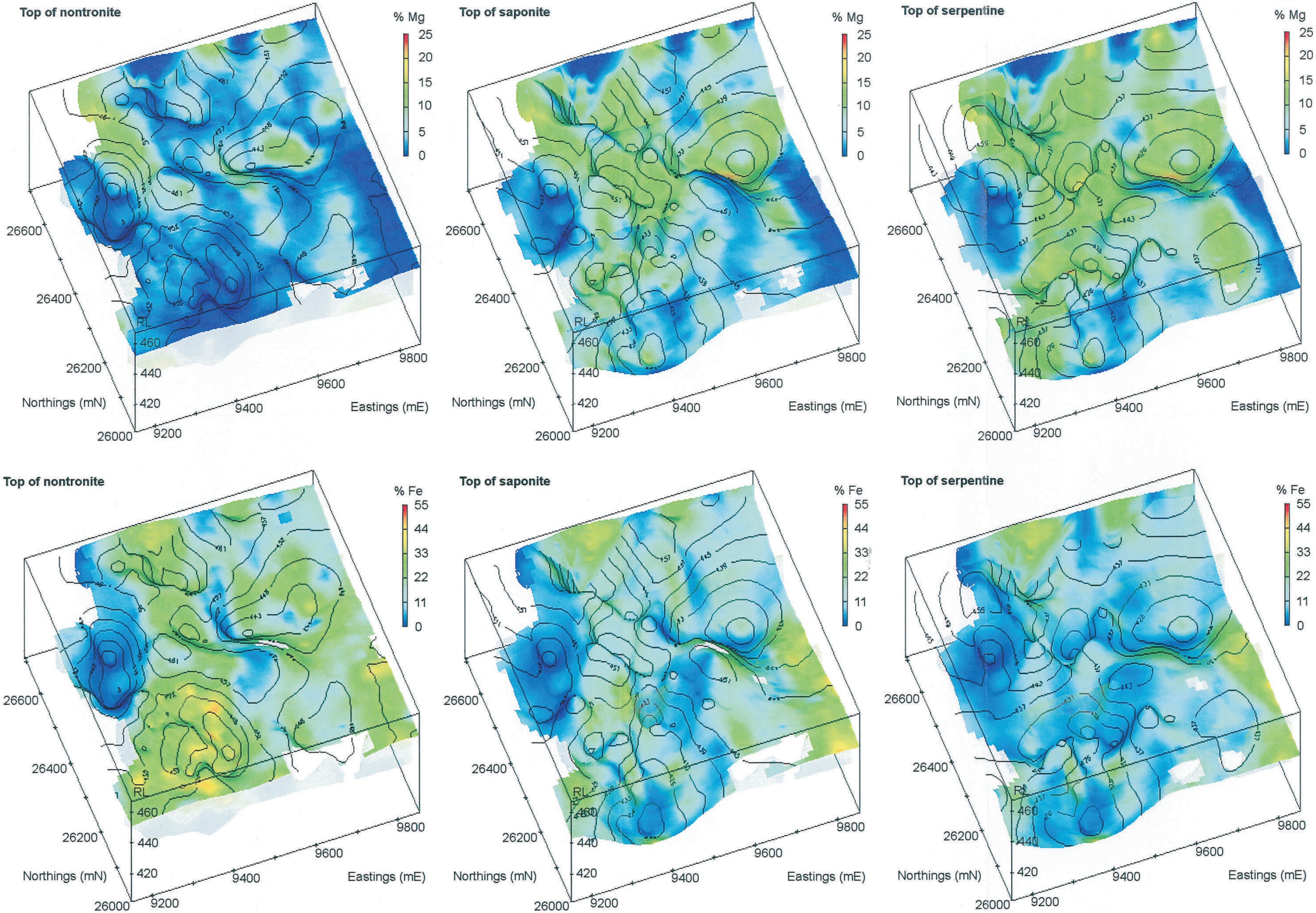

Figure 4.11. Distribution of Mg and Fe for different regolith surfaces at MM2. RL contours, at either 4 or 5 m intervals,are shown (*i.e.*, black lines) for each surface. View is at 200° azimuth and 50° elevation, with x5 vertical exaggeration. Transects for northings 26050, 26250, 26450 and 26700 mN are also shown as transparent slices through the regolith. Blocked out (*i.e.*, white) areas for some surfaces are areas of low confidence filtered out of the data.

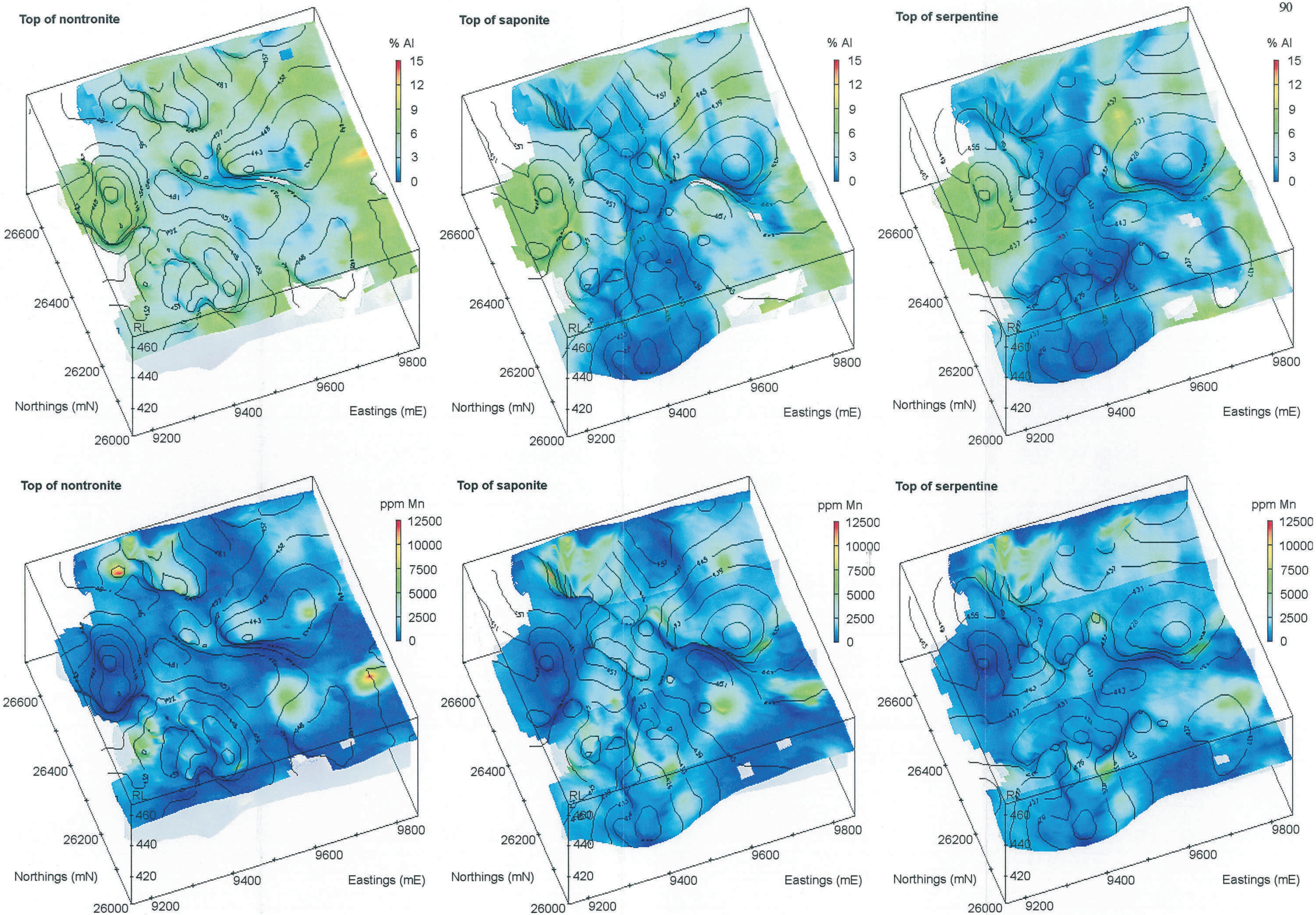

Figure 4.12. Distribution of Al and Mn for different regolith surfaces at MM2. RL contours, at either 4 or 5 m intervals, are shown (*i.e.*, black lines) for each surface. View is at 200° azimuth and 50° elevation, with x5 vertical exaggeration. Transects for northings 26050, 26250, 26450 and 26700 mN are also shown as transparent slices through the regolith. Blocked out (*i.e.*, white) areas for some surfaces are areas of low confidence that have been filtered out of the data.

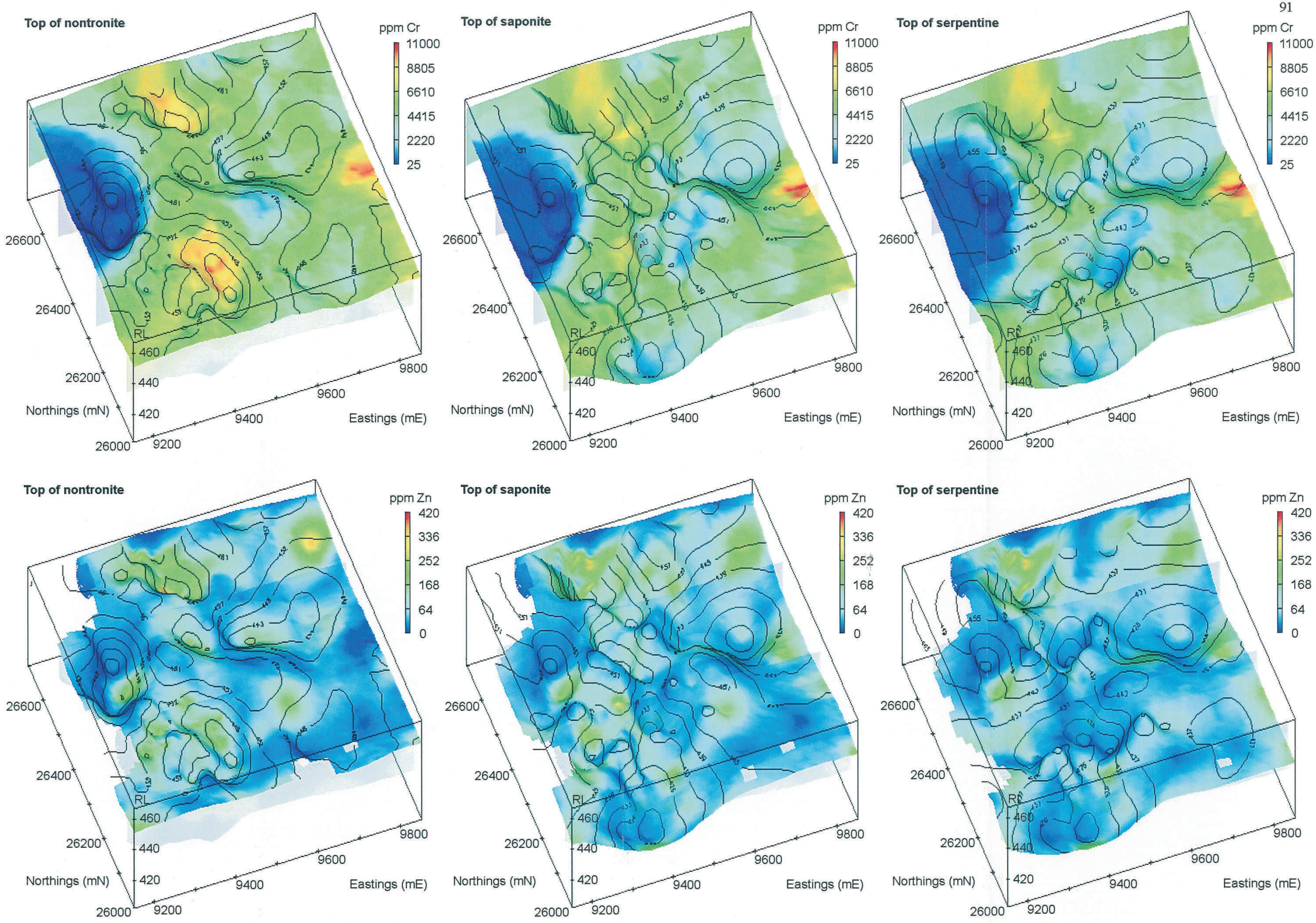

Figure 4.13. Distribution of Cr and Zn for different regolith surfaces at MM2. RL contours, at either 4 or 5m intervals, are shown (*i.e.*, black lines) for each surface. View is at 200° azimuth and 50° elevation, with x5 vertical exaggeration. Transects for northings 26050, 26250, 26450 and 26700 mN are also shown as transparent slices through the regolith. Blocked out (*i.e.*, white) areas for some surfaces are areas of low confidence that have been filtered out of the data.

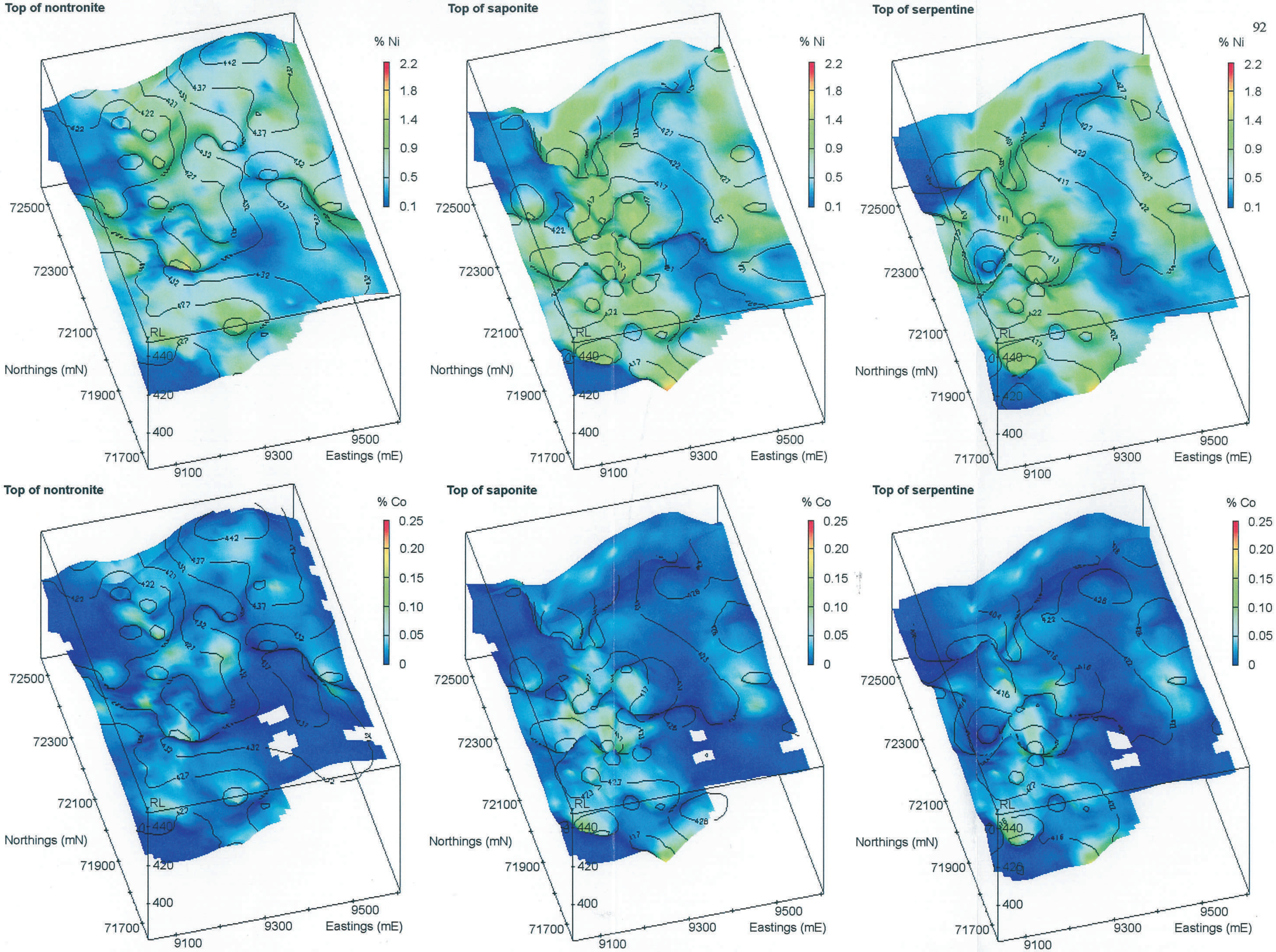

Figure 4.14. Distribution of Ni and Co for different regolith surfaces at MM3. RL contours, at either 4 or 5 m intervals, are shown (*i.e.,* black lines) for each surface. View is at 195° azimuth and 40° elevation, with x5 vertical exaggeration. Transect 72500 mN is also shown as a slice through the regolith. Blocked out (*i.e.,* white) areas for some surfaces are areas of low confidence that have been filtered out of the data.

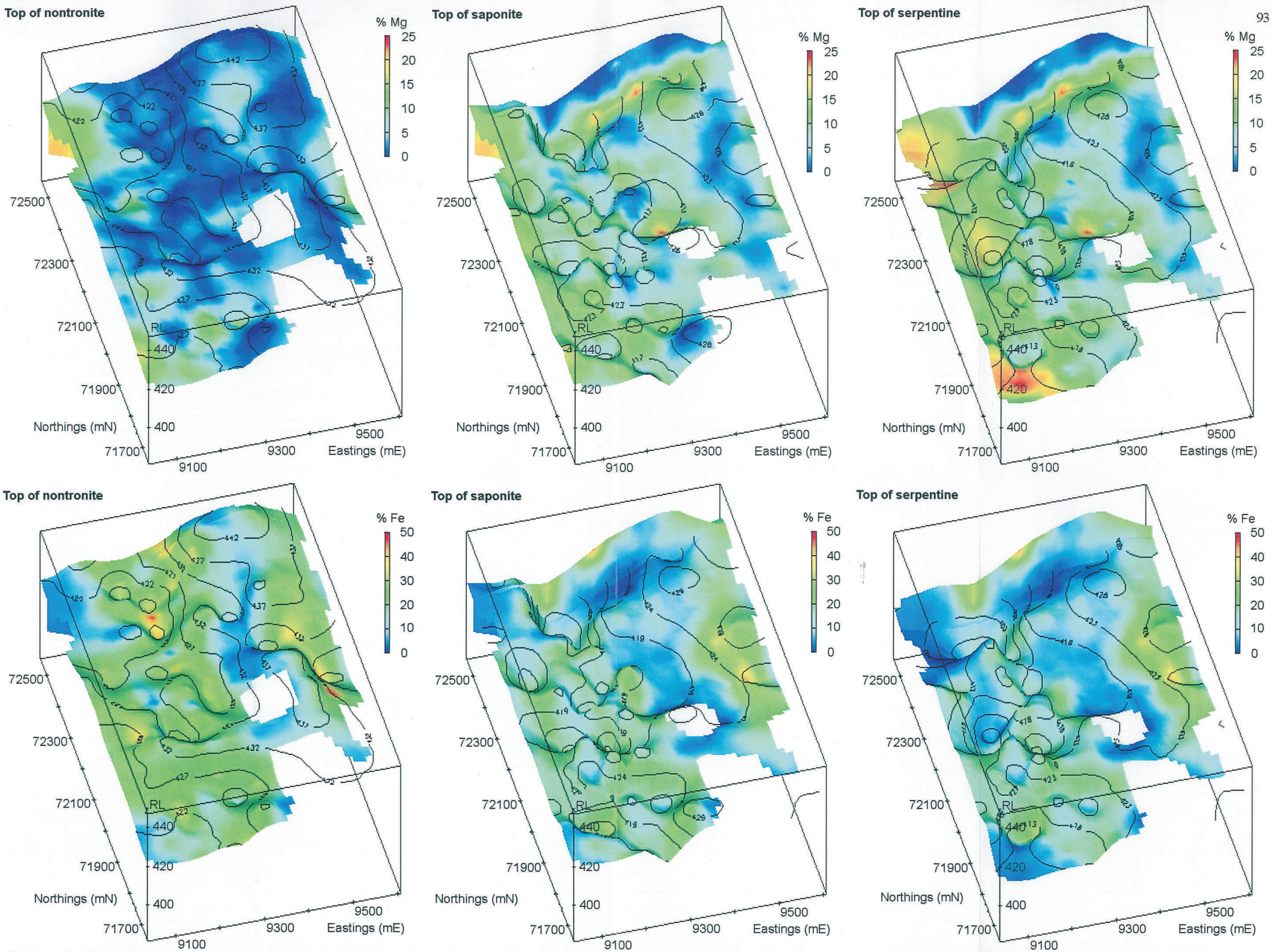

Figure 4.15. Distribution of Mg and Fe for different regolith surfaces at MM3. RL contours, at either 4 or 5 m intervals, are shown (*i.e.*, black lines) for each surface. View is at 195° azimuth and 40° elevation, with x5 vertical exaggeration. Transect 72500 mN is also shown as a slice through the regolith. Blocked out (*i.e.*, white) areas for some surfaces are areas of low confidence that have been filtered out of the data.

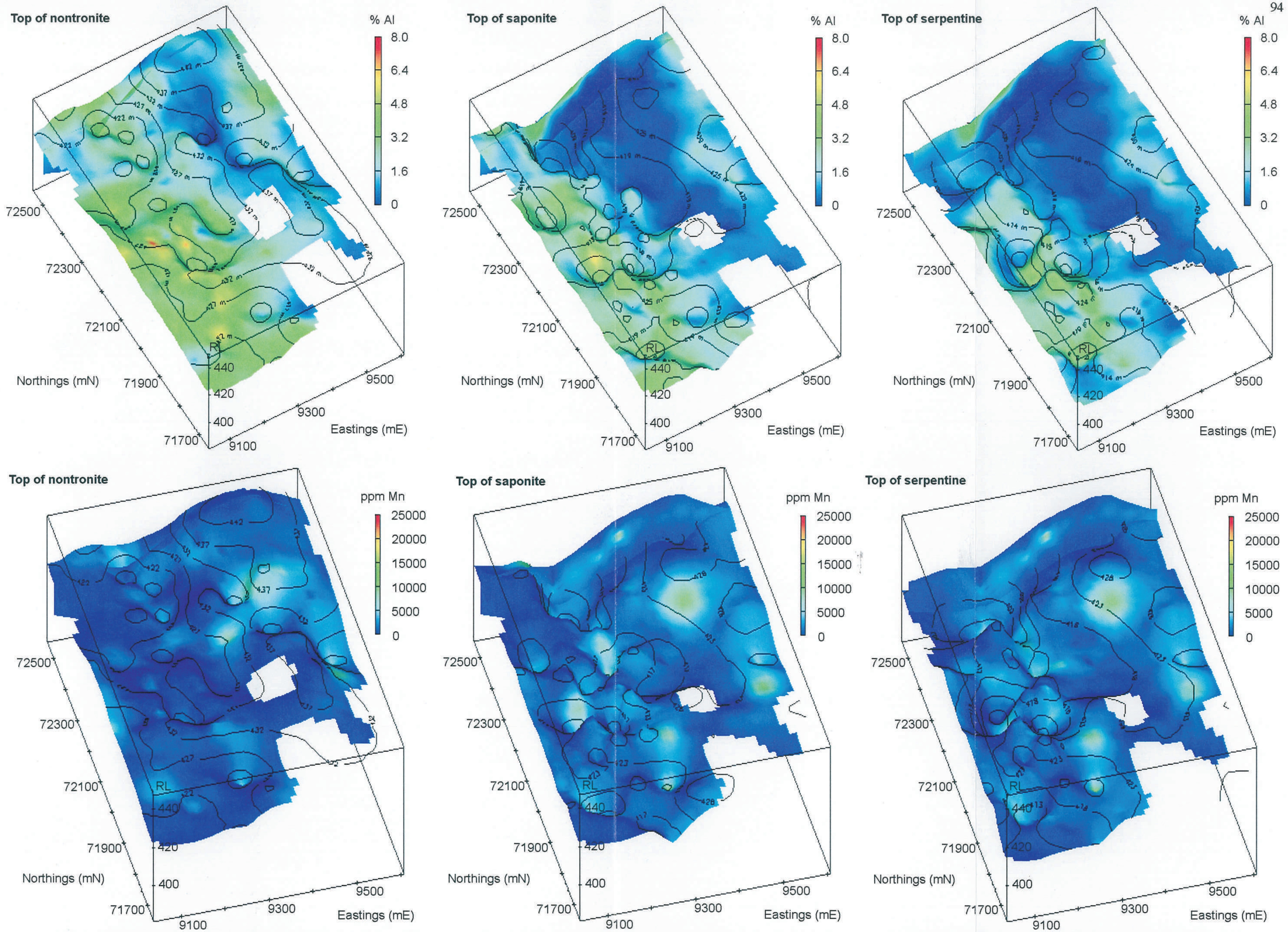

Figure 4.16. Distribution of Al and Mn for different regolith surfaces at MM3. RL contours, at either 4 or 5 m intervals, are shown (*i.e.,* black lines) for each surface. View is at 200° azimuth and 50° elevation for Al and 195° azimuth and 45° elevation for Mn, with a x5 vertical exaggeration. Transect 72500 mN is also shown as a slice through the regolith. Blocked out (*i.e.,* white) areas for some surfaces are areas of low confidence that have been filtered out of the data.

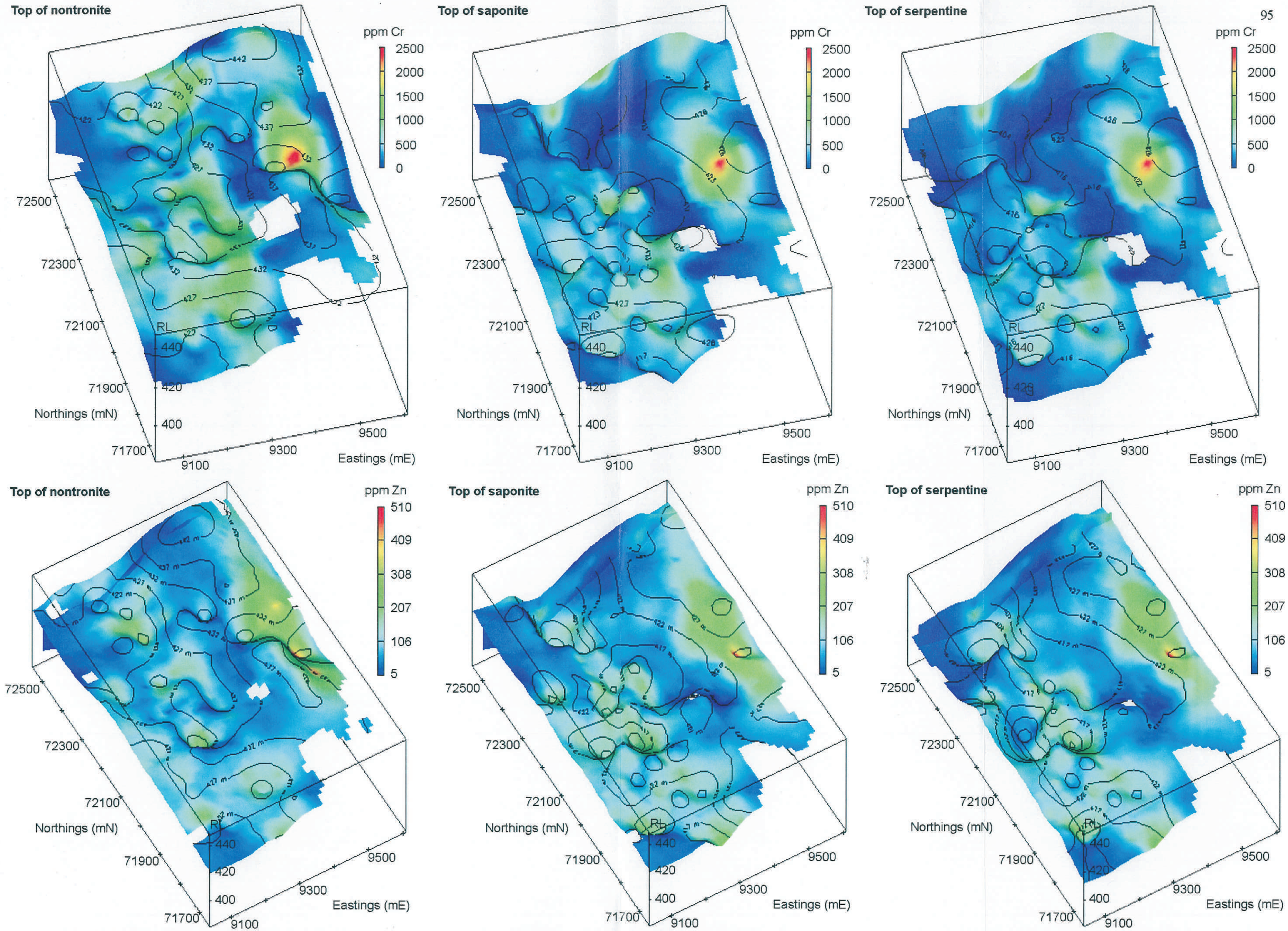

Figure 4.17. Distribution of Cr and Zn for different regolith surfaces at MM3. RL contours, at either 4 or 5 m intervals, are shown (*i.e.*, black lines) for each surface. View for Cr is at 195° azimuth and 40° elevation, with x5 vertical exaggeration. View for Zn is at 200° azimuth and 50° elevation, with x5 vertical exaggeration. Transect 72500 mN is also shown as a slice through the regolith. Blocked out (*i.e.*, white) areas for some surfaces are areas of low confidence that have been filtered out of the data.

This feature continues or is preserved to the top of the nontronite unit and becomes obscured in the 'kaolinite-2' unit (not shown) most probably due to the greater effect of weathering in the upper portion of the profile.

This feature may represent a lithological unconformity or is the result of slumping during weathering. The uniform distribution of Ni/Ni+Al values (Fig. 4.9) discounts the former possibility while the sharply defined, local nature of the feature rules out the latter possibility. More probably, this feature may represent a pre-existing conjugate (*i.e.*, intersecting) fault-set with the normal-slip fault in transects 26700 and 26450 mN (Figures 3.4 and 4.3) comprising the NW-SE striking fault. The other fault strikes approximately NNE-SSW (Fig. 4.9). Reactivation of the fault during weathering and probable normal movement along the fault-set has produced an irregular, 'egg-carton' like topography within the regolith (see Figures 4.9 to 4.13).

Nickel and Co mineralization occurs mainly within the upper half of the nontronite unit associated with topographic lows (Fig. 4.3) along the NNE-SSW striking fault (Fig. 4.10), where development of smectite (*i.e.*, nontronite and saponite) is thickest. Normal faulting within transects 26450 and 26700 mN, part of the NW-SE striking fault noted above, has resulted in two offset zones of high grade Ni (*i.e.*, > 1.0 %) within the nontronite unit (Fig. 4.3). A Ni-poor zone occurs along the plane of shearing. Faulting appears to have occurred during weathering with the Ni-poor zone most probably resulting from fluid movement along the fault plane. The distribution of Co (Fig. 4.3), Mg, Fe, Al and Mn (Fig. 4.4) for slices through the regolith all show features that relate to faulting in transects at 26450 and 26700 mN.

Mn-Co distribution

Not unexpectedly, the occurrence of Co appears generally related to the distribution of Mn (compare Figure 4.3 to 4.4 and Figure 4.10 to 4.12). However, high grades of Mn do not necessarily coincide to the highest grades of Co. Reasons for this are unclear but may indicate:

1. That Co was already depleted where the Mn oxides (*i.e.*, asbolan) initially precipitated. Cobalt may associate with Mn only if Mn and Co are both in solution and co-precipitate or Co can be adsorbed after the precipitation of Mn oxides.

2. There may be two (or more) generations of Mn oxides, with each successive generation a result of either complex weathering events or are a result of episodic wetting and drying cycles associated with fluctuating water-table levels, similar to the movement of Fe within weathering profiles. Evidence for the remobilization of Mn within the regolith is shown by the

precipitation of Mn oxides along shear planes. This may then release Co back into solution to be redistributed within the regolith.

However, such interpretation should be treated with caution. Isolated Mn 'hot-spots' within the nontronite surface (Fig. 4.12) may be due to drill hole effects (*i.e.*, are artefacts of the kriging of 'isolated' high concentrations of Mn for widely spaced drill holes).

4.3.2 MM3

General features and element distribution

A very strong lithological control on regolith geochemistry is evident at MM3 as shown by distributions of the Ni/Ni+Al ratio in both slices (Fig. 4.6) and for different regolith surfaces (Fig. 4.9). Low Ni/Ni+Al values along the western margin of the deposit are indicative of ortho- and mesocumulates lithologies. A central olivine adcumulate zone is indicated by high Ni/Ni+Al values of > 0.4 that persists from the serpentine unit through to the base of the kaolinite unit (Figures 4.6 and 4.9). This is due mainly to low Al values (Figures 4.7 and 4.16) for this zone rather than due to high Ni values (Figures 4.6 and 4.14), which is consistent to the bulk composition of adcumulates (Hill *et al.*, 1996).

A Ni-poor (*i.e.*, < 0.5 %) zone is generally coincident with the adcumulate reflected by Ni/Ni+Al values of >0.4-0.6 (Fig. 4.6). Lithology also controls the distribution of Co, with low concentrations (*i.e.*, < 0.03%) over adcumulate and higher concentrations over meso- and orthocumulates (Fig. 4.6).

The distributions of Al and Fe are broadly similar, and correlate generally with those for Ni and Co (Figures 4.7, 4.15 and 4.16). Zones of low Al- (Fig. 4.16) and Fe (Fig. 4.15), particularly for the saponite and serpentine units, generally coincide with high Ni/Ni+Al values of >0.4-0.6 (Fig. 4.9). This is consistent with the bulk chemistry of adcumulate rocks (Hill *et al.*, 1996). The distributions of Al and Fe are inversely related to Mg (Fig. 4.7). The highest grades of Mg generally occur away from the adcumulate zone, along the western margin of the deposit associated with talc-carbonate development in ortho- and mesocumulates (Figures 4.7 and 4.15). This may indicate a lateral remobilization of Mg within the regolith away from the adcumulate towards the western and eastern margins of the deposit; adcumulates generally have a greater initial Mg content than ortho- and mesocumulates and are generally more susceptible to weathering (*i.e.*, loss of Mg). The Mg content decreases up profiles but is unrelated to any regolith boundary (Fig. 4.7).

The distributions of Cr and Zn (Figures 4.8 and 4.17) are also similar to that for Fe, with a zone of low Cr and Zn coincident to the underlying adcumulate zone. The highest values of Cr correlate to high Fe values (compare Figure 4.8 to 4.7 and Figure 4.15 to 4.17), most probably due to surficial concentration of chromite. The distribution of Zn (*e.g.*, Figures 4.6 and 4.8) appears well related to that of Ni and, to a lesser extent, Co.

Structural and lithological controls

A general, lateral decrease is shown for Ni/Ni+Al values moving away from the central adcumulate zone (Fig. 4.6). This may be due to either lithological contacts being obscured during formation of the Ni laterite or to changes in the Ni/Ni+Al ratio simply indicating a gradational, rather than a discrete, change in cumulate lithology to ortho- and mesocumulates at the western and eastern margins of the deposit (Fig 4.6). The distribution of Ni/Ni+Al values within slices (Fig. 4.6) and at regolith surfaces (Fig. 4.9) within MM3 shows that the adcumulate zone either pinches out towards the south end of the deposit or plunges below the surface of the serpentine unit. The latter case would be consistent with the main structural style of cumulate lithologies at MM3 that form part of the southerly plunging, western limb of the Kilkenny syncline (see Figure 1.1).

The topography of regolith surfaces, particularly the saponite and serpentine units within and immediately adjacent to the adcumulate zone, are relatively flat (*i.e.*, show little relief) compared to the zone of ortho- and mesocumulate along the western margin at about 9250 mE (Fig. 4.9). This variable depth of weathering may reflect textural differences, such as in the packing of serpentinized olivine grains in the bedrock. Orthocumulates are defined as consisting of 50-80 % olivine, with isolated crystals floating within an intercumulus matrix. Whereas, adcumulates are comprised of >95% tightly packed olivine grains with triple-point contacts. Mesocumulates represent the intermediate condition. As olivine is easily weathered and because of the high degree of preserved, interconnected serpentinized olivine, it would be expected that adcumulates have a relatively high porosity. In contrast, the isolated nature of serpentinized olivine might result in orthocumulates having a relatively low porosity. Some evidence for this, although not conclusive, is shown for plots of cumulate porosity versus Ni/Ni+Al values for the serpentine unit of selected RC holes at MM3 (Appendix 7).

However, although adcumulates may tend to have a greater porosity than ortho- and mesocumulates (Appendix 7), extensive secondary silicification within and over adcumulates, associated with initial stages of weathering, would have either effectively acted as a physical barrier (*i.e.*, 'plugged the system' by inhibiting drainage) limiting the vertical and lateral movement of Ni and Co, or may have acted as a diluent to mineralization.

Nickel and Co occur mainly in topographic lows within the nontronite unit associated with the variably weathered ortho- and meso-cumulates, where development of smectite (nontronite) is thickest (Fig. 4.6). Cobalt occurs within primary pyroxene minerals of the intercumulus matrix (Deer *et al.,* 1980; Burger, 1996). Cobalt mineralization in MM3 along the western margin of the deposit may be a reflection of the greater amount of intercumulus material of the original ortho- and mesocumulate, as compared to adcumulate, and where, because of the limited porosity of orthocumulates, there has been little mobilization of Co during weathering away from the ortho- and mesocumulate zone.

Mn-Co mineralization

Although Mn oxides are considered to host Co mineralization in the regolith, high Co grades are not necessarily correlated to high Mn grades (*e.g.,* compare Figure 4.6 to 4.7, and Figure 4.14 to 4.16), as is also shown in MM2. The presence of high Mn grades within the adcumulate zone along transect 72300 mN (Figure 4.7) may indicate Mn oxides that have been silicified and preserved within the regolith. In this case, Mn oxides would have been unavailable to take up Co and hence appear as Co-poor. The same argument may also apply to aspects of the Mn-Co association at MM2.

4.4 Cluster Analysis

Cluster analysis of the geochemical data, supplied by Anaconda, was performed to enable a more detailed examination of element associations within and between the two study areas. Analysis was performed using STATISTICA™ (Volume III) for Windows after initial treatment of the raw data, according to Section 1.11.8. Cluster analysis was performed using Ward's method as the amalgamation or linkage rule with 1-Pearson r selected as the distance measure. Other linkage and distance measures were tried and found to give very similar results to those selected for final analysis.

The geochemical data were examined in three ways:

1. Global analysis of the combined geochemistry for MM2 and MM3, as a single 'deposit'.

2. Analysis of MM2 and MM3 as two, separate deposits.

3. Analysis of the regolith geochemistry within MM2 and MM3.

Results of the global cluster analysis for MM2 and MM3 are presented in Figure 4.18, with a summary of each examination presented in Table 4.1. Comparison of Figure 4.18 with Table 4.1 illustrates how element associations can be presented in tabular form, using parentheses to show element associations, rather than in graphical form as in Figure 4.18.

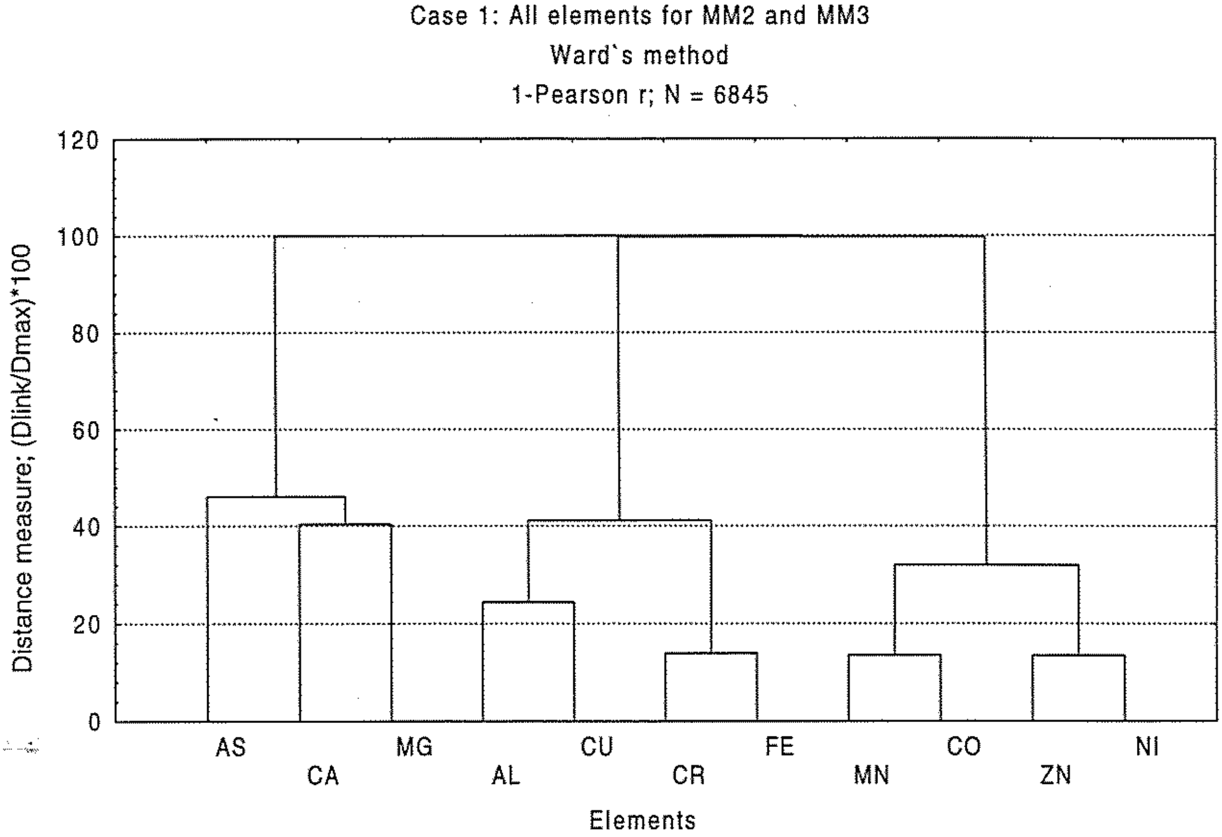

Figure 4.18. Tree diagram of the global cluster analysis of MM2 and MM3 as a 'single' deposit using the geochemical data supplied by Anaconda Nickel NL. Elements occur as three groups that are unrelated to each other. N is the number of samples analysed.

According to the clustering parameters selected for the global analysis, three element groups were identified (Figure 4.18), namely As-Ca-Mg, Al-Cu-Cr-Fe and Mn-Co-Zn-Ni. Within the latter group, Zn is strongly associated with Ni, whereas Co associates with Mn. This is presented in Table 4.1, for the global case, as; (Ni,Zn)(Mn,Co). Similar associations are shown for Al and Cu, and for Cr and Fe (Fig. 4.18), which represent another group, shown in Table 4.1 as; (Cr,Fe)(Al,Cu). Similarly, the association between Ca, Mg and As is shown accordingly as; (Ca,Mg)As (Table 4.1). These three groups are unrelated to each other as is shown by the very long tie lines that connect them in the tree diagram (Fig. 4.18). The following discussion, therefore, refers to element associations as presented in Table 4.1.

Table 4.1. Cluster analysis of regolith geochemistry for MM2 and MM3.

Case 1: Global analysis (MM2 and MM3).				Comments
	(Ni,Zn)(Mn,Co) (Cr,Fe)(Al,Cu) (Ca,Mg) As			
Case 2: Deposit analysis.				
MM2		**MM3**		
	[(Ni,Zn) (Co,Mn)] (Ca,Mg) (Cr,Fe) (As,Al,Cu)		[(Ni,Zn) (Co,Mn)] [(Fe,Cr)Al] Cu (As,Mg,Ca)	
Case 3: Analysis of regolith geochemistry.				
Unit#0 Kaolinite-1	(Ni,Cr) Fe (Zn,Co) (As,Cu) Al (Mn,Mg) Ca	**Unit#0** Kaolinite with serp.	[(Ni,Zn) (Cu,Fe,Al,Cr)] (Mn,Co) As (Ca,Mg)	**Increasing difference within and between profiles for MM2 and MM3.**
Unit#1 Kaolinite-2	(Ni,Zn) Mg (Mn,Co) Cu (Cr,Fe) As Ca,Al	**Unit#1** Kaolinite	[(Ni,Zn) (Mn,Co)] (Ca,Mg) (Cu,Fe) (As,Cr,Al)	
Unit#2 Nontronite	[(Ni,Zn) (Fe,Cr)] (Mn,Co) (Ca,Mg) As (Al,Cu)	**Unit#2** Nontronite	(Ni,Zn) (Mn,Co) (Cr,Fe) (Al,Cu) (Ca,As,Mg)	
Unit#3 Saponite	[(Ni {Zn,Fe}) (Al,Cr)] (Mn,Co) (Ca,Mg) (As,Cu)	**Unit#3** Saponite	[(Ni,Fe,Zn) Al,Cr] (Mn,Co) (As,Mg) (Ca,Cu)	**Very similar element associations.**
Unit#4 Talc	[(Ni,Zn) (Cr,Fe)] (Mn,Co) (Al,Cu) (As,Mg,Ca)	**Unit#4** Talc	[(Ni,Zn) (Fe,Cr)] (Mn,Co) (Al,Cu) As (Ca,Mg)	
Unit#5 Serpentine	[{{{(Ni,Fe) Zn} Co} Cr} Mn] (As,Mg) (Al,Cu) Ca	**Unit#5** Serpentine	[{{{(Ni,Zn) Fe} Co} Cr} Mn] (Al,Cu) (As,Mg,Ca)	
Unit#6 V.W. Serp.	[{Ni (Mn,Co)} (Zn,Fe) Cr] [(As,Mg) Ca] (Al,Cu)			

The kaolinite-1 unit at MM2 has formed by the deposition of felsic sediments (Fig. 4.1), derived from granitic outcrops that occur to the NW of the deposit (see Figure 1.1). This is the cause of the very different element associations for this unit as compared to element associations for weathered ultramafics.

4.4.1 *Cluster analysis: global and individual deposits*

Very similar element associations and groupings are indicated between the global analysis of MM2 and MM3, and for MM3 treated as a separate case (*i.e.*, 'single deposit') (Table 4.1). However, within MM2, four element sub-groups are shown rather than three. This may be a result of the input of additional felsic material at the surface of MM2. The (Ni,Zn) (Co,Mn) association is common to both deposits and reflects the similar distribution of these elements. The close association between Co and Mn is expected since some Mn oxides host Co mineralization. The close association between Zn and Ni was seen in the distributions of Zn and Ni for northing transects through and for regolith surfaces within MM2 and MM3 (Figures 4.3 and 4.5 for MM2, and Figures 4.6 and 4.8 for MM3). The (Cr,Fe) (Al,Cu) group in MM3 reflects the elements that are most resistant to weathering and are residually concentrated, especially towards the top of the regolith. The (Ca,Mg) As association is most likely related to the common weathering behaviour of the alkalie earths to which As may associate.

4.4.2 *Cluster analysis; regolith geochemistry*

Very similar element associations and groupings are shown between MM2 and MM3 for regolith units serpentine to saponite (Table 4.1). This is not unexpected, due to the very similar bulk composition of the underlying cumulate bedrock and because of the very similar mineralogy (*e.g.*, clay silicates and oxides) of these regolith units. The main clay silicates in these units, serpentine, talc and saponite, are all Mg-rich, trioctahedral minerals (*i.e.*, all cation positions are fully occupied) that have a similar major and trace element composition (Section 3.6.1). In addition, the effect of weathering is least at the base of the regolith profile so that there has been little lateral and vertical dispersion of elements.

As for the other analyses, Zn is closely associated with Ni, both of which are grouped with Fe and Cr. Manganese and Co, again, almost always occur together and within the same group as Ni, Zn, Fe and Cr (Table 4.1). The oxide mineralogy for the serpentine, talc and saponite units is very similar, comprising mainly maghemite with minor hematite, chromite and Mn oxides (see section 3.7). The intimate and finely disseminated nature of these phases within the clay silicates of these units limits the 'scale' of discrimination to which element associations may be distinguished by cluster analysis. Hence, similar element associations are indicated (Table 4.1).

Increasingly dissimilar element associations and groupings are evident upward through the regolith (*i.e.*, from the nontronite to the kaolinite units) within the deposits and between MM2 and MM3, as the effects of weathering and influence of introduced material become more pronounced (Table

4.1). An example is the association between Fe and Cr. A significant increase in Fe oxide content occurs at the nontronite/kaolinite boundary (Section 3.7). In the kaolinite unit at MM3 iron, which is present mainly as goethite and hematite, markedly weakens or lessens the association between Cr and Fe that is due to chromite (Table 4.1).

As expected, element associations and groupings within the channel clays at MM2 (*i.e.*, kaolinite-1 unit) are very different to element associations for all other units (Table 4.1). This is because of the different composition and mineralogy of this unit (derived from felsic sediments) relative to regolith developed from weathered ultramafics. The isolated occurrences of Al, Ca and, to a lesser extent, Mg (with Mn) reflects the felsic mineralogy of the this unit which is dominated by primary Al-silicates such as plagioclase, K-feldspar and muscovite towards the base of the profile, and by secondary Al-silicates such as kaolinite towards the surface (Section 3.7). The (Ni,Cr)Fe grouping in the kaolinite-1 unit at MM2 (Table. 4.1) may be related to chromite that can concentrate in the weathering profile. The (Zn,Co) and (As,Cu) groupings in the kaolinite-1 unit are difficult to interpret.

4.5 Mass balance analysis

Examination of major and trace element mobility within the regolith can only be accurately assessed from mass balance calculations (Section 1.11.6) of deposit geochemistry. Within the regolith zones that have formed by essentially isovolumetric weathering, such calculations are best determined based on bulk density. However, such calculations are invalid in zones where there has been a change in volume either due to collapse or by expansion during weathering. In such instances, emphasis is placed upon using one or more elements that can be considered geochemically immobile during weathering.

A number of mass balance studies investigating weathering processes in lateritic profiles have assumed the immobility of Zr (Colin *et al.*, 1992; Beauvais and Colin, 1993; Porto and Hale, 1995), which in most cases occurs as zircon, $ZrSiO_4$. However, Zr can also occur as hydrated Zr-silicates, which are more easily solubilized during initial stages of weathering (Porto and Hale, 1995). Other elements, of assumed immobility in the weathering profile, used in mass balance studies have included Ti, Th and Nb (Nesbitt, 1979; Esson, 1983; Braun *et al.*, 1993; Porto and Hale, 1995; Venturelli *et al.*, 1997).

For the deposits at Murrin Murrin, time constraints and the unavailability of suitable samples precluded using bulk density in calculations of mass balance. Accordingly, such calculations were performed based on Zr assays from the XRF analysis (Section 1.11.4) of pulps from selected RC drill holes across the deposits at MM2 and MM3. One major limitation of this approach, however, is that ultramafic rocks typically have very low Zr contents (between 5–10 ppm) which is often at the detection limit (5 ppm) achieved for Zr assays by XRF analysis (Table 1.2). Consequently, artefacts may be introduced in the mass balance calculations where Zr concentrations are low.

A relative comparison of element immobility can be determined by examination of the ratio of the concentration of the element in the parent material (Cp) to the concentration of the element in the weathered material (Cw) (Porto and Hale, 1995). The Cp/Cw ratio was calculated for Zr, Fe, Ti, Cr and Nb in drill holes at MM2 and MM3 with a complete weathering profile. That is, where serpentine was present, as identified by PIMA and XRD analysis, at the base of the profile (Appendix 8, Tables A8.1 and A8.2 for MM2 and MM3, respectively). Values of the Cp/Cw ratio for Fe, Ti, Cr and Nb did not give the same trends as or similar values to the Cp/Cw ratio for Zr, and were, therefore, not used in the mass balance calculations.

Only drill holes within MM2 and MM3 that contained serpentine at the base of the profile were included in the mass balance study. Investigation of the major and trace element chemistry of serpentine units at the base of those drill holes selected for analysis (Appendix 8, Figures A8.1 and A8.2 for MM2 and MM3, respectively), showed that the chemistry of the serpentine unit at both deposits was too varied for an 'average' composition for the unit to be determined, that could be used at both deposits. Thus, drill holes that did not have a complete regolith profile (*i.e.*, serpentine at depth) were excluded from study and RC holes with serpentine at the base of the profile were analyzed individually. Average compositions of the serpentine unit, for each of these drill holes at MM2 and MM3 are presented in Appendix 8 (Tables A8.3 and A8.4 for MM2 and MM3, respectively) and were used as the composition of fresh ultramafic as required in the mass balance equation (Section 1.11.6). The same approach would also have been required had bulk density determinations been used instead of Zr assays. In addition, the kaolinite-1 (*i.e.,* channel clay) unit at MM2 was not included in the mass balance study as no analysis of the parent material for this unit was available.

Mass balance profiles of the major and trace elements for RC holes, listed in Tables A8.3 and A8.4 (Appendix 8), are shown in Figure 4.19 for MM2 and in Figures 4.20 to 4.23 for MM3.

4.6 Mass balance profiles: MM2 and MM3

Concentrations of Zr within drill holes at MM2 and MM3 remain relatively constant in the weathering profile at background levels of between 5 to 10 ppm to within 3–5 m of the surface, where the Zr concentration then increased to values of between 50–100 ppm, but up to 100-200 ppm (Figures 4.19 to 4.23). High Zr values occur mainly within the upper portion of the kaolinite unit, although high Zr values also occur where other units (*e.g.*, talc, saponite and nontronite) 'outcrop' at the surface. For example, in RC hole CBRC0783 (Fig. 4.19) and ARC0786 (Fig. 4.21). Similar concentrations of Zr to 150 ppm have been reported at the surface of other Ni-laterites and were interpreted as evidence for the introduction of allochthonous material to the surface of these profiles (Butt and Nickel, 1981; Schellmann, 1989). A similar conclusion can be drawn for the deposits at MM2 and MM3, particularly where units such as talc, saponite and nontronite occur at the surface.

Enrichment of the major elements Si, Al, Fe and Mg occurs within the upper portion of the serpentine unit at or near the boundary to the overlying saponite or nontronite units. For example, as in RC holes ARC0793 (Fig. 4.20), ARC0783 and 0782 (Fig. 4.21) and ARC0126 (Fig. 4.22). This may represent a localized, relative accumulation due to the partial collapse of the upper saprock and/or lower saprolite or indicate absolute accumulation due to leaching from upper portions of the profile. This, however, may also represent an artefact of the very low Zr concentrations of serpentine in these profiles.

A strong upward depletion of Si and Mg then occurs from the top of the serpentine unit to the surface of the profile (Figures 4.19-4.23). This is consistent to observations for other Ni-laterite profiles (Esson, 1983; Schellmann, 1989; Venturelli *et al.,* 1997), and reflects the instability of Mg-silicates such as serpentine, chlorite and nontronite to conditions of more intense leaching that occur higher in the profile. Aluminium and Fe also show an upward depletion, but to a lesser degree than that shown by Si and Mg. However, Al and Fe may also show localized enrichment within the nontronite unit and the overlying kaolinite unit within both deposits. This is shown, for example, in RC holes CBRC0747 (Fig. 4.19), ARC0793 and 1257 (Fig. 4.20), ARC0782 (Fig. 4.21), and ARC0776 (Fig. 4.22). This is related to the kaolinite and Fe oxide dominated mineralogy of these units, especially for the kaolinite unit (Section 3.7). The zone of enrichment for Al and Fe in the upper portion of the profile may represent the lower extent of oxidative weathering in these profiles.

Enrichment of the trace elements Ni, Co, Cr, Mn and Zn within the upper portion of the serpentine unit is coincident to the zone of enrichment for the major elements in this unit and often represents

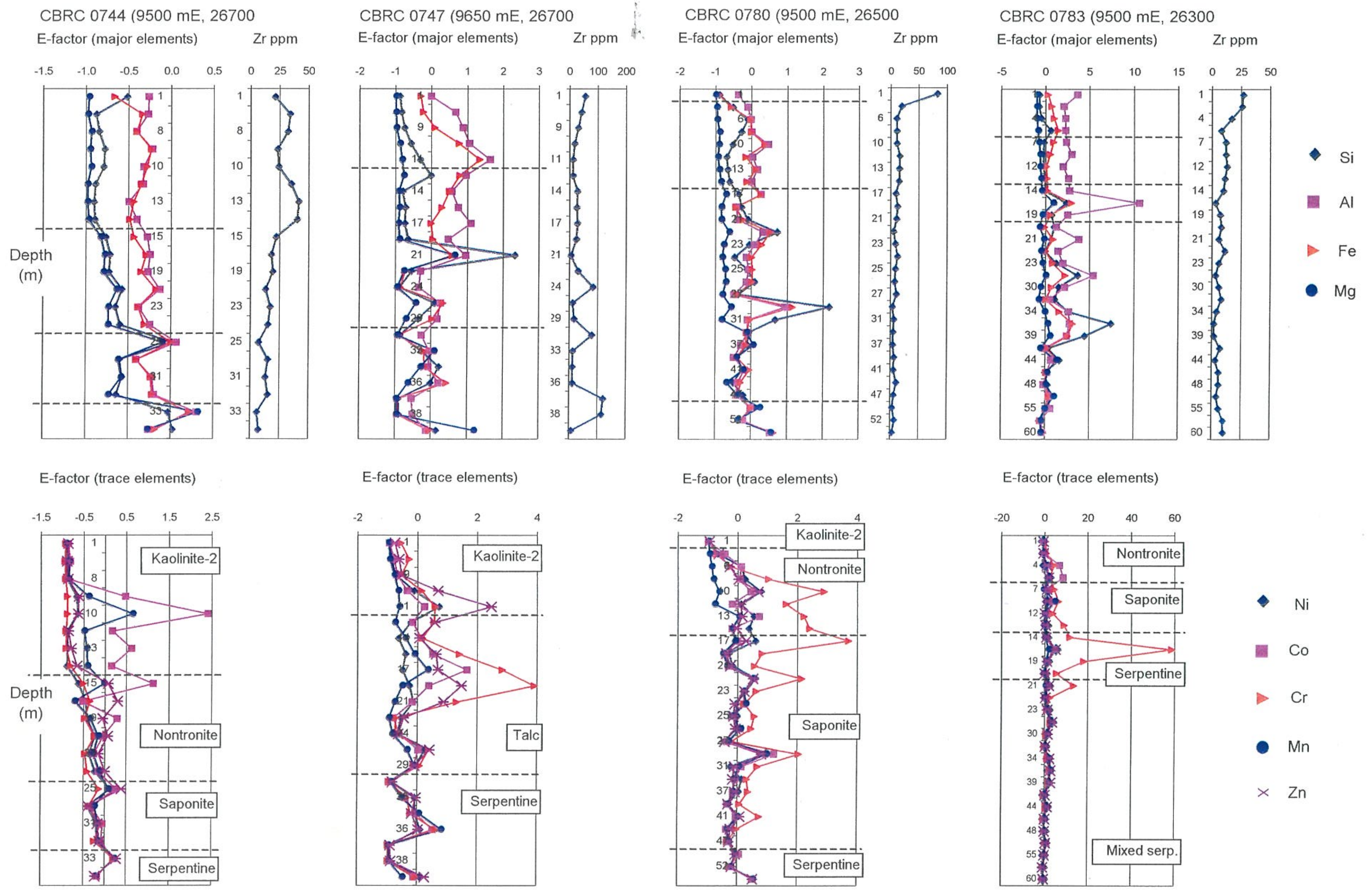

Figure 4.19. Enrichment (E) factors for major and trace elements, and Zr concentrations for selected RC drill holes at MM2. Regolith units as identified by PIMA are also shown.

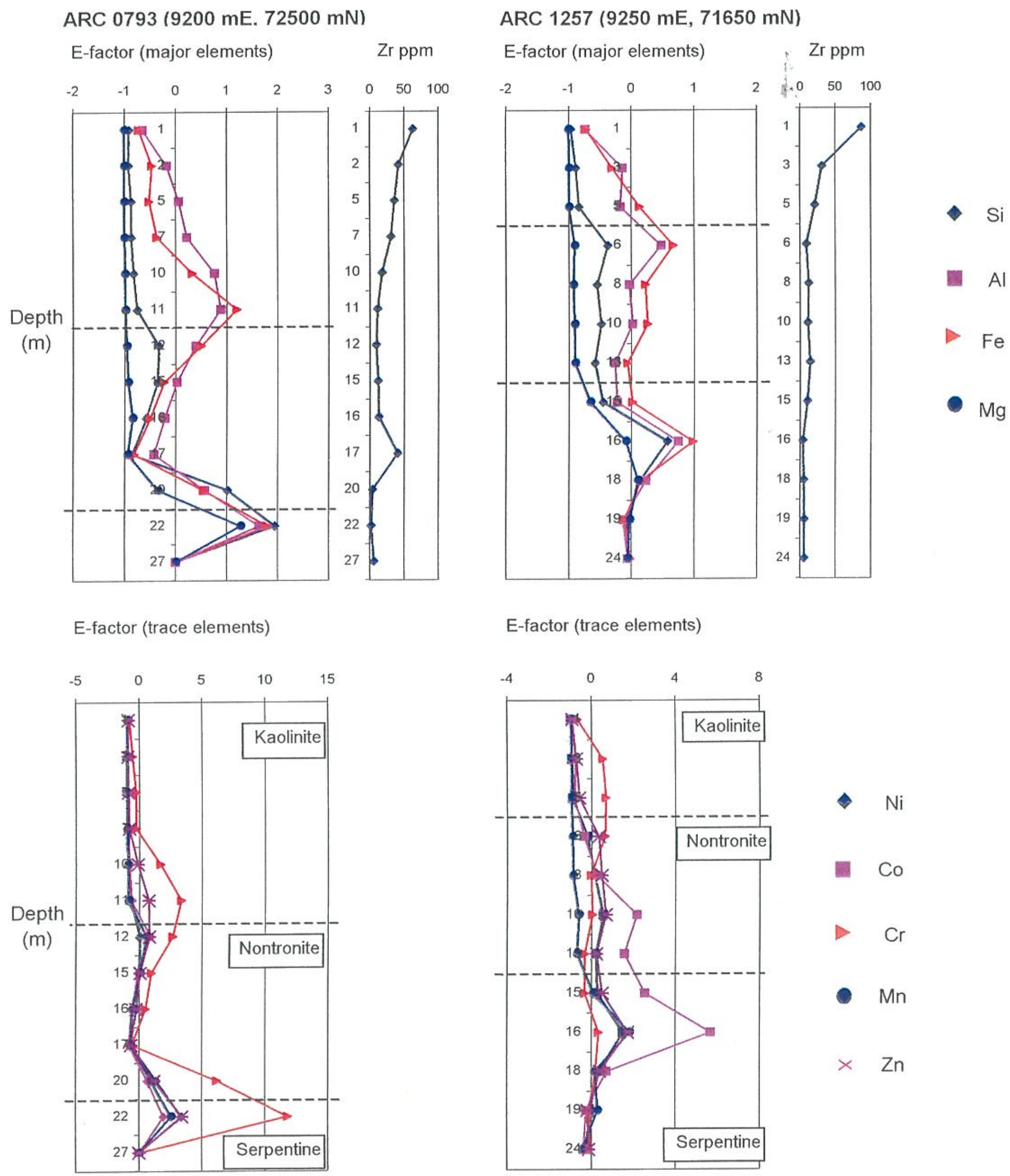

Figure 4.20. Enrichment (E) factors for major and trace elements, and Zr concenctrations for selected RD drill holes at MM3. Regolith units as identified by PIMA are also shown.

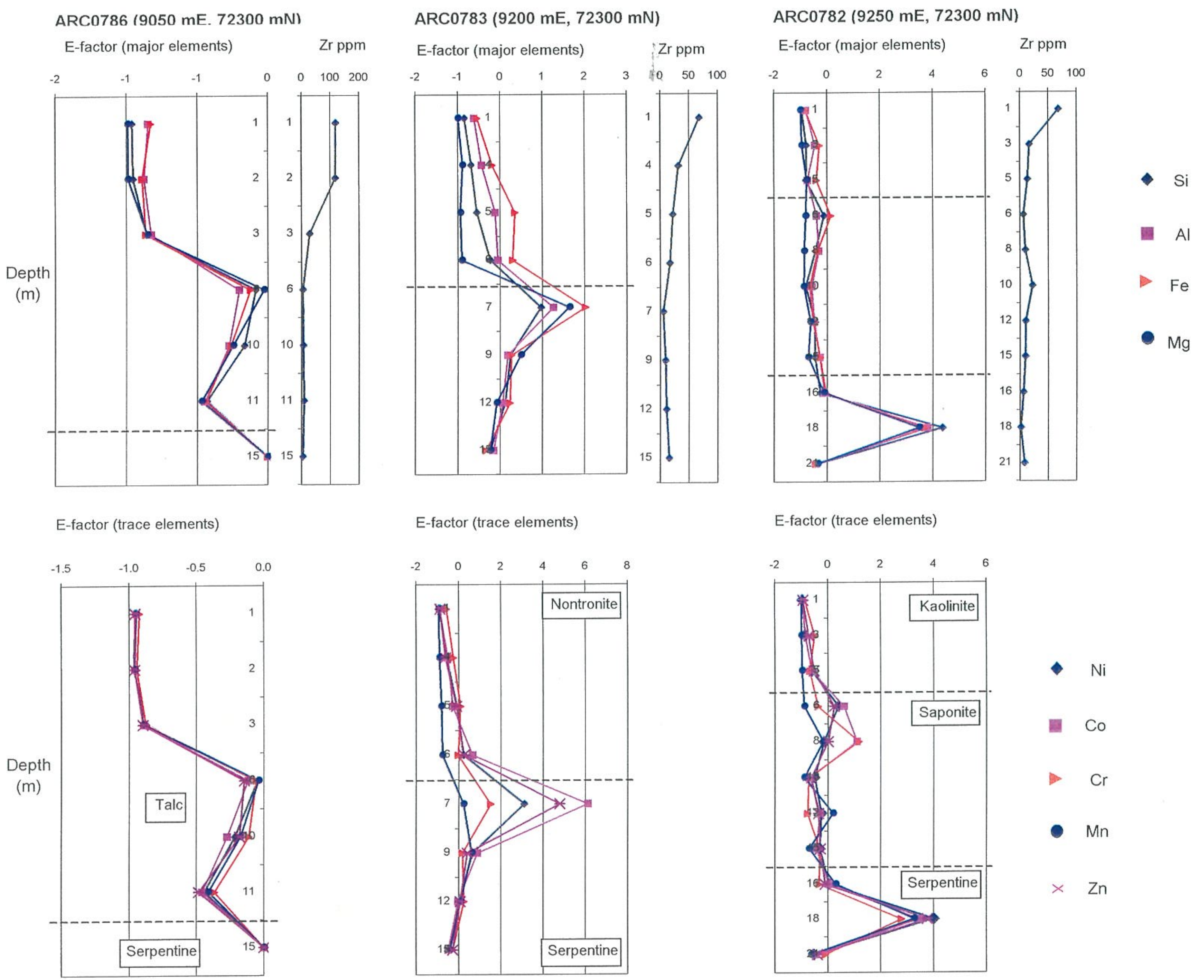

Figure 4.21. Enrichment (E) factors for major and trace elements, and Zr concentrations for selected RD drill holes at MM3. Regolith units as identified by PIMA are also shown.

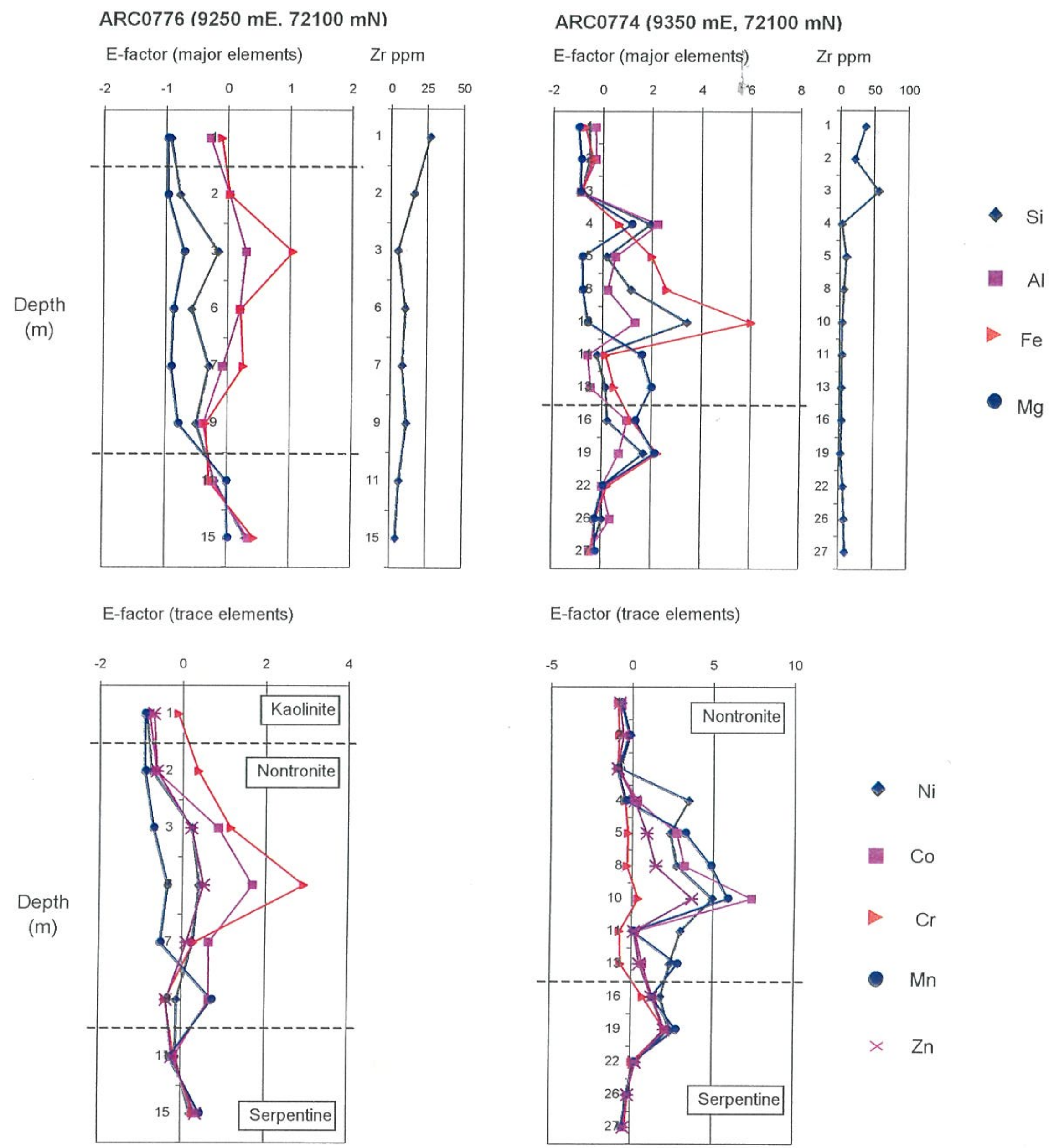

Figure 4.22. Enrichment (E) factors for major and trace elements, and Zr concentrations for selected RD drill holes at MM3. Regolith units as identified by PIMA are also shown.

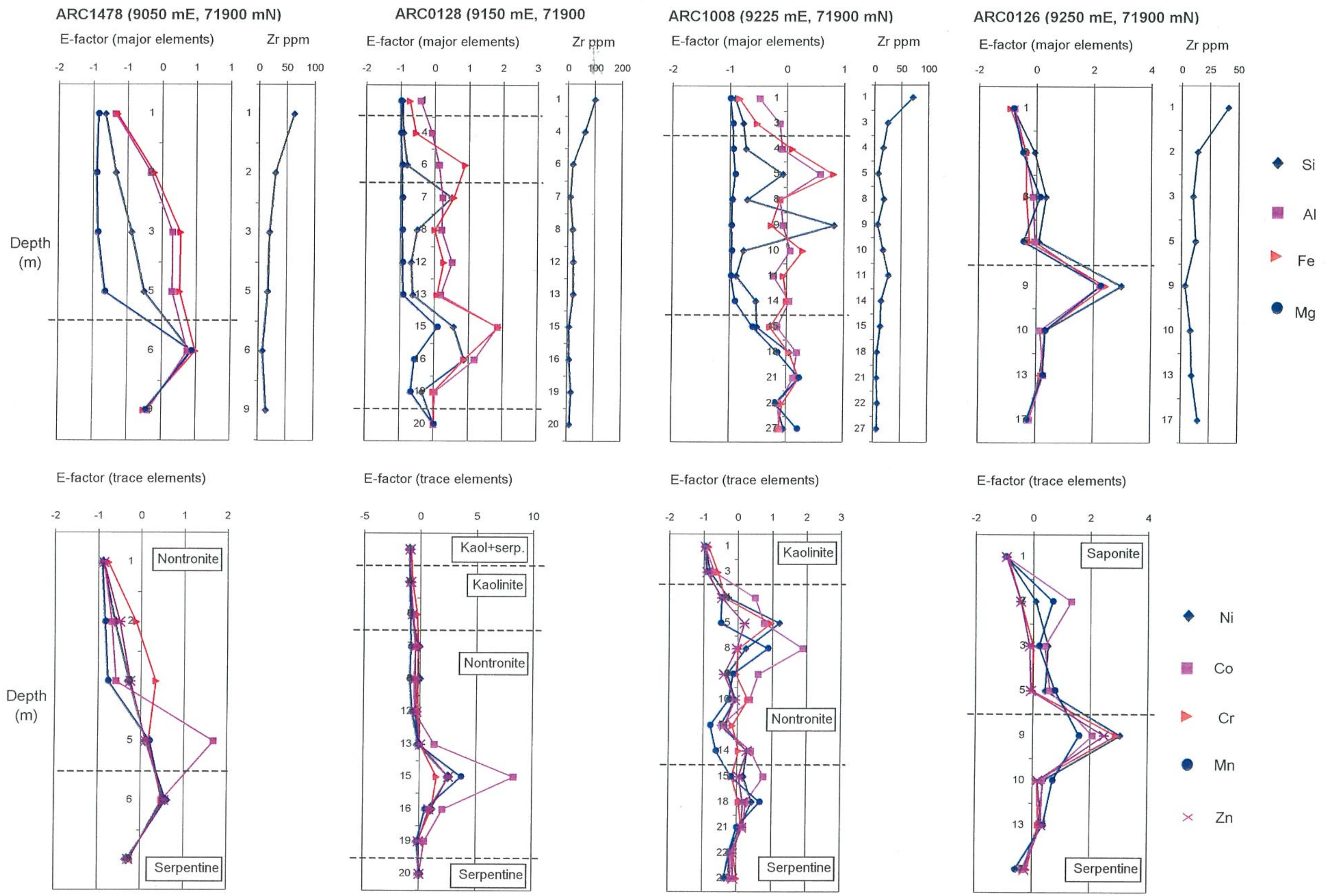

Figure 4.23. Enrichment (E) factors for major and trace elements, and Zr concentrations for selected RD drill holes at MM3. Regolith units as identified by PIMA are also shown.

the only zone of trace element enrichment in these profiles, particularly for drill holes at MM3 (*e.g.*, RC holes ARC0783 – Fig. 4.21; ARC1478 and 0128 – Fig. 4.23). A second zone of enrichment, particularly for Ni and Co, occurs higher in the profile within the upper nontronite or saponite units (*e.g.*, RC holes ARC0793 – Fig. 4.20; ARC0782 – Fig. 4.21; ARC0776 and 0774 – Fig. 4.22; ARC1008 and 0126 – Fig. 4.23), appears related to the zone of Al and Fe enrichment within these units.

4.7 Summary

The geochemical characteristics of the regolith at MM2 and MM3 were investigated by three-dimensional modelling of element-regolith associations using MVS, calculations of mass balance, and by cluster analysis. This approach has allowed local scale characterization of the lithological and structural controls to element distribution within the regolith at these deposits.

Nickel and Co mineralization within MM2 occurs mainly within the nontronite unit associated with variably weathered ortho- and meso-cumulates in topographical low areas, where development of nontronite is thickest. A strong, localized structural overprinting occurs as a conjugate fault-set, which is unrelated to primary structures within the western limb of the Kilkenny syncline. Reactivation of these faults during weathering has resulted in localized depletion of Ni and Co (and other elements) most likely due to fluid movement along fault shear planes.

A strong lithological control on Ni and Co mineralization is evident within the regolith at MM3, which is related to the primary structure of cumulates that form part of the western limb of the southerly plunging Kilkenny syncline. However, no apparent discrete change in cumulate lithology is shown. Rather, a gradational change from orthocumulates along the western and eastern margins of the deposit, through mesocumulates to a central adcumulate hosted lithology is indicated by gradational changes in the Ni/Ni+Al ratio.

Similar to the mineralization style at MM2, Ni and Co mineralization at MM3 is also associated with variably weathered ortho- and mesocumulates where nontronite development is thickest. Cobalt mineralization, as a localized enrichment, occurs mainly along the western margin of the deposit and may reflect the greater amounts of primary pyroxene phases within the intercumulus material associated with ortho- and, to a lesser extent, mesocumulates as compared to adcumulates. The variable weathering of ortho- and mesocumulates reflected in the variable topography of regolith surfaces associated with these rocks contrasts to the relatively subdued relief of regolith formed over adcumulates. The variable depth of weathering over ortho- and mesocumulates may reflect localized variations in the more open style of packing of serpentinized olivine as compared to the more tightly packed nature of serpentinized grains of olivine in adcumulates.

Nickel, Co, Fe, Al, Mg, Zn and Cr all show depleted concentrations within the cental adcumulate zone in MM3. The result for Ni and Mg is unexpected as adcumulates tend to have greater Ni and Mg contents than olivine ortho- and mesocumulates (Hill *et al.*, 1996). Mobilization of Mg away from the central adcumulate zone to the western and eastern margins may have occurred during weathering. In addition, development of a capping of secondary silica in the upper portions of profiles developed over adcumulate may have acted as a diluent to mineralization or acted to limit the mobilization of Ni within the profile.

5.0 SUMMARY AND DISCUSSION

A combined regional and deposit scale approach was employed to examine the characteristics and factors of Ni/Co enrichment within the Ni-laterite deposits at Murrin Murrin. The regional setting of the deposits and surrounding tenements was established by compilation of a 1:50000 regolith-landform map. A combined approach that incorporated aerial photographic interpretation, magnetic, radiometric and Landsat TM image analysis revealed broad, regional differences in the geomorphology and regolith-landform associations between MM north and MM south. This has implications for regolith evolution that are reflected in differences in the mineralogy and element-regolith associations in profiles at the deposit scale.

The north and south tenements at Murrin Murrin are effectively separated by a NW-SE trending, regional drainage divide, which has modified the regolith-landform associations in these areas. The regolith-landform characteristics of these areas can be summarized as follows:

MM north:

- Is dominated by depositional plains characterized by alluvial and colluvial surficial sediment.
- Has a subdued, local topography that is a result of sediment deposition and burial as the main geomorphic process. This may cause problems for exploration, as there is little outcrop.
- Local drainage is associated with the Lake Carey drainage system that drains to the NE of the area. This indicated that palaeochannel clay deposits might form a significant feature of the regolith in the area.
- Input of felsic sediments (high in Al, Si, Ca and Ti) to the sediment flux within the drainage system derive from granite/adamellite outcrops to the NW. This has implications for element-regolith associations, particularly, in upper sections of profiles.

MM south:

- The area is characterized by erosional and relict regolith-landform regimes. Landforms are dominated by low hills and rises of weathered ultramafics, which are often capped by ferruginous/siliceous duricrust forming hillcrests and ridges.
- Relict serpentine may be preserved at the surface contained within duricrust.

- Local drainage is associated with the Lake Raeside drainage system. Down-wearing by drainage incision sub-parallel to the strike of weathered ultramafics has produced a more prominent relief.

- Localized stripping of the upper portion of the weathered profile exposes the deeper regolith (*i.e.*, saprock and saprolite) at the surface; palaeochannel clays are not likely to be a feature of the regolith in the area.

- The area may be easier to explore because of the greater outcrop.

Determination of the lithological and structural factors influencing mineralization at the deposit scale was achieved by charaterization of the stratigraphy and distribution of regolith and element-regolith associations at two sites, MM2 and MM3, for the MM north and MM south tenements, respectively. Detailed mineralogical logging, using the portable infrared mineral analyser (PIMA), of RC drill hole profiles provided a qualitative means of enabling:

- Uniform and consistent description of regolith mineralogy within and between deposits, based on the main Al-Mg-silicate phase (*i.e.*, serpentine, talc, saponite, nontronite, and kaolinite) identified.

- Differences in regolith profiles within and between deposits to be more easily identified.

- A refinement of the generic Ni laterite profile established by Anaconda Nickel NL.

Profiles of the regolith stratigraphy, produced from logging using PIMA (Table 4.2), were used to provide a geological framework for modelling of element distributions using the Mining and Visualization Software (MVS) system. This enabled the three dimensional examination of the distribution of Ni and Co (and other metals) within the deposits. Cluster analysis, mass balance studies and determinations of the normative mineralogy allowed for a more detailed examination of the geochemistry, mineralogy and element-regolith associations at the two sites.

Table 4.2. Regolith characteristics for the deposits at MM2 and MM3.

MM2: PIMA unit	Normative mineralogy	Element Associations	Regolith profile: Anaconda^	Regolith profile: Generic
#0: Kaolinite-1	Kaolinite+SiO_2 ↑ up profile, to 80-90 Norm%. Plagioclase > muscovite ↓ up profile. <10% calcite in top 5m of profile	Increasingly dissimilar associations due to greater effect of weathering and input of felsic material at surface.	FZ or PC	Channel clays
#1: Kaolinite-2	Fe oxides ≥ kaolinite >> SiO_2 > nontronite > carbonate		FZ	Fe-rich, partially collapsed saprolite
#2: Nontronite	Fe oxides ≈ SiO_2 (≈ carbonate*) ≥ chlorite > nontronite		SM	Smectite
#3: Saponite	SiO_2 (≈ carbonate*) > Fe oxides ≈ chlorite > saponite	Very similar element groupings due to similar mineral compositions and minimal weathering.	SM (SA?)	Saprolite
#4: Talc	SiO_2 ≥ talc ≈ chlorite ≈ Fe oxides ≥ saponite ≈ carbonate		SA	
#5: Serpentine	Serpentine ≈ SiO_2 > Fe oxides ≈ chlorite (≈carbonate) > saponite		SA/UM	Saprock to fresh ultramafic
#6: Mixed serpentine			SA/UM	

MM3: PIMA unit				
#0: Kaolinite with serpentine	Kaolinite ≈ Fe oxides >>> serpentine > carbonate	Increasingly dissimilar associations due to greater effect of weathering at the surface.	FZ	Lateritic duricrust and preserved saprolite
#1: Kaolinite	Fe oxides ≥ SiO_2 ≈ kaolinite >> nontronite > carbonate		FZ	Fe-rich, partially collapsed saprolite
#2: Nontronite	SiO_2 (≈ carbonate*) > nontronite ≈ Fe oxides > chlorite		SM	Smectite
#3: Saponite	SiO_2 > Fe oxides ≈ saponite > chlorite ≈ carbonate	Element groupings similar due to similar mineral compositions and minimal weathering.	SM (SA?)	Saprolite
#4: Talc	Talc (≈ carbonate) > saponite ≈ chlorite ≈ Fe oxides ≈ SiO_2		SA	
#5: Serpentine	Serpentine > saponite ≈ carbonate ≈ Fe oxides ≈ SiO_2 ≈ chlorite		UM	Saprock to fresh ultramafic

^ Abbreviations of the regolith terms used by Anaconda: PC = plastic clays; FZ = ferruginous zone; SM = smectite zone; SA = saprolite; UM = ultramafic.
*Indicates that % Norm abundances of the carbonate phases, magnesite and dolomite, are highly variable, in the range 10–80 %. High SiO_2 contents correlate with low contents of carbonate, mainly as magnesite.
The 'kaolinite-2' unit at MM2 is equivalent to the 'kaolinite' unit at MM3.

A summary of the regolith characteristics for the deposits at MM2 and MM3 is presented in Table 4.2. Regolith development and mineralization styles within the Murrin Murrin deposits are very much dependent on structural and lithological factors that prevail at the deposit scale. The main differences within and between the two deposits are outlined below:

MM2

- Underlying lithology is dominantly ortho- and mesocumulate as shown from distributions of the Ni/Ni+Al ratio for values in the range 0.05 to 0.4. There is no apparent lithological control to mineralization within this variation.

- A very strong structural control to Ni and Co mineralization is expressed within the regolith as an intersecting (*i.e.,* conjugate), NW-SE/NE-SW trending fault set.

- Probable normal movement along fault planes, seemingly reactivated during weathering (probably during the early to mid-Tertiary), coupled with fluid movement along shears, has caused localized depletion within mineralized zones of the profile. Modelling of the distribution of fault systems at the deposit scale is important to understanding the distribution of Ni and Co.

- The greatest enrichment of Ni and Co occurs mainly within the nontronite unit associated with variably weathered ortho- and mesocumulates along the fault system.

- Iron oxides (*i.e.,* Fe_2O_3) and kaolinite are the dominant phases in the 'nontronite' and 'kaolinite' units of the regolith, comprising between 50-70 and 30-50 %, respectively, of the normative mineralogy. Nontronite is only a comparatively minor component of the 'nontronite' unit, with abundances of generally < 10 Norm%. Amounts of SiO_2 are highly variable, comprising up to 60-80 Norm%. Variations in the regolith mineralogy may have metallurgical implications to ore processing, concerning the fluid characteristics of these materials during ore preparation and blending.

- Within the lower units of the regolith, Al is hosted by chlorite, whereas within the upper horizons (*i.e.,* from the upper portion of the nontronite unit) Al is dominantly hosted by kaolinite.

MM3

- There is a very strong lithological control to Ni and Co mineralization related to underlying ortho- and mesocumulates. No enrichment of Ni or Co occurs within regolith developed over adcumulates.

- Enrichment of Ni and Co occurs mainly within the 'nontronite' unit formed over ortho- and mesocumulates where the development of 'nontronite' is thickest. Nickel and Co are depleted over adcumulate where silicification has either inhibited enrichment or acted as a diluent to mineralization. This may have implications for mine pit design.

- The Ni/Ni+Al ratio can discriminate cumulate lithologies in fresh rock. This discrimination holds for all horizons up to and including the lower portion of the 'kaolinite' unit and is well correlated to the underlying cumulate lithology.

- A gradational variation in values of the Ni/Ni+Al ratio indicated a gradational change in lithology from orthocumulates along the western and eastern margins of the deposit, through mesocumulate rocks to a central adcumulate zone.

- Regolith developed immediately adjacent to and over adcumulate is relatively consistent, with a uniform depth of weathering and units of uniform thickness.

- Ortho- and mesocumulates weather to variable depths that produce complex regolith profiles with units that have topographically varied boundaries. This may have implications for mine pit design.

- The variable depth of weathering over ortho- and meso-cumulates may be related to local variations in the porosity of serpentinized olivine. Drainage over and within adcumulates is inhibited by extensive secondary silicification.

- Fe oxides (*i.e.*, as Fe_2O_3) and kaolinite are the dominant phases in the 'nontronite' and 'kaolinite' units within the upper portion of the deposit, amounting to between 50-70 and 30-50 %, respectively, of the normative mineralogy. Nontronite and saponite are present in significant amounts within the smectite and saprolite and can amount to 30-50 Norm%. Chlorite is only a minor phase within the 'saponite' and 'nontronite' horizons comprising generally < 10 Norm%, reflecting the low Al-content of adcumulates. Amounts of SiO_2 are highly variable, and can comprise up to 60-80 % of the normative mineralogy. Variations in the regolith mineralogy may have metallurgical implications to ore processing, concerning the fluid characteristics of these materials during ore preparation and blending.

Mn-Co association

The presence of Co in these profiles was generally related to the occurrence of Mn. However, high grades of Mn did not necessarily indicate high grades of Co. Reasons for this are unclear but may indicate:

- That Co was already depleted where the Mn oxides initially precipitated. Cobalt may associate with Mn oxides only if Mn and Co are in solution and either co-precipitate or Co is adsorbed after Mn oxides precipitate. Manganese oxides preserved by silicification associated with initial stages of weathering of adcumulates would be unavailable to take up Co and so appear as Co-poor.

- There may be two (or more) generations of Mn oxides, with each successive generation a result either of complex weathering events or are a result of episodic wetting and drying cycles associated with fluctuating water-table levels, similar to the movement of Fe within weathering profiles. Evidence for the remobilization of Mn within the regolith is shown by the precipitation of Mn oxides along shear planes. This may then release Co back into solution to be redistributed within the regolith.

Potassium-Ar and Ar-Ar dating of K-bearing Mn oxides may have helped to establish a chronology of Mn oxide precipitation within these profiles, in relation to major weathering events preserved in the profile. However, time constraints and limited access to a suitable dating laboratory prevented such dating work to be carried out. This is something that could be considered for future research.

6.0 AKNOWLEDGEMENTS

The authors would like to thank Dr Ravi Anand for his comments on Chapter 2 of this report. Critical reviews of Chapters 3 and 4 by Dr. E. Ramanaidou and Mr. K. Scott, respectively were also appreciated. Other members of the CRCLEME staff including Dr. D. Grey, Mr. D. Longman, Dr. N. Sergeev, Mr. M. Paine and Dr. E. Nickel are thanked for their assistance and time.

The assistance of Mr. M. Hart in preparing samples for XRD and XRF analysis is also greatly appreciated. Mr. B. Bervan is thanked for his efforts in performing the PIMA measurements from which most of this work is derived. The assistance of Mr. C. Steel, Mr. A. Vartesi and Mr. T. Naughton of the CRCLEME, Visual Resources Unit in preparing a number of figures for the report are also greatly appreciated.

Finally, the authors would like to thank members of the exploration staff at Anaconda, in particular Mr. R. Monti and Mr. I. Mulholland, for allowing access to the resources of Anaconda Nickel NL in supplying geochemical and drill log data, permitting a number of field trips to the deposits and for encouraging the research into the Ni laterites at Murrin Murrin. The first author would also like thank Anaconda Nickel NL for financial support from October to December 1999.

7.0 REFERENCES

Anand, R.R., Churchward, H.M., Smith, R.E. and Grunsky, E.C. 1991. Regolith-landform development and consequences on the characteristics of regolith units, Lawlers district, Western Australia. CSIRO Australia. Division of Exploration Geoscience. Perth. Restricted Report 166R. CSIRO/AMIRA Laterite Geochemistry Project P240. 160pp. (Unpublished).

Anand, R.R., Churchward, H.M., Smith, R.E., Smith, K., Gozzard, J.R., Craig, M.A., and Munday, T.J. 1993. Classification and Atlas of regolith-landform mapping units. CSIRO Australia. Division of Exploration and Mining. Perth. Restricted Report 440R. CSIRO/AMIRA Exploration Perspectives for the Yilgarn Craton, Project 240A. (Unpublished).

Bailey, S.W. 1980. Structures of layer silicates. In: G.W. Brindley and G. Brown (Editors), Crystal sructures of clay minerals and their x-ray identification. Mineralogical Society Monograph No. 5, 1-124pp.

Beauvais, A. and Colin, F. 1993. Formation and transformation processes of iron duricrust systems in tropical humid environment. Chemical Geology 106, 77-101.

Bird, M.I. and Chivas, A.R. 1989. Stable-isotope geochronolgy of the Australian regolith. Geochimica et Cosmochimica Acta 53, 329-3256.

Brand, N.W., Butt, C.R.M. and Hellsten, K.J. 1996. Structural and lithological controls in the formation of the Cawse nickel laterite deposits, Western Australia - implications for supergene ore formation and exploration in deeply weathered terrains. In: E. J. Grimsey and I. Neuss (Editors). Nickel '96: Mineral to Market, The Australasian Institute of Mining and Metallurgy, Carlton, Victoria, Australia, 185-190pp.

Brand, N.W., Butt, C.R.M. and Elias, M., 1998. Nickel laterites: classification and features. AGSO Journal of Australian Geology and Geophysics 17, 81-88.

Brand, N.W. and Butt, C.R.M., 1999. Regolith geology of the Mt Keith, MKD5 nickel sulphide deposit, Western Australia. In: G. Taylor and C.F. Pain (Editors), New Approaches to an Old Continent. Proceedings, Regolith '98. CRC LEME, Perth, 335-341pp.

Braun, J.J., Pagel, M., Heerbillon, A. and Rosin, C. 1993. Mobilization and redistribution of REEs and thorium in a syenite lateritic profile: A mass balance study. Geochimica et Cosmochimica Acta 57, 4419-4434.

Burger, P.A. 1999. The Bulong Ni/Co laterite project, WA: a case history. In: Nickel Laterites, Workshop Notes; February 1999. Centre for Teaching and Research in Strategic Mineral Deposits, Geology Department, University of Western Australia (unpaginated).

Burger, P.A. 1996. The Bulong, Western Australia, Ni/Co laterite deposit: a case history. In: E. J. Grimsey and I. Neuss (Editors). Nickel '96: Mineral to Market, The Australasian Institute of Mining and Metallurgy, Carlton, Victoria, Australia, 37-41pp.

Butt, C.R.M. 1974. Nickel laterites and bauxites. CSIRO Australia, Division of Mineralogy, Report FP 12, 34pp.

Butt, C.R.M. and Nickel, E.H., 1981. Mineralogy and geochemistry of the weathering of the disseminated nickel sulfide deposit at Mt. Keith, Western Australia. Economic Geology 76, 1736-1751.

Camuti, K.S. and Riel, R.G. 1996. Mineralogy of the Murrin Murrin laterites. In: E.J. Grimsey and I. Neuss (Editors), Proceedings Nickel '96, The Australasian Institute of Mining and Metallurgy, Melbourne. 209-210pp.

Churchman, G.J., Whitton, J.S., Claridge, G.G.C. and Theng, B.K. 1984. Intercalation method using formamide for differentiating halloysite from kaolinite. Clays and Clay Minerals 4, 241-248.

Clayton, R.N. and Mayeda, T.K. 1963. The use of bromine pentafluoride in the extraction of oxygen from oxides and silicates for isotopic analysis. Geochimica et Cosmochimica Acta 27, 43-52.

Colin, F., Brimhall, G.H., Nahon, D., Lewis, C., Baronnet, A. and Danti, K. 1992. Equatorial rain forest lateritic mantles: A geomembrane filter. Geology 20, 523-526.

Cudahy, T.J. 1989. Improved lithological and structural mapping using Landsat thematic mapper and NS001 remotely sensed data in the Laverton region, Western Australia. CSIRO. Australia. Division of Exploration Geoscience. Perth. Restricted Report 61R. CSIRO/AMIRA Exploration for concealed gold deposits Yilgarn Block, Western Australia, Remote sensing project P243. 20pp. (Unpublished).

De Oliveira, S.M., Trescases, J.J. and Melfi, A.J. 1992. Lateritic nickel deposits of Brazil. Mineralium Deposita 27, 137-146.

Delvigne, J.E. 1998. Atlas of micromorhology of mineral alteration and weathering. R.F. Martin (Editor). The Canadian Mineralogist, Special Publication, No.3 494pp.

Denn, S. 1999. Cawse nickel laterite deposit. In: Nickel Laterites, Workshop Notes; February 1999. Centre for Teaching and Research in Strategic Mineral Deposits, Geology Department, University of Western Australia (unpaginated).

Deutscher, R.L., Mann, A.W. and Butt, C.R.M. 1980. Model for calcrete uranium mineralization. In: C.R.M. Butt and R.E. Smith (Editors), Idealized models, Section D, Conceptual models in exploration geochemistry. Special Issue, Journal of Geochemical Exploration 12, 139-161.

Dickson, B.L. and Scott, K.M. 1990. Radioelement distribution in weathered granitoids and aeolian soils in NSW. CSIRO. Australia. Division of Exploration Geoscience. Perth. CSIRO/AMIRA Improving the interpretation of airborne gamma-ray surveys, Project P263. (Unpublished).

Dickson, B.L. and Scott, K.M. 1997. Interpretation of aerial gamma-ray surveys – adding the geochemical factors. AGSO Journal of Australian Geology and Geophysics 17, 187-200.

Drury, S.A. and Hunt, G.A. 1988. Remote sensing of laterized Archaean greenstone terrain: Marshall Pool area, northeastern Yilgarn block, Western Australia. Photogrammetric Engineering and Remote Sensing 54, 1717-1725.

Drury, S.A. and Hunt, G.A. 1989. Geological uses of remotely-sensed reflected and emitted data of lateritized Archaean terrain in Western Australia. International Journal of Remote Sensing 10, 475-497.

Elias, M., Donaldson, M.J. and Giorgetta, N. 1981. Geology, mineralogy and chemistry of lateritic nickel-cobalt laterite deposits near Kalgoorlie, Western Australia. Economic Geology 76, 1775-1783.

Esson, J. 1983. Geochemistry of a nickeliferous laterite profile in Liberdade, Brazil. In: R.C.L. Wilson (Editor), Residual deposits: Surface related weathering processes and materials. Geological Society of London Special Publication 11, 91-99pp.

Fraser, S.J., Gabell, A.R., Green, A.A. and Huntington, J.F. 1986. Targeting epithermal alteration and gossans in weathered and vegetated terrains using aircraft scanners: Successful Australian case histories. In: Remote sensing for exploration geology. 5th Thematic Conference. Reno, Nevada. 1986.

Gibb, R.J. 1967. Quantitative x-ray diffraction analysis using clay minerals standards extracted from the sample to be analyzed. Clay Minerals 7, 79-90.

Girard, J.P., Razanadranorosoa, D. and Freyssinet, P. 1997. Laser oxygen isotope analysis of weathering goethite from the laterite profile of Yaou, French Guiana: paleoweathering and paleoclimatic implications. Applied Geochemistry 12, 163-174.

Golightly, J.P. 1979. Nickeliferous laterites: a general description. In: D.J.I Evans, R.S. Shoemaker and H. Veltman (Editors). International Laterite Symposium. American Institute of Mining, Metallurgical and Petroleum Engineers, Inc. 3 –23pp.

Golightly, J.P., 1981. Nickel laterite deposits. 75th Anniversary Edition, Economic Geology 76, 1775-1783.

Gower, C.F. 1976. 1:250 000 Geological Series – Explanatory Notes: Laverton, Western Australia. Geological Survey of Western Australia, Sheet SH/51-2.

Gunn, P.J., Minty, B.R.S. and Milligan, P.R. 1997. The airborne gamma-ray spectrometric response over arid Australian Terranes. In: A.G. Gubins (Editor) Proceedings of Exploration 97. Fourth Decennial International Conference on Mineral Exploration. 733-740pp.

Hill, R.E.T., Hunter, W.M., Liimatainen, J.Y. and Barnes, S.J. 1996. Ultramafic rock units in the Murrin Murrin region (Anaconda Nickel NL tenements). Exploration and Mining Report 205R. 11pp plus geological maps.

Lipton, I.T., Gaze, R.L., Horton, J.A. and Khosrowshahi, S. 1999. Recoverable resource estimation for the Halley's Lateritic nickel deposit. In: Nickel Laterites, Workshop Notes; February 1999. Centre for Teaching and Research in Strategic Mineral Deposits, Geology Department, University of Western Australia (unpaginated).

Llorca, S.M., 1993. Metallogeny of supergene cobalt mineralisation, New Caledonia. Australian Journal of Earth Science 40, 377-385.

McMurty, G.M., Wang, C-H, and Yew, H-W. 1983. Chemical and isotropic investigations into the origin of clay minerals from the Galapogos hydrothermal mounds field. Geochimica et Cosmochimica Acta 47, 475-489.

Mabbutt, J.A. 1963. Geomorphology of the Wiluna-Meekatharra area. In: J.A. Mabbutt, W.H. Litchfield, N.H. Speck, J. Sofoulis, D.G. Wilcox, J.M. Arnold, M. Brookfield and R.L. Wright General report on lands of the Wiluna-Meekatharra area, Western Australia, 1958. CSIRO Land Research Series No. 7. 107-122pp.

Monti, R., 1999. Murrin Murrin nickel-cobalt project. In: Nickel Laterites, Workshop Notes; February 1999. Centre for Teaching and Research in Strategic Mineral Deposits, Geology Department, University of Western Australia (unpaginated).

Monti, R. and Fazakerley, V.W. 1996. The Murrin Murrin nickel cobalt project. In: E.J. Grimsey and I. Neuss (Editors), Proceedings Nickel '96, The Australasian Institute of Mining and Metallurgy, Melbourne. 191-196pp.

Nahon, D., Paquet, H. and Delvigne, J. 1982. Lateritic weathering of ultramafic rocks and the concentration of nickel in the Western Ivory Coast. Economic Geology 77, 1159-1175.

Nesbitt, H.W. 1979. Mobility and fractionation of rare earth elements during weathering of a granodiorite. Nature 279, 206-210.

Pain, C., Chan, R., Craig, M., Hazell, M., Kamprad, J. and Wilford, J. 1991. RTMAP, BMR regolith database field handbook. 1st edition. Minerals and Landuse Program Series. BMR Geology and Geophysics, Australia. Regolith Series No. 4.

Parianos, J.M. and Rivers, C.J., 1996. Geology and mineralogy of the Brolga laterite deposit, Central Queensland. In: E. J. Grimsey and I. Neuss (Editors). Nickel '96: Mineral to Market, The Australasian Institute of Mining and Metallurgy, Carlton, Victoria, Australia, 63-68pp.

Porto, C.G. and Hale, M. 1995. Gold redistribution in the stone line lateritic profile of the Posse deposit, central Brazil. Economic Geology 90, 308-321.

Pringle, H.J.R., Van Vreeswyk, A.M.E. and Gilligan, S.A. 1994. An inventory and condition survey of rangelands in the northeastern Goldfields, Western Australia. Department of Agriculture Technical Bulletin, No. 87. 323pp.

Ragland, P.C. 1989. Basic Analytical Petrology. Oxford University Press. 369pp.

Schellmann, W. 1989. Allochthonous surface alteration of Ni-laterites. Chemical Geology 74, 351-364.

Short, S.A., Lowson, R.T., Ellis, J. and Price, D.M. 1989 Thorium-uranium disequilibrium dating of Late Quaternary ferruginous concretions and rinds. Geochimica et Cosmochimica Acta 53, 1379-1389.

Tapley, I.J. and Gozzard, J.R. 1992. Regolith-landform mapping in the Lawlers District. Report 4. Aerial photographic interpretation and Landsat Thematic Mapper processing for mapping regolith-landforms. CSIRO/IMEC Division of Exploration Geoscience Restricted Report 239R.

Venturelli, G., Contini, S. and Bonazzi, A. 1997. Weathering of ultramafic rocks and element mobility at Mt. Prinzera, northern Apennines, Italy. Mineralogical Magazine 61, 765-778.

Wells, M.A. 1999. Murrin Murrin region regolith-landform map: Explanatory notes. CRCLEME Restricted Report 123R, 15pp.

Wells, M.A. and Butt, C.R.M. 1998. Characterization of a "Green-spotted" rock from the Murrin Murrin Ni-laterite deposit. CRCLEME Restricted Report 88R, 5pp.

Wilford, J.R., Bierwirth, P.N. and Craig, M.A. 1997. Application of airborne gamma-ray spectrometry in soil-regolith mapping and applied geomorphology. AGSO Journal of Australian Geology and Geophysics 17, 201-216.

Yeh, H-W. 1980. D/H ratios and late stage dehydration of shales during burial. Geochimica et Cosmochimica Acta 44, 341-352.

APPENDIX 1: PALAEOMAGNETIC DATING OF REGOLITH, MURRIN MURRIN, W.A.

Brad Pillans, CRC LEME

c/- RSES, ANU, Canberra

Samples and sites

As part of a reconnaissance study on the Yilgarn Craton, to assess the suitability of regolith materials for paleomagnetic dating, samples were collected at Murrin Murrin during two field visits:

1. 2nd April, 1998. Three samples (WAA-035 to WAA-037) of grey saprolite with numerous, prominent slickensided joints, from the west wall of the test pit at MM2. [SITE 6], and six samples (WAA-038 to WAA-043) from the base of ferruginized saprolite in the south wall of the test pit at MM7. [SITE 7]

2. 8th November, 1998. Twenty samples (WAA-101 to WAA-120) from the base of ferruginized saprolite (as above) in the test pit at MM7. [SITE 7]

Samples were collected from the walls of the pits, cut back with a spade to expose a fresh, sub-vertical face. Small cube-shaped pedestals were carved with a sharp knife, onto which 6 cm^3 plastic boxes were carefully fitted. Before removal from the face, samples were oriented with a Brunton compass, and the directions later corrected for local magnetic declination.

Laboratory measurements

Samples were subject to stepwise demagnetization, using both thermal and alternating field (a.f) techniques. Thermal demagnetisation generally yields more consistent results for regolith materials, and hence a.f. demagnetization was used only for samples that were too friable for thermal treatment. Remanence was measured on a ScT 2-axis cryogenic magnetometer at the Black Mountain Palaeomagnetic Facility, Canberra. Magnetic susceptibility (as volume susceptibility, K) was measured on a Digico bulk susceptibility bridge, to monitor possible

Appendix 1. Table A1.1. Summary of paleomagnetic results.

SITE	LOCATION	COMP[1]	N(+)[2]	REMANENCE DIRECTIONS				SOUTH POLE				AGE[4]
				Decl.	Incl.	K[3]	α_{95}	Long.	Lat.	K[3]	α_{95}	
	Murrin Murrin (121.9°E, 28.8°)											
7	Test pit at MM7	LT	13(0)	009.6	-65.0	118.4	3.83	102.5E	69.7S	70.0	4.99	Czm?
		IT1	16(16)	269.1	-32.2	20.4	8.38	195.5E	07.4S	20.4	8.37	---
		IT2	12(12)	263.7	-23.3	51.2	6.12	198.1E	00.4S	64.1	5.46	---
		HT	21(21)	278.8	-51.4	23.8	6.66	184.5E	22.0S	16.8	7.99	Mz
6	Test pit at MM2	HF	3(3)	039.5	40.6	525.5	5.38	162.3E	25.5N	702.9	4.65	Pz
	Bulong (121.8°E, 30.7°S)											
10	Test Pit, 15-20 m	HT,HF	7(7)	038.4	46.7	157.8	4.29	157.8E	20.7N	128.6	5.34	Pz
	Perth Basin (Schmidt & Embleton 1976)											
PB	Permian to Cretaceous sediments	HT	128(?)					109.9E	82.7S		2.4	Czu

1 Magnetic component. LT = Low temp (<300° C); IT1 = Intermediate temp (300°-580° C); HT = High temp (>580° C); HF = High field (>20 mT).
2 N = number of specimens; (+) = number of specimens with positive inclination.
3 K = Volume magnetic susceptibility (dimensionless).
4 Czm = mid Cainozoic; Czu = upper (late) Cainozoic; Mz = Mesozoic; Pz = Proterozoic.

mineralogical changes with increasing temperature. Characteristic remanent magnetizations were identified by principal component analysis (Kirschvink 1980).

Results

Samples from the ferruginous saprolite in the test pit at MM7 all yield multicomponent magnetization directions as revealed by orthogonal plots and principal component analysis (Table 1). The four components are as follows:

1. A low temperature (LT) component, isolated at temperatures less than 300° C, in which all specimens are of normal polarity. The mean pole position is consistent with a mid-Tertiary (late Oligocene) age, based on the apparent polar wander path (APWP) of Idnurm (1985, 1994). Unfortunately, the LT component is very similar to the direction of the present day magnetic field at Murrin Murrin (declination 001°; inclination -63°), so there is a possibility that it is a modern (mining-related) remanence. That is, a magnetic remanence is induced (a chemical remanent magnetization, CRM), from exposure of previously buried saprolite by mining operations by either drying (if saprolite was below the water table) or by oxidation, in the direction of the present geomagnetic field.

2. Two intermediate temperature components (IT1 and IT2), isolated between 300° and 580°C, which yield pole positions (Table 1) that lie to the northeast of the Mesozoic segment of the APWP for Australia (Embleton 1981). The two IT components probably represent unresolved (mixed) remanence components or are laboratory-induced (by heating during thermal demagnetisation), and therefore have no age significance.

3. A high temperature component (HT), isolated above 580°C, which yields a pole position, close to, but not quite overlapping the late Jurassic segment of the APWP (Embleton 1981). The high thermal stability of this remanence suggests that it may be a reliable age indicator.

Three samples from saprolite collected from the test pit at MM2, yield a high field component (HF) which gives a mean pole position statistically identical to the pole position calculated from seven saprolite specimens from the Bulong test pit (Table 1). The poles lie well away from the Phanerozoic APWP, and appear to lie on the Proterozoic APWP (M. Idnurm pers. comm. 1998). This suggests that the magnetic remanences are not weathering-induced but, rather, represent primary remanences inherited from the rock.

Discussion

Palaeomagnetic age estimates in regolith materials are based on the assumption that weathering processes have produced secondary iron oxides that preserve a record of the magnetic field at the time they formed. The resultant ages, therefore, relate to the time of weathering, not to the age of the rocks. A good example of this principle was described by Schmidt & Embleton (1976), who reported palaeomagnetic results from Late Paleozoic and Mesozoic rocks in the Perth Basin and adjacent areas. They identified a stable high temperature magnetisation, similar in direction for all rocks, regardless of age, which they interpreted as a "blanket" remagnetization resulting from a period of regional lateritization. The age of the weathering-induced remagnetization was estimated to be Late Oligocene to Early Miocene, but more recent revisions of the APWP (Idnurm 1985, 1994) indicate a Late Miocene or Pliocene age. The Perth Basin pole (Table 1) is statistically significantly different from the Murrin Murrin LT pole (Table 1), and hence the inferred ages of weathering are also different.

Since weathering is an ongoing process, which has affected the Yilgarn Craton throughout the Phanerozoic, there is no *a priori* reason why only one weathering-induced remanence should be preserved. Thus, the regolith at Murrin Murrin could preserve imprints of more than one age. From the palaeomagnetic results discussed above, there are indications of both Tertiary and Mesozoic weathering imprints at Murrin Murrin. However, a full interpretation of the Murrin Murrin poles, and their inferred ages must await results of a rock magnetic study of the samples to isolate the phases contributing to the high temperature component of remanent magnetization.

References

Embleton, B.J. 1981. A review of the paleomagnetism of Australia and Antarctica. In: M.W. McElhinney and D.A. Valencio (Editors). Paleoreconstruction of the continents. American Geophysical Union Geodynamics Series 2, 77-92 pp.

Idnurm, M. 1985. Late Mesozoic and Cenozoic palaeomagnetism of Australia - I. A redetermined apparent polar wander path. Geophysical Journal of the Royal Astronomical Society 83, 399-418.

Idnurm, M. 1994. New Late Eocene pole for Australia, time-averaging of remanence directions, and palaeogeographic reference systems. Geophysical Journal International 117, 827-833.

Kirschvink, J.L. 1980. The least-squares line and plane and analysis of palaeomagnetic data. Geophysical Journal of the Royal Astronomical Society 45, 699-718.

Schmidt, P.W. & Embleton, B.J.J. 1976. Palaeomagnetic results from sediments of the Perth Basin, Western Australia, and their bearing on the timing of regional lateritisation. Palaeogeography, Palaeoclimatology, Palaeoecology 19, 257-273.

APPENDIX 2: SMECTITE MINERALOGY OF NI LATERITE FROM MURRIN MURRIN

Y. NOACK, A. DECARREAU and A. GAUDIN
CEREGE – Université AM III – CNRS – BP80 –13545 AIX en Provence Cedex 4 - France

Background

As part of an initial study of the crystal chemistry of Ni-bearing smectites in lateritic Ni-deposits, a combined x-ray diffraction (XRD), infrared (IR) and scanning electron microscopic (SEM) investigation was undertaken of samples from diamond drill core of the Murrin Murrin Ni-deposit. Samples were collected during two field trips to Murrin Murrin:

1. October 1997, 25 samples were collected from drill core BHG1 and 10 samplse from drill core CBDD5.

2. In November 1998, 35, 16, 46 and 6 samples were collected from cores CBDD8, CBDD3, CBDD5 and ADD3, respectively.

X-ray diffraction analysis

Bulk mineralogy

The mineralogy of the samples generally comprised serpentine (base of profile), smectite, quartz, opal, magnetite and maghemite, hematite and goethite in the oxidized zone at the top of the profile. Kaolinite is the main phase above the boundary between the smectite and the oxidized zone. Talc, chlorite, dolomite, gypsum and magnesite are also found as minor phases.

In CBDD3, maghemite (or magnetite) persists to the oxidized zone. In CBDD8, both maghemite and serpentine disappears at greater depth; the maghemite is replaced by goethite. In CBDD5, serpentine disappears near 37 m; maghemite disappears near 17m and is replaced by goethite.

Smectite mineralogy

The clay fraction (*i.e.*, <2μm) of samples were collected by standard sedimentation techniques and poorly crystalline Fe oxides removed by treatment with TAMM's solution (*i.e.*, ammonium oxalate). All samples were Ca-saturated prior to XRD analysis.

X-ray diffraction patterns show a strong reflection between 12 and 15 Å, characteristic of smectite. The d-spacing of the (06.33) peak of 1.51 Å, is characteristic of dioctahedral smectite. After glycolation, the main smectite peak shifted to 17 Å, without traces of mixed-layered phases.

Lithium treatment allows distinction of montmorillonite (with octahedral charge) from beidellite-nontronite (with tetrahedral charge). Most samples showed two peaks, one at 17 Å (beidellite or nontronite) and one at 9 Å (montmorillonite).

The smectites, therefore, appear to be mixed-layered nontronite/beidellite-montmorillonite; there is a variable contribution from the two end-members that is not related to sample depth.

Chemical composition

Drill core CBDD3 and CBDD8

Different mineralogical phases (smectites, serpentine, Fe oxides, Ti oxides and Cr oxides) of bulk samples were analyzed by SEM-EDS. Due to the intimate association of these phases in some samples, reported element concentrations should be regarded as estimates only.

For samples from CBDD3, four populations were recognized (Fig. 1):

A. A mixture of Fe oxides and silicates (serpentine or smectites), with low Ni content.

B. A mixture of Fe oxides and silicates (serpentine or smectites), with a close relationship between Fe and Ni content.

C. Particles with high Mn and Co contents.

D. Particles with high Ni contents (with 5 to 25% NiO) and various Fe and Si contents.

In samples from CBDD8, five populations were identified (Fig. 2):

A. A mixture of Fe oxides and silicates (serpentine or smectites), with low Ni content.

B. A mixture of Fe oxides and silicates (serpentine or smectites), with a close relationship between the Fe and Ni contents.

C. A population with moderately high Ni (2 to 5%), low Fe (<below 25%) and high Al contents.

D. A population with high Ni and Fe content.

E. Particles with high Mn and Co contents.

Principal componant analysis showed similar behaviour (Fig. 3 and 4) in both cores. Elements were grouped into four assocations:

1. Silicates (Si-Al-Mg).

2. Fe oxy-hydroxides (Fe).

3. Manganese oxides (Mn, Co).

4. Nickel, present as a separate group, was not associated with any of the other groups.

Drill core BHG1 and CBDD5

Pure smectites were extracted from BHG1 and CBDD5 core samples as previously described and analyzed by SEM-EDS. The Al and Fe contents of the smectites show a strong negative relationship (Figures 5 and 7, respectively). The Ni contents of smectites from BHG1 were not related to abundances of other elements. However, a positive relationship was shown between Al and Ni contents for smectites from CBDD5. The Mg content for these samples also decreased from the bottom to the top of the core.

The structural formulae of smectites from BHG1 and CBDD5 were calculated, assuming smectite with 22 charges, and plotted in the octahedral Al-Fe^{3+}-(Mg+Ni) triangle used by Guven (1988) for smectite classification. All smectite compositions fall within the Nontronite field, with a trend to the Montmorillonite-Beidellite field for BHG1 (Fig. 6) and CBDD5 (Fig. 8).

Infra-red spectrometry

Infrared characterization of smectite mineralogy was performed using two techniques:

1. Fourier Transform Infrared (FTIR) analysis of samples from cores BHG1 and CBDD5.

2. PIMA (E. Ramanaidou, CSIRO Perth) for CBDD5 samples.

FTIR

At high wavelengths (> 3500 cm^{-1}), FTIR confirmed the purity of the smectite phase and its dioctahedral composition. At low wavelengths (< 1000 cm^{-1}), the Al_2OH, $Fe^{3+}{}_2OH$ and $Fe^{3+}OHMg$ bands are well developed, with a greater intensity of the Fe band (Fig. 9).

A comparison of spectra for an Fe-rich sample (36) and an Al-rich sample (37) shows the shift of the different bands to the high wave numbers with increasing Al content (Figures 10 and 11). No obvious bands that could be attributed to Ni were evident in the FTIR spectra.

FTIR study of Ca-saturated and Li-exchanged samples allows quantification of the octahedral and tetrahedral charge characteristics of smectite. The tetrahedral charge comprised 34 to 75 %, with an average of 58%, of the total charge and was generally higher than the octahedral charge (in 17 of 21 samples). Changes in the tetrahedral and octahedral charge distribution were not related to sample depth.

A comparison of spectra for green smectites hand picked from a fracture (19V) and smectites in the bulk rock (19RT), in the same sample, shows the latter to have a greater Fe content than smectites concentrated from the fracture surface (Fig. 12).

PIMA

PIMA spectroscopy (Fig. 13) confirmed the FTIR results, with a higher contribution of the montmorillonite end-member for the Al-rich sample (CBDD5-37) and for the nontronite end-member for the Fe-rich sample (CBDD5-36).

Surprisingly, Ni contents of the Al-rich smectite end member (*i.e.*, montmorillonite) showed a good positive relationship with the intensity of the 2216 nm (montmorillonite) band. That is, Ni is enriched in the montmorillonite end-member rather than the nontronite end-member, as might have been expected.

Isotopic analysis of kaolinite

Results of the isotopic analysis of kaolinite, concentrated from RC holes CBRC0724 and CBRC0796 at MM2, are presented in Table A2.1.

Table A2.1. Oxygen isotopic composition and age data of kaolinite concentrated from the kaolinite-2 regolith unit at MM2, Murrin Murrin.

Drill hole	Sample depth (m)	$\delta^{18}O$ (‰)	Interpreted age
CBRC0724	3	+13.1	
(9325 mE, 26300 mN)	4	+16.2	
	6	+15.1	Pre-mid
	7	+16.2	Tertiary
	8	+13.0	
	9	+15.8	
	12	+15.3	
CBRC0796	1	+25.1*	Post-mid
(9200 mE, 26100 mN)	4	+19.1	Tertiary
	5	+19.3	
	6	+19.1	
	11	+18.7	

* The very high $\delta^{18}O$ value for the surface sample in RC hole CBRC0796 may be due to contamination by smectite, which was indicated as a minor to trace constituent by XRD, for some of these samples. The presence of 5-10 % smectite in the surface sample, with an isotopic composition of near +30 ‰ would contribute between +1.5 to +3.0 ‰ to give a more realistic $\delta^{18}O$ composition near +22-23 ‰ for kaolinite.

Comparison of $\delta^{18}O$ values (Table A2.1) to expected $\delta^{18}O$ values for the age ranges of kaolinite reported by Bird and Chivas (1989), indicates a mid-Tertiary age for these samples. This also presents a mid-Tertiary age as a minimum age for formation of the kaolinite-2 regolith unit in which the kaolinite occurs.

Conclusions

Smectites from the Murrin Murrin deposit appear, by XRD, FTIR and SEM characterization, as nontronite/beidellite-montmorillonite mixed-layered minerals. Ni contents increased with the aluminium content and/or the montmorillonite component in the smectite.

These mixed-layered smectites are not the phases with the greatest Ni contents. The phases richest in Ni, probably discrete Ni oxide/oxyhydroxides, were not isolated and identified in samples of the present study. Further research is required to characterize these phases.

Further research expected includes:

- Very fine characterization of the smectite crystallographic structure.
- Comparison between green smectites in cracks and yellow-brown smectite, as replacement of olivine and serpentines, in the bulk rock, at the same depth (crystallographic structure, chemical composition).
- Localization of Ni in smectite and other phases (especially with Fe products).
- Oxygen and deuterium data for smectites (temperature of formation and water composition), with different nontronite/beidellite - montmorillonite mixed-layered composition.
- Strontium compositon of carbonates and sulphates. Initial results for two dolomite samples, gave Sr^{87}/Sr^{86} values near 0.713, indicative of an external (*i.e.*, felsic) origin for Ca.
- Investigation of the evolution (*i.e.*, structure, chemical composition, nickel abundance) of smectites in exposed cracks and fractures from the bottom to the top of weathering profiles, and at the fracture surface.

Additional samples, taken during the recent field-trip to Murrin Murrin in October 1999, will help to address these problems.

References

Bird, M.I. and Chivas, A.R. 1989. Stable-isotope geochronology of the Australian regolith. Geochimica et Cosmochimica Acta 53, 3239-3256.

Fig. 1: Drill core CBDD3: SEM analysis.

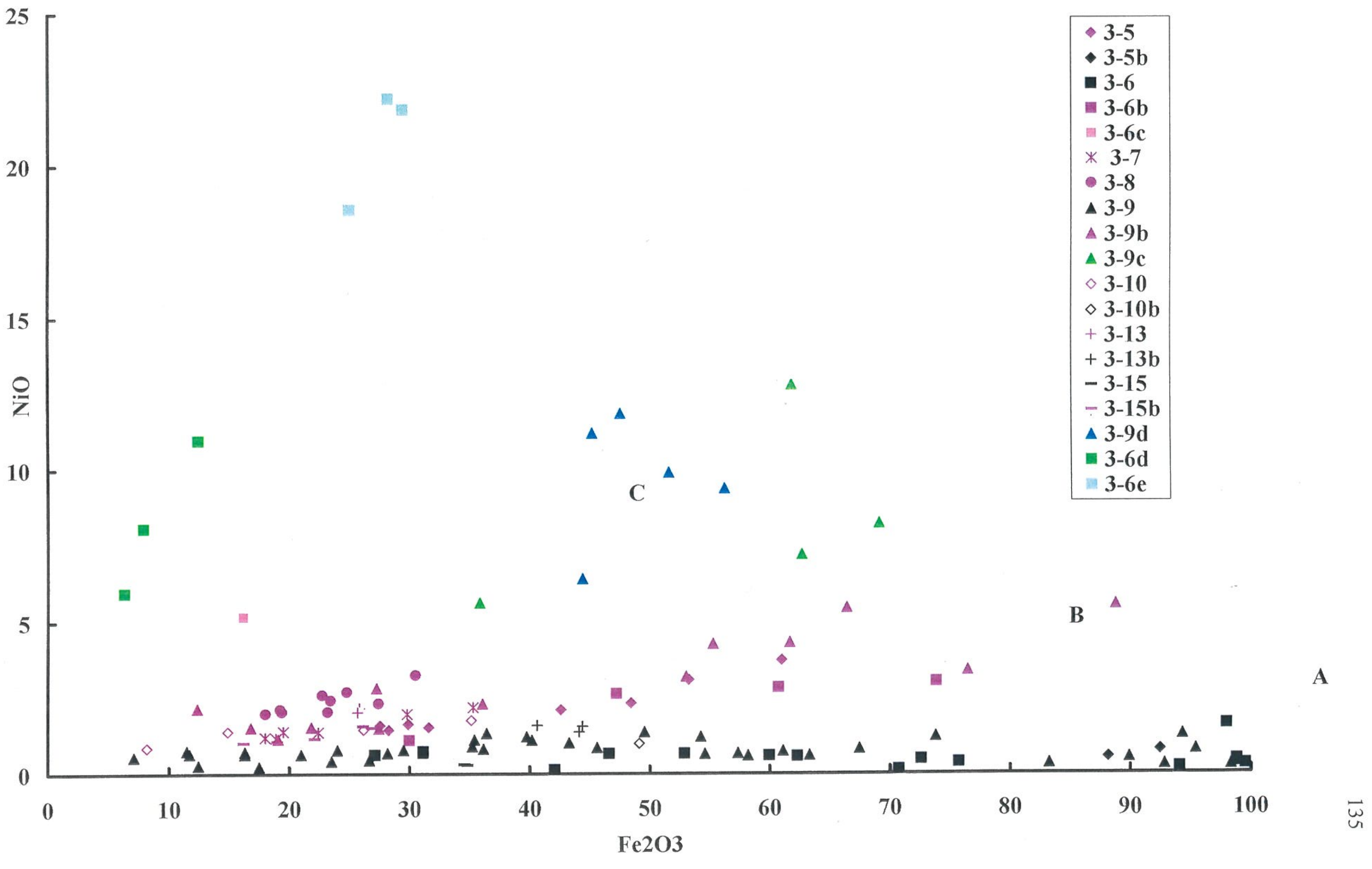

Fig. 2: Drill core CBDD8: SEM analysis.

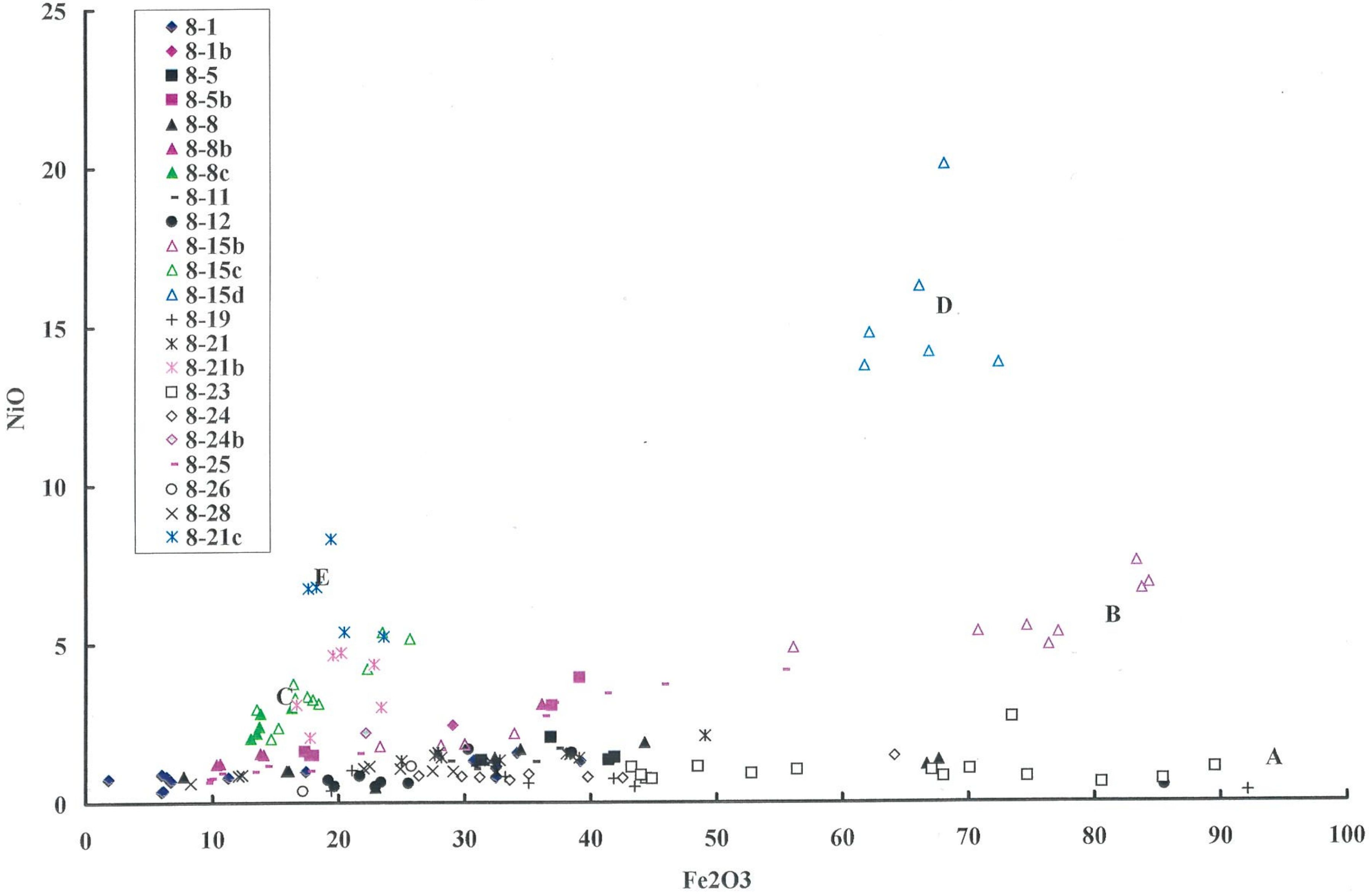

Fig. 3: Principal component analysis diagram for drill core CBDD3.

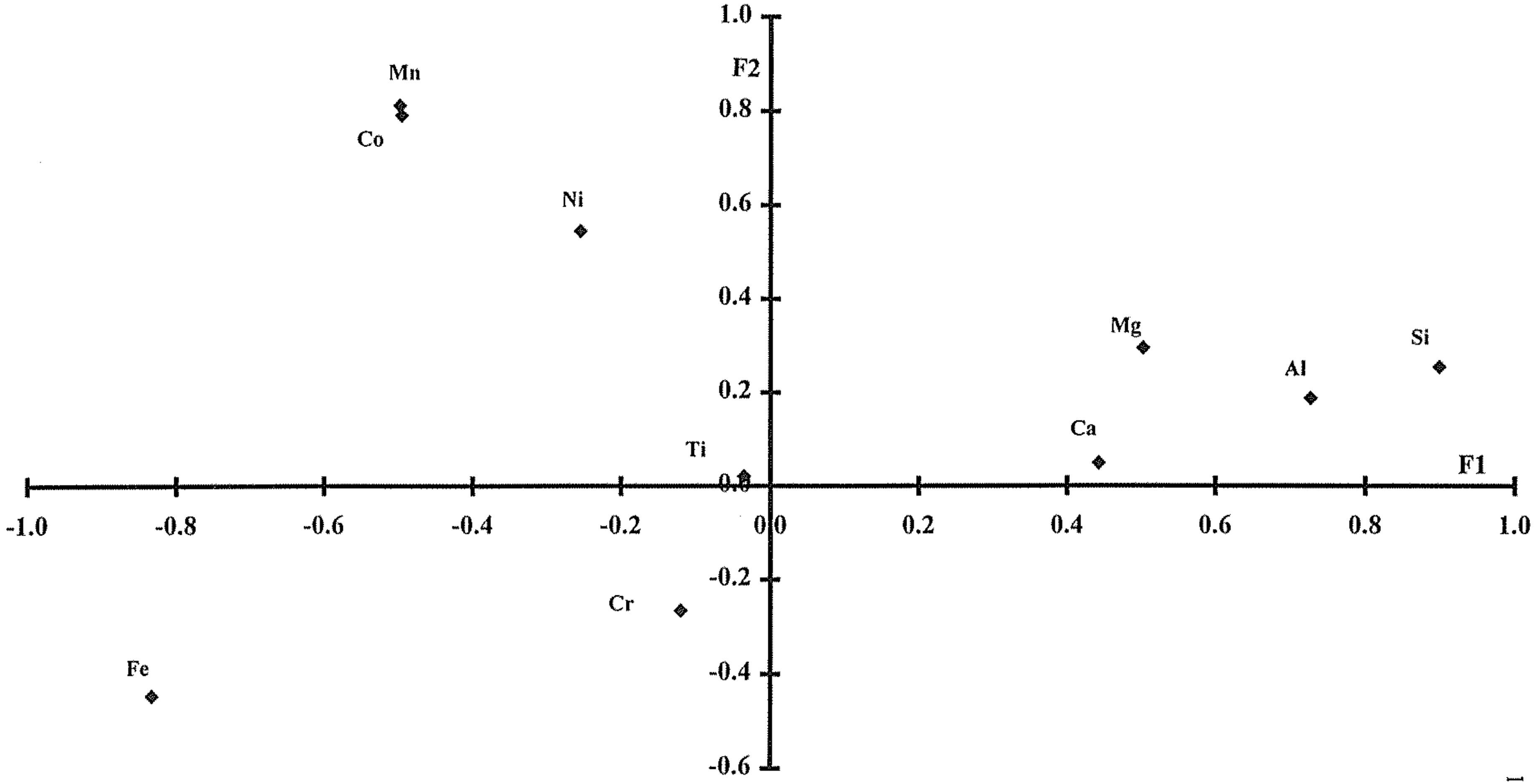

Fig. 4 : Principal component analysis diagram for drill core CBDD8.

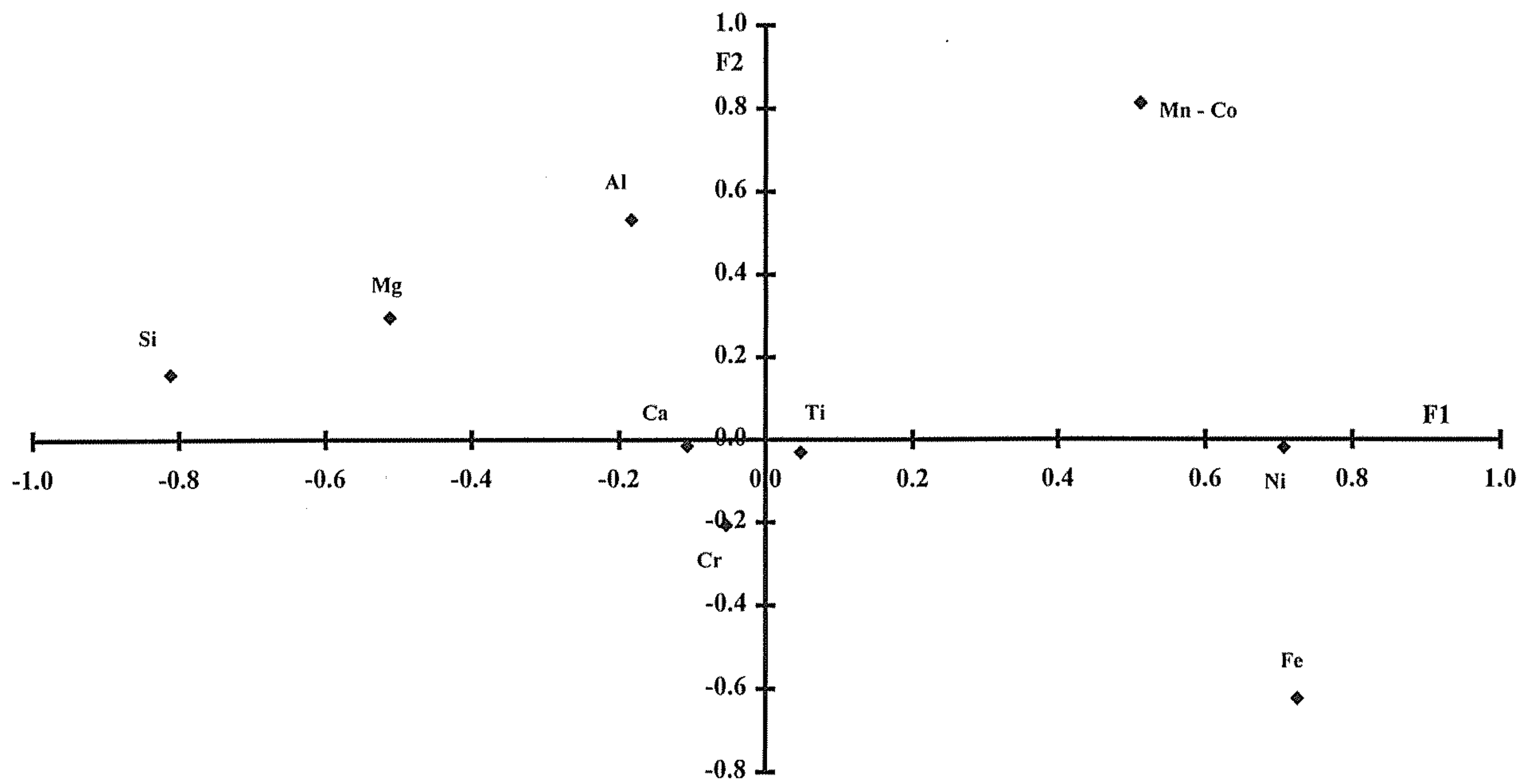

Fig. 5 : Smectites from drill core BHG1.

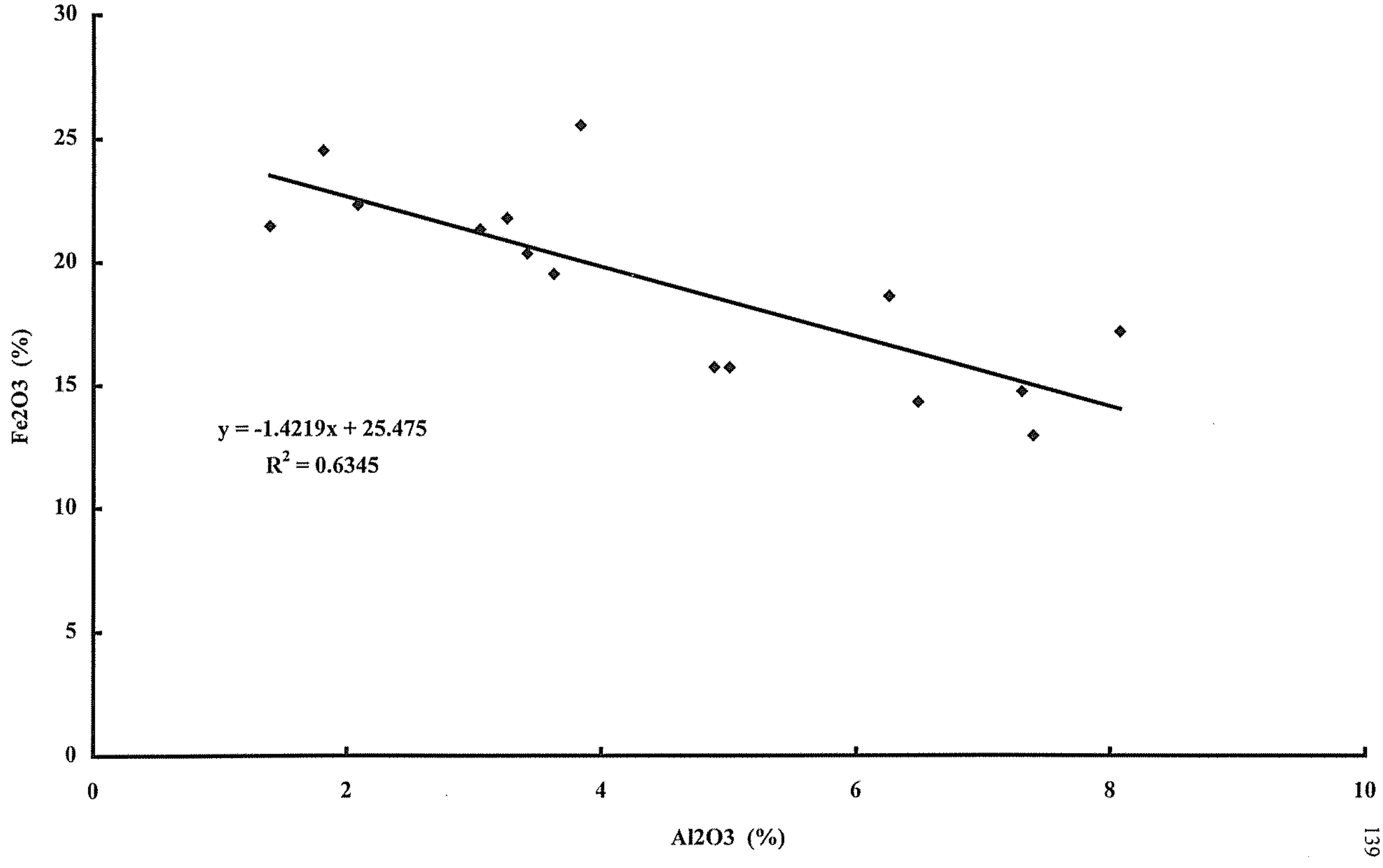

Fig. 6 : Smectites from drill core BHG1.

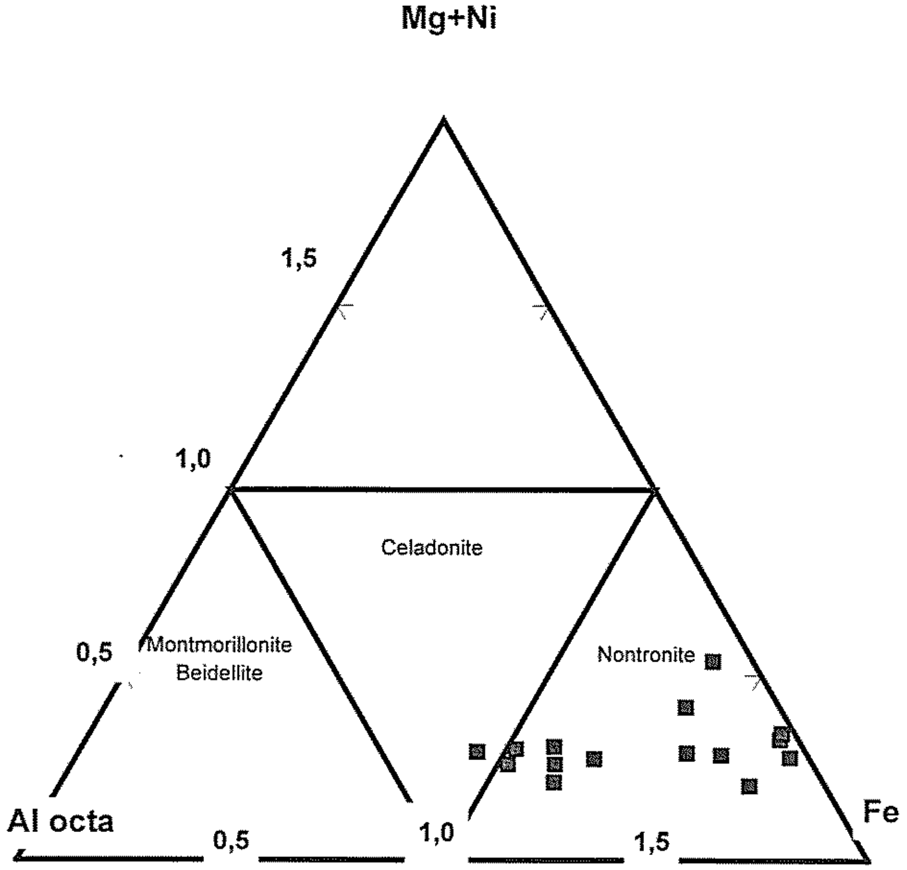

Fig. 7 : Smectites from drill core CBDD5.

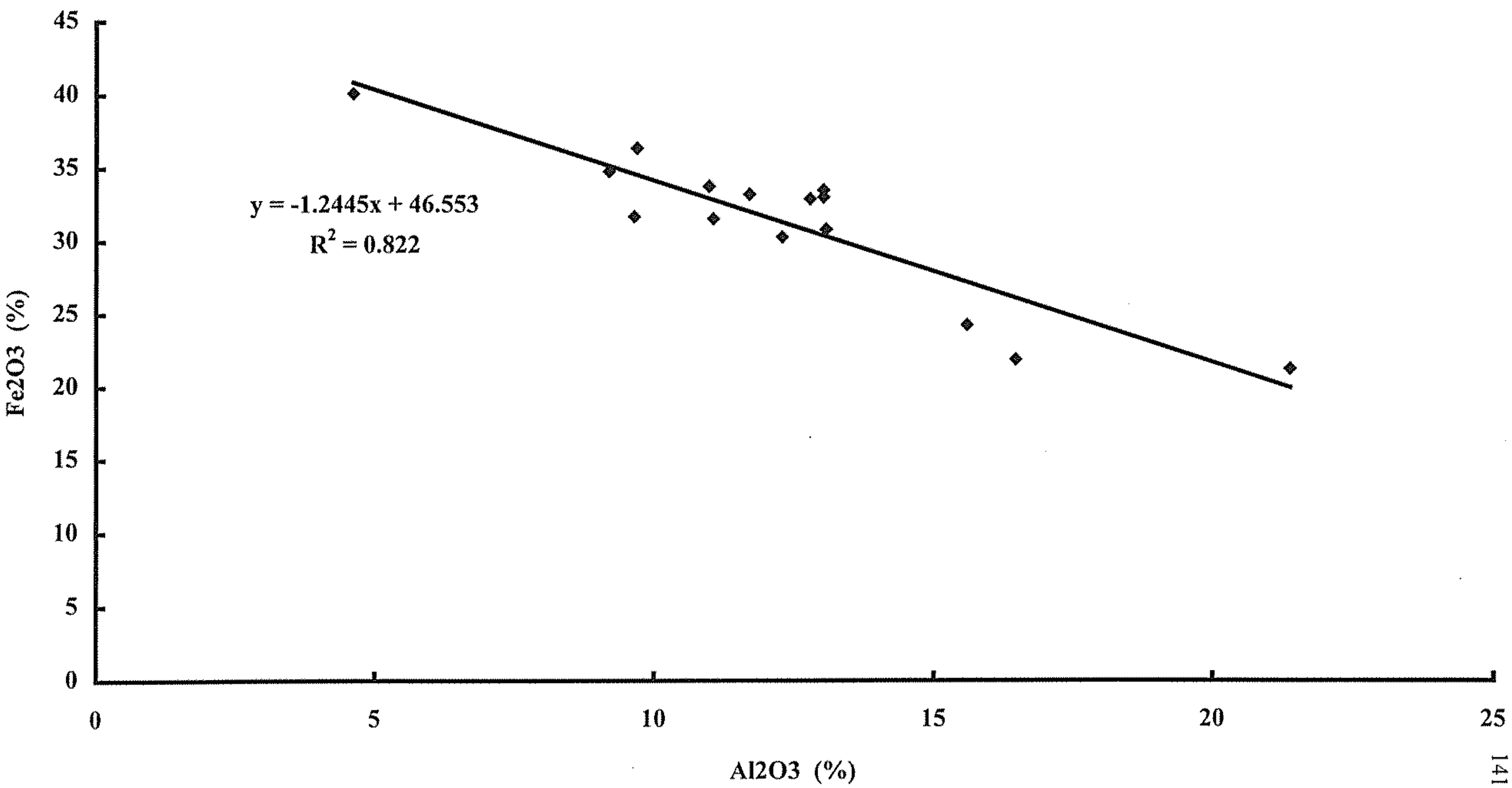

Fig. 8 : Smectites from drill core CBDD5.

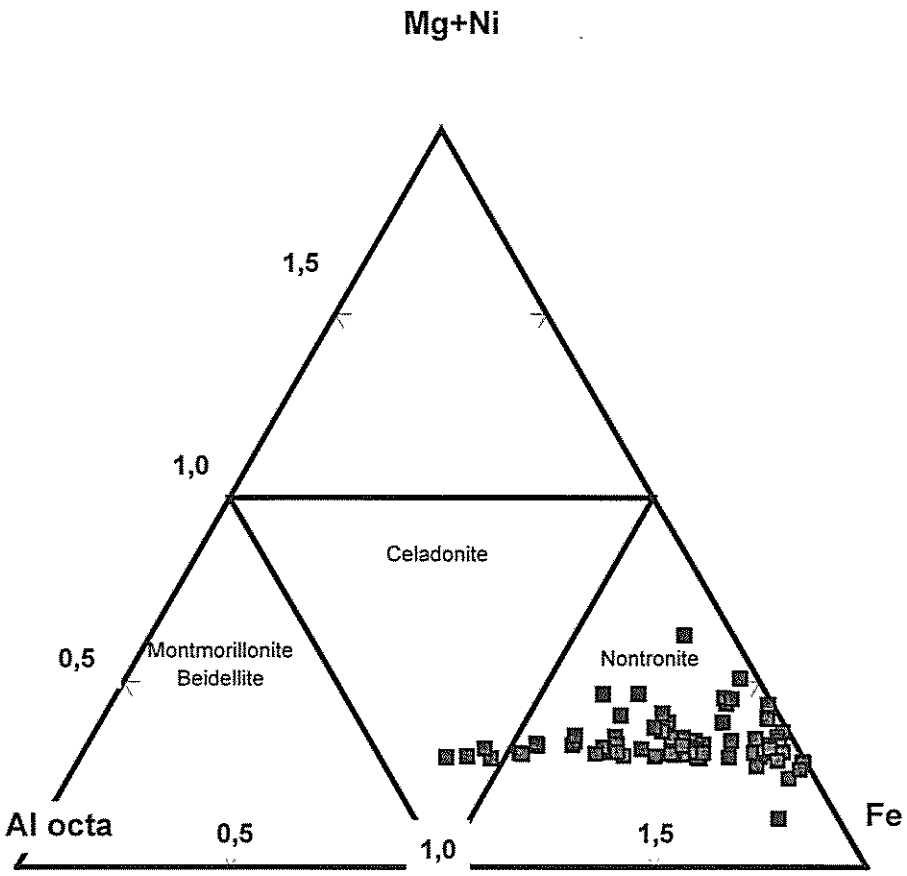

Fig. 9 : FTIR spectra

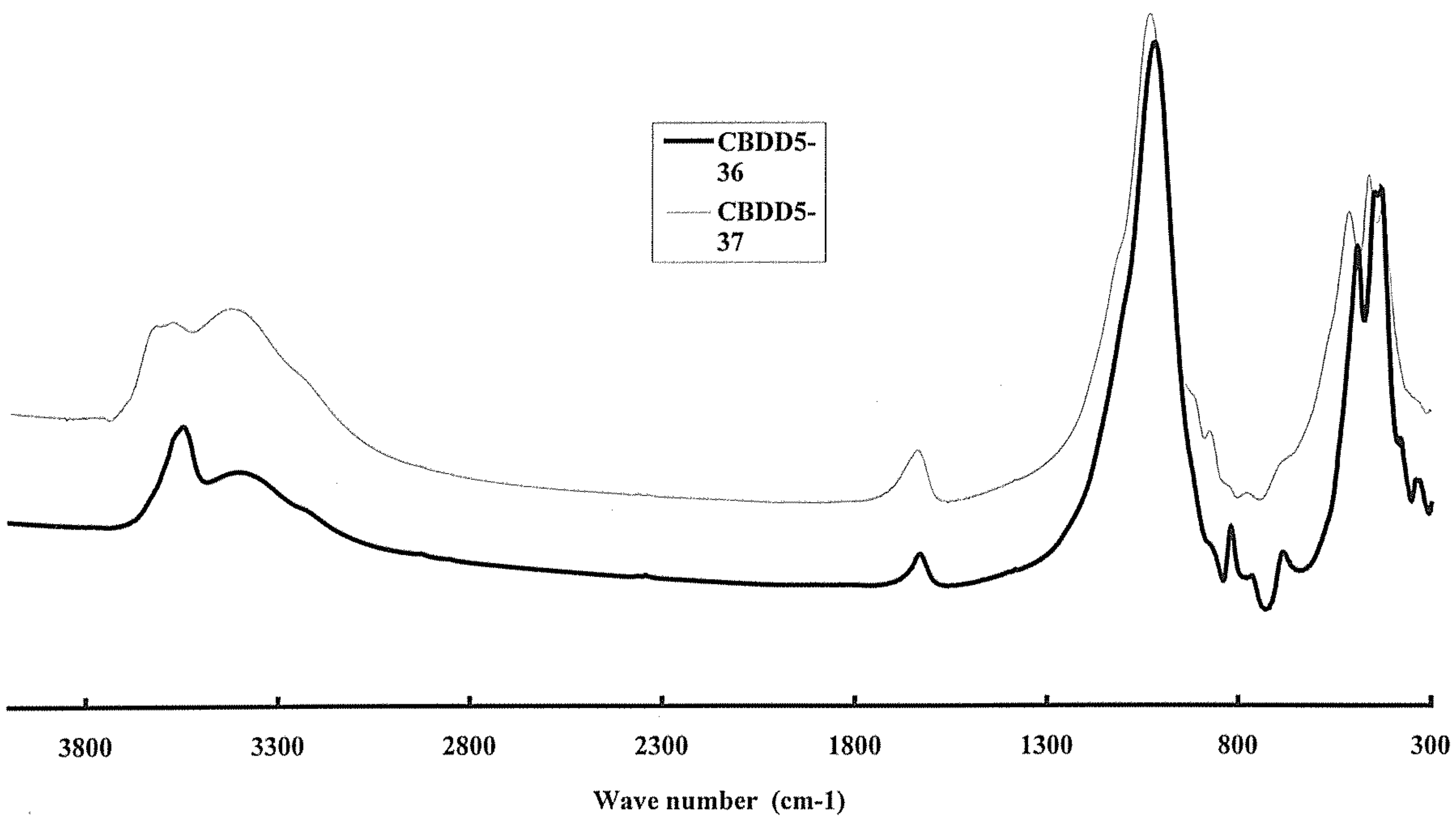

Fig. 10 : FTIR spectra

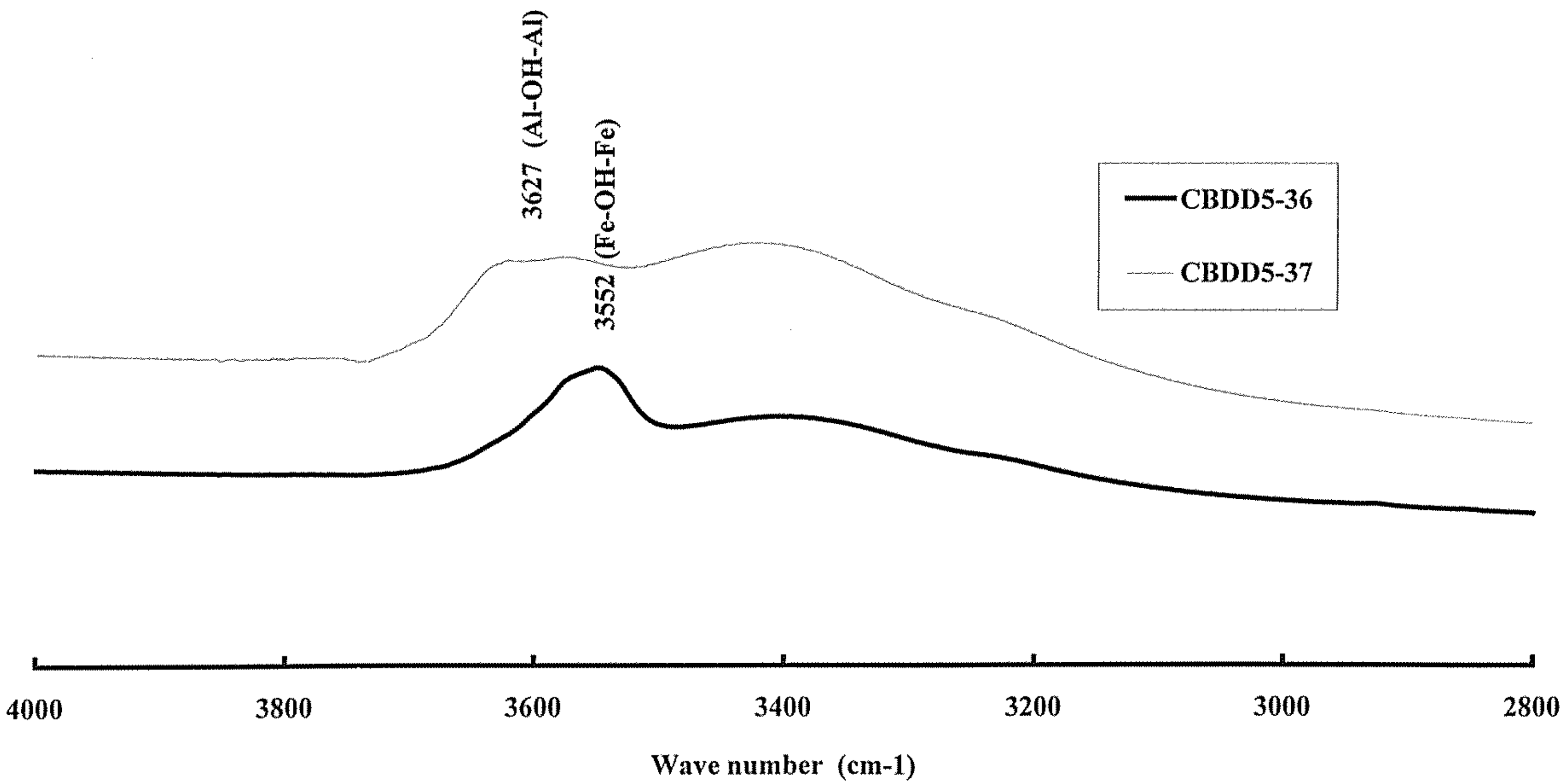

Fig. 11 : FTIR spectra

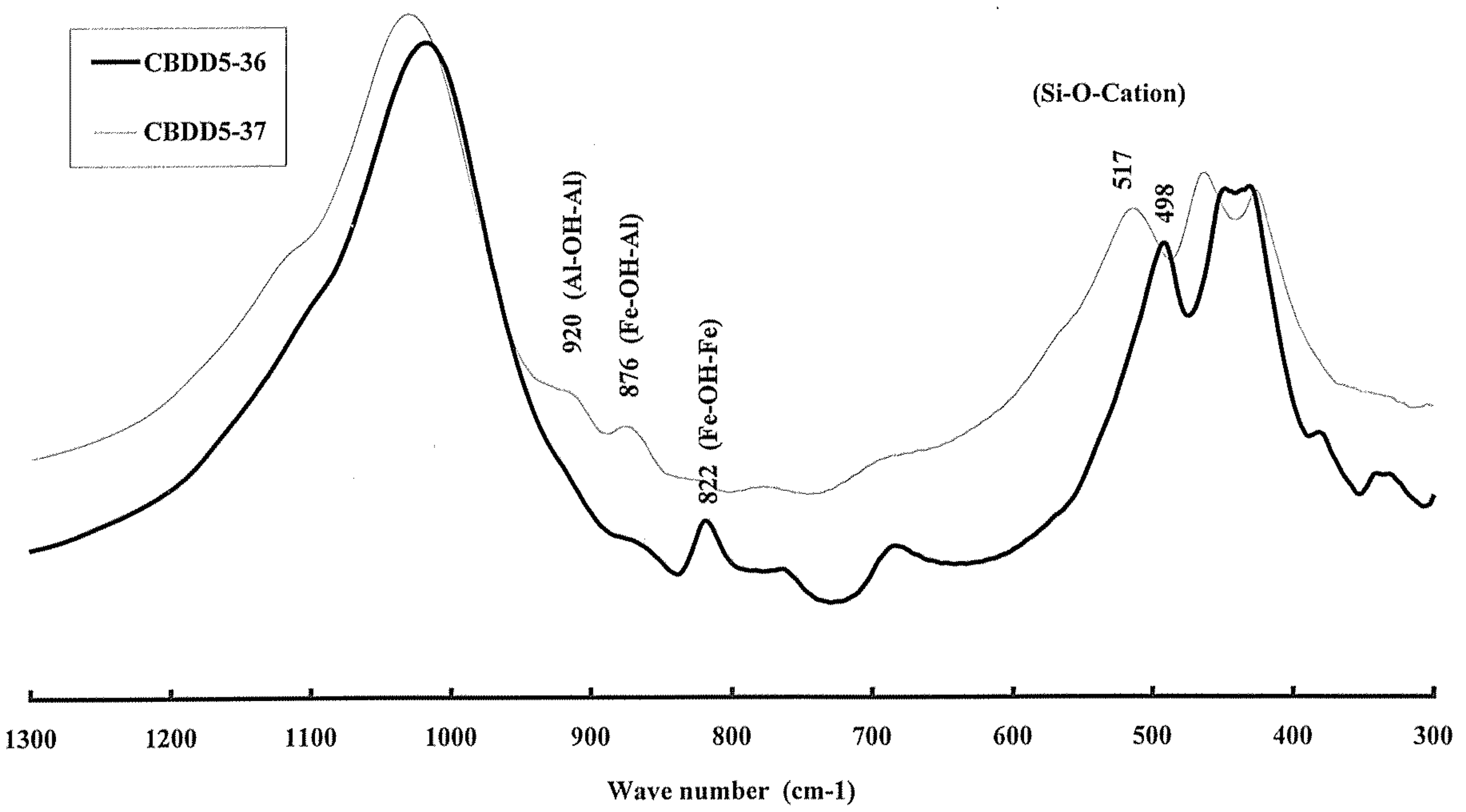

Fig. 12 : FTIR spectra for sample CBBD5-19

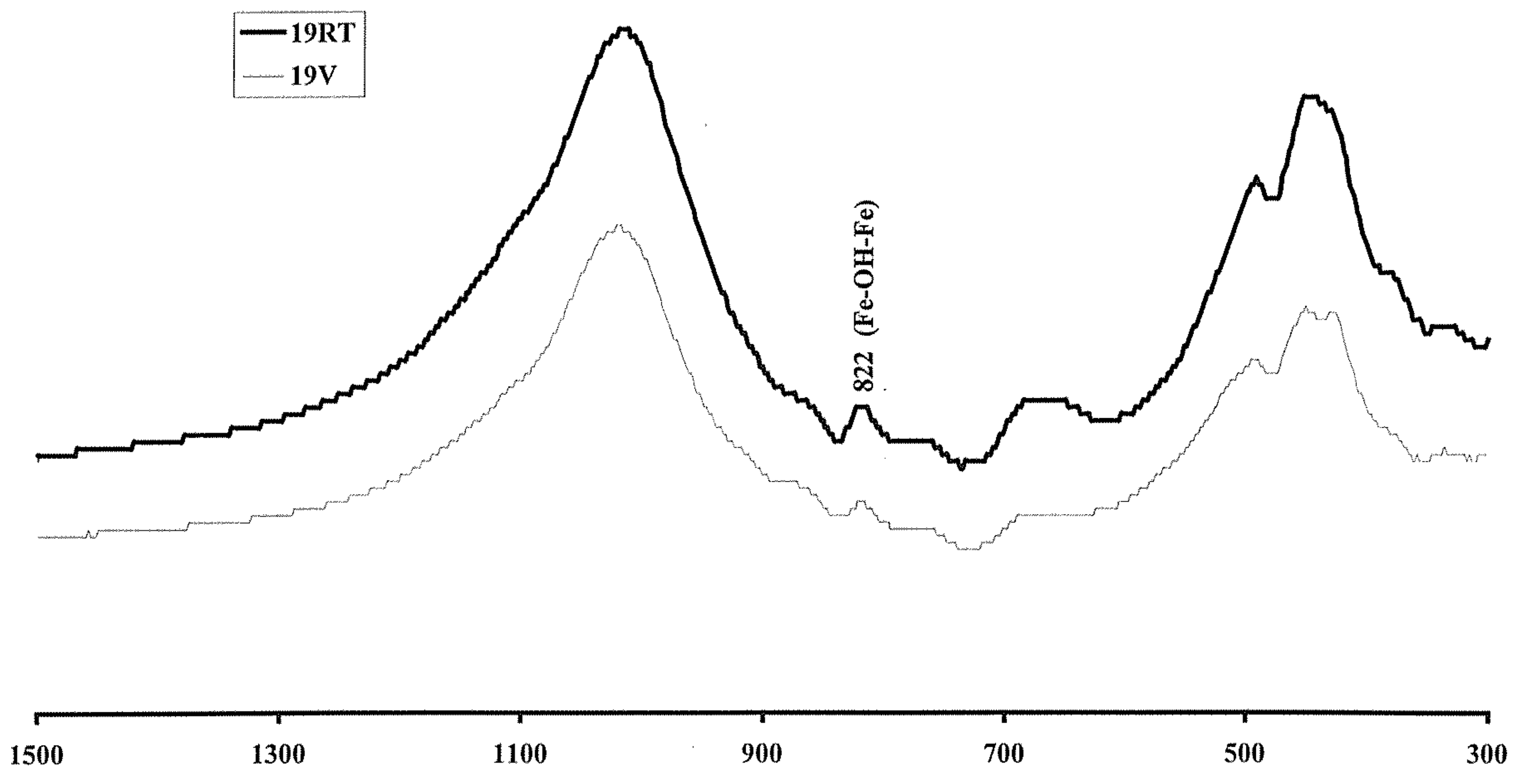

Fig. 13 : PIMA spectra

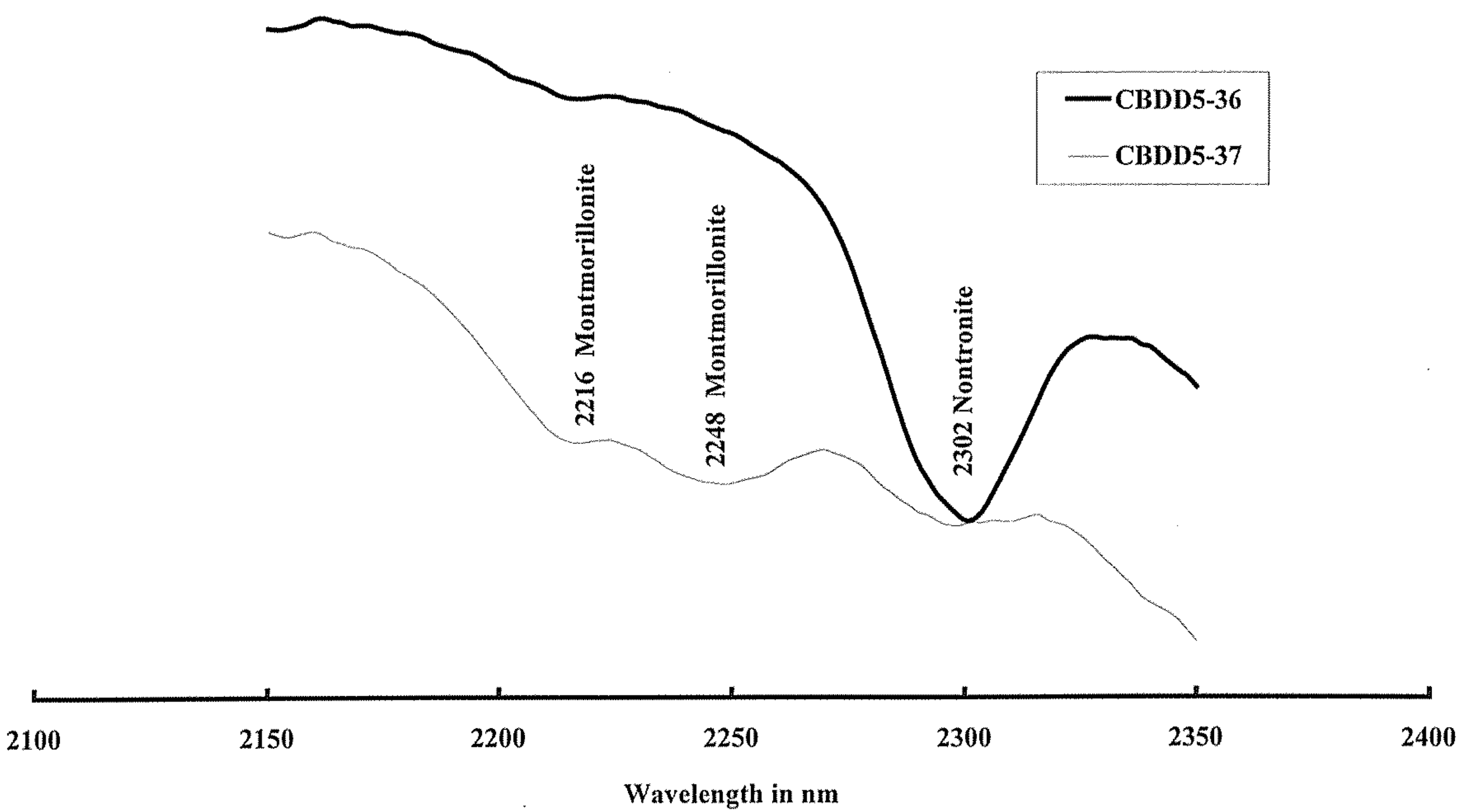

Appendix 3: Table A3.1. Drill holes selected for logging by PIMA (MM2).

Hole ID	Easting (m)	Northing (m)	RL (m)	Depth (m)	Hole ID	Easting (m)	Northing (m)	RL (m)	Depth (m)
CBRC0234	9599.46	26200.26	458.46	30	CBRC1236	9276.77	26074.6	458.02	39
CBRC0235	9550.92	26200.86	458.37	23	CBRC1241	9273.74	26251.71	459.45	27
CBRC0236	9500.14	26201.26	458.66	34	CBRC1242	9299.99	26248.15	460.3	33
CBRC0237	9449.04	26197.98	458.03	35	CBRC1245	9300.17	26148.62	459.68	21
CBRC0239	9351.13	26199.35	459.3	23	CBRC1247	9300.84	26074.25	457.44	39
CBRC0273	9597.02	26402.12	458.75	35	CBRC1256	9324.93	26074.9	457	33
CBRC0278	9352.46	26402.83	462.46	6	CBRC1260	9324.3	26249.81	460.82	39
CBRC0279	9301.51	26198.39	460.1	26	CBRC1261	9350.47	26249.86	460.85	39
CBRC0280	9251.45	26200.2	458.9	24	CBRC1384	9199.96	26300.87	457.81	12
CBRC0374	9200.62	26200.22	457.76	12	CBRC1385	9175.55	26349.59	457.9	18
CBRC0591	9549.91	26501.91	459.88	48	CBRC1386	9224.66	26349.72	458.52	27
CBRC0592	9600.16	26502.12	459.84	42	CBRC1387	9275.01	26349.96	459.77	33
CBRC0595	9749.43	26501.95	459.21	54	CBRC1388	9225	26400	458.7	30
CBRC0710	9277.52	25999.44	456.17	30	CBRC1391	9225	26450	458.9	30
CBRC0711	9250.27	26101.65	459.1	18	CBRC1392	9275	26450	459.6	39
CBRC0712	9275.53	26101.25	459.14	18	CBRC1393	9275	26400	459.6	27
CBRC0713	9300.2	26101.62	458.68	12	CBRC1395	9275	26500	459.8	33
CBRC0714	9325.02	26101.9	457.97	24	CBRC1396	9225	26500	459	6
CBRC0715	9350.21	26101.85	457.03	36	CBRC1404	9351.25	26074.91	456.26	48
CBRC0716	9375.53	26100.94	456.58	18	CBRC1501	9350.72	26149.18	458.02	40
CBRC0717	9399.84	26102.48	456.41	24	CBRC1502	9327.72	26149.32	458.76	28
CBRC0719	9326.48	26199.07	460.05	12	CBRC1505	9300.09	26700.08	463.46	16
CBRC0720	9275.76	26198.69	459.64	24	CBRC1647	9281.38	26199.99	459.73	39
CBRC0721	9249.94	26301.24	459.05	36	CBRC1657	9287.49	26199.92	459.94	45
CBRC0722	9275.17	26301.27	459.7	6	CBRC1665	9287.56	26250.13	460.02	39
CBRC0723	9299.96	26301.81	460.63	6	CBRC1672	9293.87	26249.85	460.24	39
CBRC0724	9324.96	26300.75	461.71	24	CBRC1680	9294.06	26199.7	460.01	39
CBRC0725	9350.46	26301.57	462.39	24	CBRC1728	9306.47	26249.77	460.8	42
CBRC0726	9375.08	26301.21	462.15	24	CBRC1736	9306.21	26199.79	460.26	30
CBRC0727	9400.18	26301.49	461.23	24	CBRC1749	9312.48	26249.26	460.72	42
CBRC0728	9374.85	26403.26	463.43	12	CBRC1757	9311.94	26199.85	460.18	36
CBRC0729	9424.63	26402.74	463.25	36	CBRC1771	9318.59	26200.03	460.11	24
CBRC0730	9474.2	26402.84	461.7	30	CBRC3351	9546.79	26149.65	457.45	52
CBRC0731	9350.48	26501.43	461.23	12	CBRC3352	9499.55	26150.04	457.14	58
CBRC0732	9375.3	26500.64	461.73	24	CBRC3353	9399.61	26150.11	457.23	35
CBRC0733	9399.97	26501.68	462.33	36	CBRC3359	9549.99	26251.58	459.27	50
CBRC0734	9424.98	26501.84	462.42	30	CBRC3360	9495.41	26251.72	459.92	54
CBRC0735	9449.86	26501.88	461.91	24	CBRC3364	9347.07	26349	462.89	48
CBRC0736	9376.04	26601.62	462.43	18	CBRC3365	9299.11	26601.09	461.15	3
CBRC0737	9425.22	26598.18	463.19	36	CBRC3366	9352.1	26650.89	463.46	36
CBRC0738	9475.68	26596.7	462.86	30	CBRC3367	9402.06	26650.46	464.72	54
CBRC0739	9350.31	26701.37	464.66	24	CBRC3368	9451.65	26648.7	464.33	60
CBRC0740	9374.91	26700.97	465.59	18	CBRC3369	9501.23	26650.43	463.29	48
CBRC0741	9400.21	26701.8	466.39	36	CBRC3370	9551.67	26649.59	462.68	30
CBRC0742	9424.62	26701.15	466.5	54	CBRC3456	9350.23	26550.65	461.05	18
CBRC0743	9449.79	26701.74	465.76	51	CBRC3457	9306.48	26551	460.52	12
CBRC0744	9500.03	26701.58	464.02	36	CBRC3458	9452.98	26550.13	461.59	42
CBRC0745	9539.78	26701.83	463.01	18	CBRC3459	9404.67	26548.23	461.79	24
CBRC0746	9590.08	26701.83	462.39	24	CBRC3460	9501.96	26551.48	460.98	54
CBRC0747	9649.85	26701.36	462.84	42	CBRC3461	9553.03	26551.44	460.49	48
CBRC0749	9750.55	26701.48	459.94	18	CBRC3462	9601.63	26550.13	460.78	42
CBRC0751	9850.08	26701.75	457.81	12	CBRC3467	9399	26450.1	463.01	42
CBRC0780	9499.9	26501.83	460.57	54	CBRC3468	9449.58	26450.57	462.15	54
CBRC0782	9450.62	26301.41	461.41	60	CBRC3469	9498.24	26449.5	460.48	42
CBRC0783	9500.29	26301.65	460.77	60	CBRC3470	9548.64	26449.72	459.37	36
CBRC0784	9549.8	26301.7	459.86	30	CBRC3471	9596.97	26449.2	458.8	36
CBRC0785	9599.4	26302.1	459.24	30	CBRC3487	9447.94	26349.01	462.73	36
CBRC0787	9700.34	26301.18	457.2	48	CBRC3488	9398.34	26347.93	462.97	18
CBRC0795	9149.95	26102.03	457.11	12	CBRC3850	9412.73	26199.76	458.2	36
CBRC0796	9199.99	26102.03	458.54	24	CBRC3855	9424.95	26249.72	459.45	36
CBRC0797	9449.8	26102.74	456.34	42	CBRC3859	9425.04	26200.05	458.2	36
CBRC0798	9500.08	26101.72	456.31	24	CBRC3865	9449.68	26251.33	459.7	36
CBRC0799	9550.05	26102.01	456.4	10	CBRC3870	9437.65	26200.27	458.18	36
CBRC0800	9599.66	26102.22	456.23	30	CBRC3882	9410.97	26250.53	459.42	36
CBRC0803	9749.87	26101.68	455.15	36	CBRC3892	9364.47	26199.79	458.97	36
CBRC0878	9450.21	26077.32	455.83	45	CBRC3896	9362.18	26250.2	460.86	36
CBRC0880	9450.09	26154.63	457.23	51	CBRC3904	9374.88	26250.06	460.68	36
CBRC1223	9249.92	26249.95	458.72	21	CBRC3909	9387.47	26199.92	458.39	36
CBRC1226	9249.84	26149.78	459.58	27	CBRC3913	9386.76	26250.37	460.14	36
CBRC1228	9252.03	26074.56	458.24	27					

Appendix 3: Table A3.2. Drillholes for logging by PIMA (MM3).

Hole ID	Easting (m)	Northing (m)	RL (m)	Depth (m)	Hole ID	Easting (m)	Northing (m)	RL (m)	Depth (m)
ARC0036	9498.09	71796.51	434.83	21	ARC0785	9099.32	72298.47	420.68	15
ARC0037	9100.06	72399.95	419.27	9	ARC0786	9048.38	72298.22	420.83	15
ARC0038	9499.08	71898.66	437.91	25	ARC0788	9046.45	72102.03	429.57	15
ARC0039	9446.86	71899.23	437.13	21	ARC0789	9400.82	72502.67	444.41	20
ARC0040	9544.31	72000.66	437.93	23	ARC0790	9350.31	72502	440.87	27
ARC0041	9498.86	72002.45	439.56	21	ARC0791	9301.4	72500.64	434.98	33
ARC0042	9452	72001.4	437.03	21	ARC0792	9250.77	72499.37	427.68	21
ARC0043	9498.98	72099.77	439.06	30	ARC0793	9201.03	72498.35	421.7	27
ARC0044	9449.66	72099.62	440.15	39	ARC0794	9146.71	72494.84	423.31	45
ARC0045	9499.04	72200.12	442.9	38	ARC0795	9598.4	72502.25	434.81	15
ARC0046	9449.98	72199.51	438.35	24	ARC0796	9540.34	72502.42	440.89	15
ARC0048	9448.9	72299.46	444.07	30	ARC0858	9173.58	72204.91	423.66	18
ARC0049	9398.92	72299.84	442.1	30	ARC0859	9223.68	72198.61	425.86	12
ARC0050	9499.34	72400.58	441.51	12	ARC0863	9123.78	72000.92	433.67	18
ARC0051	9450.66	72400.45	442.57	24	ARC0883	9549.06	72099.51	433.8	27
ARC0052	9494.21	72498.88	447.64	30	ARC0886	9249.62	71700.09	426.57	15
ARC0053	9450.5	72498.04	447.61	24	ARC0887	9200.17	71699.63	422.54	15
ARC0094	9197.3	72398.65	424.51	33	ARC0980	9249.88	72150.53	428.53	27
ARC0096	9292.6	72398.91	429.29	30	ARC0983	9249.47	72049.75	430.66	27
ARC0120	9348.47	71700.66	433.14	6	ARC0986	9250.47	71950.19	434.02	27
ARC0121	9306.16	71698.94	433.2	19	ARC0989	9249.21	71849.74	433.99	21
ARC0122	9324.11	71798.78	434.46	30	ARC0990	9225.2	72149.47	427.87	27
ARC0123	9277.24	71800.06	432.68	19	ARC0997	9225.99	72049.92	429.73	33
ARC0125	9299.22	71901.26	435.14	17	ARC1000	9224.45	72012.32	430.66	27
ARC0126	9247.58	71900.52	435.11	18	ARC1004	9224.85	71949.95	433.32	33
ARC0127	9198.25	71900.62	434.92	18	ARC1008	9224.38	71899.79	435.1	27
ARC0128	9149.13	71901.09	436.03	24	ARC1012	9224.93	71849.92	433.22	27
ARC0129	9100.17	71903.68	431.85	15	ARC1015	9199.84	71950.26	432.65	33
ARC0130	9299.02	72000.32	432.8	15	ARC1016	9199.94	72150.33	426.65	33
ARC0131	9249.06	72000.4	432	10	ARC1019	9200.12	72049.63	428.89	27
ARC0132	9199.28	71995.38	430.19	26	ARC1022	9150.02	72149.9	426.46	39
ARC0133	9149.92	71999.39	431.55	18	ARC1025	9149.59	72050.23	429.66	39
ARC0134	9099.18	72000.62	434.17	20	ARC1028	9149.97	71949.73	433.73	27
ARC0135	9035.98	72000.56	425.76	10	ARC1200	9175.98	72150.94	425.56	30
ARC0229	9398.6	71998.9	432.79	12	ARC1203	9175.26	72049.47	427.99	51
ARC0230	9344.55	72001.23	429.61	12	ARC1206	9174.49	71949.7	432.48	27
ARC0231	9149.24	72100.57	428.01	23	ARC1208	9175.08	71899.85	435.51	21
ARC0307	9399.13	72400.31	434.09	18	ARC1210	9174.92	71850.39	434.62	27
ARC0308	9347.41	72398.07	432.98	18	ARC1211	9150.56	71850.33	436.81	24
ARC0309	9246.88	72400.47	426.92	42	ARC1256	9300.71	71650.65	432.13	14
ARC0310	9149.48	72399.59	421.83	42	ARC1257	9249.66	71649.25	426.92	24
ARC0311	9049.93	72400.75	418.14	22	ARC1258	9200.28	71650.29	422.36	18
ARC0321	9048.16	72198.92	428.04	12	ARC1259	9099.42	71851.48	430.93	18
ARC0322	9098.82	72198.95	431.42	20	ARC1260	9049.39	71852.15	425.51	18
ARC0323	9150.29	72202.5	424.64	18	ARC1261	9399.68	72149.85	435.3	24
ARC0324	9200.53	72200.4	425.09	17	ARC1262	9350.74	72149.75	429.44	24
ARC0325	9246.33	72200.94	426.59	24	ARC1263	9300.91	72149.98	427.93	18
ARC0326	9299.34	72198.74	425.75	22	ARC1264	9100.86	72249.97	425.6	24
ARC0327	9350.53	72197.56	428.48	18	ARC1265	9150.45	72250.59	422.46	18
ARC0328	9400.69	72198.72	432.74	18	ARC1266	9199.8	72250.08	423.06	12
ARC0329	9552.87	72200.62	437.33	22	ARC1267	9249.43	72250.11	424.57	18
ARC0330	9599.27	72197.53	431.91	6	ARC1268	9300.17	72249.74	428.42	24
ARC0331	9607.16	71905.5	429.99	12	ARC1269	9350.34	72248.76	432.04	24
ARC0332	9555.79	71902.71	433.3	15	ARC1270	9398.86	72249.03	435.62	24
ARC0333	9601.28	71998.61	429.95	18	ARC1271	9348.62	72349.38	437.83	24
ARC0336	9447.96	71798.95	433.5	24	ARC1272	9300.78	72350.31	432.68	18
ARC0337	9398.55	71799.76	431.09	24	ARC1273	9249.42	72350.67	427.82	42
ARC0367	9199.69	71788.08	426.99	12	ARC1274	9200.2	72349.85	424.32	18
ARC0368	9146.68	71784.34	429.2	26	ARC1275	9150.1	72349.8	421.91	18
ARC0369	9097.71	71779.47	427.16	24	ARC1276	9105	72350.79	420.27	12
ARC0370	9060.61	71773.16	423.47	12	ARC1277	9349.61	72450.74	438.58	24
ARC0600	9149.65	71698.32	421.6	15	ARC1278	9300.18	72450.64	432.79	36
ARC0601	9099.32	71700.02	421.15	15	ARC1279	9251.18	72451.72	426.51	36
ARC0604	9102.74	71748.31	424.9	14	ARC1280	9200.65	72449.9	423.47	42
ARC0605	9149.7	71748.32	425.46	14	ARC1281	9101.39	72451.59	421.43	12
ARC0606	9149.5	71651.68	419.23	16	ARC1282	9151.27	72451.17	421.32	30
ARC0607	9100.72	71650	418.92	9	ARC1283	9052.52	72534.32	421.89	12
ARC0774	9349.09	72102.48	429.56	27	ARC1284	9101.17	72539.33	427.51	30
ARC0775	9294.1	72096.41	430.67	27	ARC1285	9151.52	72541.9	428.28	30
ARC0776	9248.76	72100.88	431.5	15	ARC1286	9199.96	72545.83	424.76	21
ARC0777	9198.39	72101.85	427.81	15	ARC1287	9250.04	72547.87	427.82	20
ARC0778	9598.96	72299.09	433.88	15	ARC1288	9299.36	72550.54	433.28	30
ARC0780	9349.44	72298.74	436.76	33	ARC1289	9400.56	72550.05	441.66	28
ARC0781	9299.87	72301.39	431.5	27	ARC1290	9349.95	72551.03	436.54	18
ARC0782	9250.3	72296.79	426.94	21	ARC1478	9049.53	71900.71	425.42	9
ARC0783	9200.36	72301.21	423.5	15	ARC1479	9297.64	72049.95	431.99	17
ARC0784	9150	72301.07	421.52	27					

Appendix 4: Table A4.1. XRF analyses of selected RC holes for MM2.

Hole ID	Depth (m)	%Ni	%Co	SiO2 %	Al2O3 %	Fe2O3 %	MnO %	MgO %	CaO %	Na2O %	K2O %	TiO2 %	P2O5 %	Ba ppm	Ce ppm	Cl ppm	Cr ppm	Cu ppm	Ga ppm	La ppm	Nb ppm	Pb ppm	Rb ppm	S ppm	Sr ppm	V ppm	Y ppm	Zn ppm	Zr ppm	OXIDES %	TotalTr ppm
CBRC0796																															
30379	1	0.19	0.004	25.77	11.60	45.90	0.051	0.66	0.85	0.15	0.07	0.51	0.021	203	-4	430	7684	77	14	-2	3	4	5	370	21	201	16	86	40	85.6	11056
30381	3	0.136	0.014	15.47	10.31	41.69	0.139	0.81	7.08	0.06	0.04	0.32	0.009	67	-2	580	3359	58	10	0	-2	2	-1	29300	42	126	11	51	26	75.9	35091
30383	4	0.133	0.013	18.05	13.83	48.24	0.117	0.63	2.44	0.11	0.04	0.45	0.008	48	21	450	3708	57	11	-4	5	-11	5	11630	35	184	5	43	40	83.9	17656
30384	5	0.164	0.016	19.47	15.09	49.18	0.126	0.63	0.61	0.09	0.04	0.67	0.016	9	4	490	4316	86	17	-10	12	-26	3	2220	21	255	4	57	69	85.9	9303
30390	10	0.278	0.055	22.28	10.39	49.04	0.146	1.02	0.26	0.16	0.06	0.45	0.003	16	34	390	5741	66	10	11	-3	-13	4	360	24	204	9	64	26	83.8	10240
30391	11	0.32	0.025	25.87	12.53	40.84	0.081	1.35	0.28	0.19	0.06	0.50	0.001	9	-25	600	13155	70	13	17	6	17	-2	295	18	204	8	232	24	81.7	18072
30392	12	0.632	0.039	29.37	7.82	39.56	0.140	3.09	0.38	0.30	0.08	0.33	0.001	16	-3	660	9166	80	12	-4	-3	14	1	370	27	163	13	231	22	81.1	17434
30393	13	1.24	0.182	36.83	5.81	26.66	0.706	7.95	0.53	0.42	0.10	0.24	0.001	148	7	1090	6326	54	7	3	4	7	-2	560	43	77	6	220	16	79.2	22761
30395	15	1.224	0.091	37.72	5.39	24.86	0.498	9.99	0.48	0.42	0.10	0.22	0.001	89	13	990	6466	51	5	3	-4	10	2	450	35	85	11	202	35	79.7	21563
30397	17	1.114	0.047	36.30	5.44	24.63	0.405	13.14	0.45	0.37	0.08	0.23	0.001	140	-15	730	6598	61	5	15	-2	6	-1	290	30	111	11	172	14	81.0	19751
30398	18	0.839	0.031	37.12	4.28	19.40	0.274	18.26	2.26	0.27	0.06	0.18	0.001	60	11	520	5439	53	8	7	-10	12	-1	220	190	91	12	123	13	82.1	15409
30404	24	0.71	0.024	39.03	4.68	19.40	0.315	19.26	0.38	0.20	0.05	0.19	0.001	76	-2	200	5340	55	7	17	0	2	-3	20	23	79	13	127	17	83.5	13282
CBRC0797																															
30405	1	0.082	0.003	40.73	17.31	27.79	0.031	0.86	0.42	0.13	0.24	0.56	0.011	237	5	30	5390	22	30	7	4	14	17	100	56	192	11	19	120	88.1	7068
30406	2	0.068	0.004	31.63	16.80	37.72	0.028	0.66	0.34	0.11	0.16	0.80	0.009	144	2	40	8601	19	38	12	7	17	10	280	43	267	8	17	152	88.3	10355
30407	3	0.04	0.01	8.80	8.58	69.48	0.029	0.34	0.12	0.03	0.04	2.29	0.027	54	-2	100	13730	18	62	-8	31	-9	7	370	23	583	8	26	262	89.7	15726
30410	6	0.085	0.011	8.97	19.98	49.93	0.020	0.39	1.00	0.04	0.06	0.88	0.036	26	-12	290	14316	32	23	4	12	-13	4	1150	36	236	8	33	197	81.3	17266
30414	9	0.318	0.022	14.28	16.73	51.94	0.047	0.49	0.14	0.06	0.03	0.43	0.037	-1	19	180	12726	42	10	3	10	-4	5	500	16	155	10	88	54	84.2	17179
30415	10	0.285	0.023	13.47	14.39	56.30	0.066	0.42	0.12	0.02	0.02	0.37	0.034	0	50	120	7846	46	8	-18	15	-16	6	430	17	168	11	80	33	85.2	11835
30417	12	0.524	0.557	21.52	18.99	38.46	2.927	0.46	0.15	0.08	0.04	0.33	0.024	808	601	50	7809	80	11	13	1	16	2	150	25	150	10	95	31	83.0	20620
30419	14	0.915	0.136	21.73	6.13	51.00	0.325	1.11	0.39	0.09	0.06	0.25	0.014	210	221	60	6848	55	7	11	7	-23	13	70	38	237	8	194	16	81.1	18452
30420	15	1.417	0.099	33.31	6.03	35.39	0.153	1.96	0.64	0.10	0.08	0.19	0.009	52	35	100	7521	48	3	10	-1	-1	-1	50	51	113	6	145	18	77.9	23275
30423	18	0.752	0.072	40.70	3.92	38.46	0.250	1.16	0.36	0.07	0.07	0.16	0.004	125	-7	180	5785	30	9	13	8	16	-6	40	34	79	8	123	9	85.1	14644
30425	19	1.128	0.08	48.03	2.95	29.09	0.280	1.89	0.50	0.13	0.08	0.13	0.001	53	-3	230	4101	21	7	20	7	11	2	50	43	57	7	103	6	83.1	16761
30426	20	1.128	0.034	53.50	2.67	23.48	0.089	2.12	0.52	0.13	0.09	0.10	0.001	41	-5	285	3755	21	3	11	-2	2	-2	60	41	44	6	120	6	82.7	15978
30429	23	0.879	0.025	57.91	1.68	22.84	0.064	1.82	0.36	0.12	0.07	0.05	0.006	13	-7	210	3375	27	5	-1	1	-2	5	40	37	49	4	99	2	84.9	12868
30430	24	0.831	0.053	64.66	1.43	17.53	0.188	1.76	0.31	0.14	0.06	0.05	0.001	36	10	200	2457	21	3	1	2	5	-5	40	32	21	6	91	6	86.1	11735
30432	26	0.918	0.043	65.45	1.29	15.97	0.168	1.79	0.31	0.14	0.07	0.04	0.007	74	3	80	2868	19	2	0	1	6	6	10	33	59	6	89	6	85.3	12850
30435	29	0.67	0.033	77.74	0.81	10.12	0.184	1.48	0.13	0.07	0.05	0.02	0.006	12	11	130	1627	16	3	1	-4	3	3	10	20	59	6	57	3	90.6	8953
30440	34	0.616	0.018	73.69	0.78	10.78	0.219	3.94	0.10	0.08	0.05	0.02	0.001	6	-1	100	1702	16	0	11	-1	-1	-3	10	22	47	7	53	6	89.7	8285
30441	35	0.816	0.024	60.38	1.52	14.87	0.246	9.46	0.13	0.12	0.06	0.05	0.002	3	10	120	2416	21	0	1	0	5	1	20	27	50	10	76	3	86.8	11137
30445	39	0.484	0.015	54.62	0.66	9.02	0.143	15.30	0.13	0.10	0.05	0.01	0.005	26	3	90	1659	9	2	2	-1	2	1	10	16	38	4	56	6	80.0	6888
30446	40	0.419	0.009	27.63	0.47	5.39	0.082	30.91	0.18	0.06	0.03	0.00	0.002	2	5	60	1150	2	0	2	-1	1	2	10	11	17	4	33	3	64.7	5546
30448	42	0.338	0.009	26.95	0.43	5.65	0.085	27.60	4.22	0.02	0.03	0.00	0.005	-7	1	40	1077	3	-2	3	0	5	-2	0	34	14	2	35	6	65.0	4647
CBRC0799																															
30475	1	0.325	0.023	48.72	10.62	23.99	0.055	1.43	0.33	0.11	0.17	0.26	0.010	161	12	-40	14371	46	12	16	2	19	7	160	37	124	14	118	58	85.7	18574
30476	2	0.533	0.022	58.15	13.22	6.96	0.031	3.25	0.71	0.16	0.22	0.30	0.001	66	38	20	1502	15	13	-5	4	7	26	20	57	46	10	32	81	83.0	7451
30479	5	0.35	0.016	58.68	13.32	5.09	0.022	3.40	0.79	0.41	0.21	0.31	0.003	52	7	40	290	10	15	20	3	14	29	0	83	48	11	22	103	82.2	4368
30480	6	0.322	0.012	58.94	13.57	5.07	0.030	3.76	0.77	0.50	0.43	0.33	0.001	42	3	90	239	7	16	4	2	8	85	0	80	27	9	31	104	83.4	4060
30481	7	0.27	0.012	58.13	13.63	5.03	0.026	3.88	0.79	0.50	0.35	0.31	0.001	1160	11	150	223	14	18	14	1	15	55	210	90	28	13	24	101	82.6	4904
30484	10	0.201	0.006	59.66	14.71	4.56	0.035	3.72	0.72	1.34	1.05	0.35	0.004	493	61	130	85	9	19	17	4	16	143	30	150	45	14	44	121	86.2	3419

Hole ID	Depth	%Ni	%Co	SiO2	Al2O3	Fe2O3	MnO	MgO	CaO	Na2O	K2O	TiO2	P2O5	Ba	Ce	Cl	Cr	Cu	Ga	La	Nb	Pb	Rb	S	Sr	V	Y	Zn	Zr	OXIDES	TotalTr
	(m)			%	%	%	%	%	%	%	%	%	%	ppm	ppm	ppm	ppm	ppm	ppm	ppm	ppm	ppm	ppm	ppm	ppm	ppm	ppm	ppm	ppm	%	ppm
CBRC0721																															
26821	1	0.052	0.002	61.96	15.60	4.90	0.029	1.07	3.96	0.16	0.15	0.61	0.015	93	22	510	318	22	21	8	6	5	6	150	98	100	10	27	123	88.4	2035
26822	2	0.041	0.002	62.00	20.89	4.93	0.030	0.67	0.66	0.15	0.08	0.81	0.009	54	25	290	247	26	21	-3	5	11	3	50	29	128	9	25	147	90.2	1474
26825	5	0.015	0.002	63.57	21.01	5.42	0.020	0.25	0.13	0.10	0.05	0.66	0.006	19	23	580	98	27	27	-5	6	5	-2	160	10	100	11	47	167	91.2	1407
26826	6	0.031	0.002	60.70	22.58	5.95	0.009	0.33	0.15	0.09	0.12	0.72	0.006	44	15	660	220	40	29	4	4	5	-1	130	11	97	12	31	180	90.7	1778
26831	11	0.045	0.002	69.63	18.46	1.39	0.007	0.81	0.14	0.18	1.00	0.60	0.005	188	37	640	331	26	23	22	2	12	13	130	16	67	10	26	138	92.2	2107
26832	12	0.047	0.004	57.88	21.46	4.08	0.015	1.78	1.56	0.19	0.63	0.77	0.011	304	29	660	918	55	27	18	3	11	18	200	32	146	12	66	161	88.4	3149
26833	13	0.021	0.004	53.97	20.80	5.17	0.018	1.84	3.19	0.25	0.99	0.73	0.020	1443	42	620	450	63	23	50	4	11	47	380	58	155	18	79	147	87.0	3812
26834	14	0.042	0.008	46.14	21.05	10.88	0.018	2.59	1.46	1.12	1.12	0.92	0.062	1284	69	550	1166	129	25	56	9	16	28	290	152	258	23	144	140	85.4	4798
26835	15	0.045	0.009	47.38	19.06	10.17	0.020	3.29	1.81	1.29	0.86	0.79	0.054	696	47	465	1565	117	20	23	4	15	27	195	192	213	19	178	131	84.7	4409
26836	16	0.046	0.009	47.33	18.99	11.43	0.028	3.74	0.66	0.68	1.07	0.82	0.064	223	35	460	1582	120	22	21	3	12	50	70	99	183	18	200	127	84.8	3736
26840	19	0.018	0.004	65.12	16.79	5.71	0.031	1.38	0.79	2.62	1.18	0.57	0.041	114	102	190	147	80	20	41	2	13	47	30	113	91	14	90	146	94.2	1421
26841	20	0.02	0.004	62.39	16.12	7.80	0.039	1.25	0.49	0.56	2.73	0.60	0.060	272	235	180	123	128	18	51	7	16	69	50	72	143	16	97	127	92.1	1801
26844	23	0.024	0.004	61.62	15.85	9.94	0.057	1.21	0.72	0.83	1.29	0.59	0.105	173	67	160	59	301	20	71	6	13	54	70	88	130	26	77	124	92.2	1685
26846	25	0.057	0.008	49.98	15.69	14.57	0.078	2.54	0.65	0.22	0.83	1.19	0.070	94	51	20	162	251	24	16	5	5	25	10	47	319	23	138	89	85.8	1884
26847	26	0.018	0.003	38.58	10.14	6.13	0.047	1.29	0.28	0.14	1.13	0.43	0.058	99	51	50	74	140	13	31	-2	2	41	30	24	104	23	69	71	58.2	996
26850	29	0.014	0.005	62.20	15.94	8.16	0.090	2.36	0.31	0.13	3.00	0.60	0.059	299	91	-50	58	87	20	33	3	37	98	150	37	156	19	195	112	92.9	1506
26853	32	0.016	0.003	62.13	15.38	8.25	0.070	2.49	0.44	0.10	2.05	0.49	0.050	187	73	-10	46	75	23	17	2	15	65	0	30	135	14	269	119	91.4	1223
26854	33	0.011	0.005	63.37	15.79	6.43	0.117	2.67	0.44	0.11	1.84	0.49	0.024	292	52	0	57	25	21	22	1	4	55	10	24	91	16	160	129	91.3	1090
26857	36	0.016	0.005	64.62	15.79	6.04	0.182	1.62	1.71	1.68	2.35	0.50	0.161	490	60	-80	88	27	30	21	1	7	57	0	92	101	15	140	116	94.7	1343
CBRC0727																															
26946	1	0.179	0.007	22.83	23.66	32.10	0.042	0.66	0.24	0.06	0.07	0.75	0.016	409	-22	10	15126	16	28	20	13	19	-1	280	30	338	15	54	164	80.5	18340
26950	5	0.339	0.015	14.48	16.28	52.84	0.072	0.64	0.12	0.03	0.03	0.47	0.016	18	19	220	9177	49	11	2	5	-1	-2	310	27	173	11	69	64	85.0	13664
26954	8	0.323	0.016	16.74	14.55	51.66	0.133	0.86	0.16	0.09	0.03	0.42	0.020	35	-9	230	19852	51	12	18	7	-2	3	270	26	215	22	102	36	84.7	24228
26955	9	0.276	0.019	13.85	11.43	60.20	0.230	0.64	0.17	0.07	0.02	0.46	0.030	17	15	170	9486	67	5	-2	11	-9	5	290	27	248	11	103	34	87.1	13388
26958	12	0.228	0.027	16.43	11.25	59.58	0.262	0.81	0.61	0.04	0.03	0.27	0.005	2	26	140	4828	54	4	-1	3	-7	0	60	26	162	12	81	16	89.3	7924
26959	13	0.382	0.028	13.10	8.72	61.36	0.113	1.35	1.45	0.04	0.03	0.33	0.008	-16	31	140	8623	80	7	8	8	-13	4	80	33	243	10	205	26	86.5	13538
26961	15	0.587	0.038	17.15	5.25	54.39	0.097	5.47	2.02	0.05	0.02	0.25	0.018	18	38	100	8913	48	7	-13	4	-5	10	40	32	307	12	243	17	84.7	15995
26962	16	0.66	0.098	30.48	4.60	37.41	0.343	7.79	2.71	0.07	0.03	0.17	0.012	175	59	20	6221	44	4	9	2	14	-3	10	37	197	13	181	13	83.6	14543
26963	17	0.709	0.093	32.90	6.48	36.36	0.234	7.47	0.60	0.06	0.04	0.20	0.005	29	9	50	6481	50	10	9	9	0	1	10	33	191	11	145	15	84.4	15047
26964	18	0.276	0.022	53.80	2.77	12.80	0.032	23.57	0.08	0.03	0.01	0.08	0.001	2	5	-20	3071	15	4	-1	0	9	1	-10	10	92	6	31	7	93.2	6167
26967	21	0.203	0.011	57.21	1.63	8.79	0.017	26.48	0.03	0.02	0.01	0.07	0.002	19	-1	-90	4592	13	2	2	1	6	0	-10	3	61	3	42	3	94.3	6751
26968	22	0.206	0.018	56.03	2.36	9.54	0.057	25.84	0.04	0.05	0.01	0.09	0.002	17	6	-50	6326	19	0	-3	-3	5	-5	0	8	65	5	57	7	94.0	8662
26970	24	0.36	0.029	52.12	1.87	15.89	0.178	21.61	0.10	0.05	0.02	0.07	0.009	150	-5	-15	5922	32	3	5	0	6	-2	0	14	120	10	46	6	91.9	10141
CBRC1384																															
60792	1	0.053	0.003	64.81	12.69	7.93	0.032	1.25	1.00	0.49	0.55	0.47	0.041	1037	49	460	1156	40	15	37	4	11	22	780	199	132	10	92	97	89.3	4663
60795	4	0.085	0.007	57.88	15.79	8.85	0.045	2.18	1.14	1.81	0.47	0.58	0.019	493	27	230	1231	60	17	27	7	10	17	400	434	185	7	78	102	88.8	4212
60796	5	0.047	0.003	52.20	15.78	8.53	0.022	2.07	3.26	0.86	0.50	0.69	0.013	580	31	250	1244	57	20	26	-1	9	14	800	251	229	7	167	117	83.9	4257
60798	7	0.012	7E-04	52.80	18.39	14.30	0.057	0.72	1.31	2.61	0.46	1.25	0.014	82	23	200	265	38	20	-3	5	6	27	60	219	335	9	26	74	91.9	1480
60799	8	0.01	0.002	52.65	17.10	14.50	0.109	2.88	3.94	3.05	0.44	1.33	0.014	238	3	190	207	46	24	2	0	7	23	80	266	365	22	45	77	96.0	1676
60801	10	0.014	0.003	51.24	15.28	14.00	0.156	5.04	6.25	3.18	0.41	1.30	0.011	112	34	110	263	41	18	9	-2	9	20	20	270	356	35	66	86	96.8	1591
60803	12	0.027	0.005	50.97	14.27	10.34	0.127	7.35	5.44	3.07	1.38	0.71	0.111	691	73	20	705	76	16	39	8	9	64	30	719	207	39	96	123	93.8	3197

Hole ID	Depth (m)	%Ni	%Co	SiO2 %	Al2O3 %	Fe2O3 %	MnO %	MgO %	CaO %	Na2O %	K2O %	TiO2 %	P2O5 %	Ba ppm	Ce ppm	Cl ppm	Cr ppm	Cu ppm	Ga ppm	La ppm	Nb ppm	Pb ppm	Rb ppm	S ppm	Sr ppm	V ppm	Y ppm	Zn ppm	Zr ppm	OXIDES %	TotalTr ppm
CBRC1395																															
66041	1	0.114	0.005	48.89	11.65	28.95	0.102	0.50	0.32	0.13	0.57	0.68	0.053	575	28	260	4025	57	19	25	2	7	24	300	47	259	31	55	148	91.8	7022
66042	2	0.023	8E-04	72.87	12.82	5.29	0.020	0.42	0.43	0.16	0.71	0.44	0.016	443	40	450	224	22	16	18	1	2	15	120	44	98	20	16	106	93.2	1846
66043	3	0.009	4E-04	61.86	14.20	4.13	0.010	0.64	6.67	0.07	0.54	0.52	0.016	151	26	190	76	19	15	24	0	13	10	150	161	100	11	8	117	88.7	1132
66045	5	0.003	3E-04	67.80	16.02	4.40	0.010	0.72	1.58	0.04	0.32	0.57	0.022	109	47	60	32	5	17	25	3	1	2	40	50	95	15	5	127	91.5	634
66047	7	0.004	3E-04	63.63	17.18	7.26	0.013	0.90	1.22	0.15	1.92	0.62	0.015	427	23	80	28	7	20	14	8	6	41	30	31	113	15	12	146	92.9	1007
66050	10	0.004	8E-04	66.85	16.62	5.49	0.008	1.04	0.68	0.10	1.20	0.54	0.035	307	75	50	32	3	22	41	1	10	24	20	32	106	15	15	129	92.6	898
66051	11	0.004	0.001	66.69	17.53	4.55	0.012	1.37	0.32	0.03	0.69	0.58	0.034	152	67	100	34	7	18	38	1	7	23	10	45	69	15	22	123	91.8	755
66052	12	0.003	0.002	64.67	15.49	7.24	0.017	1.89	0.44	0.13	1.67	0.58	0.026	261	46	10	26	0	21	20	1	-1	49	20	35	144	11	24	117	92.2	801
66056	15	0.004	0.002	65.66	15.77	5.42	0.014	2.46	0.85	0.15	1.32	0.55	0.021	305	55	-40	40	4	21	21	3	4	31	20	37	118	15	22	115	92.2	790
66057	16	0.005	0.002	57.29	14.06	6.04	0.019	4.35	4.12	0.22	1.47	0.49	0.016	611	38	-60	47	6	22	13	2	-4	36	80	85	124	11	26	106	88.1	1169
66059	18	0.005	0.002	62.79	15.95	6.77	0.024	3.24	0.82	0.16	1.41	0.57	0.038	294	62	-10	33	5	20	31	4	8	31	0	27	139	16	27	117	91.8	836
66060	19	0.01	0.003	56.57	16.82	9.07	0.035	3.83	1.09	0.07	0.55	0.64	0.080	61	61	-30	52	2	24	27	5	1	22	0	31	163	18	41	138	88.8	703
66064	23	0.007	0.003	58.64	16.49	7.69	0.032	3.97	0.65	0.11	0.78	0.63	0.033	124	64	-30	41	6	25	12	3	6	16	10	33	125	13	41	119	89.0	679
66068	27	0.005	0.003	61.16	15.47	6.97	0.052	3.38	1.63	1.22	0.55	0.58	0.147	141	41	-70	36	9	23	20	0	6	18	10	83	104	15	33	111	91.2	627
66070	29	0.01	0.002	54.63	20.68	5.93	0.042	3.10	3.38	3.20	0.63	0.69	0.154	174	95	-20	72	8	27	45	0	2	17	-10	181	106	20	31	187	92.4	1015
66071	30	0.006	0.002	63.11	16.20	5.15	0.023	3.52	1.04	0.65	2.58	0.50	0.165	669	50	-50	35	3	26	25	5	-1	47	-20	51	103	11	28	129	92.9	1155
66072	31	0.002	0.001	69.23	14.95	3.23	0.018	2.18	1.56	1.47	1.86	0.44	0.163	469	49	-25	22	7	18	15	4	2	34	-10	92	92	14	18	129	95.1	927
66074	33	0.006	0.002	72.40	12.92	3.69	0.036	2.16	2.31	2.74	0.33	0.39	0.126	127	46	-10	36	7	16	19	4	7	7	-10	136	61	15	19	112	97.1	632
CBRC0732																															
27067	1	0.194	0.01	37.49	10.77	33.26	0.104	3.16	1.01	0.11	0.26	0.43	0.013	439	11	100	8657	63	13	11	9	10	8	190	57	157	14	82	46	86.6	11890
27068	2	0.314	0.039	43.92	6.53	17.27	0.214	8.31	4.24	0.17	0.37	0.28	0.007	203	19	15	3863	45	9	7	4	13	11	165	88	89	9	76	56	81.3	8175
27069	3	0.743	0.036	30.22	4.62	18.02	0.172	8.34	7.77	0.42	0.20	0.20	0.001	502	39	2865	5745	44	5	4	3	6	-1	34430	122	60	6	132	20	70.0	51748
27071	5	1.134	0.044	38.47	5.98	21.47	0.620	11.12	0.56	0.58	0.19	0.25	0.001	828	6	3575	6709	79	7	0	2	9	2	2800	42	79	8	118	16	79.3	26043
27074	8	1.187	0.045	39.21	6.06	21.16	0.371	13.06	0.20	0.54	0.16	0.23	0.001	274	1	2115	5492	83	7	1	5	9	3	855	42	78	6	123	14	81.0	21403
27076	10	0.776	0.018	43.48	5.62	21.69	0.300	9.01	0.20	0.46	0.16	0.25	0.001	339	7	1980	5777	59	7	5	4	10	-2	705	43	86	7	117	15	81.2	17083
27077	11	0.715	0.01	40.83	6.67	23.63	0.106	7.55	0.21	0.45	0.17	0.30	0.001	51	1	1985	5809	77	8	1	3	11	1	745	46	89	7	135	17	79.9	16215
27081	15	0.555	0.005	40.77	6.76	23.18	0.063	7.25	0.71	0.46	0.16	0.30	0.001	0	-13	1625	7786	49	9	-1	8	12	-1	590	51	95	8	122	18	79.7	15941
27082	16	0.539	0.017	38.12	6.26	22.32	0.160	7.97	2.48	0.42	0.15	0.29	0.001	83	-11	1855	6448	33	7	7	7	6	-1	595	74	95	10	105	23	78.2	14880
27084	18	0.602	0.034	37.87	5.46	19.06	0.331	13.32	3.05	0.45	0.14	0.24	0.001	98	3	1390	5477	22	5	5	1	20	-2	455	75	74	15	103	18	79.9	14102
27085	19	0.453	0.014	46.87	4.97	17.03	0.120	11.75	1.39	0.40	0.13	0.22	0.001	30	-6	1117	4854	18	6	4	7	8	0	343	57	71	7	78	14	82.9	11262
27091	24	0.306	0.007	64.26	5.31	7.76	0.113	11.50	1.01	0.19	0.11	0.24	0.019	39	26	220	1764	31	8	9	3	8	0	70	37	56	8	50	32	90.5	5468

Hole ID	Depth (m)	%Ni	%Co	SiO2 %	Al2O3 %	Fe2O3 %	MnO %	MgO %	CaO %	Na2O %	K2O %	TiO2 %	P2O5 %	Ba ppm	Ce ppm	Cl ppm	Cr ppm	Cu ppm	Ga ppm	La ppm	Nb ppm	Pb ppm	Rb ppm	S ppm	Sr ppm	V ppm	Y ppm	Zn ppm	Zr ppm	OXIDES %	TotalTr ppm
CBRC0734																															
27130	1	0.231	0.022	20.95	14.00	45.90	0.101	1.50	0.27	0.07	0.06	0.47	0.027	248	10	85	11207	83	13	9	12	6	1	575	30	314	19	80	63	83.4	15270
27133	4	0.923	0.066	47.50	4.10	24.83	0.067	4.16	0.55	0.11	0.21	0.15	0.001	24	18	-60	4540	48	4	-7	0	8	6	10	49	97	11	141	16	81.7	14752
27135	6	1.379	0.046	46.78	4.31	21.54	0.093	7.32	0.41	0.18	0.15	0.18	0.001	49	11	220	6171	54	3	10	0	2	4	10	42	87	7	198	14	81.0	21101
27136	7	0.996	0.028	40.02	5.37	16.76	0.075	11.66	3.68	0.18	0.12	0.41	0.001	17	15	320	4313	45	3	3	-6	4	1	100	83	73	9	131	32	78.3	15352
27137	8	0.821	0.033	45.79	4.80	12.31	0.112	20.11	1.84	0.13	0.07	0.23	0.002	15	20	170	3209	57	6	15	0	-3	0	40	42	68	19	92	29	85.4	12288
27139	10	0.799	0.031	49.32	3.07	15.09	0.162	16.71	0.54	0.19	0.08	0.13	0.001	40	-6	210	3921	30	3	0	3	5	1	30	31	50	6	91	11	85.3	12683
27142	13	1.15	0.023	43.71	4.04	20.86	0.141	11.31	0.34	0.32	0.14	0.17	0.001	33	-1	280	5489	25	5	98	0	6	0	70	50	57	8	125	11	81.0	17952
27147	17	0.802	0.062	49.31	2.94	15.19	0.434	17.03	0.16	0.24	0.09	0.12	0.001	198	5	230	4235	91	2	12	-2	8	3	90	32	76	7	84	8	85.5	13683
27148	18	0.257	0.015	70.77	1.81	9.92	0.123	10.27	0.10	0.08	0.05	0.07	0.004	123	10	180	3051	44	2	-1	-4	15	-2	60	20	96	10	50	10	93.2	6349
27149	19	1.121	0.046	41.12	5.13	25.93	0.388	6.98	0.24	0.36	0.14	0.26	0.004	183	-18	500	7144	52	4	3	6	10	-1	200	50	52	5	129	21	80.5	19968
27152	22	1.21	0.031	39.20	4.40	21.83	0.364	12.66	0.79	0.29	0.11	0.22	0.001	81	2	320	7141	52	5	4	-3	7	0	100	61	66	14	124	17	79.9	20368
27154	24	0.79	0.024	39.60	3.53	17.12	0.270	20.33	1.29	0.20	0.08	0.18	0.001	44	-5	230	5941	32	2	2	-2	3	-1	50	46	55	10	96	12	82.6	14624
27155	25	0.915	0.025	40.76	3.81	19.22	0.341	14.17	1.53	0.27	0.10	0.17	0.001	44	-1	200	4779	38	3	0	2	4	5	40	62	79	13	112	10	80.4	14759
27157	27	0.752	0.023	41.16	3.88	18.03	0.295	15.86	1.02	0.23	0.10	0.18	0.001	45	3	170	4751	38	4	10	-3	8	0	20	56	63	9	106	9	80.8	12997
27160	30	0.427	0.017	57.33	2.78	12.42	0.236	15.34	0.24	0.15	0.08	0.11	0.001	9	12	120	3844	45	2	4	5	6	3	20	31	46	5	72	14	88.7	8655
CBRC0780																															
29168	1	0.048	0.003	57.63	15.71	10.01	0.033	1.39	0.53	0.23	0.61	0.44	0.022	475	43	140	720	36	19	33	0	18	33	100	85	101	19	44	83	86.6	2423
29170	3	0.316	0.022	63.79	5.11	13.13	0.021	3.34	0.43	0.16	0.18	0.14	0.003	202	32	180	1922	23	6	2	0	6	10	80	60	65	3	62	19	86.3	6017
29173	6	0.56	0.023	62.50	2.96	15.44	0.028	3.17	0.42	0.16	0.13	0.09	0.001	77	6	210	2822	18	2	-2	0	-9	0	40	51	30	8	67	10	84.9	9123
29175	7	0.683	0.024	55.85	3.32	17.29	0.045	9.18	0.32	0.10	0.08	0.14	0.003	120	12	120	8301	30	4	25	1	4	1	40	41	94	7	104	11	86.3	15951
29178	10	0.982	0.032	37.31	4.88	24.08	0.093	7.67	3.36	0.20	0.11	0.21	0.001	704	-24	220	15946	38	7	11	-1	4	6	160	85	69	8	171	11	77.9	27520
29179	11	0.889	0.027	35.11	4.94	21.51	0.086	7.43	7.07	0.15	0.10	0.20	0.001	374	-17	140	15623	45	6	7	-3	4	6	100	138	81	12	161	16	76.6	25822
29181	13	1.161	0.053	35.91	5.23	26.49	0.356	10.94	0.46	0.18	0.09	0.23	0.002	156	-31	195	17957	32	4	19	7	11	0	0	48	123	11	159	15	79.9	30819
29184	16	0.994	0.024	39.47	4.36	20.06	0.271	16.57	0.33	0.14	0.08	0.18	0.001	112	-32	120	18433	27	6	4	5	16	-2	5	37	94	6	129	15	81.5	29134
29186	17	0.72	0.019	41.36	3.41	18.07	0.186	19.32	0.40	0.08	0.07	0.13	0.001	65	-30	100	15824	38	6	4	2	0	-1	30	45	70	7	106	9	83.0	23628
29189	20	0.425	0.014	61.22	2.05	10.63	0.137	14.65	0.22	0.08	0.05	0.07	0.001	66	-11	20	8133	22	2	4	3	5	-1	20	20	48	2	68	12	89.1	12770
29190	21	0.417	0.014	63.71	1.87	11.97	0.149	11.76	0.17	0.10	0.05	0.07	0.001	27	7	90	5805	17	2	-9	-3	-2	-1	10	23	47	7	69	10	89.8	10384
29191	22	0.401	0.016	60.66	1.99	12.18	0.172	14.21	0.12	0.11	0.05	0.07	0.001	24	13	100	5866	26	3	-5	-3	6	-3	10	19	53	3	70	5	89.6	10326
29192	23	0.506	0.02	53.28	2.60	16.38	0.221	13.96	0.15	0.14	0.07	0.11	0.001	19	0	170	4822	16	5	-3	0	2	-2	20	23	53	6	91	8	86.9	10457
29193	24	0.571	0.03	44.87	3.12	19.19	0.346	17.52	0.57	0.17	0.07	0.13	0.004	41	-6	200	5500	31	2	-2	-1	4	2	30	39	57	1	100	12	86.0	11976
29194	25	0.402	0.013	49.83	2.21	13.01	0.146	16.46	2.68	0.09	0.06	0.10	0.003	14	-1	120	4664	44	0	-6	-4	2	0	30	72	55	6	64	8	84.6	9178
29195	26	0.336	0.016	53.84	1.82	11.32	0.176	15.08	3.03	0.08	0.05	0.07	0.001	11	14	90	3806	61	5	2	-3	-6	1	30	75	52	4	60	7	85.5	7692
29196	27	0.283	0.014	44.47	1.57	9.52	0.158	15.00	8.36	0.07	0.05	0.06	0.001	19	3	110	2973	33	4	-3	0	0	-4	20	171	38	6	52	10	79.2	6366
29197	28	0.283	0.014	67.40	1.75	10.31	0.134	9.95	0.16	0.10	0.06	0.06	0.001	15	17	100	3411	28	4	-3	-1	6	-2	20	21	57	2	50	3	89.9	6663
29200	31	0.23	0.014	70.95	1.63	9.07	0.142	7.97	0.10	0.07	0.06	0.05	0.003	18	-14	40	3740	19	0	-2	-4	10	1	0	22	51	8	50	6	90.0	6350
29201	32	0.257	0.009	29.66	1.22	6.22	0.092	29.79	0.81	0.07	0.04	0.03	0.001	14	1	-5	2198	15	2	1	-4	-3	1	5	21	25	4	35	5	67.9	4939
29206	37	0.209	0.007	25.44	0.87	5.42	0.079	32.13	0.91	0.06	0.04	0.02	0.002	6	5	30	2030	28	2	3	0	3	-4	10	16	19	4	34	4	65.0	4319
29209	40	0.219	0.009	27.86	1.02	6.33	0.103	29.27	1.60	0.08	0.04	0.03	0.001	-33	6	-5	2582	-7	1	-5	3	29	-2	-15	27	25	3	42	7	66.3	4921
29210	41	0.25	0.01	26.72	1.24	7.57	0.116	29.97	1.69	0.09	0.05	0.04	0.001	-1	9	-10	3233	12	2	-2	-5	-4	-1	10	34	22	3	50	5	67.5	5923
29213	44	0.319	0.013	35.34	1.89	11.33	0.150	24.19	1.23	0.11	0.06	0.08	0.002	0	12	30	3640	12	2	-4	-1	7	1	10	31	38	7	71	10	74.4	7159
29217	47	0.208	0.009	32.99	1.06	6.35	0.100	28.49	1.15	0.05	0.04	0.03	0.001	15	-2	-30	1497	5	3	-3	0	5	0	10	29	30	4	40	6	70.3	3737
29221	51	0.185	0.008	27.98	1.04	5.65	0.075	33.24	0.79	0.04	0.02	0.04	0.001	-28	10	-10	1339	8	1	3	6	34	-4	-15	14	27	4	31	4	68.9	3340
29222	52	0.256	0.011	33.56	1.65	8.08	0.126	33.96	0.92	0.05	0.02	0.07	0.003	9	1	210	1933	14	2	12	-2	4	2	210	20	34	6	52	7	78.4	5155
29224	54	0.235	0.009	34.20	1.39	7.86	0.105	35.31	0.92	0.06	0.02	0.05	0.004	26	1	320	1759	18	2	0	-3	5	-2	110	19	37	6	42	3	79.9	4754

Hole ID	Depth (m)	%Ni	%Co	SiO2 %	Al2O3 %	Fe2O3 %	MnO %	MgO %	CaO %	Na2O %	K2O %	TiO2 %	P2O5 %	Ba ppm	Ce ppm	Cl ppm	Cr ppm	Cu ppm	Ga ppm	La ppm	Nb ppm	Pb ppm	Rb ppm	S ppm	Sr ppm	V ppm	Y ppm	Zn ppm	Zr ppm	OXIDES %	TotalTr ppm
CBRC1505																															
58171	1	0.378	0.037	44.26	5.65	8.76	0.193	10.86	9.67	0.14	0.13	0.37	0.022	314	34	560	1407	39	5	6	3	-6	4	280	217	188	6	69	54	80.1	7300
58172	2	0.988	0.037	39.25	10.16	11.36	0.129	11.64	5.02	0.51	0.14	0.79	0.023	255	30	1770	1773	51	12	67	5	5	1	610	166	232	34	166	91	79.0	15490
58174	4	0.241	0.021	63.11	4.71	6.98	0.103	15.33	0.32	0.28	0.06	0.24	0.008	147	26	1290	2173	48	4	16	-1	5	-1	510	28	95	11	80	24	91.1	7043
58175	5	0.159	0.008	55.41	6.36	7.83	0.029	18.51	0.27	0.29	0.07	0.28	0.005	7	13	2000	3395	44	7	2	1	3	-1	360	26	85	6	82	17	89.1	7676
58179	9	0.107	0.003	72.80	4.65	6.84	0.038	5.84	0.15	0.45	0.11	0.30	0.003	31	22	1110	870	14	7	17	1	2	1	140	31	81	8	35	31	91.2	3465
58182	12	0.334	0.006	61.57	5.31	8.74	0.080	13.12	0.38	0.37	0.07	0.32	0.004	19	15	1280	1706	46	7	7	1	8	1	160	25	84	11	51	32	90.0	6821
58183	13	0.257	0.009	55.70	4.91	10.18	0.166	18.16	0.15	0.34	0.05	0.23	0.005	30	10	1330	2733	26	6	1	-3	13	0	140	23	113	9	54	14	89.9	7136
58186	16	0.221	0.011	52.58	5.32	10.12	0.224	19.76	0.99	0.30	0.05	0.24	0.003	46	-1	620	3033	20	4	4	-2	-4	-1	60	23	127	12	55	15	89.6	6306
CBRC0744																															
27467	1	0.162	0.007	67.15	7.39	15.33	0.050	2.38	0.13	0.04	0.08	0.17	0.017	152	21	20	2174	57	6	4	-2	10	4	150	23	71	11	37	21	92.7	4422
27471	5	0.171	0.016	26.56	11.77	48.53	0.153	2.74	0.05	0.04	0.05	0.39	0.005	-10	66	120	2775	42	12	4	9	1	7	210	19	146	17	51	34	90.3	5342
27474	8	0.226	0.012	32.23	9.07	41.32	0.139	6.68	0.08	0.07	0.08	0.41	0.008	30	2	150	3451	36	12	-1	2	-1	3	20	21	144	7	59	32	90.1	6318
27475	9	0.514	0.085	33.42	8.55	38.10	0.432	3.78	0.18	0.17	0.09	0.33	0.002	162	127	250	3980	52	6	13	5	5	1	40	36	112	12	121	23	85.0	10905
27476	10	0.582	0.206	33.12	7.75	37.25	1.208	4.88	0.17	0.18	0.09	0.30	0.002	816	53	220	3990	47	8	9	2	1	6	40	43	116	12	121	24	84.9	13358
27478	12	0.255	0.103	25.49	11.15	49.26	0.544	2.02	0.08	0.11	0.07	0.52	0.005	161	33	100	3983	62	9	-10	5	-22	5	10	34	167	11	69	35	89.2	8209
27480	13	0.32	0.169	25.49	9.98	50.19	0.729	2.25	0.06	0.11	0.06	0.49	0.012	128	11	100	5403	81	13	-4	5	-25	5	35	31	197	7	118	42	89.4	10998
27481	14	0.285	0.117	26.73	11.42	44.29	0.721	3.80	0.08	0.07	0.06	0.56	0.003	133	-18	60	11352	54	13	4	4	19	-1	0	36	206	6	188	40	87.7	16071
27482	15	0.561	0.118	33.69	7.55	26.78	0.665	12.58	0.18	0.23	0.09	0.34	0.001	100	-17	60	15970	59	8	106	-2	-1	-2	20	51	146	11	325	22	82.1	23614
27484	17	0.667	0.022	33.68	6.45	27.52	0.161	13.07	0.17	0.22	0.09	0.28	0.001	25	-6	60	16915	62	8	-1	-1	13	0	10	47	132	13	321	18	81.6	24473
27486	19	0.74	0.062	33.90	6.61	26.64	0.385	13.17	0.18	0.21	0.09	0.30	0.001	49	-10	60	14660	65	5	1	-3	2	1	10	40	115	8	249	19	81.5	23259
27489	22	0.669	0.031	36.55	5.41	23.22	0.335	15.76	0.27	0.16	0.08	0.26	0.001	29	-14	75	14391	32	9	3	7	3	-1	0	39	99	7	191	13	82.1	21866
27490	23	0.722	0.032	39.17	5.05	22.60	0.380	15.17	0.22	0.18	0.09	0.23	0.001	37	-1	60	13264	49	7	27	-1	-6	2	20	44	65	7	198	17	83.1	21294
27492	24	0.77	0.032	39.94	5.38	22.42	0.401	13.04	0.18	0.21	0.10	0.24	0.001	51	-21	60	12877	42	6	5	2	2	-2	0	52	74	11	206	15	81.9	21378
27493	25	0.533	0.022	46.78	3.56	15.22	0.230	20.90	0.12	0.15	0.06	0.15	0.001	46	-2	-10	8850	39	7	-9	-3	-2	2	10	32	59	6	134	7	87.2	14691
27496	28	0.599	0.026	39.47	4.24	19.37	0.351	19.27	0.38	0.15	0.06	0.18	0.003	46	-15	10	13570	33	3	8	0	-3	3	0	34	86	8	128	15	83.5	20152
27499	31	0.71	0.031	36.86	4.84	21.55	0.330	18.16	0.59	0.14	0.07	0.20	0.002	62	-25	30	17297	38	7	0	0	6	3	10	39	107	9	149	13	82.8	25128
27500	32	0.823	0.035	35.71	5.76	25.46	0.392	13.58	0.33	0.14	0.09	0.25	0.008	71	-12	30	16624	41	3	7	0	-3	-4	20	54	129	15	181	15	81.7	25712
27501	33	0.508	0.018	38.63	3.75	15.89	0.227	26.33	0.25	0.09	0.05	0.19	0.001	56	-13	0	10606	27	5	8	0	2	-1	10	26	63	4	105	6	85.4	16146
27503	35	0.369	0.015	47.63	2.47	12.38	0.172	16.96	4.81	0.04	0.03	0.09	0.004	26	0	-60	8435	21	4	1	-1	7	-1	0	32	66	23	74	7	84.6	12435

Hole ID	Depth	%Ni	%Co	SiO2	Al2O3	Fe2O3	MnO	MgO	CaO	Na2O	K2O	TiO2	P2O5	Ba	Ce	Cl	Cr	Cu	Ga	La	Nb	Pb	Rb	S	Sr	V	Y	Zn	Zr	OXIDES	TotalTr
	(m)			%	%	%	%	%	%	%	%	%	%	ppm	ppm	ppm	ppm	ppm	ppm	ppm	ppm	ppm	ppm	ppm	ppm	ppm	ppm	ppm	ppm	%	ppm
CBRC0747																															
27549	1	0.163	0.006	30.00	12.15	43.94	0.036	0.45	0.10	0.05	0.10	0.31	0.039	651	11	120	6055	97	8	0	4	27	4	480	23	162	12	64	54	87.2	9419
27554	6	0.176	0.018	32.29	15.93	37.44	0.081	0.79	0.07	0.03	0.05	0.45	0.015	0	16	10	7676	139	14	-4	-6	6	-4	240	10	213	8	81	42	87.1	10342
27558	9	0.275	0.018	36.25	13.22	39.14	0.193	1.30	0.05	0.04	0.05	0.46	0.013	-13	10	-40	3617	75	13	2	-3	25	4	70	9	149	8	72	31	90.7	6930
27559	10	0.557	0.022	35.95	8.41	36.85	0.176	4.19	0.24	0.10	0.06	0.34	0.005	4	16	-30	5221	49	6	10	6	-3	1	20	36	97	11	154	18	86.3	11385
27560	11	0.726	0.028	38.66	7.18	32.68	0.131	4.27	0.34	0.10	0.06	0.25	0.003	28	11	-90	4916	43	4	1	-1	-2	4	20	49	94	7	212	12	83.7	12813
27561	12	0.327	0.019	55.81	5.34	24.90	0.081	5.43	0.07	0.04	0.06	0.20	0.004	36	-4	-60	4790	64	6	8	2	15	2	90	12	117	7	96	12	91.9	8614
27563	14	0.356	0.059	26.55	9.94	48.51	0.475	4.61	0.02	0.02	0.04	0.56	0.010	94	60	-40	8350	64	9	3	7	-17	9	20	19	176	7	151	28	90.7	13067
27564	15	0.535	0.071	32.34	9.90	37.20	0.630	5.55	0.11	0.07	0.05	0.46	0.005	283	126	-15	15481	32	11	11	9	14	-2	-5	21	166	13	207	25	86.3	22411
27566	17	0.491	0.139	34.13	13.30	32.12	1.052	4.27	0.07	0.06	0.03	0.52	0.008	319	-38	-50	27713	27	14	10	11	15	-7	-10	15	190	12	240	28	85.6	34776
27569	20	0.631	0.064	39.67	8.18	29.51	0.339	5.01	0.10	0.09	0.04	0.40	0.027	67	-50	-40	31018	80	13	11	9	9	-4	-10	18	231	12	309	25	83.4	38620
27570	21	0.138	0.007	70.90	2.00	8.21	0.031	14.66	0.02	0.03	0.02	0.07	0.009	14	-11	-80	2680	32	5	6	0	3	-2	-5	4	61	7	43	5	96.0	4175
27573	23	0.482	0.011	63.42	4.73	9.44	0.045	14.33	0.06	0.04	0.06	0.25	0.012	4	6	-80	2192	39	6	-1	2	5	4	-10	11	84	7	83	30	92.4	7275
27574	24	0.968	0.063	47.44	12.38	12.09	0.397	7.59	0.19	0.17	0.34	0.65	0.005	387	79	-80	5670	73	10	5	-1	21	20	10	56	125	15	156	84	81.3	16904
27576	26	0.485	0.021	56.71	3.14	16.90	0.205	12.34	0.07	0.08	0.06	0.15	0.011	187	5	-30	3924	44	4	6	-1	14	2	-20	18	108	11	79	11	89.7	9399
27579	29	0.563	0.028	51.10	4.52	20.30	0.429	10.01	0.15	0.13	0.07	0.21	0.014	438	13	-70	4734	41	6	7	5	-3	-3	0	42	99	12	79	17	86.9	11303
27582	32	0.428	0.008	48.80	13.17	9.28	0.274	9.07	2.78	0.20	0.35	0.55	0.012	278	63	-90	1699	112	21	32	2	8	6	0	357	60	25	71	80	84.5	7046
27583	33	0.417	0.015	45.00	2.81	11.97	0.177	27.91	0.15	0.06	0.07	0.11	0.002	91	8	-40	2181	18	5	1	-2	3	-1	-10	34	50	11	64	13	88.3	6705
27585	35	0.359	0.02	63.27	2.32	10.44	0.325	15.63	0.05	0.09	0.06	0.09	0.007	285	5	-50	2240	22	4	14	-1	3	-1	0	29	49	7	46	11	92.3	6413
27586	36	0.47	0.034	56.15	3.28	19.85	0.607	8.52	0.07	0.11	0.08	0.15	0.014	634	4	-30	4985	51	5	4	2	3	2	0	45	94	6	63	12	88.8	10886
27588	37	0.137	0.006	52.49	12.58	9.23	0.157	9.07	11.06	0.35	0.42	0.67	0.366	208	66	-50	821	13	15	23	4	6	9	-10	712	161	17	60	120	96.4	3567
27589	38	0.254	0.006	50.63	12.98	9.16	0.157	8.92	8.78	0.28	0.56	0.71	0.366	223	73	10	768	11	18	35	3	9	23	20	549	131	16	73	114	92.5	4651
27593	42	0.304	0.013	43.46	1.57	8.86	0.115	34.91	0.06	0.01	0.02	0.06	0.001	26	6	-40	1930	8	0	-3	3	5	-1	10	10	38	4	51	8	89.1	5200

Hole ID	Depth (m)	%Ni	%Co	SiO2 %	Al2O3 %	Fe2O3 %	MnO %	MgO %	CaO %	Na2O %	K2O %	TiO2 %	P2O5 %	Ba ppm	Ce ppm	Cl ppm	Cr ppm	Cu ppm	Ga ppm	La ppm	Nb ppm	Pb ppm	Rb ppm	S ppm	Sr ppm	V ppm	Y ppm	Zn ppm	Zr ppm	OXIDES %	TotalTr ppm
CBRC0743																															
27414	1	0.055	0.006	26.89	9.54	52.77	0.037	0.53	0.15	0.03	0.05	1.06	0.020	362	13	70	8755	41	40	8	10	-13	4	530	22	393	16	22	169	91.1	11027
27416	3	0.04	0.005	8.22	18.82	51.92	0.043	0.55	1.73	0.06	0.03	1.40	0.028	38	24	355	10563	40	36	-8	19	-7	6	1145	29	449	6	30	231	82.8	13366
27417	4	0.064	0.006	9.14	17.32	56.24	0.058	0.60	0.28	0.56	0.05	0.94	0.025	32	13	1020	11732	54	26	11	3	-21	11	1330	40	367	7	36	170	85.2	15502
27422	9	0.194	0.015	15.93	17.30	49.90	0.073	0.71	0.09	0.10	0.04	0.49	0.060	17	11	170	14462	74	11	69	3	-23	6	350	27	252	10	96	96	84.7	17677
27425	12	0.24	0.01	19.38	18.36	47.82	0.099	0.51	0.06	0.10	0.04	0.57	0.024	-12	44	150	9806	97	12	1	7	-14	3	180	26	385	9	86	78	87.0	13335
27426	13	0.273	0.011	17.30	15.03	53.51	0.187	0.53	0.12	0.07	0.04	0.60	0.027	-37	284	140	11107	84	15	-12	11	4	7	110	30	412	12	84	43	87.4	15125
27432	18	0.332	0.075	19.63	15.11	52.14	0.766	0.57	0.09	0.08	0.05	0.57	0.006	53	10	40	13023	32	15	6	18	-10	2	15	53	294	14	107	33	89.0	17749
27433	19	0.861	0.131	29.08	7.88	37.98	0.656	4.76	0.28	0.17	0.10	0.34	0.003	55	-22	0	22150	37	8	12	8	14	-1	25	51	159	11	310	18	81.3	32736
27436	22	1.055	0.136	28.85	6.90	37.54	0.762	4.44	0.30	0.18	0.11	0.30	0.004	80	-41	5	28451	40	9	4	13	17	-1	0	56	147	12	413	20	79.4	41122
27437	23	0.502	0.097	16.71	10.44	55.02	0.629	1.15	0.10	0.16	0.05	0.54	0.005	83	-57	235	33403	77	13	9	6	-7	6	35	39	282	20	523	22	84.8	40669
27439	25	0.61	0.082	18.83	8.84	53.54	0.530	1.65	0.14	0.11	0.06	0.50	0.006	73	-54	55	24152	61	11	14	15	-13	2	25	38	263	28	377	23	84.2	31970
27440	26	1.41	0.09	32.69	6.10	32.83	0.597	6.74	0.30	0.21	0.11	0.26	0.001	115	-30	-20	13513	33	8	8	-3	13	-1	50	56	112	13	286	21	79.8	29144
27442	28	1.346	0.039	36.77	5.10	28.20	0.400	8.86	0.30	0.24	0.12	0.22	0.001	28	-5	35	8597	29	4	7	1	6	-1	45	53	72	11	199	19	80.2	22917
27443	29	1.443	0.037	36.18	5.41	28.49	0.446	8.02	0.31	0.21	0.12	0.24	0.001	46	-3	10	8956	29	8	9	4	1	-4	40	55	65	10	214	17	79.4	24216
27444	30	1.392	0.032	35.91	5.35	30.74	0.367	6.56	0.31	0.23	0.12	0.24	0.001	29	-6	0	8973	35	7	-5	6	20	-2	40	60	70	10	182	19	79.8	23643
27445	31	1.366	0.033	37.20	5.44	29.63	0.388	6.46	0.31	0.19	0.12	0.25	0.001	28	0	-30	9919	31	7	10	1	4	7	50	58	71	7	197	17	80.0	24336
27448	34	1.334	0.039	43.03	4.59	25.94	0.724	7.03	0.27	0.18	0.10	0.21	0.001	121	1	-40	8900	21	5	21	2	-3	0	40	61	78	19	178	8	82.1	23107
27450	35	1.372	0.032	40.48	4.98	25.54	0.427	8.34	0.27	0.21	0.11	0.22	0.001	50	-6	-20	9468	22	3	2	3	10	-1	10	52	77	15	226	14	80.6	23930
27453	38	1.253	0.041	43.79	4.81	28.78	0.433	6.25	0.20	0.15	0.08	0.24	0.005	81	-13	0	11666	37	9	15	0	3	0	30	39	119	17	278	13	84.7	25194
27454	39	0.774	0.02	54.55	2.97	15.63	0.213	16.65	0.14	0.09	0.04	0.13	0.001	12	-9	-50	6008	22	2	15	-2	6	-4	0	13	71	25	150	10	90.4	14176
27458	43	0.591	0.019	51.75	2.70	14.27	0.204	18.99	0.21	0.09	0.04	0.11	0.001	5	12	-30	6648	14	3	6	-4	6	3	0	17	61	10	100	9	88.3	12922
27463	48	0.437	0.019	55.06	2.85	14.02	0.208	16.27	0.12	0.07	0.05	0.11	0.001	20	1	-30	3421	21	5	3	3	10	1	20	20	43	8	73	7	88.8	8149
27464	49	0.23	0.012	74.27	1.73	9.58	0.144	9.11	0.09	0.04	0.03	0.06	0.007	-21	13	-50	2653	18	2	1	3	2	4	20	9	38	5	47	9	95.1	5142
27465	50	0.32	0.015	66.46	2.35	11.90	0.172	12.16	0.11	0.05	0.03	0.09	0.011	11	-6	-40	3688	22	3	-5	-3	2	-1	0	13	56	4	58	8	93.3	7111
27466	51	0.42	0.018	55.87	2.93	13.51	0.210	17.31	0.11	0.09	0.04	0.13	0.005	1	10	-40	4231	13	6	3	3	7	-1	30	14	64	5	69	9	90.2	8772
CBRC0724																															
26872	1	0.22	0.003	22.53	14.65	45.95	0.039	0.53	0.13	0.02	0.04	0.43	0.021	49	-4	140	11830	82	13	17	2	6	3	430	17	285	15	76	37	84.3	15197
26875	4	0.188	0.011	20.08	13.40	51.94	0.122	0.67	0.16	0.07	0.03	0.44	0.012	27	3	120	5398	75	10	6	1	3	5	520	28	200	23	53	34	86.9	8476
26879	8	0.22	0.017	20.69	13.84	50.44	0.157	0.68	0.14	0.06	0.03	0.56	0.012	33	18	260	5683	111	11	-2	11	-13	5	200	27	228	12	48	42	86.6	9016
26882	11	0.44	0.086	18.87	12.03	51.74	0.288	0.90	0.14	0.06	0.03	0.49	0.021	30	95	280	10185	160	8	-5	4	-24	2	160	25	237	12	102	31	84.6	16534
26885	14	0.487	0.054	19.98	9.48	51.12	0.158	1.24	0.16	0.06	0.03	0.45	0.003	34	-21	170	17799	142	9	-3	10	-10	-1	120	22	213	9	112	27	82.7	24004
26887	16	0.682	0.028	24.62	7.90	47.01	0.086	2.06	0.24	0.10	0.04	0.40	0.004	-2	3	100	11062	74	11	5	3	-15	5	140	31	317	15	189	24	82.5	19032
26890	18	1.03	0.103	34.23	6.37	31.47	0.623	4.97	0.47	0.20	0.05	0.29	0.005	248	-8	250	7991	56	7	4	2	-5	-2	180	44	157	14	175	15	78.7	20430
26893	21	1.006	0.036	38.11	4.62	23.08	0.404	14.26	0.50	0.20	0.05	0.20	0.003	77	-3	190	5906	38	6	14	4	-2	0	120	35	93	12	138	15	81.4	17033
26896	24	0.695	0.023	42.90	3.55	16.40	0.287	20.11	0.39	0.12	0.04	0.14	0.002	40	-6	130	5133	50	5	-3	-3	7	-1	80	25	63	13	107	10	84.0	12796

Hole ID	Depth	%Ni	%Co	SiO2	Al2O3	Fe2O3	MnO	MgO	CaO	Na2O	K2O	TiO2	P2O5	Ba	Ce	Cl	Cr	Cu	Ga	La	Nb	Pb	Rb	S	Sr	V	Y	Zn	Zr	OXIDES	TotalTr
	(m)			%	%	%	%	%	%	%	%	%	%	ppm	ppm	ppm	ppm	ppm	ppm	ppm	ppm	ppm	ppm	ppm	ppm	ppm	ppm	ppm	ppm	%	ppm
CBRC0725																															
26897	1	0.212	0.007	23.65	17.33	39.86	0.080	1.52	0.19	0.05	0.08	0.53	0.025	258	1	50	10141	46	17	4	-3	1	5	410	22	148	12	53	116	83.3	13436
26900	4	0.291	0.012	12.70	12.04	59.11	0.088	0.70	0.12	0.02	0.03	0.54	0.023	34	38	-20	8064	90	12	14	5	-17	3	330	24	270	28	68	44	85.4	11982
26902	6	0.159	0.015	16.25	16.21	51.66	0.181	0.54	0.09	0.06	0.02	0.49	0.020	46	23	50	9766	96	12	6	10	-15	6	290	16	228	25	56	36	85.5	12355
26905	9	1.076	0.101	35.50	7.28	31.02	0.299	4.37	0.51	0.06	0.04	0.27	0.005	42	27	-60	12597	47	8	4	5	17	4	70	41	100	9	185	24	79.4	24865
26907	11	1.105	0.054	48.26	3.49	18.87	0.140	9.66	0.54	0.09	0.05	0.14	0.001	29	-5	-30	7490	27	6	2	-3	3	0	30	40	53	8	194	8	81.2	19401
26910	14	1.171	0.042	43.73	4.08	22.68	0.172	8.72	0.65	0.10	0.05	0.17	0.001	3	-2	-40	6505	39	5	7	5	15	1	10	44	52	2	154	17	80.4	18913
26913	17	1.007	0.019	41.82	3.66	19.52	0.068	13.99	0.55	0.09	0.05	0.16	0.001	2	9	-30	6472	44	3	0	1	5	3	30	43	62	6	103	11	79.9	16984
26916	19	0.77	0.018	46.59	2.80	15.75	0.123	18.64	0.50	0.08	0.04	0.12	0.001	14	6	-50	4234	39	8	7	3	6	-2	30	28	57	7	82	9	84.6	12322
26919	22	0.711	0.022	45.55	3.14	16.47	0.236	18.56	0.52	0.10	0.04	0.13	0.001	30	17	-60	4094	38	2	-4	2	11	1	10	33	76	7	86	13	84.7	11669
CBRC0712																															
26613	1	0.186	0.007	20.45	14.64	45.70	0.040	0.47	0.16	0.01	0.04	0.51	0.020	129	-2	100	13792	52	18	14	8	21	4	480	16	265	10	55	111	82.0	16965
26615	3	0.117	0.017	24.61	12.73	45.72	0.037	0.46	0.23	0.06	0.05	0.30	0.018	33	-12	0	9973	49	13	5	9	1	-3	330	23	171	13	58	53	84.2	12016
26617	5	0.068	0.004	18.05	11.63	57.00	0.043	0.30	0.09	0.05	0.03	0.33	0.009	33	7	0	6588	43	12	-9	12	-14	2	600	20	200	6	29	41	87.5	8265
26620	8	0.244	0.032	17.65	9.26	56.77	0.117	0.57	0.09	0.05	0.03	0.38	0.012	15	-4	-20	14010	104	11	24	4	-11	5	190	17	237	9	118	25	84.9	17462
26622	10	0.431	0.034	23.87	9.67	47.50	0.078	0.91	0.18	0.07	0.04	0.38	0.006	2	11	-5	12918	106	11	-2	13	-7	1	35	21	198	9	123	24	82.7	18095
26623	11	0.842	0.061	31.99	3.72	45.40	0.176	1.44	0.27	0.08	0.05	0.14	0.001	45	-3	-60	9928	82	0	20	-4	-1	-1	20	26	110	20	171	6	83.3	19361
26624	12	1.356	0.145	37.24	4.80	32.75	0.760	4.16	0.50	0.15	0.07	0.21	0.024	257	1	-5	11810	39	7	32	5	21	-2	20	44	181	19	174	15	80.7	27608
26625	13	1.05	0.05	58.97	2.42	16.94	0.227	5.75	0.43	0.13	0.07	0.10	0.003	46	4	-50	5843	38	2	18	0	2	2	10	34	79	16	88	5	85.0	17106
26628	15	0.66	0.024	59.49	2.11	14.61	0.187	9.89	0.31	0.12	0.05	0.08	0.003	38	-4	140	5494	24	4	4	1	7	-3	0	28	73	11	77	4	86.9	12706
26631	18	0.613	0.021	57.38	2.13	14.86	0.195	11.41	0.32	0.15	0.04	0.08	0.003	60	-2	-50	6555	29	4	12	0	6	5	10	29	52	13	89	8	86.6	13116

Hole ID	Depth (m)	%Ni	%Co	SiO2 %	Al2O3 %	Fe2O3 %	MnO %	MgO %	CaO %	Na2O %	K2O %	TiO2 %	P2O5 %	Ba ppm	Ce ppm	Cl ppm	Cr ppm	Cu ppm	Ga ppm	La ppm	Nb ppm	Pb ppm	Rb ppm	S ppm	Sr ppm	V ppm	Y ppm	Zn ppm	Zr ppm	OXIDES %	TotalTr ppm
CBRC0714																															
26645	1	0.076	0.014	6.16	6.68	76.34	0.071	0.28	0.13	0.01	0.02	2.54	0.030	139	-8	50	11737	43	49	15	20	-21	6	290	22	858	17	30	238	92.2	14353
26649	5	0.139	0.006	16.99	16.55	48.88	0.026	0.34	0.11	0.04	0.04	0.71	0.022	-8	6	75	12077	33	19	-4	12	2	0	395	15	266	8	70	113	83.7	14508
26650	6	0.188	0.011	14.39	12.59	56.69	0.046	0.38	0.11	0.02	0.04	0.46	0.025	10	0	35	9895	69	12	6	5	-12	4	450	21	176	8	91	58	84.8	12781
26651	7	0.168	0.012	19.45	12.15	51.90	0.030	0.49	0.15	0.06	0.06	0.67	0.018	31	-9	120	13139	47	15	-6	14	-15	11	340	25	302	8	70	83	85.0	15933
26652	8	0.202	0.016	16.03	11.62	55.54	0.059	0.37	0.12	0.02	0.04	0.46	0.034	27	-16	90	11323	53	14	6	10	-11	4	400	18	274	8	94	72	84.3	14507
26654	10	0.209	0.02	9.56	11.32	63.43	0.122	0.29	0.05	0.03	0.02	0.31	0.051	15	-13	70	9966	60	9	96	8	-5	4	590	16	156	6	164	31	85.2	13430
26657	13	0.535	0.096	11.47	7.85	60.19	0.320	0.43	0.08	0.05	0.02	0.26	0.069	130	27	5	24248	44	8	0	15	-15	2	205	11	585	9	251	22	80.7	31843
26658	14	0.615	0.066	17.27	5.65	57.98	0.183	0.75	0.17	0.08	0.03	0.25	0.038	66	24	10	16742	50	7	-3	3	-16	2	150	24	346	10	294	16	82.4	24500
26661	16	0.749	0.023	58.08	2.53	22.34	0.090	1.84	0.42	0.10	0.06	0.10	0.001	11	32	-60	4611	26	2	15	3	-1	-2	10	31	71	6	137	7	85.6	12586
26663	18	0.606	0.025	41.44	3.28	34.74	0.139	3.05	0.51	0.13	0.06	0.15	0.004	35	3	-30	5161	63	3	17	2	6	-2	20	44	97	14	161	12	83.5	11878
26665	20	0.664	0.141	51.00	2.28	23.44	0.846	4.28	0.58	0.20	0.08	0.11	0.002	442	9	80	3119	37	3	5	-1	-6	0	40	55	58	8	98	10	82.8	11978
26666	21	0.894	0.18	43.35	3.30	25.83	1.099	5.15	0.63	0.24	0.08	0.19	0.001	321	14	80	6900	52	3	18	5	3	0	80	54	78	6	131	15	79.9	18473
26669	24	0.444	0.027	60.03	2.04	11.43	0.147	12.97	0.26	0.13	0.04	0.08	0.003	37	-5	40	8589	46	1	6	0	4	-2	30	18	54	9	70	11	87.1	13594
CBRC0783																															
29819	1	0.206	0.015	36.49	11.44	37.62	0.138	0.77	0.24	0.04	0.09	0.28	0.014	511	31	170	5005	67	6	13	-1	26	5	420	21	114	18	67	27	87.1	8688
29821	3	0.3	0.035	28.82	7.31	47.66	0.184	1.56	0.16	0.08	0.09	0.33	0.006	42	81	-20	6060	58	9	10	4	37	5	100	27	119	14	63	26	86.2	9943
29822	4	0.468	0.171	39.29	5.10	36.17	0.592	2.30	0.17	0.06	0.09	0.26	0.002	118	457	55	12436	47	9	30	8	25	-1	65	25	112	14	169	17	84.0	19965
29824	6	0.841	0.097	56.43	2.40	20.92	0.360	4.25	0.34	0.14	0.10	0.08	0.001	165	354	100	3504	40	4	16	3	2	2	20	41	39	12	121	8	85.0	13776
29825	7	0.786	0.029	42.63	3.67	24.58	0.118	12.32	0.30	0.12	0.07	0.14	0.003	49	162	250	8737	47	4	7	0	2	-3	60	31	70	9	135	12	83.9	17699
29827	9	0.901	0.074	38.99	4.37	19.62	1.140	17.84	0.31	0.17	0.06	0.18	0.001	1572	-23	870	11937	57	4	36	5	10	-3	40	37	92	12	130	12	82.7	24503
29830	12	0.829	0.024	44.78	3.57	15.05	0.233	19.19	0.30	0.12	0.05	0.15	0.002	176	-14	-70	8368	30	3	25	1	0	0	-10	26	47	10	78	13	83.4	17166
29832	13	0.709	0.018	43.51	3.62	13.57	0.126	22.41	0.25	0.12	0.05	0.14	0.001	60	-26	1000	15000	27	5	21	1	4	0	50	24	60	7	86	11	83.8	23573
29833	14	0.67	0.021	43.65	3.41	12.86	0.194	23.59	0.23	0.11	0.04	0.14	0.001	81	-12	80	17279	13	4	14	-1	-2	4	10	19	67	6	91	10	84.2	24530
29835	16	0.646	0.019	43.76	3.20	12.75	0.147	22.30	0.18	0.11	0.04	0.11	0.001	42	-42	180	24438	14	1	-3	0	3	1	20	21	60	2	96	3	82.6	31447
29838	19	0.566	0.018	51.38	2.25	11.49	0.210	18.75	0.11	0.15	0.04	0.07	0.001	72	-25	680	18225	24	3	9	1	-13	0	100	14	42	5	78	7	84.4	25032
29839	20	0.34	0.014	67.87	1.61	7.53	0.107	11.16	1.33	0.10	0.04	0.05	0.001	36	-8	210	7122	24	3	0	-3	7	-3	20	32	30	6	43	8	89.8	11025
29840	21	0.589	0.017	42.74	2.62	12.00	0.159	19.32	3.67	0.12	0.05	0.10	0.001	22	-9	0	11823	18	3	4	-3	6	-2	0	52	58	7	98	6	80.8	18104
29841	22	0.592	0.018	44.70	2.45	11.75	0.187	21.16	2.95	0.10	0.04	0.10	0.001	26	-6	0	5358	20	3	2	2	3	-1	30	41	53	6	78	11	83.4	11688
29842	23	0.574	0.018	57.82	1.64	11.74	0.213	15.95	0.55	0.15	0.05	0.06	0.001	22	7	405	1723	22	3	1	0	1	-2	25	28	34	6	71	6	88.2	8240
29845	26	0.47	0.017	60.89	1.76	10.58	0.194	11.99	0.15	0.13	0.05	0.07	0.003	12	1	-10	1482	31	3	-6	0	-1	2	10	30	47	6	73	3	85.8	6531
29849	30	0.472	0.016	64.64	1.75	11.08	0.220	11.25	0.18	0.10	0.05	0.07	0.001	5	29	190	1375	24	0	4	-4	7	0	30	29	50	3	82	6	89.3	6667
29850	31	0.359	0.012	71.24	1.08	8.96	0.175	8.67	0.13	0.12	0.04	0.03	0.001	0	13	120	1064	20	2	7	3	6	4	20	24	25	5	57	8	90.5	5053
29853	34	0.389	0.014	61.90	1.33	11.14	0.222	14.77	0.12	0.08	0.04	0.07	0.001	19	10	-20	1291	21	-1	4	1	3	2	0	24	20	3	72	4	89.7	5452
29858	38	0.223	0.009	73.44	0.69	8.90	0.138	10.07	0.11	0.09	0.03	0.01	0.008	8	17	190	937	25	3	6	0	2	-1	30	17	52	7	42	2	93.5	3632
29859	39	0.213	0.008	47.55	0.63	7.65	0.108	12.23	10.74	0.09	0.03	0.01	0.007	17	-1	50	776	12	1	8	-4	1	1	0	50	44	7	41	0	79.0	3178
29861	41	0.263	0.008	39.86	0.60	8.64	0.128	12.88	12.72	0.05	0.03	0.01	0.006	28	6	30	881	13	0	-7	0	3	0	10	89	33	4	49	7	74.9	3821
29864	44	0.24	0.007	34.06	0.46	7.76	0.101	26.86	1.72	0.04	0.02	0.00	0.010	-10	16	170	717	14	1	3	2	3	-3	10	24	37	3	38	3	71.0	3461
29866	45	0.207	0.007	25.90	0.65	7.15	0.130	28.74	4.91	0.04	0.02	0.02	0.005	-14	19	0	631	8	0	-2	-2	8	-3	-10	57	26	5	37	6	67.6	2873
29869	48	0.24	0.009	33.75	0.46	6.94	0.108	25.38	3.91	0.07	0.02	0.00	0.005	18	15	-70	963	0	0	5	-1	2	-2	-10	47	23	6	36	6	70.6	3484
29873	52	0.237	0.012	24.91	0.51	6.31	0.111	31.26	3.23	0.04	0.01	0.00	0.008	9	15	20	912	3	0	3	-1	5	-1	20	53	15	0	33	4	66.4	3542
29876	55	0.21	0.011	27.18	0.89	7.04	0.107	23.24	14.05	0.02	0.02	0.03	0.003	29	6	-40	1164	13	1	1	-3	3	3	10	180	32	7	35	6	72.6	3624
29878	57	0.204	0.005	14.61	0.55	5.17	0.098	20.63	21.47	0.04	0.02	0.01	0.001	-11	19	-40	947	11	0	6	0	8	-2	10	297	12	5	24	10	62.6	3352
29881	60	0.217	0.008	35.82	0.60	8.66	0.105	20.65	11.72	0.01	0.01	0.01	0.004	1	1	-60	814	7	-1	-1	-2	5	2	-10	111	28	2	39	10	77.6	3169

Appendix 4: Table A4.2. XRF analyses of selected RC holes for MM3.

Hole ID	Depth (m)	%Ni	%Co	SiO2 %	Al2O3 %	Fe2O3 %	MnO %	MgO %	CaO %	Na2O %	K2O %	TiO2 %	P2O5 %	Ba ppm	Ce ppm	Cl ppm	Cr ppm	Cu ppm	Ga ppm	La ppm	Nb ppm	Pb ppm	Rb ppm	S ppm	Sr ppm	V ppm	Y ppm	Zn ppm	Zr ppm	OXIDE %	TotalTr ppm
ARC1258																															
124385	1	0.246	0.015	40.83	9.45	29.00	0.109	5.27	1.58	0.23	0.38	0.48	0.045	223	33	1360	6396	64	14	0	9	9	17	680	93	155	22	86	115	87.4	11861
124386	2	0.315	0.017	52.41	3.92	9.88	0.065	17.86	1.80	0.49	0.20	0.17	0.007	78	1	3320	3879	33	3	-1	1	1	7	1610	65	68	11	69	39	86.8	12477
124387	3	0.416	0.019	54.78	3.19	10.59	0.080	21.82	0.10	0.72	0.11	0.13	0.003	37	0	1480	4958	33	6	-1	-1	-2	1	225	12	65	12	72	14	91.6	11221
124389	5	0.423	0.016	55.79	3.17	10.29	0.051	21.94	0.02	1.11	0.15	0.14	0.001	-7	24	1040	4875	9	4	-3	-1	0	3	160	8	64	9	76	7	92.7	10624
124392	7	0.417	0.016	55.66	3.06	11.14	0.075	21.62	0.02	1.21	0.13	0.13	0.001	2	-4	1150	4609	15	3	-7	1	5	3	150	5	57	15	70	8	93.0	10377
124393	8	0.396	0.017	54.54	3.12	12.39	0.148	21.28	0.02	1.16	0.15	0.13	0.001	10	15	1170	4751	19	5	-5	2	6	3	170	11	61	11	72	6	92.9	10401
124397	12	0.165	0.010	25.00	1.43	5.72	0.103	32.14	3.87	0.59	0.10	0.05	0.001	24	15	1090	2523	1	3	4	1	2	3	110	17	32	4	37	5	69.0	5578
124398	13	0.211	0.009	30.88	1.86	7.27	0.103	32.11	0.76	0.87	0.10	0.06	0.001	-1	26	640	2892	8	0	6	-2	8	-1	80	8	39	5	43	4	74.0	5926
124399	14	0.225	0.011	33.27	1.95	7.64	0.109	31.09	0.70	0.87	0.13	0.08	0.001	4	2	750	3050	14	1	1	-1	8	2	70	8	42	5	43	5	75.8	6331
124403	18	0.212	0.010	31.82	1.94	7.14	0.112	30.24	3.10	0.74	0.08	0.07	0.001	21	3	430	2428	15	3	0	-7	8	1	50	32	39	0	47	7	75.2	5256
ARC1257																															
124360	1	0.147	0.027	21.35	9.29	54.31	0.122	0.72	0.22	0.16	0.20	0.40	0.035	321	45	350	14766	72	10	10	8	-13	12	530	44	202	17	124	87	86.8	18291
124362	3	0.226	0.035	23.26	10.73	48.91	0.108	0.99	0.22	0.09	0.07	0.40	0.021	49	-18	500	23994	62	10	-3	0	-17	13	350	40	192	11	138	31	84.8	27922
124364	5	0.256	0.019	23.06	6.95	53.60	0.041	1.02	0.03	0.24	0.12	0.30	0.013	38	-20	400	17924	43	10	2	16	-1	6	180	20	115	13	147	21	85.4	21646
124365	6	0.951	0.028	37.89	5.33	33.94	0.059	4.54	0.05	0.75	0.19	0.16	0.001	-9	-1	5000	7506	53	6	5	0	1	2	790	20	80	26	203	9	82.9	23449
124368	8	1.795	0.075	36.67	4.67	33.18	0.096	4.83	0.05	1.25	0.18	0.20	0.001	19	1	14570	5876	49	7	1	1	8	0	1960	26	85	10	305	12	81.1	41603
124370	10	2.243	0.174	38.38	4.49	31.28	0.295	5.40	0.04	1.14	0.15	0.19	0.003	0	129	13430	5789	64	8	1	0	5	-1	1780	26	83	7	314	11	81.4	45790
124373	13	2.222	0.179	39.53	4.15	29.69	0.292	7.70	0.04	1.05	0.13	0.17	0.003	-1	27	12020	4740	46	4	10	2	4	1	1640	24	71	19	295	14	82.8	42881
124375	15	1.674	0.178	36.84	3.10	22.94	0.727	18.94	0.03	0.74	0.10	0.12	0.006	92	17	10790	3427	88	4	35	-2	0	-4	1510	17	56	26	255	10	83.5	34796
124376	16	1.306	0.133	42.95	2.81	17.97	0.748	20.30	0.03	0.59	0.08	0.09	0.017	262	17	6570	2698	69	2	102	-1	7	-1	980	18	61	69	185	4	85.6	25404
124378	18	0.908	0.043	38.76	2.47	13.00	0.388	30.64	0.02	0.42	0.05	0.09	0.004	38	-18	6090	2998	29	1	26	0	9	0	860	13	52	60	119	5	85.8	19758
124379	19	0.713	0.022	38.22	2.09	12.08	0.518	32.56	0.02	0.31	0.04	0.08	0.002	42	3	4210	2723	17	4	13	1	4	2	610	14	58	28	81	6	85.9	15134
124384	24	0.603	0.019	38.54	2.27	13.36	0.224	31.26	0.33	0.25	0.04	0.08	0.001	26	-2	3010	2875	87	1	4	-1	2	-5	330	12	43	8	88	6	86.3	12673
ARC1478																															
137424	1	0.343	0.014	40.60	5.84	27.95	0.121	11.03	0.75	0.17	0.20	0.44	0.023	67	0	680	6172	46	15	20	10	8	8	220	40	173	12	64	63	87.1	11135
137425	2	0.616	0.017	35.70	7.15	33.62	0.105	3.27	0.55	0.67	0.18	0.34	0.003	53	-8	2820	11447	49	7	1	5	19	4	690	60	142	5	126	30	81.6	21752
137426	3	0.745	0.014	39.04	6.34	31.20	0.101	3.15	0.34	0.84	0.19	0.28	0.001	92	-7	3740	11348	48	7	3	3	1	0	840	64	114	6	121	19	81.5	23962
137429	5	0.974	0.080	43.47	5.33	26.04	0.467	6.87	0.23	0.87	0.20	0.22	0.001	52	11	5010	8324	69	8	-5	0	1	0	1090	43	93	5	152	16	83.7	25372
137430	6	0.652	0.021	39.10	2.98	14.43	0.274	27.28	1.09	0.46	0.08	0.12	0.001	15	6	4135	4977	36	5	-1	1	3	1	750	19	46	15	100	8	85.8	16805
137433	9	0.529	0.019	39.77	3.26	13.42	0.250	27.12	2.17	0.45	0.08	0.23	0.001	-4	-2	4310	4664	31	0	8	1	4	3	620	14	54	10	86	14	86.7	15264

Hole ID	Depth	%Ni	%Co	SiO2	Al2O3	Fe2O3	MnO	MgO	CaO	Na2O	K2O	TiO2	P2O5	Ba	Ce	Cl	Cr	Cu	Ga	La	Nb	Pb	Rb	S	Sr	V	Y	Zn	Zr	OXIDE	TotalTr
	(m)			%	%	%	%	%	%	%	%	%	%	ppm	ppm	ppm	ppm	ppm	ppm	ppm	ppm	ppm	ppm	ppm	ppm	ppm	ppm	ppm	ppm	%	ppm
ARC1008																															
83610	1	0.154	0.006	47.83	13.11	24.65	0.056	0.85	0.41	0.09	0.24	0.37	0.024	338	30	170	4656	60	12	21	0	9	15	260	32	134	8	35	71	87.6	7412
83612	3	0.289	0.020	42.75	7.48	23.91	0.082	4.90	3.75	0.09	0.11	0.16	0.009	95	5	410	4804	55	5	12	-8	4	4	160	72	87	19	24	24	83.2	8836
83613	4	0.788	0.065	33.95	5.22	37.10	0.342	3.45	2.29	0.37	0.12	0.18	0.008	119	6	2930	4883	66	3	17	1	2	2	700	63	101	11	97	16	83.0	17516
83614	5	1.076	0.034	49.41	3.96	27.14	0.142	2.64	0.14	0.68	0.18	0.14	0.001	24	-4	4970	6867	51	2	14	-5	9	1	900	32	78	6	97	7	84.4	24114
83617	8	1.449	0.134	39.64	5.33	31.70	1.310	2.72	0.12	0.84	0.20	0.21	0.001	869	14	6790	8567	71	7	11	4	4	-3	1080	48	86	10	192	17	82.1	33562
83618	9	0.289	0.026	83.40	1.99	9.26	0.211	0.60	0.03	0.16	0.05	0.08	0.001	121	17	1090	2830	18	3	-5	1	6	-1	250	11	67	7	42	6	95.8	7583
83619	10	1.025	0.058	29.43	6.03	43.81	0.479	2.19	0.07	0.70	0.15	0.25	0.005	259	-2	3490	10391	76	8	9	4	12	5	750	33	136	12	174	16	83.1	26171
83620	11	0.897	0.038	22.91	7.08	51.97	0.209	1.87	0.04	0.59	0.13	0.36	0.002	48	4	2390	10941	76	6	-2	6	-14	5	760	25	156	17	186	26	85.2	23948
83623	14	1.155	0.049	45.43	4.84	27.67	0.198	4.94	0.07	0.86	0.18	0.20	0.001	27	-3	5120	6763	69	3	9	-1	2	5	880	29	90	5	194	13	84.4	25214
83624	15	0.946	0.055	42.15	3.43	17.41	0.387	19.39	0.22	0.69	0.13	0.14	0.001	27	4	6690	4818	22	4	3	6	11	-5	850	20	47	11	141	12	83.9	22659
83628	18	0.596	0.021	47.84	2.54	13.39	0.411	21.27	0.39	0.59	0.12	0.10	0.001	22	7	5020	3151	21	2	5	-5	10	-1	560	20	42	10	82	6	86.7	15091
83631	21	0.375	0.016	46.33	2.01	13.07	0.203	25.79	0.33	0.31	0.08	0.07	0.001	15	9	2470	2807	21	4	8	-3	-1	0	300	13	42	8	67	5	88.2	9645
83632	22	0.382	0.016	44.51	2.16	13.90	0.222	23.95	0.36	0.40	0.10	0.08	0.001	19	5	2810	3160	43	3	-3	-3	5	-1	350	14	38	10	72	7	85.7	10470
83637	27	0.322	0.013	43.82	1.89	11.10	0.156	30.33	0.32	0.20	0.06	0.07	0.001	4	4	1520	2999	13	7	0	-3	5	-1	190	8	47	5	63	6	87.9	8185
ARC0776																															
37749	1	0.307	0.017	20.97	6.30	55.52	0.084	1.91	0.16	0.08	0.06	0.25	0.025	362	11	550	16644	78	10	13	9	-17	1	320	21	171	8	108	27	85.4	21528
37750	2	0.374	0.019	38.30	5.32	37.83	0.050	1.93	0.41	0.05	0.10	0.17	0.006	69	-7	145	15431	34	6	14	11	13	-1	40	32	82	13	80	16	84.2	19881
37751	3	0.589	0.033	44.13	2.10	23.50	0.065	6.01	5.04	0.35	0.10	0.05	0.001	388	-2	2320	7598	50	5	10	0	10	0	440	97	51	11	83	5	81.3	17246
37755	6	1.346	0.096	43.76	3.89	27.59	0.287	5.03	0.19	0.73	0.13	0.15	0.001	32	89	5420	27768	35	4	21	1	7	3	820	37	77	6	208	10	81.8	48923
37756	7	0.964	0.047	58.51	2.39	22.93	0.168	2.78	0.12	0.56	0.11	0.09	0.001	25	8	3190	7130	32	-1	16	1	2	-1	470	24	58	11	122	8	87.7	21170
37758	9	0.927	0.065	56.82	2.19	16.24	0.858	9.43	0.15	0.77	0.13	0.07	0.001	221	6	7510	4611	31	6	5	-1	2	0	680	32	39	5	94	11	86.7	23142
37760	11	0.497	0.018	50.37	1.51	9.81	0.192	25.08	0.23	0.33	0.05	0.05	0.001	16	16	2860	3485	40	2	5	-2	-2	2	330	12	37	8	64	6	87.6	11989
37764	15	0.470	0.018	54.96	1.76	13.26	0.261	17.08	0.21	0.51	0.09	0.06	0.001	5	-4	4380	3603	17	2	0	1	4	0	420	13	33	5	75	4	88.2	13410
ARC0774																															
37693	1	0.526	0.017	73.44	4.27	9.52	0.194	2.04	0.47	0.06	0.27	0.15	0.010	120	46	180	2162	25	5	15	0	6	12	55	31	29	16	52	37	90.4	8191
37694	2	0.705	0.024	45.19	2.53	12.21	0.321	11.88	6.22	0.32	0.18	0.08	0.004	141	8	2600	2561	37	3	32	-5	8	8	2360	115	34	10	61	21	78.9	15250
37695	3	0.548	0.008	33.83	1.03	6.54	0.062	24.37	2.59	0.35	0.07	0.02	0.001	46	20	3630	1691	5	0	6	-3	10	-1	1410	1966	21	6	31	57	68.9	14426
37696	4	0.442	0.005	33.11	1.37	4.05	0.028	28.58	0.27	0.19	0.05	0.01	0.001	5	7	1320	1131	4	0	4	-1	2	-5	340	5	13	4	20	0	67.7	7284
37697	5	1.189	0.051	46.78	2.30	26.14	0.730	8.28	0.15	0.88	0.18	0.09	0.001	95	-4	6560	5507	29	3	1	3	-5	5	1490	35	35	4	120	9	85.5	26253
37700	8	0.888	0.038	58.17	1.21	20.92	0.669	6.14	0.34	0.66	0.15	0.04	0.001	47	18	4930	3294	47	3	5	0	9	-2	1050	15	23	9	104	6	88.3	18784
37703	10	0.706	0.038	59.68	1.17	20.47	0.394	6.42	0.05	0.71	0.15	0.04	0.001	25	4	5480	3449	29	-2	-2	-4	-7	-2	990	12	16	5	99	3	89.1	17504
37704	11	0.475	0.006	10.69	0.20	3.30	0.061	40.78	0.24	0.22	0.03	0.00	0.001	1	6	2850	600	2	1	2	-4	2	-1	400	2	10	2	24	3	55.5	8666
37706	13	0.332	0.006	12.81	0.22	3.61	0.182	39.30	0.61	0.19	0.04	0.00	0.001	14	11	2200	637	2	-1	9	-3	5	0	310	5	5	1	26	0	56.9	6570
37709	16	0.333	0.011	16.47	1.02	6.39	0.129	37.17	1.15	0.25	0.07	0.03	0.001	5	6	1810	4321	20	2	10	-3	9	2	250	6	15	5	48	3	62.7	9922
37712	19	0.265	0.009	24.26	0.57	6.31	0.144	32.91	2.57	0.22	0.05	0.01	0.001	4	2	1420	5185	7	-2	4	-1	7	-2	160	5	23	2	43	2	67.0	9569
37715	22	0.309	0.012	27.02	1.03	7.21	0.134	33.45	0.72	0.42	0.09	0.02	0.001	23	8	3410	5437	9	3	5	1	5	-1	410	6	31	3	53	6	70.1	12579
37719	26	0.223	0.010	36.56	1.84	5.86	0.125	30.04	0.82	0.25	0.07	0.08	0.001	-2	3	1010	5723	4	1	1	2	1	3	120	7	38	6	46	8	75.6	9266
37720	27	0.195	0.007	24.94	0.79	4.97	0.075	35.36	0.60	0.17	0.05	0.02	0.001	17	2	770	4823	17	2	-5	0	5	0	100	6	22	2	35	9	67.0	7796

Hole ID	Depth	%Ni	%Co	SiO2	Al2O3	Fe2O3	MnO	MgO	CaO	Na2O	K2O	TiO2	P2O5	Ba	Ce	Cl	Cr	Cu	Ga	La	Nb	Pb	Rb	S	Sr	V	Y	Zn	Zr	OXIDE	TotalTr
	(m)			%	%	%	%	%	%	%	%	%	%	ppm	ppm	ppm	ppm	ppm	ppm	ppm	ppm	ppm	ppm	ppm	ppm	ppm	ppm	ppm	ppm	%	ppm
ARC0786																															
37969	1	0.259	0.015	33.32	8.53	35.86	0.167	7.15	1.47	0.14	0.29	0.91	0.036	263	13	320	5833	48	22	29	5	5	3	300	83	321	17	61	120	87.9	10142
37970	2	0.190	0.011	40.33	6.90	22.84	0.131	9.67	4.78	0.15	0.40	0.80	0.026	289	36	430	4274	39	17	19	9	3	8	470	152	224	17	55	118	86.0	8129
37971	3	0.159	0.007	28.82	2.30	6.61	0.079	25.82	7.27	0.21	0.16	0.15	0.004	77	19	1150	2188	11	4	11	1	9	3	280	107	58	7	32	28	71.4	5606
37974	6	0.210	0.010	33.31	1.87	7.60	0.128	30.47	1.76	0.36	0.06	0.07	0.002	19	14	830	2905	24	2	7	-2	-1	1	210	17	38	4	47	5	75.6	6289
37978	10	0.209	0.010	36.50	2.04	7.70	0.132	28.37	2.04	0.41	0.08	0.07	0.001	19	2	1160	3276	19	3	9	-2	3	1	290	18	32	1	54	6	77.4	7038
37979	11	0.221	0.011	37.29	2.35	8.78	0.141	30.10	1.75	0.24	0.08	0.08	0.001	19	2	700	3493	21	3	1	2	6	2	140	23	40	7	51	9	80.8	6806
37983	15	0.221	0.011	36.36	2.34	8.67	0.133	31.32	1.90	0.14	0.09	0.08	0.002	28	-6	510	3072	9	3	5	-1	-4	-2	90	10	48	5	55	5	81.0	6110
ARC0782																															
37888	1	0.323	0.015	29.38	7.07	45.34	0.074	2.71	0.20	0.09	0.15	0.54	0.036	149	5	340	15548	47	18	19	13	19	5	345	21	270	20	70	68	85.6	20322
37890	3	0.347	0.012	34.78	4.66	40.95	0.026	2.19	1.21	0.06	0.05	0.17	0.013	118	-21	315	14161	50	7	15	10	14	-2	175	50	118	15	82	17	84.1	18695
37893	5	0.733	0.024	24.78	1.72	27.34	0.043	9.92	9.20	0.24	0.05	0.06	0.004	124	-3	1910	6930	22	3	-2	0	2	1	600	157	47	9	111	13	73.4	17451
37894	6	1.227	0.046	50.63	1.87	23.76	0.081	3.67	1.85	0.38	0.08	0.07	0.004	113	16	1820	6360	26	2	11	1	3	2	625	60	48	9	136	6	82.4	21930
37896	8	1.188	0.094	50.04	3.39	21.23	1.069	4.21	0.05	0.42	0.11	0.13	0.004	598	-48	2380	34901	22	3	22	5	19	-3	830	43	109	7	175	10	80.7	51886
37898	10	1.639	0.033	41.03	4.80	26.57	0.298	8.07	0.07	0.61	0.10	0.29	0.002	19	-5	4670	10378	25	6	38	2	3	0	1560	27	61	7	152	22	81.8	33649
37900	12	1.105	0.033	51.98	2.70	16.57	1.617	11.98	0.14	0.53	0.10	0.11	0.003	179	1	4770	4025	16	6	40	-2	-2	-2	1220	44	38	7	117	10	85.7	21813
37903	15	0.932	0.024	46.48	3.40	23.30	0.349	8.50	0.07	0.58	0.10	0.14	0.003	66	-19	4350	10474	29	6	96	5	12	0	980	24	68	7	118	9	82.9	25757
37904	16	0.911	0.030	42.85	2.81	20.10	1.059	16.95	0.07	0.53	0.08	0.10	0.001	142	-16	5830	6765	34	4	0	2	6	-2	1080	35	59	7	99	6	84.6	23430
37906	18	0.737	0.021	51.33	2.51	16.39	0.579	14.44	0.13	0.57	0.08	0.09	0.001	39	0	4280	6413	19	2	-1	0	4	-3	710	21	35	10	87	1	86.1	19166
37909	21	0.555	0.020	48.95	2.49	15.81	0.399	16.95	0.08	0.35	0.07	0.09	0.001	18	0	3010	12252	13	1	1	-3	4	-1	440	20	49	8	88	8	85.2	21622
ARC0783																															
37910	1	0.379	0.015	41.13	6.42	37.57	0.136	1.56	0.19	0.11	0.19	0.42	0.027	245	1	490	10266	36	10	17	10	17	5	255	29	188	15	72	68	87.8	15649
37913	4	0.784	0.033	38.31	4.42	31.48	0.113	7.04	0.46	0.49	0.14	0.35	0.013	99	3	3490	8304	42	9	2	5	16	6	620	45	165	12	97	32	82.8	21082
37914	5	1.128	0.032	37.02	4.78	35.78	0.151	2.78	0.24	0.80	0.13	0.27	0.008	86	0	5220	8232	25	10	-2	-1	0	-4	790	56	105	10	155	22	82.0	26283
37915	6	1.176	0.058	49.13	3.92	26.62	0.149	3.20	0.16	0.66	0.12	0.15	0.002	21	33	4850	5800	16	3	1	5	-1	-5	770	53	84	8	169	17	84.1	24138
37916	7	1.149	0.074	36.98	2.77	18.23	0.221	25.52	0.12	0.42	0.06	0.11	0.001	-1	11	5550	4342	25	3	11	-1	-7	1	840	16	53	9	230	5	84.4	23284
37918	9	0.835	0.035	42.07	2.61	13.80	0.529	26.04	0.48	0.42	0.07	0.11	0.001	114	-2	4100	3664	25	2	25	-2	4	0	630	21	46	16	100	9	86.1	17421
37921	12	0.637	0.022	46.23	2.86	16.35	0.431	19.44	0.48	0.49	0.09	0.13	0.001	68	2	4200	4723	16	4	26	-2	7	3	560	23	57	14	94	11	86.5	16368
37924	15	0.512	0.016	44.54	3.21	12.55	0.323	22.98	0.28	0.44	0.09	0.16	0.003	36	-11	3310	3843	1	4	16	7	26	-1	315	19	46	10	88	16	84.6	12987

Hole ID	Depth (m)	%Ni	%Co	SiO2 %	Al2O3 %	Fe2O3 %	MnO %	MgO %	CaO %	Na2O %	K2O %	TiO2 %	P2O5 %	Ba ppm	Ce ppm	Cl ppm	Cr ppm	Cu ppm	Ga ppm	La ppm	Nb ppm	Pb ppm	Rb ppm	S ppm	Sr ppm	V ppm	Y ppm	Zn ppm	Zr ppm	OXIDE %	TotalTr ppm
ARC0780																															
37825	1	0.628	0.027	42.40	3.65	29.30	0.220	5.25	3.36	0.44	0.20	0.14	0.009	100	13	2790	7589	53	3	44	0	14	2	430	71	68	12	109	28	85.0	17845
37826	2	0.424	0.024	35.47	2.92	23.07	0.066	7.89	9.11	0.18	0.09	0.07	0.005	45	5	1280	2544	50	3	-7	-2	0	1	310	138	40	6	26	20	78.9	8907
37827	3	1.055	0.059	40.03	4.90	33.23	0.085	3.22	0.55	0.69	0.21	0.12	0.001	18	12	4440	7667	82	1	-13	-2	10	2	1950	29	56	6	73	19	83.0	25463
37828	4	0.765	0.048	20.81	5.84	55.09	0.086	1.78	0.13	0.47	0.14	0.16	0.008	-1	28	2520	6322	48	5	0	5	-10	7	990	28	59	8	39	20	84.5	18160
37830	6	0.670	0.036	17.44	9.01	55.31	0.053	1.21	0.04	0.39	0.10	0.21	0.015	-7	14	2425	6850	34	9	1	15	-7	4	915	18	97	4	40	17	83.8	17466
37831	7	0.817	0.032	70.40	1.54	15.35	0.055	2.00	0.07	0.53	0.19	0.03	0.001	3	3	2780	4656	30	2	0	1	3	-1	610	16	18	6	65	5	90.2	16655
37833	9	0.712	0.039	73.14	0.97	12.25	0.424	3.00	0.05	0.53	0.13	0.02	0.001	173	20	3790	3323	17	2	5	-4	2	5	630	26	14	2	53	1	90.5	15546
37835	10	0.945	0.048	65.31	1.18	16.09	0.649	4.73	0.04	0.61	0.16	0.03	0.001	103	11	4590	4254	24	0	6	-3	-4	-1	750	27	10	6	90	4	88.8	19760
37836	11	0.691	0.028	73.16	0.59	13.02	0.677	2.81	0.03	0.53	0.17	0.00	0.001	71	8	4050	3495	26	2	4	-2	5	3	610	32	15	5	70	3	91.0	15553
37838	13	0.795	0.016	58.14	0.35	9.33	0.137	13.46	0.04	0.33	0.11	0.00	0.001	9	3	2460	2151	9	3	0	-1	1	-2	320	10	1	9	55	2	81.9	13105
37839	14	0.596	0.024	69.05	0.64	13.82	0.322	5.25	0.02	0.44	0.11	0.01	0.001	-5	8	3550	3259	13	-1	-5	0	5	-3	480	16	24	6	68	7	89.7	13581
37842	17	0.626	0.020	65.40	0.53	12.81	0.294	9.95	0.02	0.31	0.07	0.01	0.004	5	16	3070	2542	28	3	-1	-4	1	0	360	11	22	7	79	3	89.4	12577
37844	19	0.288	0.010	78.38	0.28	7.03	0.098	5.35	0.03	0.19	0.05	0.00	0.001	19	-1	1550	1984	13	0	-7	1	-6	-2	190	3	5	7	34	6	91.4	6747
37847	22	0.672	0.023	47.44	0.84	17.40	0.307	13.76	0.07	0.37	0.08	0.03	0.001	44	7	2500	3909	13	1	1	4	-4	3	390	8	20	7	87	2	80.3	13905
37848	23	0.374	0.007	17.96	0.23	4.77	0.090	36.27	0.20	0.14	0.03	0.00	0.001	8	1	1220	928	-1	-1	-2	-3	5	0	160	2	2	2	21	2	59.7	6122
37849	24	0.353	0.006	16.74	0.15	4.66	0.086	36.92	0.27	0.11	0.03	0.00	0.001	8	8	1270	1081	-2	1	2	-1	11	-3	170	2	3	1	21	2	58.9	6145
37850	25	0.281	0.012	72.54	0.34	8.78	0.089	6.58	0.05	0.20	0.06	0.00	0.001	12	8	990	2994	8	0	12	3	-1	-5	150	2	9	4	51	4	88.6	7247
37853	28	0.271	0.016	63.49	0.46	12.26	0.124	9.04	0.08	0.28	0.07	0.01	0.003	-3	10	1510	2177	12	2	9	2	4	-1	230	9	27	6	53	2	85.8	6888
37855	30	0.385	0.013	29.40	0.60	6.29	0.141	29.76	0.15	0.18	0.04	0.00	0.001	0	9	1360	1254	1	0	8	0	3	-2	170	4	13	2	38	0	66.6	6815
37858	33	0.339	0.009	17.01	0.23	6.04	0.071	36.03	0.30	0.12	0.03	0.00	0.001	6	8	860	1178	0	1	7	-1	5	-2	110	3	2	2	24	2	59.8	5649
ARC1283																															
94529	1	0.165	0.007	48.43	3.06	6.61	0.056	15.74	8.52	0.22	0.15	0.15	0.010	152	18	1830	1945	32	3	8	3	7	6	3350	321	49	3	46	42	83.0	9501
94530	2	0.196	0.010	40.21	2.48	7.41	0.106	19.11	9.32	0.27	0.11	0.12	0.008	165	3	3310	2415	27	3	-1	1	0	2	15520	142	60	7	47	25	79.1	23751
94532	4	0.322	0.014	51.59	2.90	11.79	0.200	25.26	0.16	0.33	0.05	0.12	0.006	20	-4	1870	4008	39	2	2	-2	0	3	250	13	64	7	71	6	92.4	9683
94536	7	0.313	0.014	51.94	2.95	11.32	0.184	24.52	0.55	0.25	0.05	0.12	0.010	68	6	1320	4089	30	6	8	-1	1	4	600	39	56	4	73	13	91.9	9539
94537	8	0.215	0.010	33.62	1.94	7.96	0.126	31.49	1.89	0.22	0.03	0.07	0.005	-6	15	640	2952	11	3	4	-7	5	-4	80	20	32	6	51	7	77.3	6020
94539	10	0.213	0.010	34.45	1.99	8.13	0.123	31.15	2.60	0.08	0.02	0.08	0.004	7	1	520	2714	15	2	15	1	7	-1	50	38	34	6	48	6	78.6	5655
94541	12	0.204	0.009	34.26	1.87	7.88	0.119	31.03	2.88	0.13	0.02	0.07	0.001	-8	0	640	2728	16	2	15	0	-3	-2	60	40	37	4	51	10	78.3	5695
ARC0793																															
39374	1	0.402	0.019	39.31	5.83	41.69	0.195	1.26	0.13	0.07	0.17	0.33	0.034	119	19	370	9484	60	8	13	6	12	5	320	23	155	15	102	63	89.0	14945
39375	2	0.239	0.013	22.79	9.07	52.68	0.032	0.36	0.21	0.01	0.09	0.36	0.028	94	6	0	11965	75	6	-10	0	-17	13	240	21	193	12	52	42	85.6	15182
39378	5	0.257	0.006	32.47	10.00	40.74	0.017	0.50	0.25	0.02	0.04	0.31	0.013	47	-23	0	16359	53	11	9	13	10	-3	110	22	207	7	51	36	84.4	19518
39380	7	0.305	0.009	28.10	9.93	45.57	0.025	0.56	0.19	0.03	0.02	0.33	0.018	59	-3	-50	14322	60	13	3	2	-6	0	120	18	160	12	78	31	84.8	17932
39383	10	0.296	0.014	21.34	8.05	53.84	0.062	1.02	0.07	0.07	0.03	0.30	0.019	47	-48	10	28902	92	11	-1	13	-4	4	195	19	151	5	179	18	84.8	32673
39385	11	0.381	0.012	19.18	5.58	57.69	0.051	1.17	0.04	0.09	0.04	0.19	0.016	22	-42	7	30087	121	6	-5	11	-5	2	163	19	130	12	230	11	84.0	34677
39386	12	0.829	0.056	43.89	3.48	33.05	0.526	2.10	0.10	0.20	0.08	0.12	0.001	158	-3	295	21253	60	1	18	2	13	-2	35	23	85	14	199	10	83.5	30996
39389	15	1.004	0.034	53.52	3.23	21.53	0.444	4.30	0.64	0.33	0.09	0.12	0.014	74	-12	1070	14317	30	4	15	-4	-1	1	220	29	65	13	149	12	84.2	26324
39390	16	0.838	0.018	38.29	2.67	15.03	0.206	9.88	8.49	0.35	0.09	0.10	0.001	15	-7	1370	11895	19	2	15	-1	-11	2	200	107	42	11	113	13	75.1	22314
39391	17	1.035	0.023	42.47	6.15	17.98	0.445	11.44	3.50	0.39	0.10	0.32	0.009	48	-14	1800	10506	30	4	58	2	7	3	230	34	87	50	170	41	82.8	23597
39394	20	0.795	0.021	55.65	1.65	14.29	0.271	12.62	0.55	0.25	0.06	0.05	0.001	25	-28	1810	17584	15	4	11	1	-2	1	200	19	52	10	101	4	85.4	27936
39396	22	0.740	0.019	40.72	1.38	12.97	0.249	21.88	3.56	0.21	0.04	0.04	0.001	47	-11	1800	15680	19	1	5	-2	6	0	250	34	57	12	103	2	81.0	25554
39401	27	0.509	0.019	41.46	1.57	13.87	0.211	28.86	0.16	0.07	0.02	0.05	0.001	11	5	280	3678	17	1	1	-2	4	0	50	8	44	6	70	6	86.3	9417

Hole ID	Depth (m)	%Ni	%Co	SiO2 %	Al2O3 %	Fe2O3 %	MnO %	MgO %	CaO %	Na2O %	K2O %	TiO2 %	P2O5 %	Ba ppm	Ce ppm	Cl ppm	Cr ppm	Cu ppm	Ga ppm	La ppm	Nb ppm	Pb ppm	Rb ppm	S ppm	Sr ppm	V ppm	Y ppm	Zn ppm	Zr ppm	OXIDE %	TotalTr ppm
ARC0791																															
39316	1	0.380	0.015	15.50	8.52	60.83	0.049	0.43	0.08	0.01	0.12	0.40	0.032	398	-6	30	17308	43	8	7	6	-13	13	250	26	255	14	33	79	86.0	22367
39321	5	0.534	0.023	23.09	6.28	53.11	0.059	0.86	0.26	0.08	0.10	0.26	0.029	61	-1	30	14087	49	5	7	6	-12	5	130	41	143	9	65	32	84.1	20192
39322	6	0.607	0.026	50.86	2.81	31.89	0.081	0.89	0.19	0.12	0.15	0.08	0.009	65	4	100	5615	50	6	20	-1	3	0	40	30	49	10	61	21	87.1	12372
39324	8	0.634	0.033	72.77	0.92	16.46	0.138	1.04	0.03	0.30	0.13	0.01	0.001	45	-5	1430	2796	29	2	4	-5	-2	4	230	23	27	9	60	5	91.8	11295
39325	9	0.686	0.043	76.48	0.49	13.60	0.195	1.11	0.33	0.29	0.12	0.00	0.002	27	15	1240	3055	27	1	12	0	0	3	200	26	22	7	54	3	92.6	11942
39328	11	0.680	0.035	79.04	0.43	12.85	0.171	0.99	0.03	0.20	0.08	0.00	0.001	22	3	750	3237	25	0	-1	0	6	2	180	12	17	9	54	2	93.8	11433
39329	12	1.279	0.136	66.68	0.44	20.44	1.186	1.64	0.02	0.39	0.12	0.00	0.001	369	5	1830	2782	38	-1	3	5	-2	3	340	35	6	7	91	3	90.9	19642
39334	17	1.020	0.049	69.98	0.56	13.11	0.437	4.95	0.02	0.34	0.06	0.01	0.001	80	4	2140	2335	30	0	7	2	-1	-1	390	15	13	6	82	4	89.5	15762
39336	19	0.717	0.027	65.63	1.08	15.39	0.231	6.11	0.02	0.33	0.07	0.04	0.001	33	13	1650	2721	22	0	-4	-1	2	2	310	15	8	4	69	6	88.9	12248
39337	20	0.934	0.024	24.72	1.42	13.09	0.164	28.81	0.09	0.35	0.06	0.07	0.003	0	10	2130	3147	16	2	1	-5	4	-1	380	12	6	3	80	10	68.8	15335
39339	22	0.579	0.018	15.63	0.82	9.95	0.321	34.21	0.14	0.23	0.06	0.02	0.001	17	8	1770	1659	13	1	-5	-4	-1	-1	290	14	17	8	50	7	61.4	9784
39341	24	0.331	0.014	12.76	1.01	9.25	0.172	36.49	0.16	0.30	0.05	0.03	0.001	4	20	3130	1504	7	1	-7	2	5	-1	400	13	10	4	44	4	60.2	8560
39342	25	0.259	0.008	6.29	0.51	5.03	0.117	41.89	0.24	0.18	0.03	0.00	0.001	10	4	1850	845	1	-1	1	-1	5	-2	240	7	5	2	26	0	54.3	5624
39346	29	0.268	0.010	53.28	0.28	5.93	0.094	17.57	0.14	0.10	0.04	0.00	0.001	4	16	660	1378	1	-1	1	-4	4	0	110	6	5	3	31	4	77.4	4966
39351	33	0.259	0.010	34.57	0.30	5.83	0.089	27.75	0.43	0.10	0.03	0.00	0.001	7	5	820	1391	10	0	0	-3	3	3	130	8	3	3	27	5	69.1	5065
ARC0607																															
32096	1	0.183	0.007	60.90	7.18	10.55	0.062	8.86	1.11	0.19	0.35	0.36	0.023	283	21	650	2345	43	8	16	4	12	17	2800	61	93	14	57	64	89.6	8353
32097	2	0.150	0.006	40.08	2.74	6.21	0.073	20.02	7.70	0.34	0.15	0.13	0.007	80	7	2590	1712	27	2	7	-1	14	4	1795	135	53	6	37	28	77.4	8030
32098	3	0.148	0.006	36.89	2.32	6.68	0.055	19.87	8.73	0.35	0.11	0.11	0.008	46	26	3820	1892	32	2	7	-3	2	2	570	100	62	4	40	11	75.1	8129
32099	4	0.191	0.011	59.70	3.81	11.63	0.156	7.54	3.16	0.61	0.55	0.17	0.012	71	38	3460	3570	63	7	5	3	0	5	630	76	101	10	70	13	87.3	10109
32101	6	0.134	0.006	41.00	3.00	8.07	0.077	19.73	2.59	0.35	0.54	0.13	0.004	7	34	770	2841	26	6	-2	1	8	11	170	18	82	4	60	7	75.5	5414
32104	9	0.171	0.006	59.63	3.48	10.72	0.052	9.63	1.59	0.52	0.48	0.16	0.012	23	43	1370	3176	52	2	1	0	3	10	230	17	110	8	68	11	86.3	6847
ARC0606																															
32079	1	0.180	0.012	22.37	6.68	43.64	0.097	8.81	1.59	0.02	0.11	0.66	0.044	62	-1	15	9709	70	17	-5	9	15	6	215	36	295	10	67	73	84.0	12502
32080	2	0.175	0.008	30.86	1.48	6.30	0.086	28.52	6.88	0.03	0.02	0.06	0.007	69	14	-40	1724	8	1	5	-1	-2	-3	60	129	45	6	30	9	74.2	3848
32083	4	0.200	0.009	30.67	1.73	8.52	0.101	32.69	1.21	0.06	0.03	0.07	0.009	49	5	80	2378	18	2	3	0	-3	5	20	10	36	4	43	6	75.1	4712
32087	8	0.207	0.010	38.27	1.71	9.38	0.145	28.02	1.40	0.22	0.07	0.07	0.009	4	12	800	2422	20	1	6	3	30	-3	120	6	53	3	46	8	79.3	5671
32089	10	0.207	0.010	33.00	1.84	8.11	0.135	31.68	2.02	0.11	0.03	0.07	0.003	15	-3	240	3619	21	4	1	0	-1	1	60	7	43	7	47	9	77.0	6200
32092	13	0.193	0.009	32.79	1.71	7.33	0.122	29.66	4.25	0.18	0.04	0.06	0.004	23	2	540	3169	11	1	-2	2	-4	-2	80	16	41	6	45	5	76.1	5924
32095	16	0.203	0.010	31.80	1.72	8.12	0.133	31.30	1.53	0.24	0.06	0.06	0.009	19	-8	460	3065	8	2	1	-2	3	2	100	7	54	4	46	7	75.0	5860
ARC0231																															
3908	1	0.209	0.018	51.37	6.16	10.67	0.085	3.43	11.34	0.13	0.36	0.49	0.027	342	19	410	2772	51	13	20	1	3	15	360	161	131	16	42	98	84.1	6686
3909	2	0.404	0.044	40.16	3.69	9.66	0.108	10.17	14.45	0.37	0.19	0.22	0.007	479	19	4210	2943	33	3	1	3	6	9	980	358	72	14	69	47	79.0	13696
3910	3	0.682	0.126	32.01	4.95	12.18	0.498	7.25	15.21	0.31	0.20	0.28	0.006	628	56	700	4583	25	8	18	2	-1	3	32160	291	88	16	96	45	72.9	46763
3911	4	1.262	0.151	43.01	8.41	19.90	0.411	9.55	1.58	1.09	0.20	0.40	0.003	209	-2	3460	9117	25	12	32	-1	3	2	2570	67	97	20	195	28	84.6	29940
3912	5	1.159	0.194	44.37	7.87	22.68	0.605	6.00	1.33	0.96	0.24	0.40	0.001	285	33	2930	9762	34	12	11	1	6	1	2020	71	94	16	155	35	84.5	28968
3916	8	1.484	0.309	42.38	8.97	24.26	1.172	5.95	0.57	1.24	0.23	0.45	0.003	677	55	1690	9860	43	13	22	-1	-9	3	2060	76	128	11	201	34	85.2	32759
3919	11	0.956	0.223	42.10	9.80	26.30	1.274	4.61	0.12	1.25	0.23	0.44	0.001	653	10	830	9890	29	15	7	2	11	0	1750	51	116	11	148	39	86.1	25316
3923	15	0.477	0.020	41.34	10.77	18.95	0.066	9.77	0.09	0.99	0.21	0.51	0.001	44	-15	910	7305	23	11	6	-3	13	3	860	29	91	15	84	42	82.7	14355
3924	16	0.392	0.015	48.84	9.02	17.75	0.055	11.70	0.05	0.81	0.16	0.45	0.009	15	1	1900	6263	21	11	6	1	2	-2	660	26	119	10	75	31	88.8	13178
3927	19	0.299	0.013	44.56	6.48	12.65	0.044	21.03	0.05	0.46	0.08	0.30	0.008	1	-7	1900	4342	10	7	1	4	9	-2	290	12	91	6	79	19	85.7	9859

Hole ID	Depth	%Ni	%Co	SiO2	Al2O3	Fe2O3	MnO	MgO	CaO	Na2O	K2O	TiO2	P2O5	Ba	Ce	Cl	Cr	Cu	Ga	La	Nb	Pb	Rb	S	Sr	V	Y	Zn	Zr	OXIDE	TotalTr
	(m)			%	%	%	%	%	%	%	%	%	%	ppm	ppm	ppm	ppm	ppm	ppm	ppm	ppm	ppm	ppm	ppm	ppm	ppm	ppm	ppm	ppm	%	ppm
ARC0789																															
39268	1	0.271	0.023	52.73	1.40	5.98	0.113	8.96	11.09	0.14	0.10	0.07	0.006	203	27	890	1240	27	1	17	3	3	3	370	294	67	9	25	44	80.6	6120
39270	3	0.436	0.023	80.25	0.60	8.90	0.094	2.36	1.33	0.12	0.04	0.01	0.002	38	9	650	1932	31	2	21	-2	10	1	270	319	21	4	24	16	93.7	7904
39272	5	0.644	0.037	70.20	0.51	11.43	0.175	6.96	0.04	0.21	0.05	0.01	0.001	61	0	1320	1967	28	3	4	0	7	-1	260	13	11	2	38	1	89.6	10492
39273	6	0.900	0.048	65.51	0.85	12.74	0.227	7.19	0.07	0.40	0.11	0.02	0.001	102	-4	2610	3235	33	-2	2	1	5	1	470	20	13	8	54	5	87.1	16001
39276	9	0.723	0.034	66.97	0.52	17.97	0.483	4.65	0.02	0.59	0.14	0.00	0.001	117	3	6850	2522	29	-1	1	-1	14	-5	700	18	11	6	62	-2	91.3	17858
39277	10	0.545	0.025	77.35	0.40	11.69	0.255	2.68	0.02	0.46	0.13	0.00	0.001	20	11	5510	2256	28	4	3	4	1	4	630	8	8	10	43	-1	93.0	14199
39280	13	0.847	0.031	60.82	0.50	18.74	0.276	7.23	0.02	0.37	0.09	0.01	0.001	41	9	3280	2557	35	1	7	-3	1	1	440	8	22	7	69	-1	88.1	15225
39282	15	0.621	0.012	73.44	0.27	9.52	0.095	6.71	0.01	0.21	0.07	0.00	0.001	-6	20	1450	1800	34	1	1	-2	-2	-5	210	3	14	5	36	0	90.3	9858
39283	16	0.336	0.008	83.94	0.17	7.71	0.072	2.67	0.02	0.17	0.09	0.00	0.002	16	14	1430	1431	17	0	-5	1	2	1	230	7	17	2	23	2	94.8	6589
39285	18	0.455	0.016	78.96	0.22	9.93	0.123	3.27	0.02	0.24	0.14	0.00	0.001	28	10	1310	2531	20	1	1	2	6	2	190	8	19	5	36	-2	92.9	8847
39286	19	0.348	0.012	50.20	0.23	5.22	0.092	20.11	0.24	0.16	0.06	0.00	0.001	1	8	1510	1832	11	0	0	-3	3	0	200	6	27	9	24	0	76.3	7186
39287	20	0.184	0.005	17.98	0.06	3.72	0.073	37.31	0.18	0.05	0.02	0.00	0.001	9	10	650	467	5	-1	-1	-1	0	-5	100	6	2	0	13	-1	59.4	3111
ARC0126																															
106258	1	0.151	0.007	29.88	2.28	6.14	0.042	12.14	18.60	0.22	0.17	0.12	0.006	206	26	2570	1890	19	0	1	3	5	5	4020	277	130	6	20	41	69.6	10760
106259	2	1.057	0.076	52.10	2.10	16.94	0.794	11.78	1.67	0.49	0.14	0.09	0.001	109	8	4230	3629	34	3	-4	6	10	3	1880	62	57	9	73	14	86.1	21416
106260	3	1.056	0.033	52.94	2.15	12.05	0.406	17.98	0.32	0.64	0.12	0.08	0.001	46	10	7860	4501	32	4	5	-2	10	0	500	34	37	8	81	10	86.7	23983
106262	5	1.188	0.044	51.50	2.75	17.14	0.714	10.45	0.16	1.31	0.19	0.11	0.001	55	-8	17510	5293	76	6	0	1	6	-3	1460	33	32	11	103	12	84.3	36875
106266	9	0.843	0.022	47.33	2.35	19.33	0.265	15.59	0.09	0.93	0.15	0.08	0.001	27	1	11820	5314	37	3	7	2	8	-2	1040	33	38	8	97	3	86.1	27040
106267	10	0.764	0.025	42.11	2.21	19.87	0.461	16.78	0.11	0.91	0.13	0.09	0.001	10	13	12550	4163	30	4	-5	-2	9	-2	1640	31	47	10	87	8	82.7	26453
106270	13	0.760	0.027	40.98	2.75	20.11	0.418	17.84	0.20	0.97	0.13	0.10	0.001	55	4	12540	4888	35	0	-4	1	10	1	1550	30	42	12	109	9	83.5	27112
106274	17	0.701	0.022	44.02	2.83	20.63	0.207	16.65	0.20	0.90	0.13	0.11	0.001	25	2	10600	5538	76	5	3	-4	7	-2	1280	23	57	11	102	15	85.7	24946
ARC0128																															
106294	1	0.106	0.007	22.82	15.11	43.53	0.032	0.40	0.19	0.06	0.08	0.48	0.018	331	-16	220	14922	86	13	10	-4	15	-2	560	22	208	9	44	100	82.7	17624
106297	4	0.148	0.010	20.29	14.82	45.67	0.048	0.54	0.25	0.12	0.09	0.42	0.023	25	-21	415	17723	78	13	4	9	13	2	320	22	268	9	86	63	82.3	20594
106299	6	0.285	0.021	15.10	5.22	57.13	0.059	2.34	1.83	0.27	0.08	0.20	0.013	70	-8	1340	12884	95	1	-1	6	-10	9	470	37	98	7	57	18	82.3	18090
106300	7	0.488	0.016	59.38	2.87	23.53	0.043	1.42	0.14	0.45	0.10	0.07	0.001	99	-14	2940	7478	42	2	7	4	5	5	550	23	40	7	58	9	88.0	16275
106301	8	1.035	0.023	38.61	5.01	30.31	0.040	2.88	0.15	0.94	0.21	0.21	0.002	60	-14	5390	13852	58	4	-6	1	5	1	1000	37	77	11	115	18	79.0	31158
106305	12	0.747	0.030	27.64	7.84	42.32	0.187	3.48	0.08	0.71	0.14	0.28	0.003	45	-13	4620	17108	59	7	12	-1	0	1	660	31	163	14	162	20	82.7	30634
106306	13	1.186	0.143	32.29	6.14	35.96	0.630	4.81	0.09	1.01	0.17	0.24	0.001	108	15	7080	20747	77	6	7	-3	-1	3	940	34	143	14	245	20	81.3	42706
106308	15	1.217	0.148	34.49	3.71	24.15	0.882	17.23	0.10	1.20	0.13	0.15	0.001	112	-20	15070	13191	45	2	12	5	2	-1	1700	30	69	10	215	5	82.0	44062
106309	16	0.828	0.058	49.72	3.40	18.95	0.331	7.95	0.07	0.87	0.13	0.13	0.001	44	-19	8240	12884	34	5	6	-1	9	1	1270	25	60	10	132	6	81.5	31533
106312	19	0.823	0.062	39.85	3.71	22.98	0.402	13.91	0.22	0.90	0.13	0.15	0.001	88	-8	8790	12249	42	3	8	0	2	-1	1080	21	76	10	155	14	82.3	31355
106236	20	0.587	0.027	37.58	2.22	14.37	0.320	26.89	0.51	0.89	0.08	0.08	0.002	45	-14	11520	9040	37	5	4	3	4	-3	1085	14	53	9	104	9	82.9	28024

APPENDIX 5: PIMA-II SPECTRA OF KAOLINITE.

Reflected infrared PIMA-II spectra for RC holes CBRC1391 and 0735 are presented in Figures A5.1 and A5.2, respectively. Drill hole CBRC1391 is representative of the 'kaolinite-1' regolith unit, which is characterized by a near monotonous sequence of well-ordered kaolinite as indicated by good resolution of the Al-OH absorption doublets at 1396-1414 nm and 2162-2208 nm (Fig. A5.1). In comparison, resolution of the absorption doublets of kaolinite identified in all other samples (*i.e.*, within the 'kaolinite-2' regolith unit) was not as well defined as in the 'kaolinite-1' unit (Fig. A5.2). The reflected infrared spectra for RC hole CBRC0735 also provide a good indication of the spectral characteristics of the main smectite phases (*e.g.*, nontronite and saponite) identified in these drill holes.

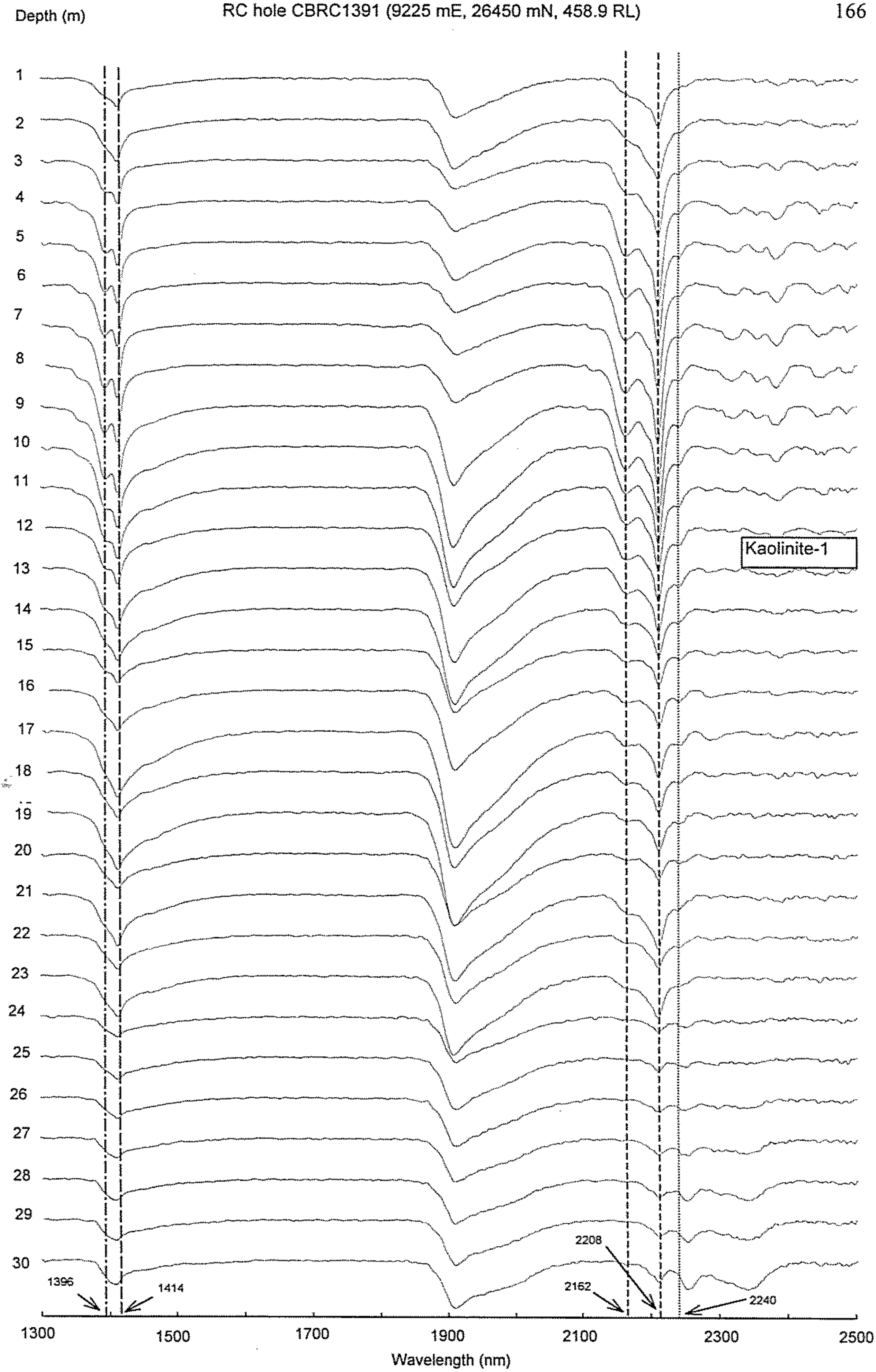

Figure A5.1. PIMA-II spectra for RC hole CBRC1391. Spectra are presented as the Hull Quotient of the raw spectra. The kaolinite-1 unit is characterized by a near monotonous sequence of well crystallized kaolinite that shows good resolution of the absorption doublets near 1400 and 2208 nm. Some Fe-substitution within kaolinite is shown by the absorption band at 2240 nm. The lower portion of the profile consists of a mixture of kaolinite and Fe-chlorite.

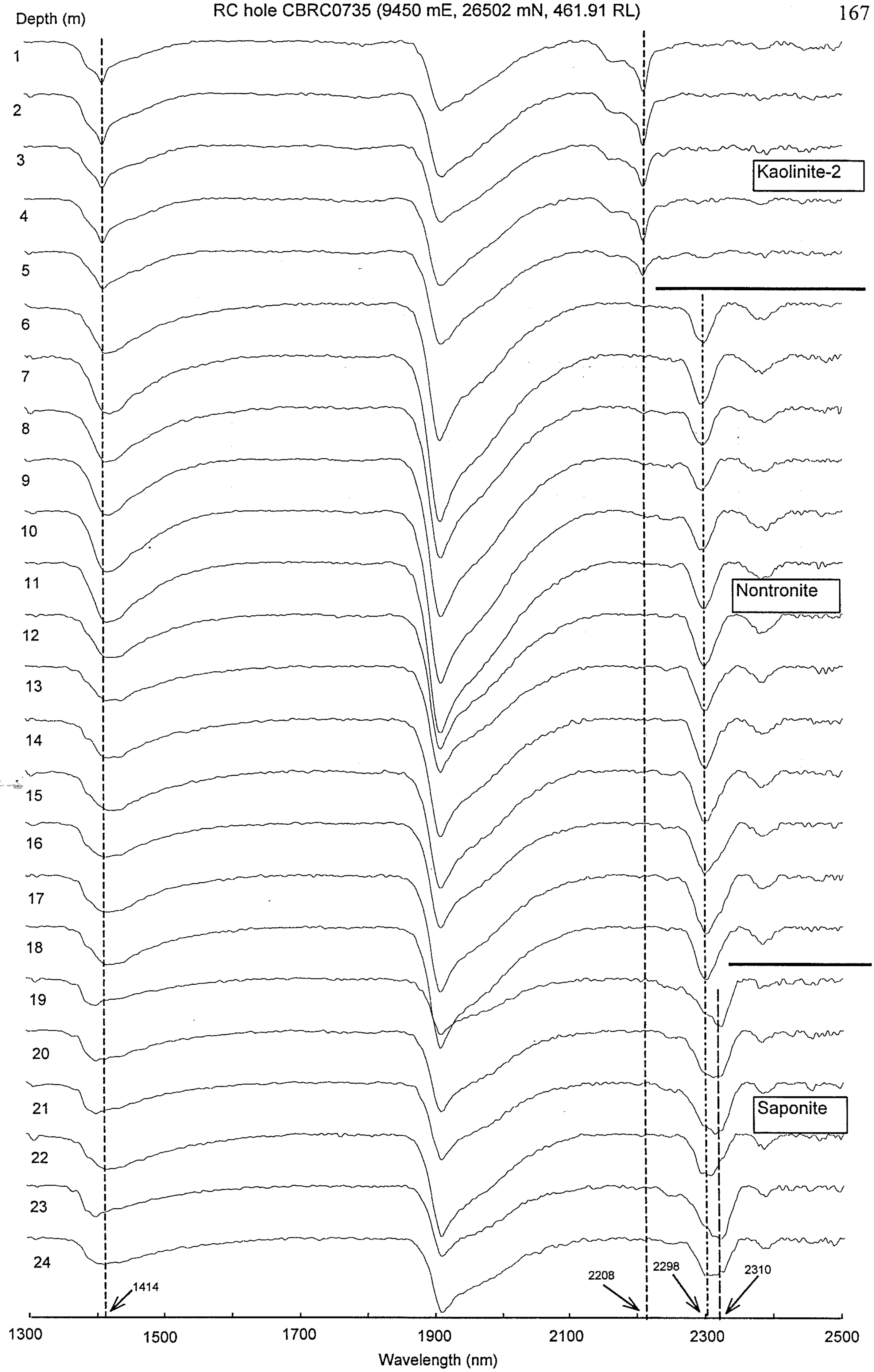

Figure A5.2. PIMA-II spectra for RC hole CBRC0735. Spectra are presented as the Hull Quotient of the raw spectra. Kaolinite at the surface of the profile shows poorer resolution of absorption doublets at 1400 and 2208 nm compared to the better crystalline kaolinite in the kaolinite-1 unit (see Figure A5.1). The main regolith units are also shown.

Appendix 6: Table A6.1. Normative mineral abundances of selected RC holes for MM2.

Hole ID	Depth (m)	Regolith Unit	Kaolinite	Opal-Si/Qtz	Fe-oxides	Illite	Nontronite	Saponite	Chlorite	Talc	Serpentine	Magnesite	Dolomite	Calcite	Gibbsite	Bassanite	Alunite	Chromite	Rutile	Apatite	Asbolan	% Total
CBRC0796																						
30379	1	Kaolinite	31.0	9.4	47.2	0.9	6.4	0.0	0.0	0.0	0.0	0.00	2.32	0.21	0.0	0.2	0.00	1.67	0.55	0.05	0.08	100.0
30381	3	Kaolinite	28.4	2.1	44.9	0.5	2.6	0.0	0.0	0.0	0.0	0.00	3.68	1.83	0.0	14.6	0.00	0.74	0.36	0.02	0.23	100.0
30383	4	Kaolinite	35.2	0.0	49.7	0.5	4.6	0.0	0.0	0.0	0.0	0.46	1.39	0.00	1.0	5.6	0.00	0.79	0.48	0.02	0.19	100.0
30384	5	Kaolinite	39.6	0.0	51.1	0.5	3.8	0.0	0.0	0.0	0.0	0.83	0.71	0.00	0.5	1.1	0.00	0.92	0.72	0.04	0.21	100.0
30390	10	Nontronite	26.5	7.4	52.1	0.8	7.0	0.0	3.1	0.0	0.0	0.00	0.71	0.00	0.0	0.2	0.00	1.29	0.51	0.01	0.30	100.0
30391	11	Nontronite	31.8	8.1	42.0	0.8	8.2	0.0	4.4	0.0	0.0	0.00	0.84	0.00	0.0	0.2	0.00	2.96	0.56	0.00	0.16	100.0
30392	12	**Nontronite**	13.3	16.3	39.8	1.1	13.6	0.0	11.9	0.0	0.0	0.00	1.19	0.00	0.0	0.2	0.00	2.11	0.38	0.00	0.29	100.0
30393	13	**Nontronite**	0.0	24.7	22.6	1.3	18.7	0.0	21.6	0.0	0.0	5.98	1.61	0.00	0.0	0.3	0.00	1.44	0.27	0.00	1.46	100.0
30395	15	**Nontronite**	0.0	25.4	20.1	1.3	18.1	0.0	19.3	0.0	0.0	11.43	1.45	0.00	0.0	0.2	0.00	1.43	0.24	0.00	0.96	100.0
30397	17	**Nontronite**	0.0	23.9	19.5	1.0	15.2	0.0	18.9	0.0	0.0	17.67	1.38	0.00	0.0	0.1	0.00	1.39	0.24	0.00	0.66	100.0
30398	18	**Nontronite**	0.0	26.0	14.4	0.7	10.2	0.0	13.8	0.0	0.0	26.07	7.07	0.00	0.0	0.1	0.00	1.05	0.17	0.00	0.41	100.0
30404	24	**Nontronite**	0.0	28.8	14.8	0.6	7.5	0.0	15.5	0.0	0.0	29.90	1.19	0.00	0.0	0.0	0.00	1.03	0.18	0.00	0.44	100.0
CBRC0797																						
30405	1	Kaolinite	43.9	17.5	26.4	2.9	5.3	0.0	0.0	0.0	0.0	0.81	1.33	0.00	0.0	0.0	0.00	1.12	0.58	0.03	0.05	100.0
30406	2	Kaolinite	43.0	9.3	36.9	1.9	4.5	0.0	0.0	0.0	0.0	0.64	0.95	0.00	0.0	0.1	0.00	1.79	0.84	0.02	0.05	100.0
30407	3	Kaolinite	17.9	0.0	71.4	0.4	1.2	0.0	0.0	0.0	0.0	0.62	0.07	0.00	2.8	0.2	0.00	2.88	2.40	0.07	0.06	100.0
30410	6	Kaolinite	17.7	0.0	51.5	0.7	1.7	0.0	0.0	0.0	0.0	0.00	1.61	0.56	21.6	0.6	0.00	3.05	0.94	0.09	0.04	100.0
30414	9	Kaolinite	29.3	0.0	53.9	0.3	2.5	0.0	0.0	0.0	0.0	0.92	0.01	0.00	9.4	0.2	0.00	2.71	0.46	0.09	0.09	100.0
30415	10	Kaolinite	29.9	0.0	60.1	0.2	0.8	0.0	0.0	0.0	0.0	0.88	0.00	0.00	5.6	0.2	0.00	1.69	0.40	0.09	0.13	100.0
30417	12	Kaolinite	48.9	0.0	40.4	0.5	0.0	0.0	0.0	0.0	0.0	0.86	0.32	0.00	1.4	0.1	0.00	1.67	0.35	0.06	5.48	100.0
30419	14	Nontronite	14.9	14.6	58.1	0.8	4.1	0.0	3.5	0.0	0.0	0.00	1.37	0.00	0.0	0.0	0.00	1.59	0.29	0.04	0.68	100.0
30420	15	Nontronite	12.7	28.7	41.3	1.1	4.7	0.0	6.8	0.0	0.0	0.00	2.42	0.00	0.0	0.0	0.00	1.79	0.22	0.03	0.33	100.0
30423	18	Nontronite	7.9	38.8	42.2	0.9	3.1	0.0	3.8	0.0	0.0	0.00	1.28	0.00	0.0	0.0	0.00	1.30	0.18	0.01	0.51	100.0
30425	19	Nontronite	3.2	48.0	31.9	1.1	5.8	0.0	6.5	0.0	0.0	0.00	1.85	0.00	0.0	0.0	0.00	0.94	0.14	0.00	0.58	100.0
30426	20	Nontronite	1.6	55.2	25.7	1.2	5.7	0.0	7.6	0.0	0.0	0.00	1.91	0.00	0.0	0.0	0.00	0.87	0.12	0.00	0.19	100.0
30429	23	Nontronite	0.0	60.7	24.5	0.9	5.3	0.0	5.9	0.0	0.0	0.39	1.29	0.00	0.0	0.0	0.00	0.77	0.06	0.02	0.13	100.0
30430	24	Nontronite	0.0	67.4	18.0	0.8	6.2	0.0	4.8	0.0	0.0	0.79	1.11	0.00	0.0	0.0	0.00	0.55	0.05	0.00	0.38	100.0
30432	26	Nontronite	0.0	68.9	16.5	0.9	6.2	0.0	4.1	0.0	0.0	1.21	1.11	0.00	0.0	0.0	0.00	0.65	0.05	0.02	0.34	100.0
30435	29	Nontronite	0.0	80.8	10.3	0.6	2.9	0.0	2.5	0.0	0.0	1.67	0.42	0.00	0.0	0.0	0.00	0.35	0.02	0.02	0.34	100.0
30440	34	**Nontronite**	0.0	75.0	10.6	0.6	3.3	0.0	2.3	0.0	0.0	7.16	0.34	0.00	0.0	0.0	0.00	0.36	0.02	0.00	0.33	100.0
30441	35	**Nontronite**	0.0	57.3	13.8	0.7	4.8	0.0	4.8	0.0	0.0	17.28	0.42	0.00	0.0	0.0	0.00	0.49	0.05	0.00	0.38	100.0
30445	39	**Nontronite**	0.0	53.0	8.2	0.6	4.0	0.0	1.7	0.0	0.0	31.53	0.41	0.00	0.0	0.0	0.00	0.34	0.01	0.01	0.22	100.0
30446	40	**Nontronite**	0.0	26.0	4.9	0.4	2.4	0.0	1.3	0.0	0.0	64.14	0.58	0.00	0.0	0.0	0.00	0.23	0.00	0.00	0.13	100.0
30448	42	**Nontronite**	0.0	26.3	5.6	0.4	0.8	0.0	1.3	0.0	0.0	51.29	14.02	0.00	0.0	0.0	0.00	0.22	0.00	0.01	0.13	100.0
CBRC0799																						
30475	1	Nontronite	24.5	36.4	22.9	2.1	4.7	0.0	4.7	0.0	0.0	0.00	1.03	0.00	0.0	0.1	0.00	3.11	0.29	0.03	0.11	100.0
30476	2	Nontronite	27.5	43.4	4.4	2.8	7.0	0.0	11.5	0.0	0.0	0.00	2.58	0.00	0.0	0.0	0.00	0.33	0.34	0.00	0.06	100.0
30479	5	Nontronite	34.6	37.6	0.2	2.7	16.3	0.0	0.0	0.0	0.0	5.39	2.83	0.00	0.0	0.0	0.00	0.06	0.34	0.01	0.04	100.0
30480	6	Nontronite	33.5	36.9	0.0	5.4	14.8	0.0	0.1	0.0	0.0	6.12	2.73	0.00	0.0	0.0	0.00	0.05	0.36	0.00	0.06	100.0
30481	7	Nontronite	34.4	36.3	0.0	4.4	15.2	0.0	0.0	0.0	0.0	6.48	2.69	0.00	0.0	0.1	0.00	0.05	0.33	0.00	0.05	100.0
30484	10	Nontronite	32.4	36.1	0.0	12.9	9.6	0.0	0.0	0.0	0.0	6.01	2.47	0.00	0.0	0.0	0.00	0.02	0.37	0.01	0.06	100.0

HoleID	Depth (m)	Regolith Unit	Kaolinite	Opal-Si/Qtz	Fe-oxides	Illite	Nontronite	Saponite	Chlorite	Talc	Serpentine	Magnesite	Dolomite	Calcite	Gibbsite	Bassanite	Alunite	Chromite	Rutile	Apatite	Asbolan	% Total
CBRC0727																						
26946	1	Kaolinite	48.8	0.0	32.6	0.9	2.5	0.0	0.0	0.0	0.0	1.02	0.61	0.00	9.2	0.1	0.00	3.26	0.81	0.04	0.08	100.0
26950	5	Kaolinite	31.2	0.0	55.5	0.4	1.2	0.0	0.0	0.0	0.0	1.26	0.16	0.00	7.5	0.1	0.00	1.95	0.50	0.04	0.14	100.0
26954	8	Kaolinite	33.3	0.0	52.4	0.3	3.7	0.0	0.0	0.0	0.0	1.52	0.30	0.00	3.3	0.1	0.00	4.22	0.44	0.05	0.22	100.0
26955	9	Kaolinite	27.9	0.0	62.8	0.3	2.9	0.0	0.0	0.0	0.0	1.11	0.28	0.00	1.6	0.1	0.00	2.02	0.49	0.08	0.36	100.0
26958	12	Kaolinite	29.5	2.3	61.6	0.3	1.6	0.0	0.0	0.0	0.0	0.72	2.04	0.00	0.0	0.0	0.00	1.01	0.28	0.01	0.42	100.0
26959	13	Kaolinite	23.3	2.0	64.6	0.3	1.7	0.0	0.0	0.0	0.0	0.61	5.00	0.00	0.0	0.0	0.00	1.84	0.36	0.02	0.22	100.0
26961	15	Talc	3.3	11.6	57.4	0.3	0.0	2.0	15.8	0.0	0.0	0.00	7.13	0.00	0.0	0.0	0.00	1.94	0.28	0.05	0.19	100.0
26962	16	Talc	0.0	24.1	39.0	0.4	0.0	2.8	17.9	3.9	0.0	0.00	9.66	0.00	0.0	0.0	0.00	1.36	0.19	0.03	0.68	100.0
26963	17	Talc	0.0	26.2	37.9	0.5	0.0	2.4	25.9	2.7	0.0	0.00	2.17	0.00	0.0	0.0	0.00	1.44	0.22	0.01	0.47	100.0
26964	18	Talc	0.0	9.3	12.0	0.1	0.0	1.1	10.2	66.3	0.0	0.00	0.26	0.00	0.0	0.0	0.00	0.62	0.08	0.00	0.06	100.0
26967	21	Talc	0.0	5.8	8.0	0.1	0.0	0.7	5.9	78.3	0.0	0.00	0.09	0.00	0.0	0.0	0.00	0.92	0.07	0.00	0.03	100.0
26968	22	Talc	0.0	6.4	8.3	0.1	0.0	1.8	8.4	73.3	0.0	0.00	0.12	0.00	0.0	0.0	0.00	1.27	0.09	0.00	0.10	100.0
26970	24	Talc	0.0	10.8	15.5	0.2	0.0	1.7	6.7	63.1	0.0	0.00	0.30	0.00	0.0	0.0	0.00	1.22	0.07	0.02	0.31	100.0
CBRC0732																						
27067	1	Kaolinite	26.6	22.6	32.4	3.1	4.5	0.0	0.0	0.0	0.0	4.99	3.28	0.00	0.0	0.1	0.00	1.81	0.45	0.03	0.16	100.0
27068	2	Nontronite	1.6	35.3	13.7	4.7	7.0	0.0	19.7	0.0	0.0	1.43	14.99	0.00	0.0	0.1	0.00	0.84	0.31	0.02	0.40	100.0
27069	3	Nontronite	0.0	17.9	12.5	2.5	18.4	0.0	15.5	0.0	0.0	7.51	6.41	0.00	0.0	17.5	0.00	1.29	0.22	0.00	0.35	100.0
27071	5	Nontronite	0.0	21.3	13.6	2.4	24.8	0.0	20.0	0.0	0.0	13.53	0.23	0.00	0.0	1.4	0.00	1.47	0.28	0.00	0.96	100.0
27074	8	Talc	0.0	18.3	21.6	2.2	0.0	23.0	21.6	10.5	0.0	0.00	0.19	0.00	0.0	0.5	0.00	1.28	0.26	0.00	0.68	100.0
27076	10	Talc	0.2	32.7	22.3	2.2	0.0	19.8	20.0	0.0	0.0	0.00	0.29	0.00	0.0	0.4	0.00	1.36	0.30	0.00	0.49	100.0
27077	11	Talc	7.8	28.5	25.5	2.3	0.0	19.4	13.8	0.0	0.0	0.00	0.31	0.00	0.0	0.4	0.00	1.39	0.36	0.00	0.19	100.0
27081	15	Talc	10.6	27.7	24.8	2.2	0.0	19.7	9.9	0.0	0.0	0.00	2.34	0.00	0.0	0.3	0.00	1.85	0.36	0.00	0.11	100.0
27082	16	Talc	9.7	25.9	23.8	2.0	0.0	17.8	9.2	0.0	0.0	0.00	9.13	0.00	0.0	0.3	0.00	1.51	0.34	0.00	0.29	100.0
27084	18	Talc	0.0	20.3	18.3	1.8	0.0	18.4	19.1	8.6	0.0	0.00	11.07	0.00	0.0	0.2	0.00	1.24	0.27	0.00	0.57	100.0
27085	19	Talc	0.0	31.2	16.2	1.7	0.0	16.6	17.4	10.2	0.0	0.00	4.95	0.00	0.0	0.2	0.00	1.10	0.25	0.00	0.21	100.0
27091	24	Talc	0.0	48.0	5.7	1.3	0.0	7.3	18.7	14.8	0.0	0.00	3.36	0.00	0.0	0.0	0.00	0.37	0.25	0.05	0.16	100.0
CBRC0734																						
27130	1	Kaolinite	38.1	3.0	48.3	0.7	3.0	0.0	0.0	0.0	0.0	2.98	0.46	0.00	0.0	0.3	0.00	2.44	0.51	0.07	0.20	100.0
27133	4	Nontronite	0.0	46.6	26.1	2.8	5.0	0.0	14.9	0.0	0.0	1.11	2.08	0.00	0.0	0.0	0.00	1.05	0.17	0.00	0.14	100.0
27135	6	Nontronite	0.0	42.5	21.0	1.9	7.9	0.0	15.6	0.0	0.0	7.94	1.49	0.00	0.0	0.0	0.00	1.37	0.20	0.00	0.19	100.0
27136	7	Nontronite	0.0	32.8	14.2	1.5	7.6	0.0	19.5	0.0	0.0	9.91	12.96	0.00	0.0	0.0	0.00	0.93	0.44	0.00	0.15	100.0
27137	8	Nontronite	0.0	35.3	8.8	0.8	4.7	0.0	15.4	0.0	0.0	28.36	5.59	0.00	0.0	0.0	0.00	0.60	0.21	0.00	0.19	100.0
27139	10	Nontronite	0.0	40.4	11.6	0.9	7.2	0.0	9.6	0.0	0.0	27.54	1.69	0.00	0.0	0.0	0.00	0.75	0.12	0.00	0.27	100.0
27142	13	Nontronite	0.0	34.5	17.2	1.7	13.4	0.0	13.4	0.0	0.0	17.03	1.14	0.00	0.0	0.0	0.00	1.17	0.18	0.00	0.25	100.0
27147	17	Nontronite	0.0	39.2	11.0	1.0	9.0	0.0	8.8	0.0	0.0	28.84	0.45	0.00	0.0	0.0	0.00	0.81	0.12	0.00	0.68	100.0
27148	18	Nontronite	0.0	64.3	7.9	0.6	3.0	0.0	5.7	0.0	0.0	17.38	0.27	0.00	0.0	0.0	0.00	0.58	0.07	0.01	0.18	100.0
27149	19	Nontronite	0.0	31.6	22.8	1.8	16.0	0.0	18.6	0.0	0.0	5.72	0.75	0.00	0.0	0.1	0.00	1.62	0.30	0.01	0.68	100.0
27152	22	Nontronite	0.0	29.9	18.3	1.3	12.0	0.0	15.1	0.0	0.0	18.36	2.67	0.00	0.0	0.0	0.00	1.51	0.23	0.00	0.56	100.0
27154	24	Nontronite	0.0	29.8	12.9	0.9	7.4	0.0	11.0	0.0	0.0	32.34	3.98	0.00	0.0	0.0	0.00	1.12	0.17	0.00	0.37	100.0
27155	25	Nontronite	0.0	31.9	15.5	1.2	10.9	0.0	12.6	0.0	0.0	21.12	5.17	0.00	0.0	0.0	0.00	0.99	0.17	0.00	0.50	100.0
27157	27	Nontronite	0.0	32.6	14.3	1.2	9.1	0.0	12.8	0.0	0.0	25.04	3.39	0.00	0.0	0.0	0.00	0.96	0.18	0.00	0.43	100.0
27160	30	Talc	0.0	30.7	12.0	1.0	0.0	5.9	9.6	38.7	0.0	0.00	0.83	0.00	0.0	0.0	0.00	0.83	0.12	0.00	0.36	100.0

Hole ID	Depth (m)	Regolith Unit	Kaolinite	Opal-Si/Qtz	Fe-oxides	Illite	Nontronite	Saponite	Chlorite	Talc	Serpentine	Magnesite	Dolomite	Calcite	Gibbsite	Bassanite	Alunite	Chromite	Rutile	Apatite	Asbolan	% Total
CBRC0780																						
29168	1	Kaolinite	38.7	39.7	9.7	7.5	0.0	0.0	0.0	0.0	0.0	2.02	1.70	0.00	0.0	0.0	0.00	0.15	0.47	0.06	0.05	100.0
29170	3	Nontronite	3.9	60.7	10.9	2.3	7.0	0.0	13.0	0.0	0.0	0.00	1.51	0.00	0.0	0.0	0.00	0.43	0.16	0.01	0.04	100.0
29173	6	Nontronite	0.0	63.1	14.3	1.7	7.1	0.0	10.4	0.0	0.0	1.00	1.53	0.00	0.0	0.0	0.00	0.64	0.10	0.00	0.06	100.0
29175	7	Nontronite	0.0	51.8	15.4	1.0	4.0	0.0	11.6	0.0	0.0	13.21	1.05	0.00	0.0	0.0	0.00	1.71	0.14	0.01	0.08	100.0
29178	10	Nontronite	0.0	31.0	21.8	1.4	8.7	0.0	18.2	0.0	0.0	2.48	12.22	0.00	0.0	0.1	0.00	3.56	0.23	0.00	0.19	100.0
29179	11	Nontronite	5.8	28.3	19.8	1.2	6.3	0.0	9.6	0.0	0.0	0.00	25.01	0.00	0.0	0.0	0.00	3.37	0.22	0.00	0.17	100.0
29181	13	Nontronite	0.0	28.5	23.7	1.1	7.6	0.0	19.2	0.0	0.0	13.59	1.61	0.00	0.0	0.0	0.00	3.85	0.25	0.01	0.63	100.0
29184	16	Nontronite	0.0	31.5	16.2	0.9	5.4	0.0	14.7	0.0	0.0	25.96	1.07	0.00	0.0	0.0	0.00	3.64	0.18	0.00	0.39	100.0
29186	17	Saponite	0.0	34.5	15.5	0.8	0.0	2.8	11.1	0.0	0.0	30.73	1.24	0.00	0.0	0.0	0.00	3.02	0.12	0.00	0.27	100.0
29189	20	Saponite	0.0	54.7	9.1	0.6	0.0	2.8	6.5	0.0	0.0	23.96	0.67	0.00	0.0	0.0	0.00	1.55	0.06	0.00	0.20	100.0
29190	21	Saponite	0.0	58.4	10.8	0.6	0.0	3.6	5.9	0.0	0.0	18.72	0.54	0.00	0.0	0.0	0.00	1.14	0.07	0.00	0.22	100.0
29191	22	Saponite	0.0	54.0	10.7	0.6	0.0	3.9	6.2	0.0	0.0	22.93	0.37	0.00	0.0	0.0	0.00	1.13	0.07	0.00	0.24	100.0
29192	23	Saponite	0.0	47.2	15.2	0.8	0.0	5.1	8.3	0.0	0.0	21.53	0.47	0.00	0.0	0.0	0.00	0.96	0.11	0.00	0.32	100.0
29193	24	Saponite	0.0	36.7	17.2	0.8	0.0	6.0	9.8	0.0	0.0	26.03	1.78	0.00	0.0	0.0	0.00	1.06	0.12	0.01	0.49	100.0
29194	25	Saponite	0.0	44.0	11.6	0.7	0.0	3.2	7.0	0.0	0.0	23.90	8.48	0.00	0.0	0.0	0.00	0.90	0.09	0.01	0.21	100.0
29195	26	Saponite	0.0	48.5	10.2	0.6	0.0	2.8	5.7	0.0	0.0	21.50	9.61	0.00	0.0	0.0	0.00	0.74	0.07	0.00	0.25	100.0
29196	27	Saponite	0.0	40.7	8.7	0.6	0.0	2.5	5.0	0.0	0.0	14.51	27.10	0.00	0.0	0.0	0.00	0.59	0.06	0.00	0.23	100.0
29197	28	Saponite	0.0	63.6	9.5	0.7	0.0	3.7	5.5	0.0	0.0	15.64	0.51	0.00	0.0	0.0	0.00	0.68	0.06	0.00	0.20	100.0
29200	31	Saponite	0.0	69.0	8.4	0.7	0.0	2.6	5.3	0.0	0.0	12.60	0.32	0.00	0.0	0.0	0.00	0.76	0.05	0.01	0.22	100.0
29201	32	Saponite	0.0	26.8	5.7	0.5	0.0	2.5	3.8	0.0	0.0	57.47	2.63	0.00	0.0	0.0	0.00	0.44	0.03	0.00	0.14	100.0
29206	37	Saponite	0.0	23.1	5.0	0.5	0.0	2.2	2.6	0.0	0.0	63.09	2.97	0.00	0.0	0.0	0.00	0.40	0.02	0.00	0.12	100.0
29209	40	Saponite	0.0	25.5	5.9	0.5	0.0	2.8	3.1	0.0	0.0	56.30	5.30	0.00	0.0	0.0	0.00	0.52	0.03	0.00	0.15	100.0
29210	41	Saponite	0.0	23.3	6.9	0.6	0.0	3.3	3.7	0.0	0.0	55.92	5.51	0.00	0.0	0.0	0.00	0.64	0.04	0.00	0.17	100.0
29213	44	Saponite	0.0	30.8	10.4	0.7	0.0	4.0	5.9	0.0	0.0	43.13	4.01	0.00	0.0	0.0	0.00	0.72	0.08	0.00	0.22	100.0
29217	47	Saponite	0.0	30.3	5.8	0.5	0.0	1.8	3.3	0.0	0.0	54.18	3.71	0.00	0.0	0.0	0.00	0.29	0.03	0.00	0.14	100.0
29221	51	Serpentine	0.0	0.0	6.3	0.3	0.0	1.5	4.2	0.0	71.5	12.76	3.07	0.00	0.0	0.0	0.00	0.32	0.04	0.00	0.13	100.0
29222	52	Serpentine	0.0	0.0	8.2	0.3	0.0	2.0	6.3	0.0	78.3	0.97	3.18	0.00	0.0	0.1	0.00	0.43	0.07	0.01	0.20	100.0
29224	54	Serpentine	0.0	0.0	7.9	0.2	0.0	2.4	5.0	0.0	78.0	2.70	3.16	0.00	0.0	0.1	0.00	0.38	0.05	0.01	0.17	100.0
CBRC1505																						
58171	1	Talc	6.2	35.6	7.6	1.5	0.0	5.2	10.4	0.0	0.0	0.00	32.23	0.00	0.0	0.1	0.00	0.29	0.38	0.05	0.35	100.0
58172	2	Talc	16.9	18.5	10.6	1.8	0.0	20.4	12.5	0.0	0.0	0.00	17.55	0.00	0.0	0.3	0.00	0.39	0.86	0.06	0.26	100.0
58174	4	Talc	0.0	37.5	4.8	0.7	0.0	10.8	16.4	27.9	0.0	0.00	0.76	0.00	0.0	0.2	0.00	0.46	0.26	0.02	0.19	100.0
58175	5	Talc	9.4	16.9	6.3	0.9	0.0	11.3	9.3	44.1	0.0	0.00	0.70	0.00	0.0	0.2	0.00	0.72	0.30	0.01	0.06	100.0
58179	9	Talc	10.3	60.1	5.9	1.4	0.0	17.7	0.3	3.3	0.0	0.00	0.43	0.00	0.0	0.1	0.00	0.19	0.33	0.01	0.06	100.0
58182	12	Talc	0.0	41.5	6.5	0.9	0.0	14.4	18.5	16.1	0.0	0.00	1.22	0.00	0.0	0.1	0.00	0.36	0.34	0.01	0.12	100.0
58183	13	Talc	0.0	24.0	8.0	0.6	0.0	13.2	17.2	35.4	0.0	0.00	0.42	0.00	0.0	0.1	0.00	0.58	0.24	0.01	0.24	100.0
58186	16	Talc	2.6	16.7	8.1	0.6	0.0	11.5	14.8	41.1	0.0	0.00	3.36	0.00	0.0	0.0	0.00	0.64	0.25	0.01	0.32	100.0

Hole ID	Depth (m)	Regolith Unit	Kaolinite	Opal-Si/Qtz	Fe-oxides	Illite	Nontronite	Saponite	Chlorite	Talc	Serpentine	Magnesite	Dolomite	Calcite	Gibbsite	Bassanite	Alunite	Chromite	Rutile	Apatite	Asbolan	% Total
CBRC0744																						
27467	1	Kaolinite	18.4	58.2	14.9	0.9	1.6	0.0	0.0	0.0	0.0	4.79	0.27	0.00	0.0	0.1	0.00	0.44	0.17	0.04	0.08	100.0
27471	5	Kaolinite	30.0	11.9	48.9	0.6	1.6	0.0	0.0	0.0	0.0	5.71	0.02	0.00	0.0	0.1	0.00	0.57	0.40	0.01	0.24	100.0
27474	8	Kaolinite	22.0	19.5	39.8	0.9	2.7	0.0	0.0	0.0	0.0	13.49	0.21	0.00	0.0	0.0	0.00	0.68	0.41	0.02	0.20	100.0
27475	9	Kaolinite	22.1	20.8	38.5	1.1	7.1	0.0	0.0	0.0	0.0	7.69	0.60	0.00	0.0	0.0	0.00	0.85	0.35	0.01	0.83	100.0
27476	10	Kaolinite	19.7	21.0	36.9	1.1	7.4	0.0	0.0	0.0	0.0	10.01	0.56	0.00	0.0	0.0	0.00	0.84	0.32	0.00	2.18	100.0
27478	12	Kaolinite	28.6	10.2	49.4	0.8	4.5	0.0	0.0	0.0	0.0	3.96	0.24	0.00	0.0	0.0	0.00	0.83	0.54	0.01	1.00	100.0
27480	13	Kaolinite	25.5	11.7	50.2	0.7	4.2	0.0	0.0	0.0	0.0	4.50	0.13	0.00	0.0	0.0	0.00	1.12	0.51	0.03	1.37	100.0
27481	14	Kaolinite	29.0	11.8	43.5	0.7	2.8	0.0	0.0	0.0	0.0	7.79	0.26	0.00	0.0	0.0	0.00	2.32	0.57	0.01	1.24	100.0
27482	15	Nontronite	0.0	22.1	21.2	1.1	9.5	0.0	27.7	0.0	0.0	12.83	0.61	0.00	0.0	0.0	0.00	3.37	0.36	0.00	1.21	100.0
27484	17	Nontronite	0.0	23.3	22.6	1.1	9.0	0.0	23.3	0.0	0.0	15.98	0.57	0.00	0.0	0.0	0.00	3.54	0.30	0.00	0.27	100.0
27486	19	Nontronite	0.0	23.7	22.0	1.1	8.6	0.0	24.0	0.0	0.0	15.91	0.61	0.00	0.0	0.0	0.00	3.08	0.31	0.00	0.68	100.0
27489	22	Nontronite	0.0	27.7	18.8	0.9	6.3	0.0	18.8	0.0	0.0	22.85	0.89	0.00	0.0	0.0	0.00	2.90	0.26	0.00	0.50	100.0
27490	23	Nontronite	0.0	30.1	18.1	1.0	7.1	0.0	17.2	0.0	0.0	22.27	0.71	0.00	0.0	0.0	0.00	2.66	0.23	0.00	0.55	100.0
27492	24	Nontronite	0.0	31.0	18.2	1.2	8.6	0.0	19.0	0.0	0.0	17.93	0.61	0.00	0.0	0.0	0.00	2.68	0.25	0.00	0.60	100.0
27493	25	Saponite	0.0	36.9	12.4	0.6	0.0	5.1	11.0	0.0	0.0	31.58	0.36	0.00	0.0	0.0	0.00	1.63	0.13	0.00	0.32	100.0
27496	28	Saponite	0.0	30.9	16.5	0.7	0.0	5.3	14.0	0.0	0.0	28.19	1.20	0.00	0.0	0.0	0.00	2.62	0.17	0.01	0.49	100.0
27499	31	Saponite	0.0	28.3	18.5	0.8	0.0	5.0	16.3	0.0	0.0	25.12	1.89	0.00	0.0	0.0	0.00	3.39	0.20	0.00	0.48	100.0
27500	32	Saponite	0.0	28.1	23.7	1.1	0.0	5.4	20.8	0.0	0.0	15.52	1.09	0.00	0.0	0.0	0.00	3.49	0.26	0.02	0.60	100.0
27501	33	Serpentine	0.0	11.4	14.6	0.6	0.0	3.4	13.6	0.0	52.8	0.00	0.85	0.00	0.0	0.0	0.00	2.21	0.20	0.00	0.34	100.0
27503	35	Serpentine	0.0	34.0	11.3	0.4	0.0	1.5	8.9	0.0	25.7	0.00	16.13	0.00	0.0	0.0	0.00	1.72	0.09	0.01	0.26	100.0
CBRC0747																						
27549	1	Kaolinite	32.3	15.4	46.1	1.2	2.1	0.0	0.0	0.0	0.0	0.83	0.00	0.00	0.0	0.2	0.00	1.30	0.33	0.06	0.06	100.0
27554	6	Kaolinite	42.1	13.4	38.6	0.6	1.2	0.0	0.0	0.0	0.0	1.63	0.03	0.00	0.0	0.1	0.00	1.62	0.47	0.04	0.16	100.0
27558	9	Kaolinite	33.9	20.1	39.5	0.6	1.6	0.0	0.0	0.0	0.0	2.63	0.07	0.00	0.0	0.0	0.00	0.74	0.47	0.03	0.29	100.0
27559	10	Kaolinite	21.7	24.9	37.5	0.7	4.1	0.0	0.0	0.0	0.0	8.54	0.79	0.00	0.0	0.0	0.00	1.09	0.35	0.01	0.29	100.0
27560	11	Kaolinite	19.0	30.1	34.4	0.7	4.2	0.0	0.0	0.0	0.0	8.80	1.18	0.00	0.0	0.0	0.00	1.06	0.27	0.01	0.26	100.0
27561	12	Talc	0.0	51.2	23.8	0.7	0.0	1.5	19.9	1.2	0.0	0.00	0.17	0.00	0.0	0.0	0.00	1.01	0.21	0.01	0.15	100.0
27563	14	Talc	12.9	15.8	48.0	0.4	0.0	0.8	18.9	0.0	0.0	0.00	0.01	0.00	0.0	0.0	0.00	1.74	0.58	0.02	0.78	100.0
27564	15	Talc	11.8	21.7	36.8	0.6	0.0	2.6	21.3	0.0	0.0	0.00	0.36	0.00	0.0	0.0	0.00	3.33	0.49	0.01	1.04	100.0
27566	17	Talc	24.2	19.0	30.1	0.4	0.0	2.1	15.9	0.0	0.0	0.00	0.20	0.00	0.0	0.0	0.00	5.83	0.55	0.02	1.77	100.0
27569	20	Talc	9.6	31.7	28.2	0.5	0.0	3.6	18.2	0.0	0.0	0.00	0.21	0.00	0.0	0.0	0.00	6.79	0.44	0.07	0.65	100.0
27570	21	Talc	0.0	43.5	7.4	0.2	0.0	0.9	7.1	40.1	0.0	0.00	0.03	0.00	0.0	0.0	0.00	0.54	0.07	0.02	0.06	100.0
27573	23	Talc	0.0	39.5	8.1	0.7	0.0	1.5	17.3	31.8	0.0	0.00	0.15	0.00	0.0	0.0	0.00	0.45	0.25	0.03	0.08	100.0
27574	24	Talc	14.7	33.4	10.6	4.5	0.0	7.0	26.3	0.0	0.0	0.00	0.68	0.00	0.0	0.0	0.00	1.29	0.74	0.01	0.75	100.0
27576	26	Talc	0.0	36.5	16.9	0.7	0.0	3.1	11.5	29.8	0.0	0.00	0.19	0.00	0.0	0.0	0.00	0.84	0.16	0.03	0.33	100.0
27579	29	Talc	0.0	37.5	20.3	0.9	0.0	5.2	17.0	16.5	0.0	0.00	0.48	0.00	0.0	0.0	0.00	1.04	0.23	0.04	0.66	100.0
27582	32	Serpentine	17.8	30.9	6.8	4.3	0.0	7.8	21.5	0.0	0.0	0.00	9.65	0.00	0.0	0.0	0.00	0.36	0.58	0.03	0.38	100.0
27583	33	Serpentine	0.0	16.4	11.3	0.8	0.0	2.2	9.7	0.0	58.3	0.00	0.49	0.00	0.0	0.0	0.00	0.45	0.11	0.00	0.26	100.0
27585	35	Serpentine	0.0	47.2	9.8	0.7	0.0	3.4	7.8	0.0	30.0	0.00	0.14	0.00	0.0	0.0	0.00	0.46	0.09	0.02	0.46	100.0
27586	36	Serpentine	0.0	49.2	19.9	1.0	0.0	4.3	11.7	0.0	11.5	0.00	0.18	0.00	0.0	0.0	0.00	1.07	0.16	0.04	0.90	100.0
27588	37	Serpentine	24.7	25.4	6.7	4.2	0.0	11.1	0.0	0.0	0.0	0.00	21.22	4.94	0.0	0.0	0.00	0.14	0.59	0.75	0.18	100.0
27589	38	Serpentine	26.1	25.2	7.1	5.9	0.0	9.3	0.0	0.0	0.0	0.00	24.41	0.21	0.0	0.0	0.00	0.14	0.65	0.78	0.19	100.0
27593	42	Serpentine	0.0	8.4	8.4	0.2	0.0	0.4	5.5	0.0	76.3	0.00	0.19	0.00	0.0	0.0	0.00	0.38	0.06	0.00	0.18	100.0

Hole ID	Depth (m)	Regolith Unit	Kaolinite	Opal-Si/Qtz	Fe-oxides	Illite	Nontronite	Saponite	Chlorite	Talc	Serpentine	Magnesite	Dolomite	Calcite	Gibbsite	Bassanite	Alunite	Chromite	Rutile	Apatite	Asbolan	% Total
CBRC0743																						
27414	1	Kaolinite	24.7	15.4	53.7	0.6	1.2	0.0	0.0	0.0	0.0	1.00	0.11	0.00	0.0	0.2	0.00	1.82	1.10	0.05	0.06	100.0
27416	3	Kaolinite	15.2	0.0	52.9	0.3	2.5	0.0	0.0	0.0	0.0	0.00	2.25	1.57	20.9	0.5	0.00	2.22	1.47	0.07	0.07	100.0
27417	4	Kaolinite	14.9	0.0	56.7	0.6	4.1	0.0	0.0	0.0	0.0	1.01	0.05	0.00	18.4	0.6	0.00	2.46	0.98	0.06	0.09	100.0
27422	9	Kaolinite	30.5	0.0	50.3	0.5	4.1	0.0	0.0	0.0	0.0	1.29	0.00	0.00	9.2	0.2	0.00	3.05	0.52	0.09	0.14	100.0
27425	12	Kaolinite	37.8	0.0	47.8	0.4	4.1	0.0	0.0	0.0	0.0	0.83	0.00	0.00	6.1	0.1	0.00	2.04	0.59	0.06	0.15	100.0
27426	13	Kaolinite	35.0	0.0	54.6	0.4	2.9	0.0	0.0	0.0	0.0	0.86	0.22	0.00	2.7	0.1	0.00	2.33	0.63	0.07	0.27	100.0
27432	18	Kaolinite	38.8	0.0	51.8	0.6	3.2	0.0	0.0	0.0	0.0	0.88	0.27	0.00	0.0	0.0	0.00	2.68	0.58	0.01	1.20	100.0
27433	19	Kaolinite	20.3	17.0	37.3	1.2	7.1	0.0	0.0	0.0	0.0	9.73	0.94	0.00	0.0	0.0	0.00	4.74	0.37	0.01	1.26	100.0
27436	22	Nontronite	5.7	20.0	36.8	1.5	7.8	0.0	18.8	0.0	0.0	0.00	1.09	0.00	0.0	0.0	0.00	6.48	0.34	0.01	1.50	100.0
27437	23	Nontronite	24.7	1.1	53.8	0.7	6.7	0.0	3.9	0.0	0.0	0.00	0.29	0.00	0.0	0.0	0.00	7.12	0.58	0.01	1.11	100.0
27439	25	Nontronite	19.4	6.9	54.9	0.8	4.5	0.0	6.4	0.0	0.0	0.00	0.46	0.00	0.0	0.0	0.00	5.27	0.54	0.01	0.96	100.0
27440	26	Nontronite	0.0	24.8	32.3	1.4	9.4	0.0	23.6	0.0	0.0	2.92	1.08	0.00	0.0	0.0	0.00	3.07	0.30	0.00	1.12	100.0
27442	28	Nontronite	0.0	29.1	26.7	1.5	10.2	0.0	18.7	0.0	0.0	9.83	1.06	0.00	0.0	0.0	0.00	1.90	0.24	0.00	0.66	100.0
27443	29	Nontronite	0.0	29.2	27.9	1.6	9.3	0.0	20.5	0.0	0.0	7.39	1.12	0.00	0.0	0.0	0.00	2.02	0.27	0.00	0.73	100.0
27444	30	Nontronite	0.0	28.9	30.5	1.6	10.3	0.0	20.4	0.0	0.0	4.12	1.13	0.00	0.0	0.0	0.00	2.05	0.28	0.00	0.61	100.0
27445	31	Nontronite	0.0	31.2	29.7	1.6	8.5	0.0	21.0	0.0	0.0	3.71	1.13	0.00	0.0	0.0	0.00	2.27	0.28	0.00	0.65	100.0
27448	34	Nontronite	0.0	37.9	25.2	1.3	7.8	0.0	17.0	0.0	0.0	6.64	0.95	0.00	0.0	0.0	0.00	1.96	0.24	0.00	1.09	100.0
27450	35	Nontronite	0.0	34.0	24.2	1.4	9.1	0.0	18.4	0.0	0.0	8.90	0.97	0.00	0.0	0.0	0.00	2.10	0.24	0.00	0.68	100.0
27453	38	Nontronite	0.0	38.5	27.7	1.0	6.4	0.0	17.9	0.0	0.0	4.36	0.67	0.00	0.0	0.0	0.00	2.53	0.26	0.01	0.70	100.0
27454	39	Nontronite	0.0	45.5	12.7	0.4	3.2	0.0	9.4	0.0	0.0	26.79	0.42	0.00	0.0	0.0	0.00	1.10	0.11	0.00	0.29	100.0
27458	43	Saponite	0.0	43.4	12.2	0.4	0.0	3.0	8.5	0.0	0.0	30.22	0.63	0.00	0.0	0.0	0.00	1.23	0.10	0.00	0.28	100.0
27463	48	Saponite	0.0	48.0	12.3	0.5	0.0	2.4	9.3	0.0	0.0	25.98	0.36	0.00	0.0	0.0	0.00	0.65	0.11	0.00	0.29	100.0
27464	49	Saponite	0.0	68.6	8.5	0.3	0.0	1.4	5.7	0.0	0.0	14.42	0.24	0.00	0.0	0.0	0.00	0.51	0.06	0.02	0.20	100.0
27465	50	Saponite	0.0	59.6	10.4	0.3	0.0	1.7	7.7	0.0	0.0	18.95	0.30	0.00	0.0	0.0	0.00	0.70	0.09	0.02	0.24	100.0
27466	51	Saponite	0.0	47.3	11.4	0.4	0.0	3.1	9.3	0.0	0.0	26.92	0.30	0.00	0.0	0.0	0.00	0.79	0.12	0.01	0.28	100.0
CBRC0724																						
26872	1	Kaolinite	40.0	5.1	48.9	0.5	0.9	0.0	0.0	0.0	0.0	1.09	0.10	0.00	0.0	0.2	0.00	2.57	0.47	0.05	0.06	100.0
26875	4	Kaolinite	35.9	2.9	54.4	0.4	2.9	0.0	0.0	0.0	0.0	1.21	0.19	0.00	0.0	0.3	0.00	1.15	0.47	0.03	0.19	100.0
26879	8	Kaolinite	37.2	3.2	53.0	0.3	2.5	0.0	0.0	0.0	0.0	1.21	0.31	0.00	0.0	0.1	0.00	1.22	0.60	0.03	0.26	100.0
26882	11	Kaolinite	32.8	3.6	55.2	0.4	2.6	0.0	0.0	0.0	0.0	1.73	0.30	0.00	0.0	0.1	0.00	2.22	0.53	0.05	0.57	100.0
26885	14	Nontronite	23.1	8.6	55.0	0.4	2.6	0.0	4.9	0.0	0.0	0.00	0.50	0.00	0.0	0.1	0.00	3.98	0.50	0.01	0.32	100.0
26887	16	Nontronite	16.4	15.3	51.0	0.5	4.4	0.0	8.4	0.0	0.0	0.00	0.79	0.00	0.0	0.1	0.00	2.51	0.45	0.01	0.18	100.0
26890	18	Nontronite	3.3	27.5	32.4	0.7	9.3	0.0	21.6	0.0	0.0	0.00	1.68	0.00	0.0	0.1	0.00	1.89	0.34	0.01	1.25	100.0
26893	21	Nontronite	0.0	30.0	20.1	0.6	8.1	0.0	16.4	0.0	0.0	21.19	1.61	0.00	0.0	0.1	0.00	1.22	0.21	0.01	0.61	100.0
26896	24	Saponite	0.0	35.2	14.5	0.4	0.0	4.2	11.7	0.0	0.0	31.28	1.17	0.00	0.0	0.0	0.00	0.98	0.13	0.00	0.40	100.0
CBRC0725																						
26897	1	Kaolinite	46.7	2.1	41.6	1.0	2.1	0.0	0.0	0.0	0.0	3.12	0.30	0.00	0.0	0.2	0.00	2.19	0.57	0.06	0.13	100.0
26900	4	Kaolinite	28.1	0.0	63.5	0.4	0.8	0.0	0.0	0.0	0.0	1.47	0.11	0.00	2.8	0.2	0.00	1.75	0.59	0.06	0.15	100.0
26902	6	Kaolinite	34.1	0.0	53.6	0.2	2.3	0.0	0.0	0.0	0.0	1.03	0.05	0.00	5.6	0.1	0.00	2.08	0.52	0.05	0.28	100.0
26905	9	Nontronite	8.0	30.6	33.5	0.5	2.7	0.0	18.9	0.0	0.0	0.00	1.87	0.00	0.0	0.0	0.00	2.92	0.31	0.01	0.63	100.0
26907	11	Nontronite	0.0	46.0	18.5	0.6	3.8	0.0	13.1	0.0	0.0	14.04	1.89	0.00	0.0	0.0	0.00	1.61	0.15	0.00	0.27	100.0
26910	14	Nontronite	0.0	41.3	22.9	0.6	4.3	0.0	15.7	0.0	0.0	10.80	2.35	0.00	0.0	0.0	0.00	1.44	0.19	0.00	0.34	100.0
26913	17	Nontronite	0.0	37.7	18.5	0.6	3.7	0.0	13.3	0.0	0.0	22.71	1.87	0.00	0.0	0.0	0.00	1.35	0.16	0.00	0.13	100.0
26916	19	Saponite	0.0	40.2	14.5	0.4	0.0	2.8	9.2	0.0	0.0	30.24	1.55	0.00	0.0	0.0	0.00	0.81	0.11	0.00	0.19	100.0
26919	22	Saponite	0.0	38.6	15.0	0.4	0.0	3.5	10.4	0.0	0.0	29.20	1.63	0.00	0.0	0.0	0.00	0.79	0.13	0.00	0.34	100.0

Hole ID	Depth (m)	Regolith Unit	Kaolinite	Opal-Si/Qtz	Fe-oxides	Illite	Nontronite	Saponite	Chlorite	Talc	Serpentine	Magnesite	Dolomite	Calcite	Gibbsite	Bassanite	Alunite	Chromite	Rutile	Apatite	Asbolan	% Total
CBRC0712																						
26613	1	Kaolinite	41.0	3.2	49.7	0.5	0.4	0.0	0.0	0.0	0.0	0.96	0.18	0.00	0.0	0.2	0.00	3.07	0.57	0.05	0.08	100.0
26615	3	Kaolinite	35.0	9.0	48.8	0.6	2.6	0.0	0.0	0.0	0.0	0.62	0.54	0.00	0.0	0.2	0.00	2.20	0.34	0.05	0.07	100.0
26617	5	Kaolinite	31.3	3.5	60.1	0.3	2.1	0.0	0.0	0.0	0.0	0.53	0.00	0.00	0.0	0.3	0.06	1.42	0.35	0.00	0.07	100.0
26620	8	Nontronite	24.1	6.3	60.9	0.3	2.2	0.0	2.2	0.0	0.0	0.00	0.15	0.00	0.0	0.1	0.00	3.10	0.42	0.03	0.23	100.0
26622	10	Nontronite	24.9	12.5	51.7	0.5	2.9	0.0	3.3	0.0	0.0	0.00	0.62	0.00	0.0	0.0	0.00	2.91	0.43	0.01	0.16	100.0
26623	11	Nontronite	6.5	29.7	50.4	0.7	3.6	0.0	5.4	0.0	0.0	0.00	1.00	0.00	0.0	0.0	0.00	2.27	0.16	0.00	0.37	100.0
26624	12	Nontronite	1.2	33.3	34.2	0.9	6.8	0.0	17.3	0.0	0.0	0.00	1.74	0.00	0.0	0.0	0.00	2.71	0.24	0.07	1.54	100.0
26625	13	Nontronite	0.0	57.8	16.4	0.9	5.5	0.0	8.5	0.0	0.0	7.63	1.51	0.00	0.0	0.0	0.00	1.26	0.11	0.01	0.45	100.0
26628	15	**Nontronite**	0.0	55.6	12.8	0.6	4.8	0.0	7.0	0.0	0.0	16.68	1.02	0.00	0.0	0.0	0.00	1.12	0.08	0.01	0.30	100.0
26631	18	**Nontronite**	0.0	52.0	12.4	0.5	5.9	0.0	7.0	0.0	0.0	19.52	1.04	0.00	0.0	0.0	0.00	1.31	0.08	0.01	0.30	100.0
CBRC0714																						
26645	1	Kaolinite	13.2	0.0	77.9	0.2	0.2	0.0	0.0	0.0	0.0	0.52	0.13	0.00	2.5	0.1	0.00	2.42	2.62	0.07	0.13	100.0
26649	5	Kaolinite	37.2	0.0	51.7	0.5	1.5	0.0	0.0	0.0	0.0	0.63	0.04	0.00	4.8	0.2	0.00	2.62	0.77	0.06	0.05	100.0
26650	6	Kaolinite	32.3	0.0	61.2	0.5	0.9	0.0	0.0	0.0	0.0	0.79	0.00	0.00	1.4	0.2	0.00	2.17	0.50	0.06	0.09	100.0
26651	7	Kaolinite	33.0	4.0	54.8	0.7	2.6	0.0	0.0	0.0	0.0	0.82	0.24	0.00	0.0	0.2	0.00	2.86	0.73	0.05	0.06	100.0
26652	8	Kaolinite	32.2	2.0	60.3	0.5	0.9	0.0	0.0	0.0	0.0	0.77	0.02	0.00	0.0	0.2	0.00	2.50	0.51	0.09	0.12	100.0
26654	10	Kaolinite	20.5	0.0	68.0	0.2	1.3	0.0	0.0	0.0	0.0	0.57	0.00	0.00	6.3	0.3	0.00	2.17	0.33	0.06	0.22	100.0
26657	13	Kaolinite	22.4	1.4	66.4	0.2	2.0	0.0	0.0	0.0	0.0	0.89	0.00	0.00	0.0	0.1	0.00	5.51	0.29	0.18	0.66	100.0
26658	14	Nontronite	14.0	10.2	64.1	0.4	3.6	0.0	2.7	0.0	0.0	0.00	0.35	0.00	0.0	0.1	0.00	3.82	0.28	0.10	0.38	100.0
26661	16	Nontronite	2.0	59.8	23.6	0.8	4.4	0.0	6.6	0.0	0.0	0.00	1.54	0.00	0.0	0.0	0.00	1.04	0.11	0.00	0.18	100.0
26663	18	Nontronite	0.5	40.4	36.9	0.8	5.8	0.0	12.0	0.0	0.0	0.00	1.89	0.00	0.0	0.0	0.00	1.18	0.17	0.01	0.28	100.0
26665	20	**Nontronite**	0.0	50.0	23.0	1.0	8.9	0.0	7.9	0.0	0.0	4.55	2.12	0.00	0.0	0.0	0.00	0.71	0.12	0.01	1.62	100.0
26666	21	**Nontronite**	0.0	40.0	25.1	1.1	10.8	0.0	12.2	0.0	0.0	4.44	2.33	0.00	0.0	0.0	0.00	1.59	0.22	0.00	2.14	100.0
26669	24	**Saponite**	0.0	54.8	10.1	0.5	0.0	4.7	6.5	0.0	0.0	20.44	0.82	0.00	0.0	0.0	0.00	1.71	0.08	0.01	0.26	100.0
CBRC0783																						
29819	1	Nontronite	28.8	23.8	39.5	1.1	1.7	0.0	2.7	0.0	0.0	0.00	0.53	0.00	0.0	0.2	0.00	1.08	0.31	0.04	0.23	100.0
29821	3	Nontronite	15.4	20.5	50.6	1.2	3.5	0.0	6.2	0.0	0.0	0.00	0.49	0.00	0.0	0.1	0.00	1.34	0.37	0.02	0.36	100.0
29822	4	Nontronite	7.1	36.4	38.2	1.2	2.4	0.0	9.8	0.0	0.0	0.00	0.58	0.00	0.0	0.0	0.00	2.80	0.29	0.01	1.21	100.0
29824	6	**Nontronite**	0.0	56.0	20.9	1.3	6.1	0.0	8.3	0.0	0.0	4.65	1.22	0.00	0.0	0.0	0.00	0.77	0.09	0.00	0.72	100.0
29825	7	**Saponite**	0.0	37.6	24.0	0.8	0.0	4.5	12.8	0.0	0.0	17.02	0.97	0.00	0.0	0.0	0.00	1.81	0.14	0.01	0.22	100.0
29827	9	**Saponite**	0.0	30.6	17.5	0.7	0.0	6.1	14.7	0.0	0.0	25.35	0.98	0.00	0.0	0.0	0.00	2.36	0.18	0.00	1.58	100.0
29830	12	**Saponite**	0.0	37.3	13.3	0.6	0.0	4.2	11.8	0.0	0.0	29.83	0.94	0.00	0.0	0.0	0.00	1.62	0.14	0.00	0.34	100.0
29832	13	**Saponite**	0.0	34.5	10.7	0.5	0.0	4.1	11.5	0.0	0.0	34.84	0.73	0.00	0.0	0.0	0.00	2.78	0.13	0.00	0.19	100.0
29833	14	Serpentine	0.0	19.6	11.4	0.5	0.0	4.2	12.4	0.0	47.0	0.00	0.79	0.00	0.0	0.0	0.00	3.65	0.14	0.00	0.31	100.0
29835	16	Serpentine	0.0	21.3	10.9	0.5	0.0	4.3	11.7	0.0	45.1	0.00	0.62	0.00	0.0	0.0	0.00	5.23	0.12	0.00	0.25	100.0
29838	19	Serpentine	0.0	33.0	10.3	0.5	0.0	5.9	7.8	0.0	37.8	0.00	0.32	0.00	0.0	0.0	0.00	3.92	0.08	0.00	0.33	100.0
29839	20	Mix. Serp.	0.0	58.5	6.8	0.5	0.0	3.8	5.3	0.0	18.9	0.00	4.53	0.00	0.0	0.0	0.00	1.48	0.05	0.00	0.18	100.0
29840	21	**Mix. Serp.**	0.0	25.9	11.2	0.6	0.0	4.7	9.3	0.0	32.6	0.00	12.88	0.00	0.0	0.0	0.00	2.52	0.10	0.00	0.26	100.0
29841	22	**Mix. Serp.**	0.0	25.4	11.4	0.5	0.0	3.8	8.7	0.0	38.5	0.00	10.17	0.00	0.0	0.0	0.00	1.13	0.10	0.00	0.29	100.0
29842	23	Mix. Serp.	0.0	42.7	12.0	0.6	0.0	5.6	5.3	0.0	31.2	0.00	1.88	0.00	0.0	0.0	0.00	0.36	0.06	0.00	0.33	100.0
29845	26	Mix. Serp.	0.0	52.3	11.1	0.6	0.0	5.3	6.1	0.0	23.4	0.00	0.53	0.00	0.0	0.0	0.00	0.33	0.08	0.01	0.32	100.0
29849	30	Mix. Serp.	0.0	55.5	11.4	0.6	0.0	3.9	5.9	0.0	21.3	0.00	0.61	0.00	0.0	0.0	0.00	0.29	0.07	0.00	0.33	100.0
29850	31	Mix. Serp.	0.0	65.2	9.2	0.5	0.0	4.7	3.3	0.0	16.1	0.00	0.44	0.00	0.0	0.0	0.00	0.23	0.04	0.00	0.26	100.0
29853	34	Mix. Serp.	0.0	48.5	11.4	0.5	0.0	3.1	4.4	0.0	31.0	0.00	0.41	0.00	0.0	0.0	0.00	0.27	0.07	0.00	0.33	100.0
29858	38	Mix. Serp.	0.0	64.3	8.9	0.4	0.0	3.4	1.9	0.0	20.4	0.00	0.32	0.00	0.0	0.0	0.00	0.19	0.01	0.02	0.20	100.0
29859	39	**Mix. Serp.**	0.0	42.9	7.6	0.4	0.0	3.4	1.7	0.0	7.5	0.00	36.24	0.00	0.0	0.0	0.00	0.16	0.01	0.02	0.16	100.0
29861	41	**Mix. Serp.**	0.0	36.7	8.9	0.4	0.0	1.9	1.8	0.0	6.7	0.00	43.37	0.00	0.0	0.0	0.00	0.18	0.01	0.01	0.19	100.0
29864	44	**Mix. Serp.**	0.0	9.7	9.5	0.3	0.0	1.8	1.6	0.0	69.8	0.00	6.86	0.00	0.0	0.0	0.00	0.18	0.00	0.03	0.17	100.0
29866	45	**Mix. Serp.**	0.0	0.2	8.4	0.3	0.0	1.8	2.5	0.0	67.0	0.00	19.40	0.00	0.0	0.0	0.00	0.15	0.02	0.01	0.21	100.0
29869	48	**Mix. Serp.**	0.0	12.4	8.1	0.3	0.0	3.1	1.4	0.0	59.0	0.00	15.32	0.00	0.0	0.0	0.00	0.23	0.00	0.01	0.19	100.0
29873	52	**Mix. Serp.**	0.0	0.0	7.4	0.1	0.0	1.7	1.9	0.0	64.6	11.10	12.59	0.00	0.0	0.0	0.00	0.22	0.00	0.02	0.20	100.0
29876	55	**Mix. Serp.**	0.0	13.8	6.9	0.2	0.0	0.7	3.0	0.0	28.2	0.00	46.63	0.00	0.0	0.0	0.00	0.23	0.03	0.01	0.16	100.0
29878	57	**Mix. Serp.**	0.0	9.0	5.1	0.2	0.0	1.5	1.7	0.0	10.2	0.00	71.90	0.00	0.0	0.0	0.00	0.19	0.01	0.00	0.14	100.0
29881	60	**Mix. Serp.**	0.0	23.4	8.6	0.1	0.0	0.4	2.1	0.0	26.6	0.00	38.48	0.00	0.0	0.0	0.00	0.16	0.01	0.01	0.15	100.0

Appendix 6: Table A6.2. Normative mineral abundances of selected drill holes for MM3.

Hole ID	Depth (m)	Regolith Unit	Kaolinite	Opal/Qtz	Fe-oxides	Illite	Nontronite	Saponite	Chlorite	Talc	Serpentine	Magnesite	Dolomite	Calcite	Gibbsite	Bassanite	Alunite	Chromite	Rutile	Apatite	Asbolan	% Total
ARC1258																						
124385	1	Talc	17.1	25.9	28.8	4.72	0.0	9.0	7.9	0.0	0.0	0.0	4.9	0.0	0.0	0.33	0.00	0.52	0.52	0.11	0.19	100.0
124386	2	Talc	0.0	21.3	7.8	2.51	0.0	19.4	11.4	30.9	0.0	0.0	5.4	0.0	0.0	0.79	0.00	0.19	0.19	0.02	0.13	100.0
124387	3	Talc	0.0	12.3	8.3	1.35	0.0	28.0	8.0	41.4	0.0	0.0	0.2	0.0	0.0	0.11	0.00	0.14	0.14	0.01	0.15	100.0
124389	5	Talc	0.0	11.8	7.1	1.80	0.0	43.1	5.6	30.1	0.0	0.0	0.0	0.0	0.0	0.06	0.03	0.14	0.14	0.00	0.10	100.0
124392	7	Talc	0.0	12.1	7.8	1.57	0.0	47.0	4.9	26.1	0.0	0.0	0.0	0.0	0.0	0.06	0.02	0.14	0.14	0.00	0.14	100.0
124393	8	**Talc**	0.0	11.7	9.1	1.80	0.0	45.0	5.2	26.5	0.0	0.0	0.0	0.0	0.0	0.06	0.04	0.14	0.14	0.00	0.24	100.0
124397	12	**Talc**	0.0	0.0	4.0	1.22	0.0	22.8	1.8	18.3	0.0	38.2	13.4	0.0	0.0	0.05	0.00	0.05	0.05	0.00	0.16	100.0
124398	13	**Talc**	1.3	0.0	5.1	1.23	0.0	33.7	0.2	17.5	0.0	38.0	2.6	0.0	0.0	0.04	0.00	0.07	0.07	0.00	0.16	100.0
124399	14	**Talc**	0.4	0.0	5.3	1.61	0.0	33.9	1.6	21.5	0.0	32.9	2.4	0.0	0.0	0.03	0.00	0.08	0.08	0.00	0.17	100.0
124403	18	**Talc**	0.0	0.0	5.0	0.98	0.0	28.6	3.2	23.7	0.0	27.4	10.7	0.0	0.0	0.02	0.00	0.08	0.08	0.00	0.17	100.0
ARC1257																						
124360	1	Kaolinite	24.3	7.1	56.4	2.55	6.9	0.0	0.0	0.0	0.0	1.0	0.3	0.0	0.0	0.27	0.00	0.45	0.45	0.09	0.25	100.0
124362	3	Kaolinite	30.0	9.6	52.0	0.86	4.0	0.0	0.0	0.0	0.0	1.8	0.5	0.0	0.0	0.18	0.00	0.45	0.45	0.06	0.22	100.0
124364	5	Kaolinite	18.5	10.8	56.1	1.62	10.5	0.0	0.0	0.0	0.0	1.7	0.0	0.0	0.0	0.09	0.01	0.34	0.34	0.00	0.08	100.0
124365	6	Nontronite	0.2	18.8	26.5	2.06	34.1	0.0	17.4	0.0	0.0	0.0	0.0	0.0	0.0	0.15	0.38	0.18	0.18	0.00	0.12	100.0
124368	8	Nontronite	0.0	6.4	20.1	0.76	56.5	0.0	12.3	0.0	0.0	1.8	0.0	0.0	0.0	0.15	1.25	0.24	0.24	0.00	0.20	100.0
124370	10	Nontronite	0.0	11.2	19.9	0.46	50.6	0.0	12.1	0.0	0.0	3.5	0.0	0.0	0.0	0.12	1.14	0.21	0.21	0.00	0.61	100.0
124373	13	Nontronite	0.0	14.4	18.8	0.33	44.5	0.0	10.8	0.0	0.0	9.1	0.0	0.0	0.0	0.11	0.99	0.19	0.19	0.00	0.57	100.0
124375	15	Serpentine	0.0	10.3	24.6	0.02	0.0	30.2	7.6	0.0	24.5	0.0	0.0	0.0	0.0	0.09	0.97	0.14	0.14	0.00	1.48	100.0
124376	16	Serpentine	0.0	17.0	18.5	0.26	0.0	23.5	7.4	0.0	31.2	0.0	0.0	0.0	0.0	0.08	0.57	0.10	0.10	0.00	1.41	100.0
124378	18	Serpentine	0.0	3.4	12.7	0.00	0.0	16.1	6.9	0.0	59.5	0.0	0.0	0.0	0.0	0.05	0.46	0.10	0.10	0.00	0.63	100.0
124379	19	Serpentine	0.0	2.2	11.8	0.04	0.0	11.8	6.1	0.0	66.8	0.0	0.0	0.0	0.0	0.05	0.33	0.08	0.08	0.00	0.72	100.0
124384	24	Serpentine	0.0	4.5	12.9	0.48	0.0	9.5	7.2	0.0	63.8	0.0	0.9	0.0	0.0	0.16	0.00	0.09	0.09	0.00	0.34	100.0
ARC1478																						
137424	1	**Nontronite**	0.0	31.4	23.9	2.38	6.8	0.0	19.8	0.0	0.0	12.2	2.3	0.0	0.0	0.10	0.00	0.46	0.46	0.06	0.19	100.0
137425	2	Nontronite	10.9	15.3	27.5	2.44	30.5	0.0	10.3	0.0	0.0	0.0	1.6	0.0	0.0	0.37	0.00	0.40	0.40	0.01	0.21	100.0
137426	3	Nontronite	8.5	16.0	22.4	2.59	38.8	0.0	9.6	0.0	0.0	0.0	0.7	0.0	0.0	0.45	0.00	0.33	0.33	0.00	0.19	100.0
137429	5	Nontronite	0.0	21.1	14.7	2.58	38.0	0.0	16.5	0.0	0.0	5.1	0.1	0.0	0.0	0.55	0.00	0.25	0.25	0.00	0.89	100.0
137430	6	Serpentine	0.0	7.0	13.3	0.98	0.0	17.8	8.7	0.0	47.9	0.0	3.3	0.0	0.0	0.36	0.00	0.12	0.12	0.00	0.41	100.0
137433	9	**Serpentine**	0.0	8.6	11.7	0.95	0.0	16.9	9.6	0.0	44.1	0.0	7.0	0.0	0.0	0.29	0.00	0.23	0.23	0.00	0.37	100.0
ARC1008																						
83610	1	Kaolinite	33.9	31.4	24.6	2.98	3.8	0.0	0.0	0.0	1.1	0.0	1.2	0.0	0.0	0.13	0.00	0.40	0.40	0.06	0.09	100.0
83612	3	**Kaolinite**	19.5	32.0	24.4	1.38	3.8	0.0	0.0	0.0	5.2	0.0	13.2	0.0	0.0	0.08	0.00	0.17	0.17	0.02	0.16	100.0
83613	4	**Nontronite**	8.4	22.2	35.7	1.55	16.2	0.0	6.6	0.0	0.0	0.0	7.9	0.0	0.0	0.35	0.00	0.20	0.20	0.02	0.67	100.0
83614	5	Nontronite	2.5	34.6	20.5	2.29	30.5	0.0	8.5	0.0	0.0	0.0	0.0	0.0	0.0	0.42	0.07	0.16	0.16	0.00	0.30	100.0
83617	8	Nontronite	6.2	18.0	23.9	2.29	38.1	0.0	8.1	0.0	0.0	0.0	0.0	0.0	0.0	0.36	0.29	0.24	0.24	0.00	2.29	100.0
83618	9	Nontronite	3.3	80.1	7.3	0.53	6.5	0.0	1.7	0.0	0.0	0.0	0.0	0.0	0.0	0.08	0.05	0.08	0.08	0.00	0.34	100.0
83619	10	Nontronite	10.2	8.7	39.6	1.66	31.7	0.0	6.4	0.0	0.0	0.0	0.0	0.0	0.0	0.21	0.26	0.28	0.28	0.00	0.87	100.0
83620	11	Nontronite	13.9	2.5	49.4	1.13	26.0	0.0	5.4	0.0	0.0	0.0	0.0	0.0	0.0	0.12	0.39	0.41	0.41	0.00	0.41	100.0
83623	14	Nontronite	0.0	24.0	17.7	1.90	38.2	0.0	14.8	0.0	1.9	0.0	0.0	0.0	0.0	0.21	0.35	0.22	0.22	0.00	0.41	100.0
83624	15	Serpentine	0.0	15.7	17.2	1.69	0.0	28.2	9.4	0.0	26.1	0.0	0.2	0.0	0.0	0.43	0.00	0.16	0.16	0.00	0.71	100.0
83628	18	Serpentine	0.0	20.8	12.5	1.51	0.0	23.4	6.1	0.0	33.6	0.0	1.0	0.0	0.0	0.27	0.00	0.11	0.11	0.00	0.60	100.0
83631	21	Serpentine	0.0	17.4	12.3	0.97	0.0	11.8	5.5	0.0	50.4	0.0	0.9	0.0	0.0	0.14	0.00	0.07	0.07	0.00	0.31	100.0
83632	22	Serpentine	0.0	16.8	13.3	1.25	0.0	15.8	5.7	0.0	45.3	0.0	1.1	0.0	0.0	0.17	0.00	0.09	0.09	0.00	0.34	100.0
83637	27	Serpentine	0.0	11.4	10.3	0.71	0.0	7.5	5.7	0.0	62.9	0.0	1.0	0.0	0.0	0.09	0.00	0.08	0.08	0.00	0.23	100.0

Hole ID	Depth (m)	Regolith Unit	Kaolinite	Opal/Qtz	Fe-oxides	Illite	Nontronite	Saponite	Chlorite	Talc	Serpentine	Magnesite	Dolomite	Calcite	Gibbsite	Bassanite	Alunite	Chromite	Rutile	Apatite	Asbolan	% Total
ARC0776																						
37749	1	Kaolinite	17.2	13.1	60.0	0.83	3.5	0.0	0.0	0.0	0.0	4.1	0.3	0.0	0.0	0.16	0.00	0.28	0.28	0.07	0.17	100.0
37750	2	Nontronite	9.7	35.9	41.3	1.34	2.3	0.0	7.5	0.0	0.0	0.0	1.5	0.0	0.0	0.02	0.00	0.20	0.20	0.02	0.10	100.0
37751	3	Nontronite	0.0	37.6	20.1	1.27	15.0	0.0	6.2	0.0	0.0	1.5	17.9	0.0	0.0	0.22	0.00	0.05	0.05	0.00	0.13	100.0
37755	6	Nontronite	0.0	28.0	19.0	1.76	33.5	0.0	12.4	0.0	0.0	3.8	0.2	0.0	0.0	0.44	0.00	0.17	0.17	0.00	0.61	100.0
37756	7	Nontronite	0.0	48.4	17.1	1.41	24.2	0.0	6.4	0.0	0.0	1.5	0.1	0.0	0.0	0.24	0.00	0.10	0.10	0.00	0.34	100.0
37758	9	Nontronite	0.0	38.9	6.4	1.55	31.0	0.0	4.3	0.0	0.0	16.1	0.1	0.0	0.0	0.32	0.00	0.08	0.08	0.00	1.26	100.0
37760	11	Serpentine	0.0	22.5	9.3	0.61	0.0	12.7	3.8	0.0	49.9	0.0	0.6	0.0	0.0	0.16	0.00	0.05	0.05	0.00	0.30	100.0
37764	15	Serpentine	0.0	34.2	12.7	1.13	0.0	20.2	3.7	0.0	26.9	0.0	0.5	0.0	0.0	0.21	0.00	0.07	0.07	0.00	0.40	100.0
ARC0774																						
37693	1	Nontronite	4.9	71.3	8.7	3.34	2.5	0.0	7.0	0.0	0.0	0.0	1.6	0.0	0.0	0.03	0.00	0.16	0.16	0.03	0.30	100.0
37694	2	Nontronite	0.0	36.4	7.9	2.15	12.9	0.0	6.8	0.0	0.0	12.3	19.7	0.0	0.0	1.10	0.00	0.08	0.08	0.01	0.47	100.0
37695	3	Nontronite	0.0	25.7	2.2	0.83	14.0	0.0	2.0	0.0	0.0	46.6	7.9	0.0	0.0	0.65	0.00	0.02	0.02	0.00	0.10	100.0
37696	4	Nontronite	0.0	27.8	1.5	0.59	7.5	0.0	4.0	0.0	0.0	57.6	0.7	0.0	0.0	0.16	0.00	0.01	0.01	0.00	0.05	100.0
37697	5	Nontronite	0.0	26.7	15.7	1.62	36.2	0.0	3.7	0.0	0.0	14.0	0.0	0.0	0.0	0.41	0.43	0.10	0.10	0.00	1.08	100.0
37700	8	Nontronite	0.0	44.1	13.3	1.81	26.9	0.0	0.8	0.0	0.0	11.0	0.5	0.0	0.0	0.50	0.00	0.04	0.04	0.00	0.96	100.0
37703	10	Nontronite	0.0	44.7	11.9	1.18	28.8	0.0	0.3	0.0	0.0	11.9	0.0	0.0	0.0	0.13	0.47	0.04	0.04	0.00	0.61	100.0
37704	11	Nontronite	0.0	7.5	2.1	0.35	5.0	0.0	0.0	0.0	0.0	84.2	0.6	0.0	0.0	0.18	0.00	0.00	0.00	0.00	0.09	100.0
37706	13	Nontronite	0.0	9.7	2.2	0.46	4.9	0.0	0.0	0.0	0.0	80.5	1.8	0.0	0.0	0.14	0.00	0.00	0.00	0.00	0.24	100.0
37709	16	Serpentine	0.0	0.0	5.9	0.87	0.0	9.8	2.2	0.0	24.8	52.2	3.9	0.0	0.0	0.12	0.00	0.03	0.03	0.00	0.20	100.0
37712	19	Serpentine	0.0	0.0	6.3	0.66	0.0	9.2	0.8	0.0	50.1	23.0	9.6	0.0	0.0	0.08	0.00	0.01	0.01	0.00	0.23	100.0
37715	22	Serpentine	0.0	0.0	6.5	1.18	0.0	17.3	1.2	0.0	44.1	26.7	2.4	0.0	0.0	0.21	0.00	0.03	0.03	0.00	0.22	100.0
37719	26	Serpentine	0.0	4.5	5.1	0.95	0.0	10.8	5.9	0.0	69.2	0.0	3.1	0.0	0.0	0.06	0.00	0.10	0.10	0.00	0.21	100.0
37720	27	Serpentine	0.0	0.0	4.7	0.66	0.0	7.1	2.0	0.0	54.0	29.2	2.2	0.0	0.0	0.05	0.00	0.02	0.02	0.00	0.13	100.0
ARC0786																						
37969	1	Talc	6.7	21.7	34.9	3.57	0.0	5.4	20.4	0.0	0.0	0.0	4.8	0.0	0.0	0.14	0.00	0.97	0.97	0.09	0.26	100.0
37970	2	Talc	4.9	27.2	20.8	4.79	0.0	5.7	15.0	3.7	0.0	0.0	15.9	0.0	0.0	0.22	0.00	0.83	0.83	0.06	0.20	100.0
37971	3	Talc	0.0	0.0	5.6	2.02	0.0	8.4	6.7	37.1	0.0	13.8	25.8	0.0	0.0	0.14	0.00	0.16	0.16	0.01	0.13	100.0
37974	6	Talc	0.0	0.0	6.4	0.74	0.0	14.0	5.0	39.9	0.0	27.5	6.0	0.0	0.0	0.10	0.00	0.07	0.07	0.01	0.19	100.0
37978	10	Talc	0.0	0.0	6.4	1.00	0.0	16.3	5.4	44.0	0.0	19.4	7.1	0.0	0.0	0.14	0.00	0.08	0.08	0.00	0.20	100.0
37979	11	Talc	0.0	0.0	7.5	0.95	0.0	9.0	7.1	48.2	0.0	21.0	5.8	0.0	0.0	0.07	0.00	0.08	0.08	0.00	0.21	100.0
37983	15	Serpentine	0.0	4.6	8.0	1.12	0.0	5.5	7.8	0.0	66.0	0.0	6.7	0.0	0.0	0.04	0.00	0.09	0.09	0.01	0.21	100.0
ARC0782																						
37888	1	Kaolinite	18.5	20.7	47.6	1.91	3.7	0.0	0.0	0.0	0.0	5.8	0.3	0.0	0.0	0.17	0.00	0.59	0.59	0.09	0.15	100.0
37890	3	Kaolinite	12.8	31.6	44.6	0.65	2.4	0.0	0.0	0.0	0.0	3.0	4.3	0.0	0.0	0.09	0.00	0.19	0.19	0.03	0.05	100.0
37893	5	Kaolinite	3.7	19.0	26.6	0.63	10.2	0.0	0.0	0.0	0.0	7.0	32.4	0.0	0.0	0.29	0.00	0.07	0.07	0.01	0.08	100.0
37894	6	Saponite	3.7	48.0	28.0	1.08	0.0	14.9	0.0	0.0	0.0	0.0	0.0	3.6	0.0	0.33	0.00	0.08	0.08	0.01	0.17	100.0
37896	8	Saponite	8.1	46.6	23.3	1.00	0.0	18.1	0.0	0.0	0.0	0.0	0.0	0.0	0.0	0.16	0.43	0.16	0.16	0.00	1.94	100.0
37898	10	Saponite	5.4	27.6	30.0	0.20	0.0	26.2	8.2	0.0	0.0	0.0	0.0	0.0	0.0	0.21	0.88	0.34	0.34	0.00	0.54	100.0
37900	12	Saponite	0.0	40.9	16.5	0.86	0.0	20.7	7.0	0.0	0.0	10.9	0.0	0.0	0.0	0.39	0.29	0.12	0.12	0.00	2.20	100.0
37903	15	Saponite	0.0	36.6	24.9	0.78	0.0	25.0	10.5	0.0	0.0	0.7	0.0	0.0	0.0	0.21	0.44	0.16	0.16	0.00	0.58	100.0
37904	16	Serpentine	0.0	21.8	20.8	0.39	0.0	21.7	7.9	0.0	24.9	0.0	0.0	0.0	0.0	0.20	0.49	0.12	0.12	0.00	1.53	100.0
37906	18	Serpentine	0.0	33.3	16.3	1.04	0.0	23.3	6.7	0.0	18.0	0.0	0.0	0.0	0.0	0.36	0.00	0.10	0.10	0.00	0.85	100.0
37909	21	Serpentine	0.0	30.7	15.4	0.91	0.0	14.3	7.8	0.0	29.8	0.0	0.0	0.0	0.0	0.22	0.00	0.10	0.10	0.00	0.61	100.0
ARC0783																						
37910	1	Kaolinite	16.2	33.4	38.7	2.39	4.7	0.0	0.0	0.0	0.0	3.0	0.4	0.0	0.0	0.13	0.00	0.46	0.46	0.07	0.23	100.0
37913	4	Nontronite	0.0	25.7	26.5	1.81	21.5	0.0	14.9	0.0	0.0	7.0	1.2	0.0	0.0	0.31	0.00	0.39	0.39	0.03	0.23	100.0
37914	5	Nontronite	5.1	16.9	29.3	1.76	36.7	0.0	8.4	0.0	0.0	0.0	0.4	0.0	0.0	0.42	0.00	0.32	0.32	0.02	0.32	100.0
37915	6	Nontronite	0.9	35.1	20.3	1.59	29.6	0.0	11.2	0.0	0.0	0.0	0.1	0.0	0.0	0.40	0.00	0.17	0.17	0.01	0.31	100.0
37916	7	Serpentine	0.0	6.7	18.8	0.61	0.0	16.6	8.4	0.0	47.8	0.0	0.0	0.0	0.0	0.34	0.11	0.12	0.12	0.00	0.43	100.0
37918	9	Serpentine	0.0	11.6	13.3	0.86	0.0	16.3	7.5	0.0	47.8	0.0	1.3	0.0	0.0	0.30	0.00	0.12	0.12	0.00	0.79	100.0
37921	12	Serpentine	0.0	22.5	15.8	1.13	0.0	19.4	8.2	0.0	30.4	0.0	1.4	0.0	0.0	0.28	0.00	0.14	0.14	0.00	0.64	100.0
37924	15	Serpentine	0.0	17.5	11.6	1.14	0.0	17.7	9.9	0.0	40.3	0.0	0.8	0.0	0.0	0.16	0.00	0.17	0.17	0.01	0.48	100.0

Hole ID	Depth (m)	Regolith Unit	Kaolinite	Opal/Qtz	Fe-oxides	Illite	Nontronite	Saponite	Chlorite	Talc	Serpentine	Magnesite	Dolomite	Calcite	Gibbsite	Bassanite	Alunite	Chromite	Rutile	Apatite	Asbolan	% Total
ARC0780																						
37825	1	Nontronite	0.4	31.1	24.2	2.51	18.7	0.0	10.5	0.0	0.0	0.0	11.7	0.0	0.0	0.21	0.00	0.15	0.15	0.02	0.37	100.0
37826	2	Nontronite	3.3	29.7	21.5	1.10	7.4	0.0	5.0	0.0	0.0	0.0	31.4	0.0	0.0	0.15	0.00	0.07	0.07	0.01	0.13	100.0
37827	3	Nontronite	3.7	22.4	27.2	2.80	31.1	0.0	10.5	0.0	0.0	0.0	0.8	0.0	0.0	1.02	0.00	0.14	0.14	0.00	0.18	100.0
37828	4	Nontronite	10.7	4.5	55.5	1.57	21.0	0.0	5.6	0.0	0.0	0.0	0.0	0.0	0.0	0.38	0.18	0.19	0.19	0.00	0.18	100.0
37830	6	Nontronite	18.9	0.0	57.0	0.63	17.1	0.0	3.5	0.0	0.0	0.0	0.0	0.0	1.7	0.12	0.50	0.24	0.24	0.00	0.11	100.0
37831	7	Nontronite	0.0	61.5	9.3	2.18	22.4	0.0	2.2	0.0	0.0	1.9	0.0	0.0	0.0	0.20	0.15	0.03	0.03	0.00	0.11	100.0
37833	9	Nontronite	0.0	64.2	6.0	1.28	22.0	0.0	0.5	0.0	0.0	5.0	0.0	0.0	0.0	0.14	0.24	0.02	0.02	0.00	0.67	100.0
37835	10	Nontronite	0.0	53.6	9.1	1.49	25.2	0.0	0.6	0.0	0.0	8.5	0.0	0.0	0.0	0.11	0.36	0.03	0.03	0.00	0.98	100.0
37836	11	Nontronite	0.0	72.8	11.9	1.69	6.6	0.0	0.0	0.0	0.0	5.7	0.0	0.0	0.0	0.08	0.30	0.00	0.00	0.00	0.96	100.0
37838	13	Nontronite	0.0	57.2	9.1	1.23	3.4	0.0	0.0	0.0	0.0	28.7	0.0	0.0	0.0	0.11	0.06	0.00	0.00	0.00	0.22	100.0
37839	14	Nontronite	0.0	63.2	9.8	1.00	14.7	0.0	0.0	0.0	0.0	10.5	0.0	0.0	0.0	0.05	0.25	0.01	0.01	0.00	0.48	100.0
37842	17	Nontronite	0.0	57.6	9.1	0.60	12.0	0.0	0.2	0.0	0.0	19.8	0.0	0.0	0.0	0.05	0.16	0.01	0.01	0.00	0.41	100.0
37844	19	Nontronite	0.0	76.4	5.1	0.58	6.6	0.0	0.0	0.0	0.0	11.1	0.0	0.0	0.0	0.08	0.01	0.00	0.00	0.00	0.15	100.0
37847	22	Nontronite	0.0	40.2	13.4	0.97	15.1	0.0	1.1	0.0	0.0	28.5	0.0	0.0	0.0	0.18	0.00	0.03	0.03	0.00	0.46	100.0
37848	23	Nontronite	0.0	14.7	3.3	0.35	5.5	0.0	0.1	0.0	0.0	75.4	0.6	0.0	0.0	0.07	0.00	0.00	0.00	0.00	0.13	100.0
37849	24	Nontronite	0.0	14.8	3.9	0.35	3.1	0.0	0.0	0.0	0.0	76.8	0.8	0.0	0.0	0.08	0.00	0.00	0.00	0.00	0.12	100.0
37850	25	Nontronite	0.0	70.6	6.4	0.72	8.2	0.0	0.0	0.0	0.0	13.8	0.1	0.0	0.0	0.07	0.00	0.00	0.00	0.00	0.15	100.0
37853	28	Nontronite	0.0	59.3	9.0	0.85	11.4	0.0	0.1	0.0	0.0	18.9	0.1	0.0	0.0	0.11	0.00	0.01	0.01	0.01	0.20	100.0
37855	30	Nontronite	0.0	25.0	4.1	0.47	7.1	0.0	1.2	0.0	0.0	61.4	0.4	0.0	0.0	0.08	0.00	0.00	0.00	0.00	0.21	100.0
37858	33	Nontronite	0.0	14.2	4.8	0.35	4.7	0.0	0.2	0.0	0.0	74.8	0.9	0.0	0.0	0.05	0.00	0.00	0.00	0.00	0.11	100.0
ARC1283																						
94529	1	Kaolinite	5.8	36.7	3.3	1.60	8.0	0.0	0.0	0.0	0.0	18.8	24.1	0.0	0.0	1.40	0.00	0.14	0.14	0.02	0.08	100.0
94530	2	Talc	0.0	12.7	6.0	1.33	0.0	10.3	7.3	32.1	0.0	0.0	22.6	0.0	0.0	7.31	0.00	0.12	0.12	0.02	0.16	100.0
94532	4	Talc	0.0	2.8	10.3	0.60	0.0	12.5	9.1	63.7	0.0	0.0	0.4	0.0	0.0	0.12	0.00	0.12	0.12	0.01	0.29	100.0
94536	7	Talc	0.0	5.4	10.0	0.60	0.0	9.4	9.6	62.7	0.0	0.0	1.5	0.0	0.0	0.28	0.00	0.13	0.13	0.02	0.27	100.0
94537	8	Talc	0.0	0.0	6.9	0.36	0.0	8.3	6.1	44.0	0.0	27.7	6.3	0.0	0.0	0.04	0.00	0.07	0.07	0.01	0.19	100.0
94539	10	Talc	0.0	0.0	7.3	0.24	0.0	3.0	6.9	49.4	0.0	24.1	8.7	0.0	0.0	0.02	0.00	0.08	0.08	0.01	0.18	100.0
94541	12	Talc	0.0	0.0	7.0	0.24	0.0	4.8	6.3	47.7	0.0	23.9	9.6	0.0	0.0	0.03	0.00	0.07	0.07	0.00	0.17	100.0
ARC0793																						
39374	1	Kaolinite	14.7	32.8	43.5	2.12	3.0	0.0	0.0	0.0	0.0	2.5	0.1	0.0	0.0	0.16	0.00	0.35	0.35	0.09	0.32	100.0
39375	2	Kaolinite	25.1	13.0	58.1	1.18	0.4	0.0	0.0	0.0	0.0	0.5	0.5	0.0	0.0	0.12	0.00	0.40	0.40	0.07	0.07	100.0
39378	5	Kaolinite	28.4	23.0	45.0	0.53	0.7	0.0	0.0	0.0	0.0	0.8	0.8	0.0	0.0	0.06	0.00	0.36	0.36	0.03	0.03	100.0
39380	7	Kaolinite	28.1	17.7	50.1	0.26	1.3	0.0	0.0	0.0	0.0	1.0	0.5	0.0	0.0	0.06	0.00	0.37	0.37	0.05	0.05	100.0
39383	10	Kaolinite	23.0	11.9	58.6	0.40	2.9	0.0	0.0	0.0	0.0	2.2	0.0	0.0	0.0	0.10	0.00	0.34	0.34	0.05	0.13	100.0
39385	11	Kaolinite	16.0	12.4	63.8	0.58	4.0	0.0	0.0	0.0	0.0	2.6	0.0	0.0	0.0	0.09	0.00	0.23	0.23	0.03	0.11	100.0
39386	12	Nontronite	3.3	42.1	34.1	1.09	9.2	0.0	8.6	0.0	0.0	0.0	0.4	0.0	0.0	0.02	0.00	0.14	0.14	0.00	0.94	100.0
39389	15	Nontronite	0.0	48.7	18.3	1.18	14.7	0.0	11.3	0.0	0.0	2.5	2.2	0.0	0.0	0.11	0.00	0.14	0.14	0.04	0.72	100.0
39390	16	Nontronite	0.0	30.5	10.5	1.14	15.0	0.0	8.5	0.0	0.0	3.4	30.4	0.0	0.0	0.10	0.00	0.10	0.10	0.00	0.33	100.0
39391	17	Nontronite	0.0	29.0	11.5	1.21	16.0	0.0	21.3	0.0	0.0	7.8	11.9	0.0	0.0	0.11	0.00	0.33	0.33	0.02	0.63	100.0
39394	20	Nontronite	0.0	49.2	10.2	0.70	9.9	0.0	4.7	0.0	0.0	23.0	1.7	0.0	0.0	0.09	0.00	0.05	0.05	0.00	0.39	100.0
39396	22	Serpentine	0.0	20.4	12.8	0.51	0.0	8.4	4.1	0.0	40.6	0.0	12.6	0.0	0.0	0.12	0.00	0.04	0.04	0.00	0.39	100.0
39401	27	Serpentine	0.0	12.4	14.1	0.24	0.0	2.7	5.5	0.0	64.1	0.0	0.5	0.0	0.0	0.02	0.00	0.06	0.06	0.00	0.33	100.0

Hole ID	Depth (m)	Regolith Unit	Kaolinite	Opal/Qtz	Fe-oxides	Illite	Nontronite	Saponite	Chlorite	Talc	Serpentine	Magnesite	Dolomite	Calcite	Gibbsite	Bassanite	Alunite	Chromite	Rutile	Apatite	Asbolan	% Total
ARC0791																						
39316	1	Kaolininite	23.4	5.4	67.0	1.60	0.4	0.0	0.0	0.0	0.0	0.9	0.0	0.0	0.0	0.13	0.00	0.45	0.45	0.08	0.10	100.0
39321	5	Kaolininite	17.3	15.7	59.0	1.37	3.6	0.0	0.0	0.0	0.0	1.4	0.8	0.0	0.0	0.07	0.00	0.29	0.29	0.08	0.12	100.0
39322	6	Nontronite	4.8	50.2	34.0	1.95	5.3	0.0	2.7	0.0	0.0	0.0	0.6	0.0	0.0	0.02	0.00	0.09	0.09	0.02	0.17	100.0
39324	8	Nontronite	0.0	69.7	13.7	1.56	12.6	0.0	1.3	0.0	0.0	0.8	0.0	0.0	0.0	0.08	0.04	0.01	0.01	0.00	0.27	100.0
39325	9	Nontronite	0.0	75.1	11.9	1.47	8.7	0.0	0.0	0.0	0.0	1.4	1.0	0.0	0.0	0.10	0.00	0.00	0.00	0.00	0.37	100.0
39328	11	Nontronite	0.0	77.5	11.2	0.96	8.2	0.0	0.2	0.0	0.0	1.5	0.0	0.0	0.0	0.08	0.01	0.00	0.00	0.00	0.32	100.0
39329	12	Nontronite	0.0	66.6	20.9	1.27	5.9	0.0	0.0	0.0	0.0	3.2	0.0	0.0	0.0	0.05	0.15	0.00	0.00	0.00	1.95	100.0
39334	17	Nontronite	0.0	64.6	10.0	0.48	13.9	0.0	0.2	0.0	0.0	9.8	0.0	0.0	0.0	0.05	0.19	0.01	0.01	0.00	0.70	100.0
39336	19	Nontronite	0.0	59.8	11.9	0.67	13.5	0.0	2.2	0.0	0.0	11.3	0.0	0.0	0.0	0.05	0.13	0.04	0.04	0.00	0.37	100.0
39337	20	Nontronite	0.0	15.5	8.9	0.69	13.6	0.0	3.4	0.0	0.0	57.2	0.1	0.0	0.0	0.17	0.00	0.07	0.07	0.01	0.27	100.0
39339	22	Nontronite	0.0	9.8	7.3	0.70	9.1	0.0	1.7	0.0	0.0	70.6	0.3	0.0	0.0	0.13	0.00	0.02	0.02	0.00	0.44	100.0
39341	24	Nontronite	0.0	5.2	5.3	0.58	11.7	0.0	2.2	0.0	0.0	74.3	0.3	0.0	0.0	0.18	0.00	0.03	0.03	0.00	0.25	100.0
39342	25	Nontronite	0.0	1.8	2.8	0.35	7.0	0.0	1.0	0.0	0.0	86.2	0.6	0.0	0.0	0.11	0.00	0.00	0.00	0.00	0.16	100.0
39346	29	Nontronite	0.0	52.3	4.9	0.48	4.0	0.0	0.3	0.0	0.0	37.3	0.4	0.0	0.0	0.05	0.00	0.00	0.00	0.00	0.15	100.0
39351	33	Nontronite	0.0	32.1	4.6	0.35	3.9	0.0	0.5	0.0	0.0	57.0	1.3	0.0	0.0	0.06	0.00	0.00	0.00	0.00	0.14	100.0
ARC0607																						
32096	1	Talc	6.7	44.3	8.5	4.28	0.0	7.3	14.1	10.4	0.0	0.0	2.1	0.0	0.0	1.34	0.00	0.38	0.38	0.06	0.10	100.0
32097	2	Talc	0.5	11.7	4.8	1.89	0.0	13.5	7.2	32.6	0.0	0.0	26.4	0.0	0.0	0.89	0.00	0.14	0.14	0.02	0.12	100.0
32098	3	Talc	0.0	11.0	5.4	1.40	0.0	14.1	6.6	29.6	0.0	0.0	31.3	0.0	0.0	0.28	0.00	0.12	0.12	0.02	0.09	100.0
32099	4	Talc	4.9	44.6	9.9	6.95	0.0	24.3	0.0	0.0	0.0	0.0	5.2	3.1	0.0	0.31	0.00	0.19	0.19	0.03	0.24	100.0
32101	6	Talc	0.1	3.7	6.9	7.61	0.0	15.6	5.8	49.5	0.0	0.0	10.2	0.0	0.0	0.09	0.00	0.15	0.15	0.01	0.14	100.0
32104	9	Talc	1.3	44.4	8.9	6.20	0.0	21.2	5.1	6.6	0.0	0.0	5.6	0.0	0.0	0.12	0.00	0.18	0.18	0.03	0.09	100.0
ARC0606																						
32079	1	Talc	5.5	8.5	45.8	1.42	0.0	0.8	18.4	12.3	0.0	0.0	5.5	0.0	0.0	0.11	0.00	0.74	0.74	0.12	0.17	100.0
32080	2	Talc	0.0	0.0	5.9	0.24	0.0	1.1	5.4	47.1	0.0	16.5	23.5	0.0	0.0	0.03	0.00	0.06	0.06	0.02	0.13	100.0
32083	4	Talc	0.0	0.0	8.0	0.36	0.0	2.3	6.0	44.8	0.0	34.2	4.0	0.0	0.0	0.01	0.00	0.07	0.07	0.02	0.15	100.0
32087	8	Talc	0.0	0.0	8.9	0.87	0.0	8.7	5.1	54.0	0.0	17.2	4.8	0.0	0.0	0.06	0.00	0.07	0.07	0.02	0.22	100.0
32089	10	Talc	0.0	0.0	7.3	0.36	0.0	4.1	6.2	46.7	0.0	28.2	6.8	0.0	0.0	0.03	0.00	0.07	0.07	0.01	0.20	100.0
32092	13	Talc	0.0	0.0	6.5	0.48	0.0	6.8	5.3	44.7	0.0	21.3	14.5	0.0	0.0	0.04	0.00	0.06	0.06	0.01	0.18	100.0
32095	16	Talc	0.0	0.0	7.2	0.73	0.0	9.2	5.0	41.3	0.0	30.9	5.2	0.0	0.0	0.05	0.00	0.07	0.07	0.02	0.20	100.0
ARC0231																						
3908	1	Kaolinite	13.3	40.5	8.5	4.20	5.1	0.0	0.0	0.0	0.0	0.0	14.7	12.2	0.0	0.16	0.00	0.49	0.49	0.06	0.16	100.0
3909	2	Kaolinite	7.1	26.6	4.6	2.14	14.1	0.0	0.0	0.0	0.0	0.0	43.1	1.4	0.0	0.43	0.00	0.21	0.21	0.02	0.19	100.0
3910	3	Kaolinite	10.6	19.0	8.2	2.32	12.2	0.0	0.0	0.0	0.0	0.0	31.4	0.1	0.0	14.61	0.00	0.28	0.28	0.01	0.91	100.0
3911	4	Nontronite	0.0	11.5	3.6	2.48	45.7	0.0	27.1	0.0	0.0	2.9	4.0	0.0	0.0	1.25	0.00	0.43	0.43	0.01	0.80	100.0
3912	5	Nontronite	4.9	16.3	9.3	3.05	41.2	0.0	18.6	0.0	0.0	0.0	3.5	0.0	0.0	1.00	0.00	0.44	0.44	0.00	1.21	100.0
3916	8	Nontronite	6.6	6.3	7.1	2.90	52.8	0.0	19.3	0.0	0.0	0.0	0.7	0.0	0.0	1.02	0.00	0.49	0.49	0.01	2.32	100.0
3919	11	Nontronite	19.8	4.3	10.0	1.86	51.8	0.0	2.2	0.0	0.0	5.8	0.0	0.0	0.0	0.33	0.73	0.46	0.46	0.00	2.32	100.0
3923	15	Nontronite	24.6	11.5	8.3	2.21	32.7	0.0	0.3	0.0	0.0	18.8	0.0	0.0	0.0	0.24	0.23	0.53	0.53	0.00	0.12	100.0
3924	16	Talc	11.1	23.9	15.2	1.67	0.0	32.2	14.5	0.0	0.0	0.0	0.0	0.0	0.0	0.14	0.26	0.49	0.49	0.00	0.11	100.0
3927	19	Talc	2.0	5.4	10.4	1.03	0.0	18.5	20.7	41.1	0.0	0.0	0.0	0.0	0.0	0.14	0.00	0.34	0.34	0.00	0.09	100.0

Hole ID	Depth (m)	Regolith Unit	Kaolinite	Opal/Qtz	Fe-oxides	Illite	Nontronite	Saponite	Chlorite	Talc	Serpentine	Magnesite	Dolomite	Calcite	Gibbsite	Bassanite	Alunite	Chromite	Rutile	Apatite	Asbolan	% Total
ARC0789																						
39268	1	Nontronite	0.2	48.5	3.9	1.17	5.5	0.0	3.6	0.0	0.0	0.0	36.6	0.0	0.0	0.17	0.00	0.07	0.07	0.01	0.20	100.0
39270	3	Nontronite	0.0	78.9	7.7	0.47	4.8	0.0	1.5	0.0	0.0	2.0	4.3	0.0	0.0	0.13	0.00	0.01	0.01	0.00	0.17	100.0
39272	5	Nontronite	0.0	66.5	9.4	0.56	8.4	0.0	0.7	0.0	0.0	14.0	0.0	0.0	0.0	0.11	0.02	0.01	0.01	0.00	0.32	100.0
39273	6	Nontronite	0.0	58.2	8.5	1.27	16.3	0.0	0.7	0.0	0.0	14.2	0.0	0.0	0.0	0.19	0.05	0.02	0.02	0.00	0.43	100.0
39276	9	Nontronite	0.0	65.1	17.1	1.16	5.9	0.0	0.0	0.0	0.0	9.6	0.0	0.0	0.0	0.05	0.39	0.00	0.00	0.00	0.71	100.0
39277	10	Nontronite	0.0	78.6	11.7	1.11	2.2	0.0	0.0	0.0	0.0	5.6	0.0	0.0	0.0	0.05	0.35	0.00	0.00	0.00	0.40	100.0
39280	13	Nontronite	0.0	56.2	16.5	0.79	10.8	0.0	0.0	0.0	0.0	14.9	0.0	0.0	0.0	0.05	0.22	0.01	0.01	0.00	0.44	100.0
39282	15	Nontronite	0.0	72.2	9.0	0.69	3.8	0.0	0.0	0.0	0.0	14.0	0.0	0.0	0.0	0.03	0.10	0.00	0.00	0.00	0.15	100.0
39283	16	Nontronite	0.0	85.3	8.1	0.73	0.0	0.0	0.0	0.0	0.0	5.7	0.0	0.0	0.0	0.05	0.08	0.00	0.00	0.00	0.11	100.0
39285	18	Nontronite	0.0	81.1	10.5	1.05	0.0	0.0	0.0	0.0	0.0	7.0	0.0	0.0	0.0	0.05	0.05	0.00	0.00	0.00	0.20	100.0
39286	19	Nontronite	0.0	48.4	4.3	0.70	3.6	0.0	0.0	0.0	0.0	42.1	0.7	0.0	0.0	0.09	0.00	0.00	0.00	0.00	0.15	100.0
39287	20	Nontronite	0.0	17.5	3.7	0.23	0.5	0.0	0.0	0.0	0.0	77.4	0.5	0.0	0.0	0.05	0.00	0.00	0.00	0.00	0.10	100.0
ARC0126																						
106258	1	Saponite	4.3	23.0	5.5	2.05	0.0	8.4	0.0	0.0	0.0	0.0	46.7	7.9	0.0	1.89	0.00	0.13	0.13	0.01	0.07	100.0
106259	2	Saponite	0.0	41.2	16.7	1.70	0.0	18.8	4.5	0.0	0.0	10.1	4.6	0.0	0.0	0.89	0.00	0.09	0.09	0.00	1.24	100.0
106260	3	Saponite	0.0	37.3	10.8	1.40	0.0	23.5	4.0	0.0	0.0	21.3	0.8	0.0	0.0	0.23	0.00	0.08	0.08	0.00	0.59	100.0
106262	5	Saponite	3.1	32.2	17.9	2.03	0.0	42.5	0.0	0.0	0.0	0.0	0.0	0.0	0.0	0.48	0.41	0.12	0.12	0.00	1.16	100.0
106266	9	Serpentine	0.0	22.9	19.2	1.46	0.0	38.4	3.4	0.0	13.3	0.0	0.0	0.0	0.0	0.26	0.38	0.10	0.10	0.00	0.43	100.0
106267	10	Serpentine	0.0	16.9	20.7	0.75	0.0	38.8	3.0	0.0	17.8	0.0	0.0	0.0	0.0	0.33	0.76	0.10	0.10	0.00	0.74	100.0
106270	13	Serpentine	0.0	13.0	20.2	1.34	0.0	41.0	5.2	0.0	17.5	0.0	0.0	0.0	0.0	0.60	0.30	0.12	0.12	0.00	0.68	100.0
106274	17	Serpentine	0.0	18.3	20.3	1.57	0.0	37.2	5.8	0.0	15.5	0.0	0.0	0.0	0.0	0.59	0.10	0.13	0.13	0.00	0.36	100.0
ARC0128																						
106294	1	Pres. Serp.	42.8	3.7	47.3	1.05	2.7	0.0	0.0	0.0	0.7	0.0	0.3	0.0	0.0	0.29	0.00	0.55	0.55	0.05	0.07	100.0
106297	4	Kaolinite	42.0	0.1	49.0	1.19	5.2	0.0	0.0	0.0	0.0	0.6	0.6	0.0	0.0	0.17	0.00	0.48	0.48	0.06	0.10	100.0
106299	6	Kaolinite	13.8	3.4	60.4	1.09	12.1	0.0	0.0	0.0	0.0	1.8	6.5	0.0	0.0	0.24	0.00	0.23	0.23	0.04	0.12	100.0
106300	7	Nontronite	3.6	51.8	19.1	1.29	19.7	0.0	3.9	0.0	0.0	0.0	0.2	0.0	0.0	0.28	0.00	0.08	0.08	0.00	0.09	100.0
106301	8	Nontronite	7.0	14.5	20.9	2.82	45.0	0.0	8.7	0.0	0.0	0.0	0.0	0.0	0.0	0.47	0.11	0.25	0.25	0.00	0.09	100.0
106305	12	Nontronite	11.4	4.2	36.3	1.69	32.4	0.0	12.6	0.0	0.0	0.0	0.0	0.0	0.0	0.24	0.15	0.33	0.33	0.00	0.37	100.0
106306	13	Nontronite	2.1	4.9	24.3	1.90	46.8	0.0	17.5	0.0	0.0	0.0	0.0	0.0	0.0	0.28	0.33	0.29	0.29	0.00	1.35	100.0
106308	15	Nontronite	0.0	5.3	7.7	0.54	46.8	0.0	7.9	0.0	0.0	29.0	0.0	0.0	0.0	0.26	0.73	0.15	0.15	0.00	1.49	100.0
106309	16	Nontronite	0.0	31.2	7.3	0.86	38.2	0.0	9.0	0.0	0.0	11.7	0.0	0.0	0.0	0.20	0.63	0.15	0.15	0.00	0.64	100.0
106312	19	Nontronite	0.0	17.2	10.3	1.57	36.7	0.0	9.6	0.0	0.0	23.0	0.1	0.0	0.0	0.51	0.00	0.15	0.15	0.00	0.70	100.0
106236	20	Serpentine	0.0	0.2	13.0	1.05	0.0	36.7	3.9	0.0	42.8	0.0	1.2	0.0	0.0	0.55	0.00	0.09	0.09	0.00	0.53	100.0

Appendix 6. Table A6.3. Normative mineral abundances for the channel clay regolith unit for MM2.

Hole ID	Depth (m)	Regolith Unit	Kaolinite	Opal-Si/	Iron Oxides	Vermiculite	Nontronite	Illite	Muscovite	Plagioclase	Magnesite	Dolomite	Calcite	Chromite	Rutile	Apatite	Asbolan	CIPW % Total
CBRC0721																		
26821	1	Chnl Clays	37.80	43.40	4.79	3.28	0.00	0.00	1.31	1.40	0.00	0.00	7.26	0.07	0.63	0.04	0.04	100.0
26822	2	Chnl Clays	52.03	36.96	4.87	2.03	0.00	0.00	0.69	1.30	0.00	0.00	1.18	0.05	0.83	0.02	0.04	100.0
26825	5	Chnl Clays	52.85	38.73	5.43	0.75	0.00	0.00	0.43	0.86	0.00	0.00	0.22	0.02	0.67	0.01	0.03	100.0
26826	6	Chnl Clays	55.72	33.99	5.97	0.99	0.00	0.00	1.03	1.49	0.00	0.00	0.00	0.04	0.73	0.01	0.02	100.0
26831	11	Chnl Clays	37.22	47.52	1.22	2.46	0.00	0.00	8.64	2.23	0.00	0.00	0.00	0.07	0.61	0.01	0.01	100.0
26832	12	Chnl Clays	41.98	32.14	3.78	5.59	0.00	0.00	5.64	9.80	0.00	0.00	0.00	0.19	0.82	0.03	0.03	100.0
26833	13	Chnl Clays	29.84	29.49	5.08	5.98	0.00	0.00	9.17	19.45	0.00	0.00	0.00	0.10	0.80	0.05	0.04	100.0
26834	14	Chnl Clays	33.98	16.36	11.19	8.50	0.00	0.00	10.48	18.02	0.00	0.00	0.00	0.26	1.02	0.16	0.04	100.0
26835	15	Chnl Clays	27.96	19.26	10.33	10.96	0.00	0.00	8.13	21.92	0.00	0.00	0.00	0.35	0.89	0.14	0.04	100.0
26836	16	Chnl Clays	33.79	21.28	11.47	12.34	0.00	0.00	10.06	9.57	0.00	0.00	0.00	0.35	0.91	0.17	0.06	100.0
26840	19	Chnl Clays	17.74	34.98	5.48	4.21	0.00	0.00	10.27	26.56	0.00	0.00	0.00	0.03	0.58	0.10	0.05	100.0
26841	20	Chnl Clays	13.69	42.27	7.85	3.90	0.00	0.00	24.30	7.13	0.00	0.00	0.00	0.03	0.63	0.15	0.06	100.0
26844	23	Chnl Clays	23.23	40.33	10.03	3.74	0.00	0.00	11.37	10.32	0.00	0.00	0.00	0.01	0.62	0.26	0.08	100.0
26846	25	Chnl Clays	30.06	31.59	15.43	8.36	0.00	0.00	7.79	5.12	0.00	0.00	0.00	0.04	1.32	0.18	0.13	100.0
26847	26	Chnl Clays	22.55	41.19	9.53	6.31	0.00	0.00	15.75	3.61	0.00	0.00	0.00	0.02	0.71	0.23	0.11	100.0
26850	29	Chnl Clays	12.44	42.69	7.83	7.30	0.00	0.00	26.48	2.35	0.00	0.00	0.00	0.01	0.63	0.15	0.13	100.0
26853	32	Chnl Clays	18.63	43.75	7.97	7.79	0.00	0.00	18.28	2.84	0.00	0.00	0.00	0.01	0.52	0.12	0.10	100.0
26854	33	Chnl Clays	21.14	44.30	5.98	8.34	0.00	0.00	16.39	3.11	0.00	0.00	0.00	0.01	0.52	0.06	0.17	100.0
26857	36	Chnl Clays	5.48	39.53	5.80	4.98	0.00	0.00	20.61	22.42	0.00	0.00	0.00	0.02	0.52	0.39	0.24	100.0
CBRC1384																		
60792	1	Chnl Clays	26.01	49.93	8.05	3.95	0.00	0.00	4.95	4.42	0.00	0.00	1.80	0.25	0.50	0.10	0.05	100.0
60795	4	Chnl Clays	28.30	32.36	8.78	6.88	0.00	0.00	4.23	16.31	0.00	0.00	2.12	0.26	0.62	0.05	0.08	100.0
60796	5	Chnl Clays	33.29	31.25	8.67	6.73	0.00	0.00	4.63	7.98	0.00	0.00	6.34	0.27	0.76	0.03	0.04	100.0
60798	7	Chnl Clays	26.45	21.31	14.73	2.23	0.00	0.00	4.06	29.75	0.00	0.00	0.00	0.06	1.30	0.03	0.07	100.0
60799	8	Chnl Clays	6.47	18.75	14.08	8.79	0.00	0.00	3.83	46.50	0.00	0.00	0.00	0.04	1.37	0.03	0.14	100.0
60801	10	Chnl Clays	0.00	16.75	12.67	15.07	0.00	0.00	3.50	46.03	0.00	0.00	4.40	0.05	1.31	0.03	0.20	100.0
60803	12	Chnl Clays	0.00	16.31	8.40	22.24	0.00	0.00	11.91	32.27	0.00	0.00	7.56	0.14	0.73	0.27	0.17	100.0
CBRC1395																		
66041	1	Chnl Clays	24.73	35.55	29.75	1.54	0.00	0.00	5.01	1.14	0.00	0.00	0.46	0.84	0.71	0.13	0.14	100.0
66042	2	Chnl Clays	26.25	58.28	5.32	1.28	0.00	0.00	6.16	1.39	0.00	0.00	0.75	0.05	0.45	0.04	0.03	100.0
66043	3	Chnl Clays	31.13	45.03	4.02	1.93	0.00	0.00	4.64	0.60	0.00	0.00	12.06	0.02	0.52	0.04	0.01	100.0
66045	5	Chnl Clays	37.85	49.11	4.28	2.18	0.00	0.00	2.76	0.35	0.00	0.00	2.82	0.01	0.58	0.05	0.01	100.0
66047	7	Chnl Clays	21.48	43.53	7.26	2.76	0.00	0.00	16.81	7.46	0.00	0.00	0.00	0.01	0.64	0.04	0.02	100.0
66050	10	Chnl Clays	28.80	47.43	5.36	3.18	0.00	0.00	10.46	4.10	0.00	0.00	0.00	0.01	0.55	0.09	0.01	100.0
66051	11	Chnl Clays	37.12	46.05	4.28	4.18	0.00	0.00	6.00	1.66	0.00	0.00	0.00	0.01	0.59	0.08	0.02	100.0
66052	12	Chnl Clays	22.27	46.21	7.00	5.85	0.00	0.00	14.73	3.24	0.00	0.00	0.00	0.01	0.61	0.06	0.03	100.0
66056	15	Chnl Clays	23.36	46.27	4.92	7.60	0.00	0.00	11.63	5.56	0.00	0.00	0.00	0.01	0.57	0.05	0.02	100.0
66057	16	Chnl Clays	0.00	40.72	5.41	14.53	0.00	0.00	14.00	24.59	0.00	0.00	0.11	0.01	0.55	0.04	0.03	100.0
66059	18	Chnl Clays	22.64	42.54	6.13	10.06	0.00	0.00	12.49	5.40	0.00	0.00	0.00	0.01	0.60	0.09	0.04	100.0
66060	19	Chnl Clays	31.87	35.60	8.57	12.17	0.00	0.00	4.98	5.85	0.00	0.00	0.00	0.01	0.69	0.20	0.05	100.0
66064	23	Chnl Clays	30.44	37.87	7.03	12.59	0.00	0.00	7.06	4.20	0.00	0.00	0.00	0.01	0.67	0.08	0.05	100.0
66068	27	Chnl Clays	21.06	37.46	6.38	10.63	0.00	0.00	4.93	18.48	0.00	0.00	0.00	0.01	0.62	0.37	0.08	100.0
66070	29	Chnl Clays	16.73	15.53	5.16	9.39	0.00	0.00	5.44	43.68	0.00	2.93	0.00	0.01	0.70	0.37	0.06	100.0
66071	30	Nontronite	24.99	33.40	0.21	0.00	2.29	28.98	0.00	0.00	4.59	4.64	0.00	0.01	0.48	0.38	0.03	100.0
66072	31	Nontronite	25.85	43.36	0.04	0.00	0.52	20.58	0.00	0.00	1.33	7.51	0.00	0.00	0.43	0.37	0.02	100.0
66074	33	Nontronite	32.26	57.88	2.53	0.00	1.92	4.02	0.00	0.00	0.60	0.00	0.00	0.01	0.41	0.31	0.05	100.0

APPENDIX 7: BULK AND PARTICLE DENSITY MEASUREMENTS, MM3.

Introduction

The bulk density and particle density of fragments and nodules of serpentinized cumulate from the serpentine unit of selected RC drill holes at MM3 were determined to provide a measure of the porosity of the weathered (*i.e.*, serpentinized) cumulate. At least eight, representative fragments or nodules of cumulate were handpicked from each bulk, one meter composite RC drill sample collected from the sample farm at MM3. Two each were used for the measurement of bulk density, particle density and two for determining the moisture content correction. Remaining cumulate fragments were kept in storage for reference purposes.

Bulk density

The bulk density of cumulate fragments were determined using the clod method described by Blake and Hartge (1986a), where bulk density p_b (g/cm^3) is given by the equation:

$$p_b = p_w W_{ods}/[W_{sa} - W_{spw} + W_{pa} - (W_{pa} p_w / p_p)]$$

where:

p_w = density of water at the temperature of determination.
W_{ods} = oven-dry weight of the sample (at 105° C).
W_{sa} = weight of uncoated sample in air.
W_{spw} = weight of wax coated sample in water.
W_{pa} = weight of wax coating in air.
p_p = density of paraffin wax, taken to be 0.91 g/cm^3.

Particle density

Particle density was determined using the pycnometer method described in Blake and Hartge (1986b) where particle density, p_p (g/cm^3) is given by the equation:

$$p_p = p_w (W_s - W_a)/[(W_s - W_a) - (W_{sw} - W_w)]$$

where:

p_w = density of water (g/cm^3) at the temperature of measurement.
W_s = weight of the pycnometer and sample (corrected to oven dry weight).
W_a = weight of the empty pycnometer.

W_{sw} = weight of the pycnometer, sample and water.

W_w = weight of the pycnometer (without sample) filled with water at the temperature of measurement.

Cumulate fragments and nodules were gently crushed in an agate mortar and pestle before determination of particle density, which, in most cases, were performed in duplicate.

Porosity

The porosity of the serpentinized cumulate nodules was calculated from measurements of bulk and particle densities by the method of Danielson and Sutherland (1986) from the equation:

$$S_t = (1-p_b/p_p) \times 100$$

where:

S_t = total porosity as a percentage.
p_b = bulk density (g/cm^3).
p_p = particle density (g/cm^3).

Limitations of the method

The cumulate nodules, hand-picked from each composite sample were small, generally about 1-2 g in weight, but were mostly 0.5 to 1.0 g in weight. These fragments, therefore, may not be representative of the cumulate comprising the serpentine unit from which they derive, and may only represent those nodules and fragments robust enough to have survived the drilling and recovery process. In addition, their small size may have introduced errors in determinations of particle density and, especially, bulk density.

As a test of the methodology, measurements of bulk and particle density were conducted on samples of diamond drill core. Samples from diamond drill core CBDD5 were collected from the major regolith units identified with enough material collected to enable duplicate measurements to be performed using samples each of mass 4 to 5 g. Results for bulk and particle densities, and sample porosity are presented in Table A7.1.

The very low standard deviation for measurements of bulk and particle density indicates that good sample precision can be obtained by the methods used. Values of bulk density, particularly for regolith towards the base of the profile (saprolite and smectite clay units) are comparable to bulk densities determined by Anaconda Nickel NL for the smectite zone (SM) and saprolite zone (SA) material. Bulk density values show a gradual increase from the bottom of the profile towards the surface where at the nontronite/kaolinite boundary a marked increase occurs. This is also indicated by a significant decrease in porosity and may indicate a partial collapse of the profile or is due to the illuviation of clay from upper portions of the profile.

Table A7.1. Bulk density, particle density and porosity of samples from diamond drill core CBDD5.

Sample depth (m)	Particle density (g/cm^3)	SD N=2	Bulk density (g/cm^3)	SD N=2	Porosity (%)	Regolith unit
3.8	2.97	0.08	2.18	0.01	27	Kaolinite
6.3	3.42	0.06	2.42	0.41	29	(FZ)*
8.3	2.94	0.26	2.79	0.36	5	
11.5	2.91	0.03	1.95	0.34	33	Smectite
13.5	2.86	0.00	1.91	0.08	33	
16.5	2.50	0.00	1.98	0.01	21	(SM)*
18	2.39	0.01	1.64	0.00	32	
23.3	2.63	0.03	1.63	0.02	38	Saprolite
31.5	2.84	0.05	1.76	0.08	38	(SA)*
38.6	2.73	0.04	1.58	0.15	42	
42.6	2.91	0.14	1.71	0.17	41	Saprock (UM)*

SD = standard deviation. N = number of samples.

* Profile logging terms used by Anaconda Nickel NL.

Porosity of serpentinized cumulate

Results for bulk density, particle density and porosity of serpentinized cumulate nodules from the serpentine unit of selected RC drill holes in MM3 are presented in Table A7.2. Values of porosity were plotted against values of the N/Ni+Al ratio for the serpentine unit of each drill hole (Fig. A7.1). The Ni/Ni+Al ratio has been used as a means of discriminating olivine cumulate (*i.e.*, ortho-, meso-, adcumulate) lithologies in fresh rock (Hill *et al.*, 1996). It has been used in this study to determine if there is a difference in porosity due to textural differences in the packing of serpentinized olivine grains preserved in the cumulate.

A general increase in porosity is shown with increasing Ni/Ni+Al values (Fig. A7.1.). The result is expected as the tightly packed, interconnecting nature of serpentinized olivine grains within adcumulates would likely result in a greater porosity than shown by orthocumulates, which consist

Appendix 7. Table A7.2. Bulk density, particle density and porosity data of serpentine for selected RC drill holes in MM3.

Hole ID (depth m)	Particle density (g/cm3)	SD	Bulk density (g/cm3)	SD	Porosity (%)
ARC0793					
21	2.22	0.68 (N=2)	2.15	0 (N=2)	**3.2**
22	2.38	0.42 (N=2)	1.7	0.21 (N=2)	**28.5**
23	2.26	0.03 (N=2)	1.61	0.09 (N=2)	**28.8**
24	2.41	0.16 (N=2)	1.63	0.02 (N=2)	32.5
25	2.18	(N=1)	1.5	(N=1)	31.2
26	2.39	(N=1)	1.56	(N=1)	34.7
27	2.46	(N=1)	1.88	0.16 (N=2)	23.6
ARC0786					
12	2.52	0.10 (N=2)	2.48	0.15 (N=6)	1.5
13	2.52	0.03 (N=2)	2.51	0.19 (N=6)	0.4
14	2.61	0.00 (N=2)	2.49	0.11 (N=6)	4.6
15	2.49	0.14 (N=2)	2.48	0.04 (N=6)	0.5
ARC0776					
10	2.43	0.20 (N=2)	1.61	0.36 (N=2)	33.6
11	2.46	0.26 (N=2)	2.1	0.08 (N=2)	**14.7**
12	2.48	0.19 (N=2)	1.91	0.11 (N=2)	**22.9**
13	2.50	0.06 (N=2)	1.76	0.19 (N=2)	29.7
14	2.73	0.39 (N=2)	1.51	0.12 (N=2)	44.7
15	2.36	0.00 (N=2)	1.79	0.38 (N=2)	24.1
ARC1008					
16	2.62	0.04 (N=2)	1.59	0.08 (N=2)	39.4
17	2.83	0.23 (N=2)	1.7	0.07 (N=4)	**40.0**
18	2.60	0.11 (N=2)	1.47	0.04 (N=2)	**43.4**
19	2.69	0.09 (N=2)	1.7	0.07 (N=3)	**36.7**
20	2.56	0.04 (N=2)	1.85	0.06 (N=4)	27.8
21	2.59	0.01 (N=2)	1.89	0.06 (N=4)	27.0
22	2.70	0.09 (N=2)	2.06	0.48 (N=4)	23.8
23	2.86	0.38 (N=2)	1.86	0.03 (N=4)	34.9
24	2.47	0.10 (N=2)	1.83	0.11 (N=4)	25.8
25	2.62	0.00 (N=2)	2	0.08 (N=4)	23.6
26	2.60	0.06 (N=2)	2.09	0.04 (N=4)	19.8
27	2.61	0.05 (N=2)	2.04	0.08 (N=4)	21.8

Hole ID (depth m)	Particle density (g/cm3)	SD	Bulk density (g/cm3)	SD	Porosity %
ARC0783					
11	2.55	0.05 (N=-2)	2.64	1.34 (N=2)	**-3.4**
12	2.65	0.00 (N=2)	1.5	0.10 (N=3)	43.3
13	2.78	0.13 (N=2)	1.53	0.12 (N=3)	**45.0**
14	2.61	0.09 (N=2)	1.48	0.07 (N=3)	43.4
15	2.57	0.01 (N=2)	1.79	0.07 (N=2)	30.4
ARC0126					
9	2.51	(N=1)	1.02	0.19 (N=2)	**59.4**
10	3.00	0.24 (N=2)	1.36	0.03 (N=2)	54.6
11	2.73	0.07 (N=2)	1.35	0.11 (N=2)	50.6
12	2.57	0.01 (N=2)	1.4	0.07 (N=2)	45.6
13	2.76	0.02 (N=2)	1.33	0.07 (N=2)	51.8
14	2.65	0.09 (N=2)	1.52	0.18 (N=2)	42.5
15	2.68	0.06 (N=2)	1.41	0.11 (N=2)	47.4
16	2.76	0.32 (N=2)	1.53	0.04 (N=2)	44.6
17	2.59	0.07 (N=2)	1.56	0.05 (N=2)	39.8

Hole ID (depth m)	Particle density (g/cm3)	SD	Bulk density (g/cm3)	SD	Porosity %
ARC0782					
16	2.55	0.05 (N=2)	1.56	0.10 (N=2)	38.7
17	2.57	0.13 (N=2)	1.85	0.26 (N=2)	28.0
18	2.52	0.25 (N=2)	1.61	0.08 (N=2)	**36.1**
19	2.29	0.25 (N=2)	1.57	0.09 (N=2)	31.3
20	2.43	0.22 (N=2)	1.54	0.03 (N=2)	36.7
21	2.63	00.12 (N=2)	1.69	0.06 (N=2)	35.9

SD = Standard deviation. N = Number of replilcate samples. Samples where the porosity is highlighted in bold were not included in further analysis because of marked differences in their %MgO contents. Only samples with similar %MgO contents within the serpentine unit of each drill hole were plotted in Figure A7.1. This was to ensure that for each drill hole, samples for each meter interval of the serpentine unit had a similar degree of weathering. For example, the presence of magnesite, which would adversely affect measurements of porosity, may be indicated by an increase in %MgO content.

of fewer, isolated olivine grains floating within an intercumulus matrix. The result, however, is not unequivocal. Further analysis is required on a larger number of samples with a more even distribution of Ni/Ni+Al values, particularly for Ni/Ni+Al ratios of < 0.2 and > 0.4, before a definitive conclusion can be established.

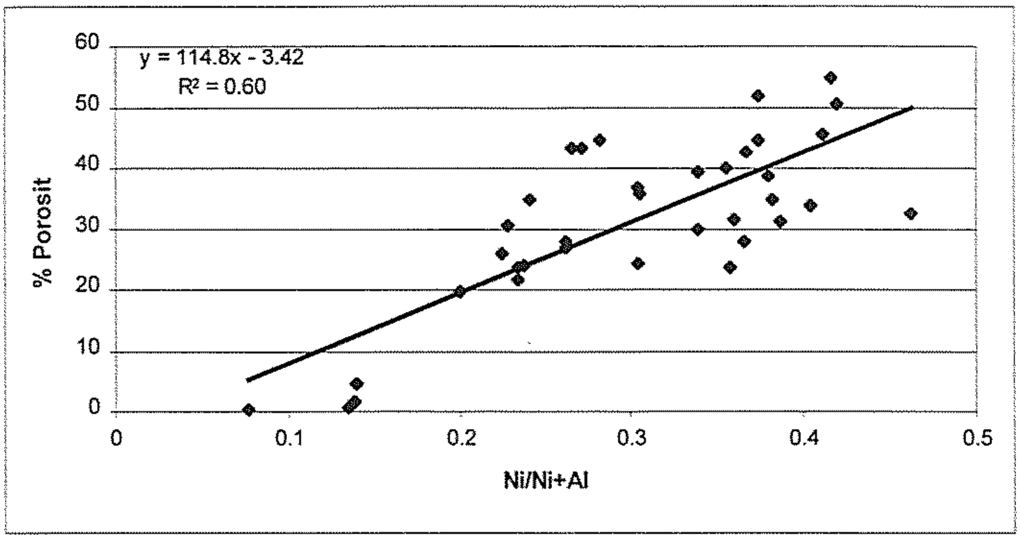

Figure A7.1. Porosity of nodules of serpentinized, olivine cumulate versus the Ni/Ni+Al ratio of the serpentine unit of RC drill holes presented in Table A7.2. Values of the Ni/Ni+Al ratio were calculated from the geochemical data supplied by Anaconda Nickel NL for these drill holes. Only porosity values for those samples with comparable %MgO values within each drill hole are shown (*i.e.*, samples in Table A7.2 with values of porosity highlighted in bold were not plotted). This was to ensure that only serpentine units with a similar degree of 'weathering' were compared.

References

Blake, G.R. and Hartge, K.H. 1986a. Bulk density. In: A. Klute (Editor) Methods of soil analysis. Part 1: Physical and mineralogical methods. 2nd edition. Soil Science Society of America, Inc., Madison, Wisconsin, USA. 363-376pp.

Blake, G.R. and Hartge, K.H. 1986b. Particle density. In: A. Klute (Editor) Methods of soil analysis. Part 1: Physical and mineralogical methods. 2nd edition. Soil Science Society of America, Inc., Madison, Wisconsin, USA. 377-382pp.

Danielson, R.E. and Sutherland, P.L. 1986. Porosity. In: A. Klute (Editor) Methods of soil analysis. Part 1: Physical and mineralogical methods. 2nd edition. Soil Science Society of America, Inc., Madison, Wisconsin, USA. 443-462pp.

APPENDIX 8: MASS BALANCE, MM2 AND MM3

Introduction

Major element (*i.e.,* Si, Al, Fe and Mg) composition of the serpentine unit for drill holes in MM2 and MM3, as listed in Tables A8.1 and A8.2, respectively, are shown for values of the Ni/Ni+Al ratio in Figures A8.1 and A8.2. Values of the Ni/Ni+Al ratio have been used to discriminate cumulate lithologies (*i.e.,* ortho-, meso- and adcumulate) in fresh rock (Hill *et al.,* 1996). The same approach was used here to determine if major element compositions were related to the various cumulate types.

Examination of the major element chemistry was required to determine if an 'average' composition for the serpentine unit at both deposits could be obtained to provide a 'fresh rock' composition for those drill holes that did not show serpentine at depth. This is a requirement of the mass balance equation used (Section 1.11.6) and would otherwise have allowed examination of those drill holes that do not have a complete weathering profile (*i.e.,* serpentine at depth).

One limitation of this approach is that the serpentine unit at the base of each drill hole may not be truly representative of 'fresh' serpentinized ultramafic; drill holes were not deep enough to intersect fresh bedrock. In addition, mass balance calculations do not take into account any lateral mobilization of elements within the regolith.

Regolith chemistry

Although some degree of lithological discrimination was evident for drill holes at MM2 on the basis of their % Al_2O_3 contents, in general, the wide range in values of the major elements for the serpentine unit at both deposits (Figures A8.1 and A8.2) indicated that an 'average' composition could not be determined for this unit, as a whole, at either site particularly for drill holes at MM3. In addition, the results indicated that each drill hole needed be treated separately in the mass balance analysis.

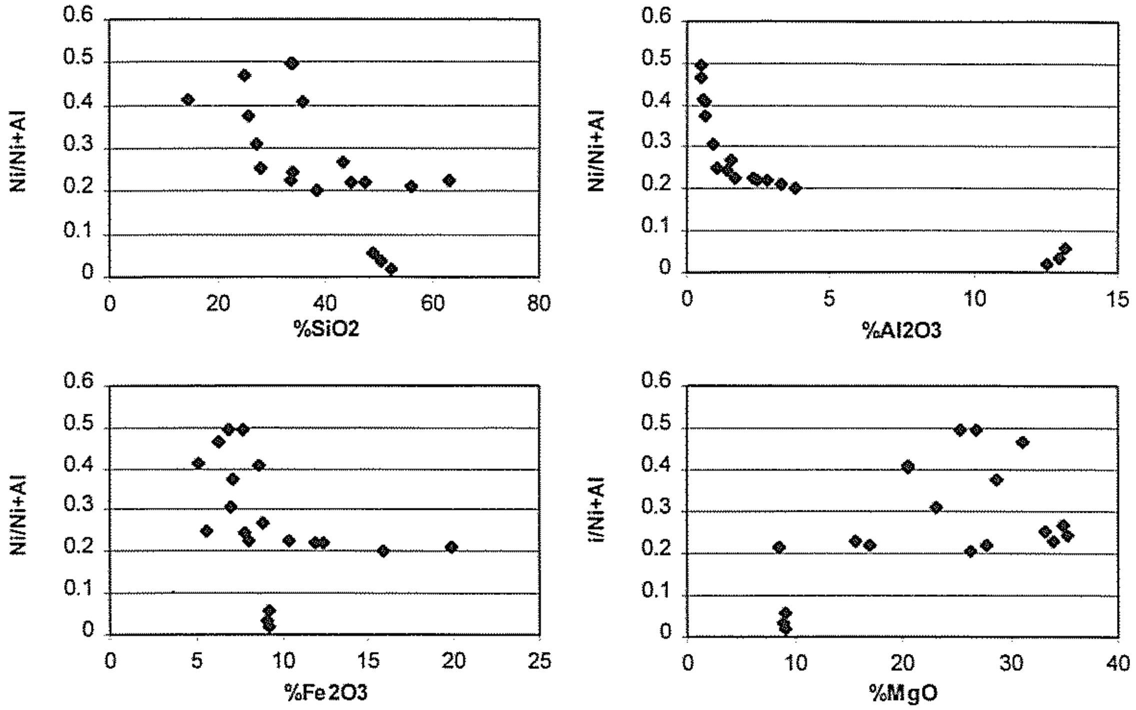

Figure A8.1. Weight % of Si, Al, Fe and Mg for Ni/Ni+Al values of serpentine units within drill holes at MM2. Results are for the XRF analysis of RC drill pulps (Section 1.11.4).

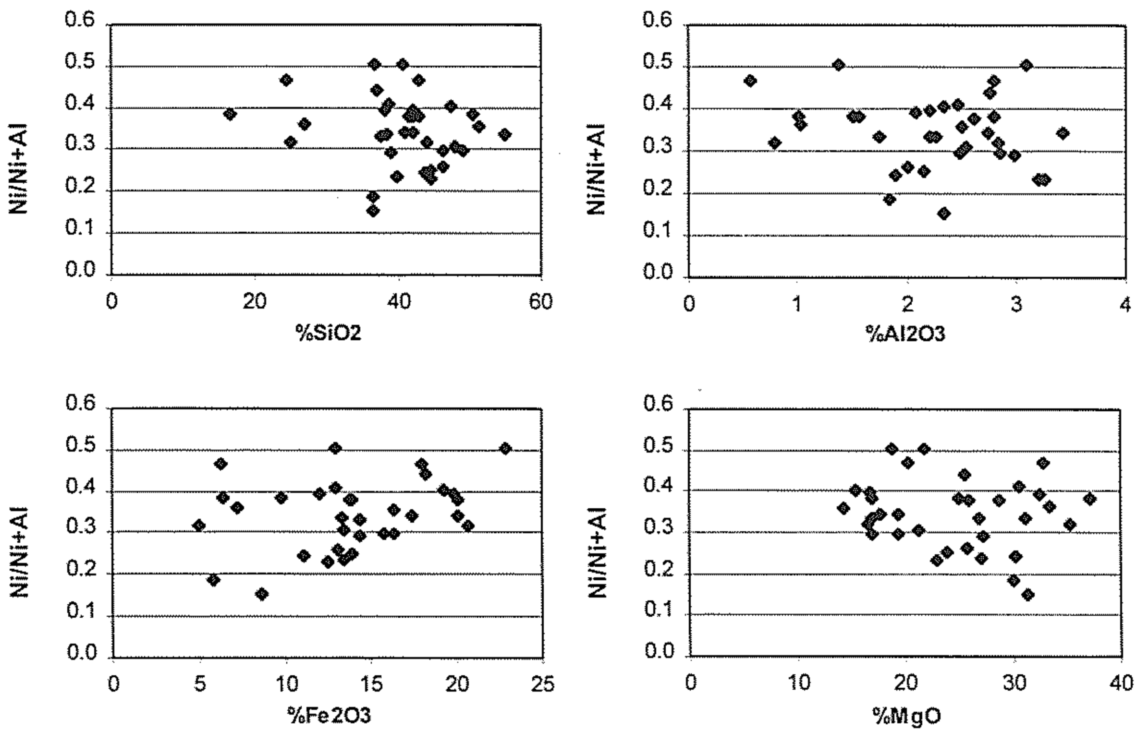

Figure A8.2. Weight % of Si, Al, Fe and Mg for Ni/Ni+Al values of serpentine units within drill holes at MM3. Results are for the XRF analysis of RC drill pulps (Section 1.11.4).

Appendix 8: Table A8.1. Cp/Cw ratios for Zr, Fe, Cr, Ti and Nb for RC drill holes at MM2.

Hole ID	Regolith Unit	Depth to (m)	Cp/Cw Zr	Fe	Ti	Cr	Nb
CBRC0780							
29168	Kaolinite-2	1	0.05	0.72	0.11	2.33	2.67
29170	Nontronite	3	0.24	0.55	0.36	0.87	2.67
29173	Nontronite	6	0.45	0.47	0.57	0.59	2.67
29175	Nontronite	7	0.41	0.42	0.37	0.20	2.67
29178	Nontronite	10	0.41	0.30	0.24	0.11	2.67
29179	Nontronite	11	0.28	0.33	0.25	0.11	2.67
29181	Nontronite	13	0.30	0.27	0.22	0.09	0.41
29184	Nontronite	16	0.31	0.36	0.27	0.09	0.59
29186	Saponite	17	0.50	0.40	0.38	0.11	1.33
29189	Saponite	20	0.38	0.68	0.77	0.21	0.89
29190	Saponite	21	0.45	0.60	0.74	0.29	2.67
29191	Saponite	22	0.90	0.59	0.71	0.29	2.67
29192	Saponite	23	0.56	0.44	0.45	0.35	2.67
29193	Saponite	24	0.38	0.38	0.39	0.30	2.67
29194	Saponite	25	0.56	0.55	0.52	0.36	2.67
29195	Saponite	26	0.64	0.64	0.74	0.44	2.67
29196	Saponite	27	0.45	0.76	0.88	0.56	2.67
29197	Saponite	28	1.50	0.70	0.79	0.49	2.67
29200	Saponite	31	0.75	0.79	1.04	0.45	2.67
29201	Saponite	32	1.00	1.16	1.59	0.76	2.67
29206	Saponite	37	1.13	1.33	2.78	0.83	2.67
29209	Saponite	40	0.69	1.14	1.52	0.65	0.89
29210	Saponite	41	0.90	0.95	1.28	0.52	2.67
29213	Saponite	44	0.45	0.64	0.66	0.46	2.67
29217	Saponite	47	0.75	1.13	1.61	1.12	2.67
	Serpentine*	>51	1.00	1.00	1.00	1.00	1.00
CBRC0744							
27467	Kaolinite-2	1	0.31	0.92	0.83	4.38	1.00
27471	Kaolinite-2	5	0.19	0.29	0.36	3.43	0.11
27474	Kaolinite-2	8	0.20	0.34	0.34	2.76	0.50
27475	Kaolinite-2	9	0.28	0.37	0.43	2.39	0.20
27476	Kaolinite-2	10	0.27	0.38	0.46	2.39	0.50
27478	Kaolinite-2	12	0.19	0.29	0.27	2.39	0.20
27480	Kaolinite-2	13	0.16	0.28	0.29	1.76	0.20
27481	Kaolinite-2	14	0.16	0.32	0.25	0.84	0.25
27482	Nontronite	15	0.30	0.53	0.41	0.60	1.00
27484	Nontronite	17	0.36	0.51	0.49	0.56	1.00
27486	Nontronite	19	0.34	0.53	0.47	0.65	1.00
27489	Nontronite	22	0.50	0.61	0.55	0.66	0.15
27490	Nontronite	23	0.38	0.63	0.62	0.72	1.00
27492	Nontronite	24	0.43	0.63	0.59	0.74	0.50
27493	Saponite	25	0.93	0.93	0.96	1.08	1.00
27496	Saponite	28	0.43	0.73	0.79	0.70	1.00
27499	Saponite	31	0.50	0.66	0.70	0.55	1.00
27500	Saponite	32	0.43	0.56	0.57	0.57	1.00
	Serpentine*	>33	1.00	1.00	1.00	1.00	1.00

Serpentine* = Indicates that Cp/Cw ratios have been calculated for averaged compositions of the serpentine regolith unit.

Appendix 8: Table A8.1. continued..

Hole ID	Regolith Unit	Depth to (m)	Cp/Cw Zr	Fe	Ti	Cr	Nb
CBRC0747							
27549	Kaolinite-2	1	0.20	0.29	0.34	0.47	0.44
27554	Kaolinite-2	6	0.26	0.34	0.23	0.37	1.75
27558	Kaolinite-2	9	0.35	0.33	0.22	0.78	1.75
27559	Kaolinite-2	10	0.61	0.35	0.31	0.54	0.29
27560	Kaolinite-2	11	0.92	0.39	0.42	0.58	1.75
27561	Talc	12	0.92	0.51	0.53	0.59	0.88
27563	Talc	14	0.39	0.26	0.19	0.34	0.25
27564	Talc	15	0.44	0.34	0.23	0.18	0.21
27566	Talc	17	0.39	0.40	0.20	0.10	0.17
27569	Talc	20	0.45	0.43	0.26	0.09	0.21
27570	Talc	21	2.44	1.56	1.44	1.06	1.75
27573	Talc	23	0.37	1.35	0.42	1.29	0.88
27574	Talc	24	0.13	1.06	0.16	0.50	1.75
27576	Talc	26	1.00	0.76	0.71	0.72	1.75
27579	Talc	29	0.65	0.63	0.50	0.60	0.35
27582	Serpentine	32	0.14	1.38	0.19	1.67	0.88
	Serpentine*	>33	1.00	1.00	1.00	1.00	1.00
CBRC0783							
29819	Nontronite	1	0.24	0.19	0.04	0.18	1.14
29821	Nontronite	3	0.25	0.15	0.03	0.14	0.29
29822	Nontronite	4	0.38	0.19	0.04	0.07	0.14
29824	Nontronite	6	0.80	0.33	0.13	0.25	0.38
29825	Saponite	7	0.54	0.28	0.07	0.10	1.14
29827	Saponite	9	0.54	0.36	0.06	0.07	0.23
29830	Saponite	12	0.49	0.47	0.07	0.10	1.14
29832	Saponite	13	0.58	0.52	0.07	0.06	1.14
29833	Serpentine	14	0.64	0.54	0.07	0.05	1.14
29835	Serpentine	16	2.14	0.55	0.09	0.04	1.14
29838	Serpentine	19	0.92	0.61	0.14	0.05	1.14
29839	Mixed serp.	20	0.80	0.93	0.21	0.12	1.14
29840	Mixed serp.	21	1.07	0.58	0.10	0.07	1.14
29841	Mixed serp.	22	0.58	0.60	0.10	0.16	0.57
29842	Mixed serp.	23	1.07	0.60	0.17	0.51	1.14
29845	Mixed serp.	26	2.14	0.66	0.14	0.59	1.14
29849	Mixed serp.	30	1.07	0.63	0.15	0.64	1.14
29850	Mixed serp.	31	0.80	0.78	0.29	0.83	0.38
29853	Mixed serp.	34	1.61	0.63	0.15	0.68	1.14
29858	Mixed serp.	38	3.21	0.79	0.77	0.94	1.14
29859	Mixed serp.	39	3.21	0.92	0.83	1.13	1.14
29861	Mixed serp.	41	0.92	0.81	0.91	1.00	1.14
	Serpentine*	>44	1.00	1.00	1.01	1.00	1.00

Serpentine* = Indicates that Cp/Cw ratios have been calculated for averaged compositions of the serpentine regolith unit.

Appendix 8: Table A8.2. Cp/Cw ratios for Zr, Fe, Ti, Cr and Nb for RC drill holes at MM3.

Hole ID	Regolith Unit	Depth to (m)	Cp/Cw Zr	Fe	Ti	Cr	Nb
ARC1257							
124360	Kaolinite	1	0.065	0.236	0.208	0.194	0.125
124362	Kaolinite	3	0.183	0.262	0.209	0.119	1.000
124364	Kaolinite	5	0.270	0.239	0.285	0.160	0.063
124365	Nontronite	6	0.630	0.378	0.542	0.382	1.000
124368	Nontronite	8	0.473	0.386	0.412	0.488	1.000
124370	Nontronite	10	0.515	0.410	0.444	0.495	1.000
124373	Nontronite	13	0.405	0.432	0.483	0.604	0.500
124375	Serpentine	15	0.567	0.559	0.689	0.836	1.000
124376	Serpentine	16	1.418	0.713	0.913	1.062	1.000
	Serpentine*	>18	1.001	1.000	0.996	1.000	1.000
ARC1478							
137424	Nontronite	1	0.171	0.498	0.387	0.781	0.100
137425	Nontronite	2	0.364	0.414	0.505	0.421	0.200
137426	Nontronite	3	0.566	0.446	0.614	0.425	0.333
137429	Nontronite	5	0.672	0.535	0.768	0.579	1.000
	Serpentine*	>6	1.000	1.000	1.003	1.000	1.000
ARC1008							
83610	Kaolinite	1	0.085	0.522	0.220	0.651	1.000
83612	Kaolinite	3	0.250	0.538	0.519	0.631	1.000
83613	Nontronite	4	0.375	0.347	0.458	0.620	1.000
83614	Nontronite	5	0.857	0.474	0.586	0.441	1.000
83617	Nontronite	8	0.353	0.406	0.400	0.354	0.250
83618	Nontronite	9	1.000	1.389	1.025	1.070	1.000
83619	Nontronite	10	0.375	0.294	0.335	0.292	0.250
83620	Nontronite	11	0.231	0.248	0.228	0.277	0.167
83623	Nontronite	14	0.462	0.465	0.418	0.448	1.000
83624	Serpentine	15	0.522	0.739	0.586	0.629	0.167
	Serpentine*	>18	1.000	1.000	1.006	1.000	1.000
ARC0776							
37749	Kaolinite	1	0.185	0.208	0.218	0.213	0.111
37750	Nontronite	2	0.313	0.305	0.326	0.230	0.091
37751	Nontronite	3	1.000	0.491	1.100	0.466	1.000
37755	Nontronite	6	0.500	0.418	0.377	0.128	1.000
37756	Nontronite	7	0.625	0.503	0.604	0.497	1.000
37758	Nontronite	9	0.455	0.710	0.753	0.769	1.000
	Serpentine*	>11	1.000	1.000	1.000	1.000	1.000
ARC0774							
37693	Nontronite	1	0.171	0.639	0.223	2.448	1.250
37694	Nontronite	2	0.298	0.499	0.425	2.066	1.250
37695	Nontronite	3	0.110	0.931	2.125	3.130	1.250
37696	Nontronite	4	2.500	1.503	4.857	4.679	1.250
37697	Nontronite	5	0.694	0.233	0.374	0.961	0.417
37700	Nontronite	8	1.042	0.291	0.810	1.607	1.250
37703	Nontronite	10	2.083	0.297	0.919	1.534	1.250
37704	Nontronite	11	2.083	1.845	22.667	8.820	1.250
37706	Nontronite	13	2.500	1.686	22.667	8.308	1.250
37709	Serpentine	16	2.083	0.953	1.360	1.225	1.250
	Serpentine*	>19	1.000	1.000	1.000	1.000	1.000

Serpentine* = Indicates that Cp/Cw ratios have been calculated for averaged compositions of the serpentine regolith unit.

Appendix 8: Table A8.2. continued..

Hole ID	Regolith Unit	Depth to (m)	Cp/Cw Zr	Fe	Ti	Cr	Nb
ARC0786							
37969	Talc	1	0.042	0.242	0.088	0.527	0.200
37970	Talc	2	0.042	0.380	0.100	0.719	0.111
37971	Talc	3	0.179	1.312	0.552	1.404	1.000
37974	Talc	6	1.000	1.141	1.176	1.057	1.000
37978	Talc	10	0.833	1.126	1.081	0.938	1.000
37979	Talc	11	0.556	0.987	0.976	0.879	0.500
37983	Serpentine	15	1.000	1.000	1.000	1.000	1.000
ARC0782							
37888	Kaolinite	1	0.074	0.385	0.172	0.545	0.102
37890	Kaolinite	3	0.303	0.426	0.552	0.599	0.140
37893	Kaolinite	5	0.385	0.638	1.525	1.223	1.330
37894	Saponite	6	0.833	0.734	1.368	1.333	1.330
37896	Saponite	8	0.526	0.821	0.735	0.243	0.266
37898	Saponite	10	0.227	0.656	0.324	0.817	0.665
37900	Saponite	12	0.500	1.052	0.830	2.106	1.330
37903	Saponite	15	0.556	0.748	0.689	0.809	0.266
	Serpentine*	>16	1.000	1.000	1.000	1.000	0.998
ARC0783							
37910	Kaolinite	1	0.174	0.379	0.312	0.397	0.283
37913	Nontronite	4	0.370	0.452	0.378	0.491	0.566
37914	Nontronite	5	0.538	0.398	0.487	0.495	2.830
37915	Nontronite	6	0.696	0.535	0.873	0.703	0.566
37916	Serpentine	7	2.367	0.781	1.202	0.939	2.830
	Serpentine*	>9	1.000	1.000	1.003	1.000	0.999
ARC0793							
39374	Kaolinite	1	0.095	0.333	0.165	0.388	0.167
39375	Kaolinite	2	0.143	0.263	0.150	0.307	1.000
39378	Kaolinite	5	0.167	0.340	0.172	0.225	0.080
39380	Kaolinite	7	0.194	0.304	0.165	0.257	0.500
39383	Kaolinite	10	0.343	0.258	0.183	0.127	0.080
39385	Kaolinite	11	0.529	0.240	0.277	0.122	0.094
39386	Nontronite	12	0.632	0.420	0.458	0.173	0.667
39389	Nontronite	15	0.500	0.644	0.439	0.257	1.000
39390	Nontronite	16	0.462	0.923	0.563	0.309	1.000
39391	Nontronite	17	0.146	0.771	0.171	0.350	0.500
39394	Nontronite	20	1.500	0.971	1.149	0.209	1.000
39396	Serpentine	22	3.000	1.069	1.500	0.235	1.000
39401	Serpentine*	27	1.000	1.000	1.000	1.000	1.000
ARC0126							
106258	Saponite	1	0.260	3.290	0.815	2.573	0.333
106259	Saponite	2	0.762	1.193	1.161	1.340	0.167
106260	Saponite	3	1.067	1.677	1.263	1.080	1.000
106262	Saponite	5	0.889	1.179	0.962	0.919	1.000
106266	Serpentine	9	3.556	1.045	1.202	0.915	0.500
	Serpentine*	>10	1.000	1.000	1.000	1.000	1.000

Serpentine* = Indicates that Cp/Cw ratios have been calculated for averaged compositions of the serpentine regolith unit.

Appendix 8: Table A8.2. continued..

Hole ID	Regolith Unit	Depth to (m)	Cp/Cw Zr	Fe	Ti	Cr	Nb
ARC0128							
106294	Kaol+serp	1	0.085	0.330	0.165	0.606	3.000
106297	Kaolinite	4	0.136	0.315	0.189	0.510	0.353
106299	Kaolinite	6	0.472	0.251	0.392	0.702	0.500
106300	Nontronite	7	0.944	0.610	1.111	1.209	0.750
106301	Nontronite	8	0.472	0.474	0.390	0.653	3.000
106305	Nontronite	12	0.425	0.339	0.283	0.528	3.000
106306	Nontronite	13	0.425	0.399	0.328	0.436	3.000
106308	Nontronite	15	1.700	0.595	0.537	0.685	0.600
106309	Nontronite	16	1.417	0.758	0.597	0.702	3.000
106312	Nontronite	19	0.607	0.625	0.541	0.738	3.000
106236	Serpentine	20	1.000	1.000	1.000	1.000	1.000

Serpentine* = Indicates that Cp/Cw ratios have been calculated for averaged compositions of the serpentine regolith unit.

Appendix 8: Table A8.3. Average composition of serpentine units in RC drill holes at MM2.

Hole ID		%SiO2	%Al2O3	%Fe2O3	%MgO	%CaO	%Na2O	%K2O	%TiO2	%Ni	%Co	Cr ppm	Mn ppm	Zn ppm	Zr ppm	Nb ppm
CBRC0780	Average	31.91	1.36	7.20	34.17	0.88	0.05	0.02	0.05	0.226	0.009	1677	790	42	5	3
	SD	3.42	0.31	1.34	1.05	0.08	0.01	0.00	0.02	0.036	0.002	306	199	10.8	2.2	3
	(N = 3)															
CBRC0744	Average	43.13	3.11	14.14	21.65	2.53	0.07	0.04	0.14	0.439	0.016	9521	1545	90	7	1
	SD	6.36	0.91	2.48	6.63	3.22	0.04	0.01	0.07	0.099	0.003	1535	301	21.9	0.7	0
	(N = 2)															
CBRC0747	Average	51.97	2.50	12.78	21.74	0.08	0.07	0.06	0.10	0.387	0.021	2834	2370	56	11	2
	SD	9.42	0.73	4.88	11.88	0.05	0.04	0.03	0.04	0.072	0.010	1440	1697	8.9	2.2	1
	(N = 4)															
CBRC0783	Average	28.03	0.59	7.00	25.25	8.72	0.04	0.02	0.01	0.222	0.008	878	841	35	6	1
	SD	7.36	0.15	1.09	4.03	7.27	0.02	0.00	0.01	0.016	0.002	176	81	5.1	2.7	0
	(N = 7)															

SD = Standard deviation. N = The number of one meter interval, composite samples, that comprise the serpentine unit of each drill hole, used to determine the average composition of the serpentine unit.

Appendix 8: Table A8.4. Average composition of serpentine units in RC drill holes at MM3.

Hole ID		%SiO2	%Al2O3	%Fe2O3	%MgO	%CaO	%Na2O	%K2O	%TiO2	%Ni	%Co	Cr ppm	Mn ppm	Zn ppm	Zr ppm	Nb ppm
ARC1257	Average	38.51	2.28	12.81	31.49	0.12	0.33	0.04	0.08	0.741	0.028	2865	2917	96	5.7	1
	SD	0.27	0.19	0.66	0.98	0.18	0.09	0.01	0.01	0.154	0.013	138	1141	20.2	0.6	0
	(N = 3)															
ARC1478	Average	39.43	3.12	13.92	27.20	1.63	0.46	0.08	0.17	0.590	0.020	4820	2027	92.75	10.8	1
	SD	0.48	0.20	0.71	0.11	0.77	0.01	0.00	0.08	0.086	0.001	221	129	9.5	4.6	0
	(N = 2)															
ARC1008	Average	45.63	2.15	12.87	25.34	0.35	0.38	0.09	0.08	0.419	0.016	3029	1921	71	6.0	1
	SD	1.82	0.28	1.23	3.81	0.03	0.17	0.03	0.01	0.121	0.003	166	869	8.2	0.8	0
	(N = 4)															
ARC0776	Average	52.67	1.64	11.54	21.08	0.22	0.42	0.07	0.06	0.483	0.018	3544	1754	69.5	5.0	1
	SD	3.25	0.18	2.44	5.66	0.01	0.13	0.03	0.01	0.019	0.001	83	378	7.8	1.4	0
	(N = 2)															
ARC0774	Average	28.20	1.06	6.09	32.94	1.18	0.27	0.07	0.03	0.248	0.010	5292	925	44.3	6.3	1
	SD	5.70	0.55	0.93	2.20	0.93	0.11	0.02	0.03	0.050	0.002	382	237	7.5	3.1	1
	(N = 4)															
ARC0786	Average	36.36	2.34	8.67	31.32	1.9	0.14	0.09	0.08	0.221	0.011	3072	1030	55	5.0	1
	SD															
	(N = 1)															
ARC0782	Average	47.71	2.60	17.43	16.11	0.09	0.48	0.08	0.09	0.734	0.024	8477	5259	91.3	5.0	1
	SD	4.37	0.18	2.33	1.45	0.03	0.12	0.01	0.01	0.178	0.005	3274	2642	6.7	3.6	1
	(N = 3)															
ARC0783	Average	44.28	2.89	14.23	22.82	0.41	0.45	0.08	0.13	0.662	0.024	4077	3312	93.8	11.8	3
	SD	2.09	0.30	1.94	3.30	0.12	0.04	0.01	0.02	0.163	0.010	567	798	6.3	3.3	3
	(N = 3)															
ARC0793	Average	41.46	1.57	13.87	28.86	0.16	0.07	0.02	0.054	0.509	0.019	3678	1634	70	6.0	1
	SD															
	(N = 1)															
ARC0126	Average	42.37	2.60	20.20	17.09	0.17	0.93	0.13	0.10	0.742	0.025	4863	2804	99.3	10.7	1
	SD	1.54	0.34	0.39	0.65	0.05	0.04	0.00	0.01	0.035	0.003	688	1053	11.2	3.8	0
	(N = 3)															
ARC0128	Average	37.58	2.22	14.365	26.885	0.51	0.89	0.08	0.08	0.587	0.027	9040	2478	103.5	8.5	3
	SD															
	(N = 1)															

SD = Standard deviation. N = The number of one meter interval, composite samples, that comprise the serpentine unit of each drill hole, used to determine the average composition of the serpentine unit. For some drill holes, only a single one meter composite sample was available for analysis.